Biochemical characterization of the IRT1 transporter and of its regulatory mechanism

Virginia Cointry

université PARIS-SACLAY

Biochemical characterization of the IRT1 transporter and of its regulatory mechanism

Thèse de doctorat de l'université Paris-Saclay

École doctorale n° 567 : Sciences du Végétal : du gène à l'écosystème (SEVE)
Spécialité de doctorat: Biologie
Unité de recherche : Laboratoire de Recherche en Sciences Végétales UMR 5546
CNRS-UPS Pôle de Biotechnologies Végétales, Auzeville
Référent : Faculté des sciences d'Orsay

Thèse présentée et soutenue à Toulouse, le 30 Mars 2021, par

Virginia COINTRY

Composition du Jury

Sébastien THOMINE Directeur de recherche, I2BC Gif sur-Yvette	Président
Youssef BELKHADIR Directeur de recherche, GMI Vienna	Rapporteur & Examinateur
Chloé ZUBIETA Directrice de recherche, LPCV Grenoble	Rapportrice & Examinatrice
Guillaume LENOIR Maître de conférences, I2BC Gif sur-Yvette	Examinateur
Hugues NURY Chargé de recherche, IBS Grenoble	Examinateur
Grégory VERT Directeur de recherche, LRSV Toulouse	Directeur de thèse

Thèse de doctorat

NNT : 2021UPASB019

Table of contents

Abbreviations

AHA2: Arabidopsis H+-ATPase 2

AUC: analytical ultracentrifugation

bHLH: basic Helix-Loop-Helix

BIFC: bimolecular fluorescence complementation

BRI1: Brassinosteroid Insensitive 1

CDF: Cation Diffusion Facilitator

Cd: Cadmium

CD: Circular Dichroism

CIPK23: CBL-Interacting Protein Kinase 23

Co: Cobalt

Co-IP: co-Immunopurification

CryoEM: cryogenic electron microscopy

DDM: n-Dodecyl β-D-maltoside

DNA: deoxyribonucleic acid

DNase: deoxyribonuclease

EDTA: Ethylenediaminetetraacetic acid

EE: Early endosome

ER: endoplasmic reticulum

FC16: Fos-choline 16

Fe: iron

Fe^{2+}: ferrous iron

Fe^{3+}: ferric iron

GFP: Green Fluorescent Protein

H: histidine

Hygro: Hygromycin B

HRP: Horseradish Peroxidase

ICP-MS: Inductively coupled plasma mass spectrometry

IDF: IRT1 Degradation Factor

IP: Immunoprecipitation

IRT1: Iron Regulated Transporter 1

K: lysine

Kana: Kanamycin

kDa: kilo Dalton

LE: Late endosome

Leu: Leucine

M: Molar

Mn: Manganese

MS: Murashige and Skoog medium

NA: Nicotianamine

NMR: nuclear magnetic resonance

OD: Optical Density

PAGE: polyacrylamide gel electrophoresis

PCR: polymerase chain reaction

PM: plasma membrane

PVDF: Polyvinylidene difluoride

RNA: ribonucleic acid

ROS: reactive oxygen species

SDS: Sodium Dodecyl Sulfate

(F-)SEC: (Fluorescence coupled) Size Exclusion Chromatography

Spec: Spectinomycin

SSR: sepharose streptavidin resin

TM: Transmembrane domain

Trp: tryptophan

Ub: ubiquitin

Ura: Uracil

Wp: Pellet weight

WT: Wild Type

ZIP: ZRT-IRT-like Protein

Zn: Zinc

Abstract

Iron is a key nutrient for all living organisms and it is involved in many cellular processes. Despite being one of the most abundant elements on earth, iron often is unavailable because it precipitates in soil, forming insoluble complexes. Plants take up iron from the soil through the epidermic cells of the root using the IRT1 iron transporter that belongs to the widely distributed ZIP family of transporters. Aside from iron, IRT1 can also transport non-iron metals (Zn, Mn, Co and Cd), which we also refer to as the secondary substrates. It was recently shown by our team that IRT1 acts as a transceptor, directly sensing non-iron metals using a histidine-rich stretch in an unstructured intracellular loop (Dubeaux et al., 2018). Shortly, under non-iron metal excess, metals bind to the histidines recruiting the CIPK23 kinase. Phosphorylation, in turn, allows the recruitment of the IDF1 E3 ligase that ubiquitinates IRT1 and targets it for degradation through the endocytic pathway.

To date, we still know very little about the structural characteristics of IRT1, its transport mechanisms, the basis of IRT1 transport selectivity and the molecular mechanisms driving regulation events such as the recruitment of the CIPK23 kinase. Such a gap exist for all the eukaryotic ZIPs. During the course of this work, we initiated crucial steps for achieving the biochemical characterization of this protein. Here, we are the first to report having established an optimized protocol for the heterologous expression, solubilization and purification of an IRT1 variant protein in yeast cells. Also, we determined a technical procedure for the study of the IRT1 transporter in proteoliposomes. Both technical approaches reported here set ground in the future of the structural and mechanical characterization of IRT1, and eukaryotic ZIPs in general. The sample generated by our protocol resulted in a quality enough for preliminary characterization of the structure by cryogenic electron microscopy together with our collaborators. Additionally, we were able to investigate the oligomeric properties of IRT1 in vitro, by subjecting the pure sample to fluorescent coupled size exclusion chromatography and analytical ultracentrifugation, and by in vivo techniques such as co-immunoprecipitation and bimolecular fluorescence complementation.

Furthermore, we investigated the nature of the molecular mechanism driven by metal binding on the loop of IRT1. We determined by circular dichroism and NMR the absence of tridimensional structure on said portion of the protein, even in presence of the secondary substrates that trigger the regulatory path of IRT1. We provide here, further evidence of metal binding on the histidine loop, as well as a quantification of this interaction in vitro. Additionally, we inferred on the role of an aspartic acid residue, present in the regulatory loop as well, which appears to have a role in metal binding.

Résumé

Le fer est un nutriment clé pour tous les organismes vivants et il est impliqué dans de nombreux processus cellulaires. Bien qu'il soit l'un des éléments les plus abondants sur terre, le fer est souvent indisponible car il précipite dans le sol, formant des complexes insolubles. Les plantes absorbent le fer du sol à travers les cellules épidermiques de la racine en utilisant le transporteur de fer IRT1 qui appartient à la famille de transporteurs ZIP largement répandue. Outre le fer, l'IRT1 peut également transporter des métaux non ferreux (Zn, Mn, Co et Cd), que nous appelons également les substrats secondaires. Notre équipe a récemment montré que l'IRT1 agit comme un transcepteur, détectant directement les métaux non ferreux à l'aide d'un motif riche en histidine dans une boucle intracellulaire non structurée (Dubeaux et al. 2018). Brièvement, sous un excès de métal non ferreux, les métaux se lient aux histidines recrutant la kinase CIPK23. La phosphorylation, à son tour, permet le recrutement de la ligase IDF1 E3 qui ubiquitine IRT1 et la cible pour la dégradation par la voie endocytique.

À ce jour, nous en savons encore très peu sur les caractéristiques structurelles de l'IRT1, ses mécanismes de transport, la base de la sélectivité de transport de l'IRT1 et les mécanismes moléculaires à l'origine des événements de régulation tels que le recrutement de la kinase CIPK23. Un tel écart existe pour toutes les ZIP eucaryotes. Au cours de ce travail, nous avons initié des étapes cruciales pour réaliser la caractérisation biochimique de cette protéine. Ici, nous sommes les premiers à rapporter avoir établi un protocole optimisé pour l'expression hétérologue, la solubilisation et la purification d'une protéine variante IRT1 dans les cellules de levure. En outre, nous avons déterminé une procédure technique pour l'étude du transporteur IRT1 dans les protéoliposomes. Les deux approches techniques rapportées ici ont jeté les bases de l'avenir de la caractérisation structurelle et mécanique de l'IRT1 et des ZIP eucaryotes en général. L'échantillon généré par notre protocole a abouti à une qualité suffisante pour la caractérisation préliminaire de la structure par microscopie électronique cryogénique en collaboration avec nos collaborateurs. De plus, nous avons pu étudier les propriétés oligomères de l'IRT1 in vitro, en soumettant l'échantillon pur à une chromatographie d'exclusion de taille couplée par fluorescence et à une ultracentrifugation analytique, et par des techniques in vivo telles que la co-immunoprécipitation et la complémentation de fluorescence bimoléculaire.

En outre, nous avons étudié la nature du mécanisme moléculaire induit par la liaison du métal sur la boucle de l'IRT1. Nous avons déterminé par dichroïsme circulaire et RMN l'absence de structure tridimensionnelle sur ladite partie de la protéine, même en présence des substrats secondaires qui déclenchent la voie régulatrice de l'IRT1. Nous fournissons ici, des preuves supplémentaires de la liaison des métaux sur la boucle de l'histidine, ainsi qu'une quantification de cette interaction in vitro. De plus, nous avons déduit le rôle d'un résidu d'acide aspartique, également présent dans la boucle de régulation, qui semble avoir un rôle majeur dans la liaison directe des métaux.

Acknowledgements

I want to thank my supervisor Gregory Vert for giving me the chance of working in his laboratory during the past years, where I learned more than I could have imagined. I'm very thankful to everyone in the lab, Alvaro, Ulla, Maria, Reyes, Florian, Julie, Julien, Charlotte and past members, Amanda and Natalie, for the incredible help and support and also for the fun times out of the lab. I was very lucky to work alongside people that are also close friends. Thank you!!

Thank you to my family for being so supportive during this time living an ocean away. Fer, I can't thank you enough, without your support I would probably not have gotten to this point. To my friends in Argentina, always rooting for me, my friends in Paris, which were there in difficult and good times and my friends in Toulouse that have been there for me, especially during this last period and helped me through.

I want to specially thank Cedric Montigny and Guillaume Lenoir, for hosting me in their lab, and sharing all their knowledge with me, it was an extremely enriching experience and I am very happy I got to work with you. Thank you to my collaborators Nelly Morellet at ICSN, Hugues Nury and Eva Pebay Peroula at IBS Grenoble.

1 Introduction

1.1 Metal nutrition in living organisms

1.1.1 Essential micronutrients for living organisms: the role of transition metals

Living organisms require nutrients to perform fundamental processes. According to the amount in which they are required by cells, nutrients can be classified into two groups. Macronutrients are those present at much higher quantities than micronutrients. Macronutrients, such as carbon (C), hydrogen (H), nitrogen (N), oxygen (O), phosphorous (P) and sulfur (S), are required in high amounts and are directly implicated as the building blocks in the synthesis of basic cell components, such as proteins, lipids, carbohydrates, etc. Certain ions such as calcium (Ca), sodium (Na), potassium (K), magnesium (Mg), and chloride (Cl) are considered macronutrients as well, for being required in much higher quantity than micronutrients. Such macronutrient ions are rather involved in maintaining electrical and osmotic balance, communication among cells, etc.

On the other hand, first-row transition metals; i.e. iron (Fe), cobalt (Co), chromium (Cr), copper (Cu), manganese (Mn), selenium (Se), nickel (Ni), molybdenum (Mo) and the soft metal zinc (Zn) are categorized as micronutrients. Despite being needed in minute amounts (5–100 $mg.kg^{-1}$ dry mass), micronutrients are critical for the correct development of cell functions (Alloway 2013). Chemical properties, such as coordination geometries and redox potentials, make every individual metal relevant and suitable for specific tasks; meaning that in most cases they cannot be replaced by other elements.

More than one third of proteins in the whole-cell proteome bind metals (Waldron et al. 2009) and the purpose of these metal-bound proteins vary. In most cases, metals are bound to proteins to serve as cofactors catalyzing biological reactions that would not be viable instead (Waldron et al. 2009). A classic example are the Fe-S containing Ferredoxins (FNR) involved in the electron transfer chain during photosynthesis. Besides functioning as cofactors, metals can be bound to proteins for structure stabilization reasons such as zinc (Zn) in zinc finger motifs; or for storage purposes, like iron (Fe) in the chelator protein ferritin. In vivo binding of metals needs to be precise and specific. The misplacing of a metal atom could cause severe impairment in protein function (Merchant 2010). For example, in DNA binding proteins, replacement of Zn^{2+}; a divalent metal without redox activity; for a redox active divalent cation, could cause radical formation and potential DNA damage.

For the purposes of this thesis, the importance, primary uptake mechanisms and homeostasis of Zn and Fe will be described in the following chapters, with a focus on IRT1-related ZIP transporters when possible.

1.1.2 Importance and molecular mechanisms governing iron and zinc acquisition in eukaryotes

1.1.2.1 Humans

Dietary metal incorporation is at the heart of metal nutrition in higher organisms. For vertebrates, like humans, one of the main sources of micronutrients are crops and depending on the soil where these are cultivated, this is very often a problem due to poor micronutrient bioavailability in most agricultural soils. Fe and Zn deficient diets for example can cause a number of physiological disorders, anemia resulting from lack of Fe being the predominant one. The World Health Organization estimates 1.96 billion people suffer from this condition (De Benoist and Mclean 2008). Some of the health consequences of severe Fe deficiency anemia are increased risk of maternal and child mortality (Macgregor 1963; Scholl and Hediger 1994). Additionally, impaired cognitive and physical functions in children and adults are also linked to Fe deficiency anemia (Jáuregui-Lobera 2014). This health issue affects very unevenly developing countries, specifically affecting women of reproductive age and children. Dietary differences are one of the main causes of this problem, given that cereals are the main food source in developing countries and contain low amount of bioavailable Fe (Yip and Ramakrishnan 2002). Similarly, Zn malnutrition affects approximately one third of the global population. In addition to food production in deficient soils, phytates in cereals that are mostly consumed by impoverished populations, negatively affect Zn absorption (Welch and Graham 2004). Immune deficiency, hypogonadism, growth retardation, diarrhea and dermatitis are among the consequences of a severe to moderate Zn deficiency (Prasad 1991).

The mechanisms of Fe and Zn intake in humans have been largely characterized in the last two decades. Nutrient absorption takes place through the apical surface of epithelial cells in the duodenum (*Figure 1-1*). In the process of Fe absorption from non-haem iron sources (mainly from plant-based foods), it is speculated that ascorbic acid in gastric acid allows the reduction of ferric (Fe^{3+}) to ferrous iron (Fe^{2+}) by the Duodenal Cytochrome B (DCYTB) reductase (McKie et al. 2001; Ganasen et al. 2018). Fe^{2+} is then transported inside the enterocyte through the Divalent Metal Ion Transporter 1 (DMT1), also referred to as Natural Resistance Associated Macrophage Protein 2 (NRAMP2) from the NRAMP family of transporters (Gulec, Anderson, and Collins 2014; Garrick 2011). On the other hand, haem-iron (derived from meat based foods) enters the epithelium through the Haem Carrier Protein 1 (HCP1) and is later a substrate to the Haem-Oxygenase (HO) which catalyzes the reduction of haem-iron into Fe^{2+}, carbon oxide and biliverdin IXa (Shayeghi et al. 2005). Further on the uptake path, ferroportin 1 (FPN1) located at the basolateral side of the cell, exports Fe into the blood for distribution (McKie et al. 2000).

Regarding Zn intake, it has been demonstrated that the main actor in incorporating Zn through the apical membrane of enterocytes is the Zrt-Irt-like protein 4 (ZIP4) (Küry et al. 2002; Wang et al. 2002). Moreover, Zn Transporter 1 (ZnT-1) functions in regulating the intracellular Zn concentration through efflux out of the cell into the portal blood to be distributed to other tissues (Mcmahon and Cousins

1998). ZnT-1 exports Zn through the basolateral side of the epithelial cell. Likewise, ZIP5 and ZIP14, also located at the basolateral face of enterocytes, work as the counterpart of ZnT-1, absorbing Zn from the blood flux helping to balance nutrient requirements (Wang et al. 2004; Guthrie et al. 2015).

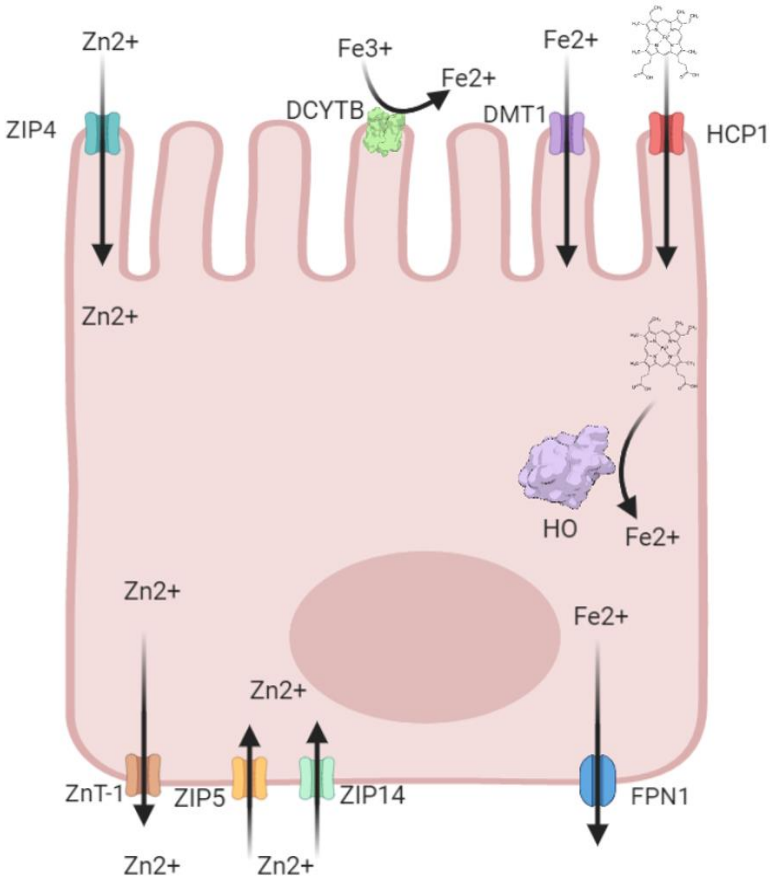

Figure 1-1 Iron and Zn uptake by human enterocytes. Dietary non-haem iron is reduced by DCYTB. Fe^{2+} is then internalized by the DMT1 transporter. Haem iron on the other hand, is transported by HCP1 into the cytosol, where it is converted into $Fe^{2+}$and biliverdin by the HO. In order to be distributed to other tissues, Fe^{2+} is loaded to the bloodstream thanks to FPN1. Zn^{2+} is carried into the enterocyte by the ZIP4 transporter. Znt-1 in turn, excretes Zn^{2+} into the blood for distribution. ZIP4 and ZIP5 enact the opposite function, absorbing Zn^{2+} from the blood flow. Created with BioRender.com.

Nutritional deficit is not the only source of metal-related health issues. Genetic diseases caused by malfunctioning of the aforementioned metal transporters can have a tremendous impact on human health. An example of these are loss of function mutations in the Zn transporter ZIP13 causing Ehler-Danlos syndrome (EDS) (Bin et al. 2014). ZIP13 is present in connective tissue and bone and is critical for its development. People who suffer from EDS exhibit a series of bone abnormalities such as skeletal dysplasia of the spine and malformation of the hands and teeth, due to the fact that Zn is essential for bone mineralization (Yamaguchi 1998). Similarly, Acrodermatitis Entheropatica is a rare recessive genetic disorder caused by mutations in the ZIP4 transporter, impairing dietary Zn absorption (Dufner-Beattie et al. 2003). Acrodermatitis Entheropatica causes skin disease and frequent infections in children and can be treated by Zn supplementation. Same as for Zn transporters, genetic diseases associated with

mutations of Fe transporters also exist. Ferroportin disease is the most common cause of hyperferritinemia and is caused by a mutation in the previously mentioned FPN1 transporter (Przybyszewska and Zekanowska 2014). This disease can cause liver damage from mild to severe cirrhosis, joint pain and heart disease such as arrhythmias.

1.1.2.2 Yeast

Yeast, being simple unicellular eukaryotic organisms, are subjected to variable environmental and nutritional conditions, and compete with other microorganisms for nutrient acquisition. Early studies in *Saccharomyces cerevisiae* found the involvement of two separate zinc uptake machinery. A high affinity and a low affinity one, that implicate the ZIP transporters ZRT1 and ZRT2, respectively (Zhao and Eide 1996a; 1996b). *ZRT1* was first identified by sequence comparison to the *IRT1* Arabidopsis gene, expressing the Iron Regulated Transporter 1 (IRT1) (Eide et al. 1996). *ZRT2* was then found by sequence analysis of the yeast genome, because of its similarity to the *ZRT1* gene (Zhao and Eide 1996b). The function of these genes, was discovered thanks to the mutant *zrt1* inability to grow unless growth media is supplemented with high concentrations of Zn. These transporters were characterized in wild type yeast by using the radioisotope ^{65}Zn. Kinetic assays showed Km values of 10 and 1 μM for yeast grown in Zn replete and in Zn deficient conditions respectively, indicating the presence of low and high affinity mechanisms. The same experiment done in the *zrt1* mutant demonstrated that uptake in both Zn depleted and Zn replete conditions, presented only low affinity uptake, indicating that *zrt1* is indeed responsible for high affinity uptake. Conversely, the mutant *zrt2* presented only high affinity uptake in the same conditions. The presence of a dual mechanism, allows cells to adapt and overcome their changing environmental metal availability. The concentration of this metal has to be raised 10^5-fold to complement said mutant strain, which points out to the ZRT1/2 system to be the main entry point of Zn (Zhao and Eide 1996b).

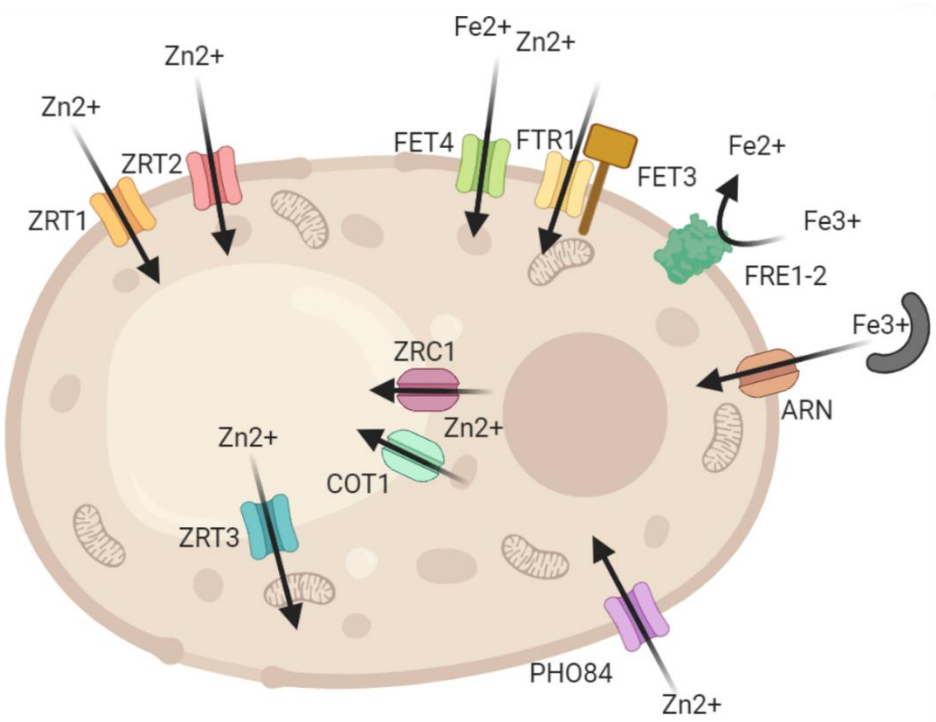

Figure 1-2 Iron and Zinc uptake in yeast. ZRT1 and ZRT2 constitute the high and low affinity Zn^{2+} transporters. Vacuolar transporters ZRC1 and COT1 storage Zn^{2+}, whereas ZRT3 exports it from the vacuole into the cytosol in deficiency conditions. The PHO84 transporter also constitutes a minor system for uptake of Zn^{2+}. Insoluble Fe^{3+} is reduced by FRE1 and FRE2. Fe^{2+} is incorporated through the FET3/FTR1 complex or by the FET4 transporter. The latter, is also able to transport Zn^{2+}. Insoluble iron is chelated and extruded through the ARN transporters. Created with BioRender.com

A mutant strain of *Saccharomyces cerevisiae*, lacking both *zrt1* and *zrt2* genes is still viable when grown in higher amounts of Zn, presumably indicating the presence of additional uptake mechanisms of lower affinity. The low-affinity iron transporter FET4 was shown to transport Zn in such conditions. On the other hand, a Δ*zrt1*Δ*zrt2*Δ*fet4* strain was still able to incorporate Zn when supplied in massive amounts suggesting the possibility of additional low-affinity mechanisms (Waters and Eide 2002). The phosphate and manganese transporter PHO84 is one of the systems thought to take part in Zn uptake with low affinity since a knockout mutation of this gene confers zinc resistance (Jensen, Ajua-Alemanji, and Culotta 2003). Additional Zn transporters and channels are coordinated to control the cytosolic Zn concentration. Detoxification by importing ions into the vacuole is a common strategy used by yeast. Vacuolar storage of Zn is undertaken by the ZRC1 and the COT1 channels, two proteins belonging to the cation diffusion facilitator family (CDF). Studies revealed that the overexpression of these proteins, conferred tolerance to toxic levels of Zn^{2+}, while null mutants *cot1* and *zrc1* present impaired uptake (Douglas S. Conklin, Culbertson, and Kung 1994; Kamizono et al. 1989; D S Conklin et al. 1992). When Zn availability decreases, the vacuolar ZIP transporter ZRT3 replenishes the Zn pool. The role of ZRT3 was discovered through an assay of the triple mutant *zrt1zrt2zrt3* which required 10-fold more Zn that the double mutant *zrt1zrt2*, indicating the overlapping function of these genes. Its location was then

mapped thanks to immunofluorescence microscopy to the vacuolar membrane (MacDiarmid, Gaither, and Eide 2000).

The Fe uptake machinery in yeast is also divided into high and low-affinity systems. The multicopper oxidase FET3 and the permease FTR1 form a complex that make up the high-affinity uptake machinery of Fe^{2+} (Askwith et al. 1994; De Silva et al. 1997; Kwok, Severance, and Kosman 2006). Studies showed that the *fet3* and *ftr1* mutants were unable to take up Fe^{2+} in low concentration conditions, unlike wild type yeast which presented uptake that was saturated at 5 μM (Dix et al. 1994; Stearman et al. 1996). The *fet3* mutant did however show uptake at concentrations above 5 μM, due to the remaining FET4 low-affinity transporter (Dix et al. 1994; Dix et al. 1997). Overexpression of *FET4* gene increased low affinity uptake whereas its disruption prevented yeast from any uptake at elevated concentrations of 5 to 200 μM (Dix et al. 1994). While Fe^{3+} is the predominant form of Fe in nature, FET3 and FET4 can only import Fe^{2+}. The activity of the FRE1 and FRE2 reductases on Fe^{3+} salts and chelates reduces this cation into Fe^{2+} (Georgatsou and Alexandraki 1994; Dancis et al. 1992). Yeast null mutants *fre1* have a decreased iron uptake rate when Fe^{3+} is supplied, even when said mutant overexpresses FET3. This effect can be reverted by addition of an external reducing agent like ascorbate (Dix et al. 1994). Also, a study measured the reductase activity in *fre1* and *fre2* mutant strains and showed it was severely decreased compared to the wild type (Georgatsou and Alexandraki 1994). Given the low bioavailability of Fe in soil due to its majoritarian presence as insoluble Fe hydroxides, many microorganisms count with a chelating non-reducing system for its uptake. This consist in the synthesis, excretion and sequestration of siderophores. Some organisms have the ability to incorporate not only self-secreted siderophores but also the ones released by different organisms (Byers and Arceneaux 1998). Interestingly, *Saccharomyces cerevisiae* is unable to produce siderophores by itself, but it has developed uptake strategies to incorporate ones from fungi and bacteria present in its environment. In this yeast there are four siderophore transporters from the ARN family, ARN1-4 (Yun, Ferea, et al. 2000). Three of them, ARN1-3 are specific to siderophores of the hydroxamate type, such as ferrichrome (FC), ferrichrome A (FC-A) and triacetylfusarinine C (TAFC), secreted by ascomycetous fungi like *Aspergillus* and *Penicillium* (Yun, Tiedeman, et al. 2000; Heymann, Ernst, and Winkelmann 2000; Charlang et al. 1981; Wallner et al. 2009). Mutation of the *ARN*1 and *ARN3* genes simultaneously abolishes growth when FC or FC-A are the main sources of Fe. On the other hand, disruption of *ARN1* alone has little effect on uptake and mutant *arn3* presents partially inhibited siderophore-Fe uptake. *ARN2* has been seen mostly involved in the uptake of TAFC complexes, given that null mutants on this gene had no effect on TC and TCA but did have partially impaired growth on TAFC. However, *ARN2* appears to be helped by the other *ARN* genes in the process of TAFC incorporation, as shown by the difference of growth on the *arn2* strain compared to the inviable double mutants *arn1arn2* and *arn2arn3* (Yun, Tiedeman, et al. 2000). The remaining *ARN*, *ARN4* is specific to the bacterial exclusive catecholate siderophore, enterobactin. This was demonstrated by ^{55}Fe-labeled enterobactin in vivo uptake experiments that presented a completely impaired incorporation in *arn4* mutants (Heymann, Ernst, and Winkelmann 2000). The siderophore-Fe uptake mechanisms consist in binding of the Fe-

siderophore chelate to the ARN protein, the whole complex being endocytosed into the cell in an ubiquitin-dependent manner and then, once in the intracellular space, the translocation of Fe chelates across the membrane (Philpott 2006).

1.1.2.3 Plants

As stated in the previous section, metals are of great importance for plant growth and development. Root systems constitute the primary entry point for micronutrients in plants. Even though Fe is one of the most abundant elements on earth, in soils it is mostly found as insoluble Fe^{3+} compounds. Oxide, hydroxide and phosphate forms are among the most common ones. Despite the relative abundance of iron, its low bioavailability impacts very deeply several aspects of plant production including yield or harvest quality. This is mostly due to the very strong requirement of iron for photosynthesis and respiration since many proteins from the corresponding electron transfer chains use as various forms of iron as cofactors, such as ferredoxins (Kroh and Pilon 2020). Also, it is well established that iron is of huge importance in the biosynthesis and metabolism of chlorophylls (Marsh, Evans, and Matrone 1963). Fe shortage can consequently cause severe plant growth arrest. Likewise, excess of metals, and in particular Fe, can be toxic to plants. This is encountered upon flooding where anaerobic conditions produce Fe^{2+}, which is readily transported into plant cells, as frequently observed in rice for bronzing symptoms. This is also inherent to acidic soils where the bioavailability of iron is higher, or to soils with high levels of iron, such as laterite soils. This type of soil is widespread in warm humid climates and tends to be poor in organic material, besides containing elevated concentration of Fe oxides. Because of its redox reactivity, an excess of iron can be deleterious by production of hydroxyl radicals through the Fenton reaction. This reaction consist of oxidation of Fe^{2+} by hydrogen peroxide (H_2O_2) into $Fe^{3+}$and reduction back to Fe^{2+} also by H_2O_2, generating in total a water molecule, a hydroxyl radical ($HO\bullet$) and a hydroperoxyl radical ($HOO\bullet$) that can damage cellular components and biomolecules (Gratão et al. 2005).

In order to absorb Fe, plants developed different acquisition mechanisms that can be classified as strategy I and strategy II (*Figure 1-3*). Strategy I uptake is based on the solubilization/reduction of the soil Fe^{3+} chelates into Fe^{2+}. The solubilization is achieved via proton pumps that export protons into the rhizosphere and secreting phenolic compounds. This strategy is adopted by dicots and non-graminaceous plants. *Arabidopsis thaliana* is the model plant used to exemplify strategy I Fe acquisition. In Arabidopsis, the proton pump responsible for acidification of the soil is the H^+-ATPase 2 (AHA2), which works together with the Ferric Reduction Oxidase 2 (FRO2) ferric chelate reductase to reduce Fe^{3+}. There are twelve AHA isoforms in Arabidopsis, however, analysis of media acidification by *aha* mutants showed only the AHA2 proton pump to be involved in proton extrusion in response to Fe-deficiency conditions (Santi and Schmidt 2009; Robinson et al. 1999). This acidification step is of tremendous importance for Fe uptake, given that Fe^{3+} solubility increases 1000-fold with each unit drop in pH. Additionally, phenolic compounds in root exudates, mainly coumarins, excreted by the ABCG37 transporter enhance Fe^{3+} solubility (Ziegler et al. 2017). In accordance with its function, an *abcg37*

Arabidopsis mutant is hypersensitive to Fe deficiency and accumulates less Fe (Fourcroy et al. 2014). *ABCG37* and genes from the biosynthesis pathway of coumarins, like the *2-oxoglutarate Fe(II) oxygenase Feruloyl-CoA 6´-Hydroxylase* (*F6'H1*), an essential gene for the synthesis of coumarins like scopoletin and scopolin, are upregulated by Fe deficiency (Kai et al. 2008; Lan et al. 2011). Besides H^+ and coumarins, low molecular weight organic acids like citric acid, malic acid, oxalic acid and tartaric acid also contribute to soil acidification. The nature of the anionic exporters involved in this task is yet to be elucidated, however homologs of the xylem citrate effluxer FERRIC REDICTASE DEFECTIVE 3 (FRD3), may be suspected (Durrett, Gassmann, and Rogers 2007). Posterior to soil acidification and Fe reduction by FRO2, the Iron Regulated Transporter 1 (IRT1) is then responsible for translocation of Fe^{2+} into the cell (Vert et al. 2002). Knock out mutants of the components of the Strategy I system, *irt1* and *fro2*, have similar phenotypical characteristics such as impaired growth, low Fe accumulation and are extremely chlorotic, demonstrating their essential roles in Fe acquisition.

On the other hand, strategy II plants, namely grasses, require phytosiderophore (PS) secretion to solubilize and chelate Fe^{3+}. PS-Fe complexes are then taken up through the roots to deliver iron into plant cell. In *Zea mays*, the efflux transporter TOM1 releases PS into the soil, followed by transport of the PS-Fe^{3+} complex through the Yellow Stripe 1 transporter (YS1) (Curie et al. 2001; Mori and Nishizawa 1987; Nozoye, Nakanishi, and Nishizawa 2013). The distinction between strategy I and II is however not strict. For example rice, a grass species, possess transporters homologous to IRT1 that constitute an additional strategy I type of uptake (Ishimaru et al. 2006; Lee and An 2009). The contribution of both types of transporters in these species is still not clear.

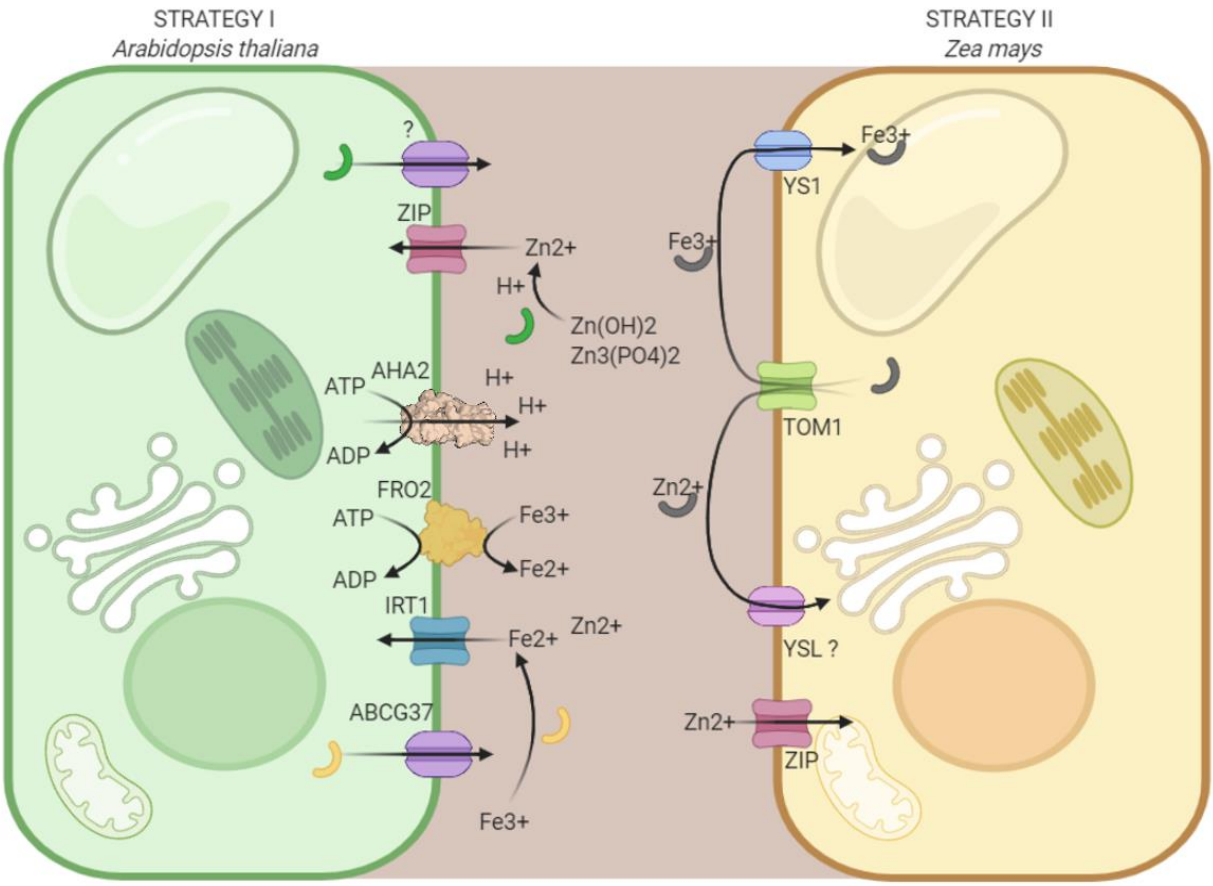

Figure 1-3 Fe and Zn primary uptake in plants. Strategy I plants such as *Arabidopsis thaliana*, incorporate Fe through a reduction mechanisms involving rhizosphere acidification by AHA2 and reduction of Fe^{3+} to Fe^{2+}. Reduced Fe is then take up by IRT1. The ABCG37 transporter releases coumarins (represented by yellow semi-circles) into the soil, which allows further solubilization of ferric compounds. Strategy II plants, here exemplified by *Zea mays*, export phytosiderophores (grey semi-circles) through the TOM1 transporter, that chelate insoluble iron. Chelated iron complexes are then imported by YS1. Zinc is solubilized thanks to soil acidification by proton extrusion and organic acid exudates (green semi-circles). Zn^{2+} is taken up by ZIP transporters. In grasses, chelated $Zn^{2+}$is thought to be incorporated through YSL proteins. ZIP transporters may also be involved. Created with BioRender.com.

Similar to Fe, Zn deficiency in plants can cause chlorosis and growth retardation. Moreover, it affects carbohydrate metabolism, defense against diseases and production of seeds (Marschner 1995). In crops, Zn scarcity impacts deeply in cereal grain yield. This metal is also essential for the stability of the genetic material. In contrast to Fe deficiency, signs of Zn deficiency show only under severe limitation. Moderate Zn insufficiency often causes mild yield losses in crops and is challenging to detect. The availability of Zn is greatly impacted by pH, moisture levels, calcareous and sodic soils and elevated amount of nitrogen and phosphate (Alloway 2004).

Plants mostly take up Zn in its divalent form (Zn^{2+}), indicating that in contrast to iron, prior reduction is not necessary. Mechanisms for Zn acquisition resemble those of Fe to a certain extent. Like Fe Strategy I uptake, many plants secrete molecules that enhance solubility of Zn hydroxides and phosphates, releasing Zn^{2+}. One unit drop in pH increases Zn solubility 30 to 45-fold. As previously detailed for Fe^{3+}, H^+ and low molecular weight organic acids contribute to Zn^{2+} solubilization too. Transporters from the ZIP family are involved in the transport of Zn^{2+}across the membrane, as well as

passive diffusion nonspecific cation channels (Grotz et al. 1998; Williams, Pittman, and Hall 2000; Demidchik et al. 2002). Additionally, in Arabidopsis, Zn^{2+} is part of the secondary substrates transported by the iron transporter IRT1 that also belongs to the ZIP family (Korshunova et al. 1999; Eide et al. 1996; Vert, Briat, and Curie 2001; Vert et al. 2002). IRT3 was also shown to be involved in Zn uptake at the root cell plasma membrane (Lin et al. 2009). There's however little agreement about which specific ZIPs are part of the primary uptake of Zn^{2+}. Detailed analysis of the ZIP transporter family and their transport spectrum is provided below. As for grasses, ZIP transporters have also been vastly described to be involved in Zn deficiency response in rice and maize (Huang et al. 2020; S. Li et al. 2013). On the other hand, conflicting evidence suggests the existence of a Strategy II Zn primary uptake mechanism in certain cereals. Early studies have reported that in maize, like Fe, Zn can be taken up complexed with PS, presumably through YS-type of transporters, but that a non-PS uptake system is present in this organism as well (Von Wirén, Marschner, and Romheld 1996). Posterior studies, refuted this idea, by demonstrating that the maize YS1 transporter is unable to complement the yeast *zrt1zrt2* mutant deficient in Zn uptake, even when PSs are supplemented to the media (Roberts et al. 2004). Moreover, PS production upon Zn^{2+} deficiency and PS-Zn^{2+} absorption has been stablished in barley (Suzuki et al. 2006). Interestingly, analyses in barley using ^{62}Zn, demonstrated an uptake preference for the PS deoxymugineic acid (DMA) complexed Zn (DMA-Zn) than for soluble Zn^{2+}, which together with the elevated PS excretion during Zn deficiency, suggests this to be the main entry route of this metal (Suzuki et al. 2006). Rice, on the other hand, appears to utilize PS-Zn transport mostly as a long-distance mobilization mechanism throughout the plant rather than as a primary uptake strategy (Suzuki et al. 2008). Biochemical evidence of PS-Zn transport by YSL transporters or by a different family of PS-Zn transporters is missing, however, the evidence so far suggests that different uptake mechanisms of Zn uptake exist across organisms, and that they are not conserved among cereals.

1.2 Iron and zinc transport across membranes in plant cells

1.2.1 Metal transporter families implicated in iron and zinc plant homeostasis

To provide enough Fe and Zn for cell function and metabolism, both metals have to be transported across membranes into the cytosol or into organelles where they are utilized by proteins for different tasks. Metal transporters of different kinds are involved in the process of metal uptake, intracellular distribution/compartmentalization, cell-cell transfer or long distance transport. This section will focus on the general characteristics of the main families of transporters involved in the abovementioned processes, while section 3 will focus deeper on the ZIP family of transporters.

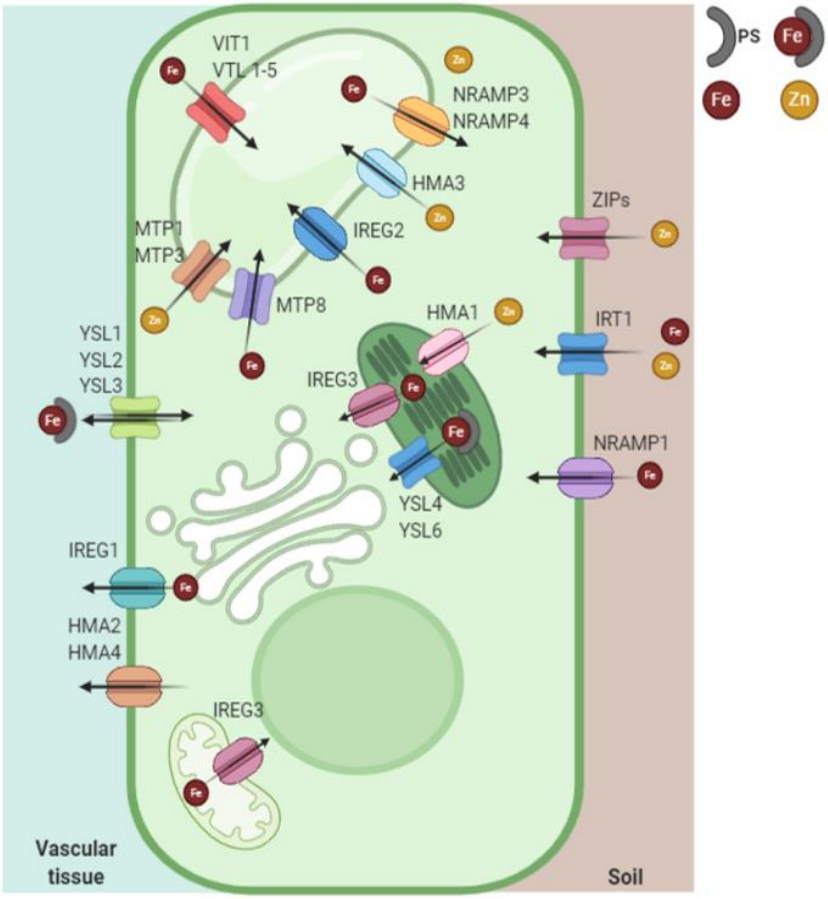

Figure 1-4 Main Fe and Zn transporters in Arabidopsis (Except ZIPs). The principal Fe transporter IRT1 takes up nutritional Fe from the soil. NRAMP1 confers a low-affinity uptake of Fe. Export through the plasma membrane is carried out by IREG1. Phytosiderophore-complexed Fe is mobilized by YSL1, YSL2 and YSL3 into and out of vascular tissue. Vacuolar Fe storage takes places thanks to VIT, VTLs 1-5, MTP8 and IREG2. Restoration of cytosolic Fe levels from the vacuole is processed by NRAMP3 and NRAMP4. IREG3 functions in mobilization of Fe from chloroplasts and mitochondria, whereas YSL4 and YSL6 extrude Fe-phytosiderophore complexes. Zinc is taken up by ZIP transporters (these will be better illustrated in section 3). IRT1 is a low-affinity Zn transporter. Export of Zn through the PM into the xylem is carried out by HMA2 and HMA4. MTP1, MTP3 and HMA3 incorporate Zn to the vacuolar pool. In turn, HMA1 delivers Zn to chloroplasts. Created with BioRender.com

1.2.2 Principal families of proteins involved in iron and zinc transport in plants

1.2.2.1 NRAMPS

The first Natural Resistance Associated Macrophage Protein (NRAMP) transporter was identified in human macrophage cells and found to be involved in response to pathogen attack (Vidal et al. 1993; Cellier, Belouchi, and Gros 1996). NRAMP1 was found in the lysosomal compartment of macrophages where, after phagocytosis, it changes the intraphagosomal metal availability to inhibit microbial growth (Forbes and Gros 2001). Later on, homologous proteins were found both in eukaryotes and prokaryotes and made their involvement in metal trafficking more evident. NRAMPs have high sequence similarities among members from different kingdoms of life. For example, the *Arabidopsis* NRAMPs are 50% identical to the *Saccharomyces cerevisiae* NRAMP SMF1, and 40% identical to the mouse NRAMP1. Notably, the predicted transmembrane domains (TMDs) are the regions of higher identity (Kerppola and Ames 1992).

Metal ion transport by NRAMPs requires a proton gradient as driving force and, as other metal transporters, its substrate range is broad, being able to transport Mn^{2+}, Zn^{2+}, Cu^{2+}, Fe^{2+}, Cd^{2+}, Ni^{2+}, and Co^{2+}. The widely accepted transport mechanism of NRAMPs is that of a symporter, where both metal ions and H^{+} are transported simultaneously, based on data from mammalian and yeast members (Gunshin et al. 1997; Chen et al. 1999; Tandy et al. 2000). The rat DCT1 NRAMP and the yeast SMF1 protein were both characterized in Xenopus oocytes, where transport was proton dependent and generated acidification of the intracellular milieu, suggesting a co-transport mechanism (Gunshin et al. 1997; Chen et al. 1999).

NRAMPs are transmembrane proteins, with large C-terminal tails. Topology predictions suggest between 11 and 12 TMs depending on the particular orthologue (Courville et al. 2004). In 2014, the first NRAMP 3D structure was published, which was the *Staphylococcus capitis* NRAMP orthologue (Ehrnstorfer et al. 2014). Later on, structures of further bacterial NRAMPs were published as well (Ehrnstorfer et al. 2017; Bozzi et al. 2016; 2019). NRAMP structures revealed a pseudo-symmetry, where TMs 1-5 are aligned in opposite direction to TMs 6-10. TMs 1 and 6 are in proximity of each other, and share the particularity of being unwound in the center of the membrane. It has been revealed that conserved residues in this partially unstructured region constitute the metal binding center of NRAMPS. The remaining TM 11 and 12 in some cases, are positioned in the periphery of the 1-5 and 6-10 structures, and possess no apparent transport properties (Ehrnstorfer et al. 2014; 2017; Bozzi et al. 2016; 2019).

In plants, there are a high number of NRAMP homologues. Arabidopsis possess 6 NRAMPs, named NRAMP1-6, with NRAMP2-5 being the most closely related to each other and NRAMP1 and NRAMP6 forming a separate cluster. NRAMP1, 3, 4 and 5 were shown to complement yeast mutants defective in high and low-affinity Fe uptake systems and in manganese uptake, called *Δfet3Δfet4* and *Δsmf1* respectively (Thomine et al. 2000; Curie et al. 2000). Furthermore, NRAMP4 is able to complement not

only *Δfet3Δfet4* and *Δsmf1* but also the zinc uptake deficient yeast strain *Δzrt1Δzrt2*. Plant NRAMPs are expressed both in the roots as well as in the shoots, demonstrating their participation in metal homeostasis along the whole organism. Arabidopsis NRAMPs were shown to localize in different compartments/organelles. NRAMP3 and NRAMP4 function at the vacuolar membrane, as shown by transient expression of a GFP fusion to the C-terminal side of AtNRAMP3 in onion epidermal cells and by immunolocalization in cotyledons for AtNRAMP4; where it works in restoring cytoplasmic Fe levels during deficiency (Thomine et al. 2003; Lanquar et al. 2005). Recently a role for NRAMP2 at the Trans-Golgi network has been proposed, where it is expected to work remobilizing Mn in deficiency conditions (Gao et al. 2018). In contrast, NRAMP1 was found by confocal microscopy of a GFP fusion, to be expressed in the plasma membrane. The latter was pointed out to be the major Mn^{2+} uptake system in Arabidopsis, besides constituting a low-affinity Fe^{2+} transporter, given that a knock-out mutation in Arabidopsis in this gene confers hypersensitivity to Mn deficiency. Symptoms of said hypersensitivity were chlorosis, shorter roots and overall lower biomass production (Cailliatte et al. 2010).

1.2.2.2 P_{IB} type ATPases

P-type ATPases are a large family of transporters that, like the aforementioned NRAMPs, are found in all kingdoms of life. A great variety of substrates is transported by this family, giving place to the classification of P-Type ATPases into subfamilies. The class that is implicated in the transport of metal micronutrients is called P_{IB}-type ATPases. This subtype shares a common highly conserved characteristic, which is the presence of a CPx-motif, mainly formed by either of these three amino acid combinations: C-P-C, C-P-H or C-P-S. For this reason, P_{IB}-type ATPases - also referred to as heavy metal P-type ATPases (HMA) - are also frequently called CPx-type ATPases. The CPx motif is found in the intramembranous region and is directly involved in the translocation of metals.

Sequence alignment of several CPx-type ATPases further subdivided this subfamily into six subclasses. Substrate preference varies between subclasses, as well as the sequence of other specific conserved motifs besides the CPx. One of these is the P_{IB2} Type ATPases, which present a CPC motif and is mainly involved in the transport of Zn^{2+} (Argüello, Elif, and González-Guerrero 2007). Additionally, subclass P_{IB4} has been proved to be involved in Co^{2+}, Zn^{2+}, Fe^{2+} and Cd^{2+} (Purohit et al. 2018). A sixth subclass, the P_{IB6}-type ATPases, was recently classified. Members of this category in bacteria are thought to transport Fe^{2+} due to their genomic location in relation to the ferric uptake regulator (Fur) binding sites that resemble the organization of the bacterial Feo Fe^{2+} uptake operon (Smith, Smith, and Rosenzweig 2014). However, biochemical evidence is still lacking.

In Arabidopsis, eight members belong to the P_{IB}-type ATPases family, HMA1-8. HMA1-4 are implicated in Zn transport and homeostasis in diverse organelles. For instance, HMA1 is present in plastids and is involved in Zn^{2+} and Cu^{2+} import; HMA2 and HMA4 work as Zn^{2+} exporters at the plasma membrane in xylem loading, and HMA3 localizes at the vacuolar membrane where it helps in cell detoxification of Zn (Takahashi et al. 2012; Verret et al. 2004; Kim et al. 2009; Hussain et al. 2004).

Interestingly, except HMA1, the remaining three HMAs were shown to aid in Cd^{2+} detoxification as well.

CPx-type ATPases display eight TMs, with both N and C termini facing the cytosol, and have two large intracellular loops. As other P-type ATPases, HMAs, contain ATP binding domains at the N-terminus, where ATP is hydrolyzed phosphorylating, in turn, a conserved asparagine residue. The hydrolysis of ATP provides sufficient energy for translocation of the substrates. There's a wealth of information about the tridimensional structure of HMA transporters, particularly of the soluble ATPase domain. To date, there are available structures of ATPase domains from 27 different species, ranging from humans, yeast, plants and bacteria in the Protein Data Bank repository. Full-length structures are however less abundant. As of today, only the structures of the prokaryotic *Shigella sonnei* Zn-HMA and the *Legionella pneumophila* Cu-HMA are available (Gourdon et al. 2011; Wang et al. 2014). Like other P-type ATPases, these structures showed that HMAs contain the three typical cytoplasmic A-domain (actuator), P-domain (phosphorylation) and the N-domain (nucleotide binding). The transmembrane domain is composed of six helixes forming a core, also conserved across P-Type ATPases. Two additional helixes are present in this domain, which are a particular characteristic of P_{IB}-Type ATPases.

1.2.2.3 CDF

Prokaryotes and eukaryotes share a common mechanism of metal toxicity response. Cation Diffusion Facilitators (CDF) enact this mechanism. The CDF family is also referred to as Solute Carrier 30 (Slc30), ZnT for Zinc Transporters and, in plants, as Metal Tolerance Proteins (MTP). Proteins from this family are efflux transporters, with the ability to mobilize several divalent metals from the cytoplasm into the extracellular space, the vacuole (in plants and yeast) or into other organelles. CDF members were found to be involved in the extrusion of Fe^{2+}, Ni^{2+}, Mn^{2+}, Co^{2+}, Cd^{2+} and Zn^{2+}, suspectedly, through an antiporter type of transport, where H^+ or K^+ are the counter ion to the metals as exemplified by the CzcD of *Bacillus subtilis*, YiiP from *Escherichia coli*, *Arabidopsis thaliana* MTP1 and others (Guffanti et al. 2002; Grass et al. 2005; Kawachi et al. 2008).

Early phylogenetic studies have separated this family into three subgroups. Substrate preference seems to be overall conserved along with phylogenetic relations, and accordingly the subfamilies were classified as Zn^{2+}-CDFs, Zn^{2+}/Fe^{2+}-CDFs and Mn^{2+}-CDFs (Montanini et al. 2007). Later on, this classification expanded, separating the Zn/Fe-CDFs into Zn^{2+}/Cd^{2+}, Co^{2+}/Ni^{2+}, Fe^{2+} and $Zn^{2+}/Cd^{2+}/Fe^{2+}/Mn^{2+}$ groups.

For the most part, CDFs are predicted to form six TMDs with both C and N termini facing the cytoplasmic side. They contain a large cytoplasmic loop with histidine motifs HX ranging between 3 and 6 repeats, where X can be G or S residues. These characteristics resemble those of the ZIP family of transporters, to which CDFs are phylogenetically related (Kambe et al. 2006). The first crystal structure of a CDF transporter to be determined was the one of the *Escherichia coli* YiiP transporter. The resolved structure showed a Y-shaped homodimer, with transported Zn^{2+} and Cd^{2+} atoms tetra-coordinated between three D and one H residues located in TM2 and TM5 (Lu and Fu 2007). Interestingly, a point

mutation in one of the D residues to H, promotes loss of affinity towards Cd^{2+}, rendering the transporter selective to Zn^{2+} (Hoch et al. 2012). In nature, this HD/HD transport site occurs in mammalian CDFs, which are able to transport Zn^{2+} but not Cd^{2+}. Structures of the homologue CDFs from the prokaryotes *Shewanella oneidensis* and the extremely thermophilic bacterium *Thermus thermophilus* were also achieved in the following years by CryoEM and X-ray crystallography respectively (Coudray et al. 2013; Cherezov et al. 2008).

Eleven members of this family have been reported in *Arabidopsis thaliana*, from which four have been characterized to date. MTP1 and MTP3 correspond to the Zn-CDF subclass and are involved in vacuolar storage of Zn^{2+}, the MTP8 transporter is also localized at the vacuole and is responsible for Fe^{2+} and Mn^{2+} localization in seeds and MTP11, a Mn^{2+}-CDF type localized at the trans-Golgi/pre-vacuolar compartment (Desbrosses-Fonrouge et al. 2005; Arrivault, Senger, and Krämer 2006; Delhaize et al. 2007; Eroglu et al. 2016; Chu et al. 2017; Eroglu et al. 2017).

1.2.2.4 YSL

Oligopeptide transporters (OPT) are a small family of proteins that transport amino acid-derived substrates. This family is separated into two subgroups: Oligopeptide transporters (PT) and Yellow Stripe Like (YSL) transporters. The latter mediates the transport of phytosiderophores (PS)-metal and nicotianamine-metal complexes across membranes. PS are organic substances produced by plants for chelating divalent metals that help plants incorporate these essential micronutrients in scarcity conditions. PS are classified in different families according to their substrate preferences. For instance, coumarins are PS which are capable of binding Fe^{2+}, whereas mugineic acid type PS do not require prior reduction of Fe and have affinity to Fe^{3+} (Schmidt et al. 2014; Mino et al. 1983). Nicotianamine on the other hand, is a biosynthetic intermediate of mugineic acid and it is a structural analog of the latter, with chelating properties for Fe, Zn, Mn, Co, Ni and Cu (Shojima et al. 1990; Haydon and Cobbett 2007). YSLs take their name from the yellow striped leaf phenotype that arises from disruption of the YS1 gene in maize. YSLs are widely distributed among plant species. Graminaceous plants rely on YSL transporters largely for their primary uptake of Fe from the soil using phytosiderophores, whereas non-graminaceae on the other hand, mostly utilize this family of transporters for translocation of complexed metals throughout the plant.

YSLs are large integral transmembrane proteins with a predicted architecture of 9 to 16 TMs, although no structural data has been reported yet (Wiles, Naider, and Becker 2006). YS1 from maize (ZmYS1) requires a proton gradient to function, as shown in Xenopus oocyte experiments, where transport was dependent on pH but not on other ions, like sodium (Schaaf et al. 2004). Unlike other transporters, YSLs can transport both Fe^{2+} and Fe^{3+} when complexed with PS like nicotianamine (NA) or deoxymugineic acid (DMA), with a preference for DMA metal complexes as exemplified by oocyte-based experiments on ZmYS1 (Schaaf et al. 2004). Besides Fe, it has been observed that other metals are transported in this same way. Among them, Ni, Cu and Zn complexes. Furthermore, the rice closest homologue of ZmYS1, OsYSL15, is also a Fe-PS transporter with wide substrate specificity.

A much debated question is the involvement of YSLs in Zn-PS transport. Maize *ys1* mutants show decreased Zn-PS uptake (Von Wirén, Marschner, and Romheld 1996). Also, other grasses; like barley and wheat were found to secrete elevated amounts of PS when undergoing Zn deficiency and reversion to normal PS levels when Zn was resupplied (Gries et al. 1995; F. Zhang, Römheld, and Marschner 1989; Cakmak et al. 1994). Further biochemical evidence of the transport of Zn-PS by YSL is however lacking. Whether specific Zn-PS-affine YSL exist remains unanswered to date.

Arabidopsis counts with eight YSLs. The characterized AtYSL1, AtYSL2 and AtYSL3 appear to be expressed in xylem in roots, shoots and leaves, pointing to their involvement in Fe-PS distribution (DiDonato et al. 2004; Waters et al. 2006). AtYSL1 participates in loading of Fe-NA in seeds and inflorescences together with AtYSL3 (Chu et al. 2010). A double mutant plant with impairments in both these genes presents interveinal chlorosis, low leaf Fe contents and impaired metal mobilization from leaf during senescence (Waters et al. 2006). Interestingly, single mutants in said genes, and in YSL2, do not exhibit any noticeable phenotype (DiDonato et al. 2004; Waters et al. 2006). Contrary to this, AtYSL4 and AtYSL6 function at the chloroplast envelope, exporting Fe to prevent overload on the plastids. Again, single mutants of YSL4 and YSL6 do not show strong phenotypical differences to the wild-type plants when exposed to Fe excess. The double mutants however, presents marked Fe toxicity effects such as growth impairment (Divol et al. 2013).

1.2.2.5 IREG

Iron regulated proteins (IREG) define a widely distributed protein family. Human ferroportin1 (Fpn1) is the most known example. Its function is the distribution of Fe in humans from the enterocyte, where primary uptake takes place, into the bloodstream. IREGs have been suspected of transport of other divalent metals than Fe, such as Co, Zn, Ni and Mn (Schaaf et al. 2006; Morrissey et al. 2009). The involvement of Ca^{2+} in metal transport by IREGs was recently demonstrated for the human Fpn1 where Ca^{2+} acts as an essential cofactor. Additionally, a Ca^{2+} bound structure of the *Bdellovibrio bacteriovorous* Fpn suggested a conserved role for this cation in the function of IREGs (Deshpande et al. 2018).

IREGs are formed by 9 to 12 putative TMs and present a highly conserved H residue proven to be important for Fe transport (Zohn et al. 2007). Bacterial IREG structures were obtained by X-ray crystallography and they suggest a homologous structure to one of the Major Facilitator Superfamily (MFS), where TMs 1-6 form the N terminal lobe and TMs 7-12 the C terminal lobe (Taniguchi et al. 2015). Both halves are connected through a large cytosolic loop. Also, a transition metal ion binding site is found at the interface of both.

Three IREG proteins are encoded in Arabidopsis, AtIREG1-3. Their localization varies, AtIREG1 is present at the plasma membrane of roots and shoots, AtIREG2 at the tonoplast in root cells and AtIREG3 at the chloroplast and mitochondria membranes (Morrissey et al. 2009; Conte et al. 2009; Schaaf et al. 2006). AtIREG1, besides transporting Co^{2+}, was the only member established to be implicated in Fe^{2+} transport out of the cell, extruding Fe^{2+} into xylem for transport to the shoot (Morrissey et al. 2009). AtIREG2 was found to be involved in Ni^{2+} internalization in the vacuole in

roots, thus preventing loading of toxic metals into the vasculature (Schaaf et al. 2006; Morrissey et al. 2009). IREG2 function in Fe^{2+} has long been suspected, since Fe deficiency response in *ireg2* mutants is delayed or impaired, suggesting that inability to sequester Fe^{2+}in the vacuole impacts Fe^{2+} deficiency sensing (Morrissey et al. 2009). Very recently, Kim et al. 2020 reported on the involvement of IREG3 in Fe^{2+} export from organelles. Interestingly, IREG3 was suggested previously to transport a metal chelator, like citrate or NA, into plastids (Conte et al. 2009).

1.2.2.6 VIT

Arabidopsis thaliana Vacuolar Iron Transporters (VITs) were first identified for their homology to the vacuolar CCC1 transporter from yeast. The action of VIT1 in plants is crucial for Fe^{2+} storage in the vacuole, whereas yeast CCC1 was found responsible for Fe^{2+} and Mn^{2+} detoxification (Li et al. 2001; Kim et al. 2006). This family of transporters spans from eukaryotes to bacteria and archaea.

The resolution of the crystal structure of the *Eucalyptus grandis* VIT homologue was recently achieved, allowing the recognition of important motifs for metal transport. EgVIT is composed of 5 TMs with a large cytosolic loop that contains 3 alfa-helixes between TM2 and TM3. The N and C termini face opposite sides, with N terminus on the cytoplasm and C terminus on the vacuolar lumen. EgVIT forms a homodimer, where the interface between the two monomers creates a channel through which the metal ions are extruded. Conserved W, M, D and N residues in this region provide a hydrophilic cavity for proper ion translocation. This channel is open from the cytosolic side but closed by hydrophobic residues on the interior side of the vacuole. Upon transport, G and P residues undergo conformational changes that open the gate to allow the passing of metal ions (Kato et al. 2019).

The sequence similarity is low across this family of transporters, however, the structure and specific transport residues are highly conserved. Biochemical data on EgVIT1 and yeast CCC1 suggested an antiporter type of transport mechanism, by counter transport of H^+ out of the vacuole (Cockrell et al. 2014; Kato et al. 2019). The main substrate of VIT-like transporters appears to be Fe^{2+}; however, other divalent ions like Mn^{2+} and $Zn^{2+}$are suspected of being lower affinity substrates (Li et al. 2001; Kim et al. 2006; Zhang et al. 2012). EgVIT presented Co^{2+} transport as well (Kato et al. 2019).

Besides VIT1, in Arabidopsis five more members of this family have been identified. AtVTL1-5 are too vacuolar transporters (Gollhofer et al. 2014). Research to date has not yet determined whether each homologue participates at a certain stage of plant nutrition or development, or if their functions are redundant.

1.3 ZIP family of proteins

The ZIP family of proteins was founded by the IRT1 transporter from *Arabidopsis thaliana*, first identified in 1996, and the Zrt1 Zn transporter from *Saccharomyces cerevisiae*. Since then, Zrt-Irt like Proteins (ZIPs) were found across all phyla, in 5205 species to this date (Pfam database). ZIP transporters are involved in the transport of Zn^{2+}, Fe^{2+} and other divalent metals, such as Cd^{2+} and Mn^{2+} into the cytoplasmic space. This section describes the mechanisms, classification, structure and regulation of ZIP transporters.

1.3.1 Mechanisms of ZIP transporters: an area of great disparity

To date there has been little agreement on what is the transport mechanism of ZIPs and whether this is a conserved characteristics. Zhao and Eide proposed during early reports on the *Saccharomyces cerevisiae* ZRT1 and ZRT2 that these two proteins might function through an energized type of transport, potentially driven by metabolic energy like the electrochemical gradient (Zhao and Eide 1996a; 1996b). This prediction was based on the observation that yeast Zn uptake requires metabolic energy (White and Gadd 1987). In addition, Cd^{2+} uptake by the mouse mZIP8 and mZIP14, in mouse fetal fibroblast cell cultures was hindered by mitochondrial respiratory chain inhibitor KCN, suggesting an energy dependent mechanism (He et al. 2006; Girijashanker et al. 2008). Opposed to this, a cell-based study of the human hZIP2 also involving electron transport inhibitors, revealed an energy-independent transport (Gaither and Eide 2000).

A symporter mechanism was proposed for both mZIP8 and mZIP14, where Cd^{2+} or Zn^{2+} are mobilized together with HCO_3^- (Liu et al. 2008; Girijashanker et al. 2008). It is worth pointing out that in the case of mZIP14, addition of HCO_3^- increased significantly the uptake, whereas experiments on mZIP8 were performed only in presence of HCO_3^-. Likewise, research on the hZIP2 expressed in mammalian cell cultures suggested a symport mechanism of Zn^{2+}/HCO_3^-, considering that addition of HCO_3^- accelerated considerably the uptake rate (Gaither and Eide 2000). However, further work on hZIP2 showed contradictory data. In the latter, HCO_3^- did not affect radio-labeled Zn^{2+} transport in any way when expressed in *Xenopus laevis* oocytes (Franz et al. 2018). In turn, extracellular pH did affect transport activity. At acidic pH values the greatest uptake rate was recorded, while at values above 7.5 activity was abolished. Electrogenecity, Na^+ and Cl^- gradient dependency and H^+ or K^+ coupled transport were also assayed by Franz et al. 2018, where they found none of these to be involved, except for the electrogenic nature of the transporter that remained elusive. On the other hand, transport of Cd^{2+} and Zn^{2+} by hZIP2 did seem to be voltage-dependent. The overall mechanism of hZIP2 in this study suggested a passive transport across the membrane contrasting with previous reports.

Furthermore, proteoliposome-reconstituted ZIPB from the pathogenic bacteria *Bordetella bronchiseptica* was assayed for transport in a fluorescence-based approach. In line with the latest data on hZIP2, ZIPB behavior *in vitro* was that of a voltage-dependent electrodiffusion channel and was able to transport Zn^{2+} in absence of physiological ions (Lin et al. 2010). In accordance with this, the structure

of the ZIPB monomer (described in a following section) displays a metal transport channel (Zhang et al. 2017).

Taking together all these conflicting reports, it is worth pointing out the importance of further research on the mechanism of transport of ZIP transporters from different organisms. Evidence to date indicates no common transport mechanisms throughout this family, and maybe even divergence across organisms.

1.3.2 Classification of ZIPs

ZIPs can be classified into four subfamilies based on their sequence and domain composition. These are subfamily I, subfamily II, gufA and LIV-1/LZT (Gaither and Eide 2001; Guerinot 2000). Common domain composition and sequence identity is shared throughout these groups, in particular between the first three. The latter, the LIV-1 subfamily, which takes its name from a breast cancer-related gene, is the least similar to the rest and presents an additional N-terminal extracellular domain (ECD). This subfamily is one of the most studied in terms of conservation of particular characteristics. The ECD of LIV-1 type proteins varies in length. Few isoforms of other subfamilies may contain small ECDs but not as significant as those in LIV-1. Members of the LIV-1 subfamily have been reported to oligomerize through a proline-alanine-leucine motif (PAL motif) present in their ECD (Zhang, Sui, and Hu 2016). Additionally, this subgroup of proteins contains a unique metalloprotease motif HEXPHEXGD within TM5, with conserved proline and glutamic acid residues. It stands out that this subfamily is specific of eukaryotes, especially of mammals. Additionally, a subgroup appears to emerge from the LIV subfamily, referred to as KE4. This subclade shares the HEXPHEXGD motif, but lacks a conserved CPALLY motif present in human, mouse and monkey LIV-1 ZIPs at TM1, believed to be important for structural stabilization. Some members of the KE4 subgroup were found to be expressed in intracellular membranes, unlike LIV-1 members that have been found in plasma membrane (Lasswell et al. 2000; Taylor and Nicholson 2003).

Plant and fungal ZIPs fall mainly in subfamily I. Section 1.4 describes the IRT1 protein, a model ZIP of this subfamily. Subfamily II includes some mammalian members as well as insect and nematode isoforms. Studies in mice revealed that subfamily II genes were dispensable in zinc replete conditions but do have an important role in zinc deficiency conditions (Kambe et al. 2008).

The gufA subfamily was named after the gufA protein of *Myxococcus xanthus* of unknown function but predicted to be a metal ion transporter. Many bacterial ZIPs are found in this clade. The ZIP11 transporter, the only human member of this subfamily, was described mainly as a zinc transporter with significantly less histidine and cysteine residues as the other ZIPs (Yu et al. 2013). It is speculated that its transport mechanism may differ from the other ZIPs due to this particular characteristic.

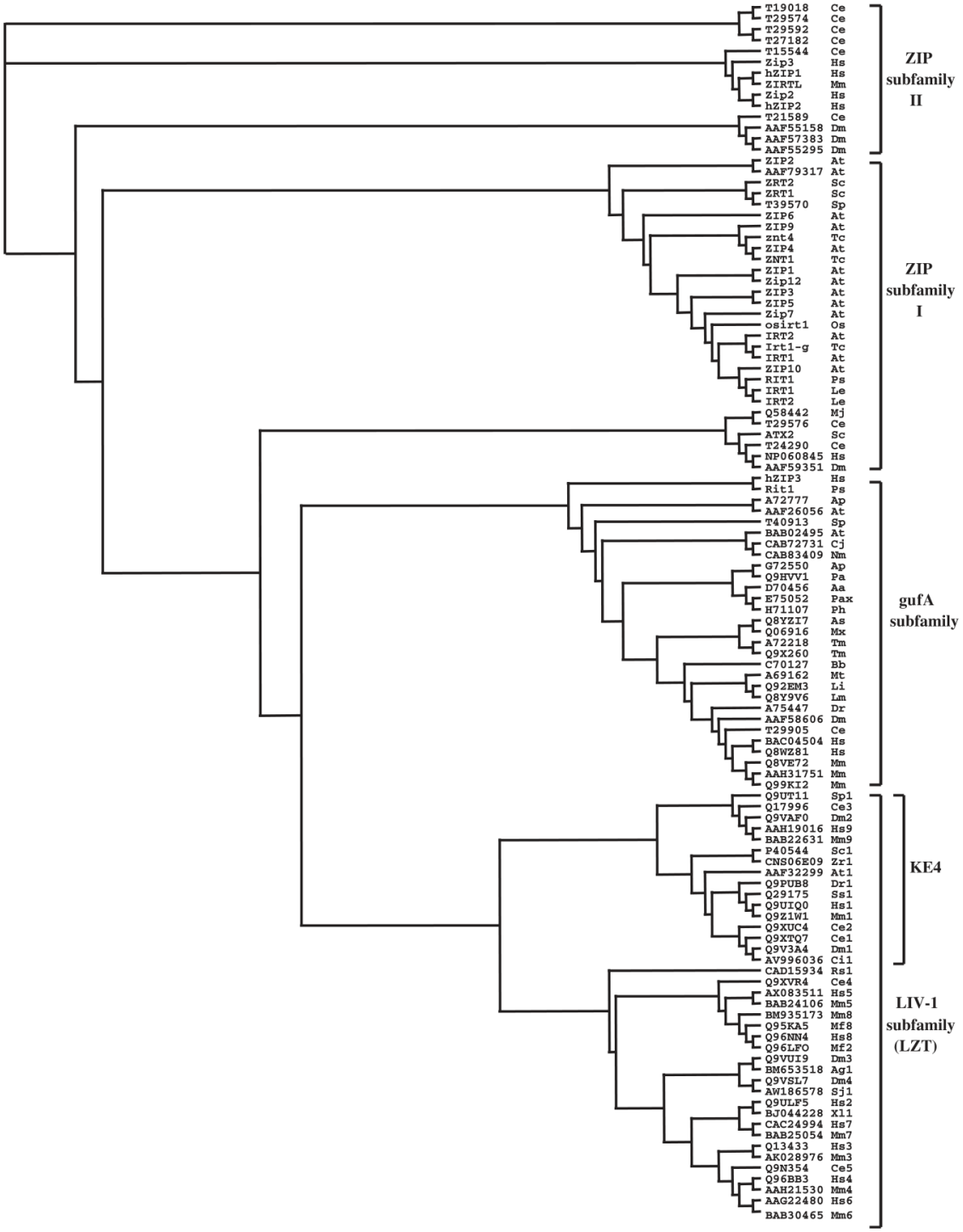

Figure 1-5 Phylogenetic tree of the ZIP family sequences (Adapted from Taylor et al. 2003). The association of different ZIP family sequences was determined using the Clustal V program to perform an alignment. The two-letter species abbreviations are Ag= Anopheles gambiae,Ap = Aeropyrum pernix, As = Anabaena sp., At = Arabidopsis thaliana,Bb = Borrelia burgdorferi,Br = Brachydanio rerio,Ce = Caenorhabditis elegans, Ci = Ciona intestinalis, Cj = Campylobacter jejuni,Dm= Drosophila melanogaster,Dr = Deinococcus radiodurans,Hs =Homo sapiens,Le = Lycopersicon esculentum,Li = Listeria innocua,Lm= Listeria monocytogenes,Mf= Macaca fascicularis,Mj = Methanococcus jannaschii,Mm= Mus musculus,Mx = Myxococcus xanthus, Nm= Neisseria meningitides,Os = Oryza sativa,Pa = Pseudomonas aeruginosa, Pax = Pyrococcus abyssi,Ph = Pyrococcus horikoshii,Ps = Pisum sativum, Rs = Ralstonia solanacearum,Sc = Saccharomyces cerevisae,Sj = Schistosoma japonicum,Sp = Schizosaccharomyces pombe,Ss = Sus scrofa,Tc = Thlaspi caerulescens,Tm= Thermotoga maritime,Xl = Xenopus laevii,Zr = Zygosaccharomyces rouxxii.

1.3.3 Topology and structure of ZIPs

Proteins from the ZIP family are predicted to share similar structural architectures, however, transmembrane topology prediction servers yield rather inconsistent results. The consensus is that most ZIPs are composed of eight TM spans, with fairly good agreement for the three first and three last TMs. For some ZIPs, algorithms predict TM4 and TM5 with significant less accuracy if not at all (Mathews et al. 2005). Both N and C termini are expected to face the extracellular space, with some exceptions where an additional TM/signal peptide on the N terminus is predicted. The presence of signal peptides has been analyzed for some plant members of this family. Work on *Malus xiaojinensis'* IRT1 stablished the presence of an uncleavable signal peptide that is needed for the correct targeting to the plasma membrane (Zhang et al. 2014). Prediction softwares indicate the presence of signal peptides for several other ZIPs as well (Alagarasan et al. 2017; Bin et al. 2011; Mathews et al. 2005). Furthermore, several studies have assessed the presence of highly conserved histidine residues within TM2, TM4 and TM5 that are suspected of being implicated in transport (Eide et al. 1996; Zhao and Eide 1996a; Grotz et al. 1998; Guerinot 2000; J. Wu et al. 2009; López-Millán, Ellis, and Grusak 2004; Moreau et al. 2002; Burleigh, Kristensen, and Bechmann 2003; S. Li et al. 2013).

Another interesting topological feature of ZIPs is the large cytosolic loop between TM3 and TM4. This loop is of variable lengths and amino acid composition across members of the family; however, a common shared characteristic is the high histidine content. In the loop, histidines are often arranged in motifs, sometimes spaced by other residues, like in the Arabidopsis IRT1, where four H are spaced by G (HGHGHGHG). This motifs tend to be positioned in the middle of the loop. Sequence analyzes of the human ZIP4 and related mammalian ZIPs revealed that the length of the histidine stretch is roughly proportional to the length of the loop (T. Zhang et al. 2019). For example, the loop of the human hZIP4 is 33 aminoacid long and has 4 histidines, whereas *Sarcophilus harrisi* and *Musca domestica* have 46 aminoacid long loops with 8 and 10 histidines respectively. Extensive research has established that this intracellular loop is important for regulation of ZIPs mediated by post-translational modifications upon direct metal binding (Dubeaux et al. 2018; R. Gitan et al. 2003). However, certain human isoforms lack this loop, such as ZIP11, ZIP12, and ZIP13 (Kambe et al. 2006).

To date, the structure of only one protein from the ZIP family has been published. The crystal structure of ZIPB from the prokaryote *Bordetella bronchiseptica* was reported by Zhang et al. in 2017. The crystal structure of ZIPB confirmed the predicted eight TMs and also revealed a series of metal binding sites. Crystals of ZIPB were described to nucleate only in presence of Cd^{2+}. The structure of the Cd-bound ZIPB presents four metal binding sites (M1-M4), two of which, M1 and M2, are inserted mid-way through the membrane area forming a binuclear metal center. Two motifs in TM4 and TM5, HNhPEG and QD/NhPEG respectively, were found to be responsible for Cd^{2+} binding in this intramembranous region. These motifs are highly conserved among bacterial ZIPs. M3 and M4 were found in the surface area exposed to the solvent. Cd^{2+} replacement by soaking crystals in $ZnCl_2$ revealed additional binding sites for Zn^{2+} in the cytosol exposed area. The internal site M1 was successfully

occupied by Zn^{2+}, while M2 failed in displacing the previously bound Cd^{2+} atom. This suggests that the first site has better accessibility and potentially blocks the second site. A putative transport pathway was described in detail thanks to directed mutagenesis and residue conservation analyses (Zhang et al. 2017). It was proposed that bound metal ions in M1 and M2 are released thanks to a series of H, D and E chelating residues located in the proximity of the exit cavity, with help from the large cytosolic loop between TM3 and TM4. It is expected that release by the chelating residues, elicits conformational changes that set an open conformation at the extracellular side of the cavity, where two D residues are thought to recruit substrate metals. This work sets a very important precedent for the study of the ZIP family. However, the low sequence identity among ZIPs from different organisms impedes the identification of equivalent residues. Further work on eukaryotic members of the family are crucial for the validation of common mechanical characteristics as well as specific ones.

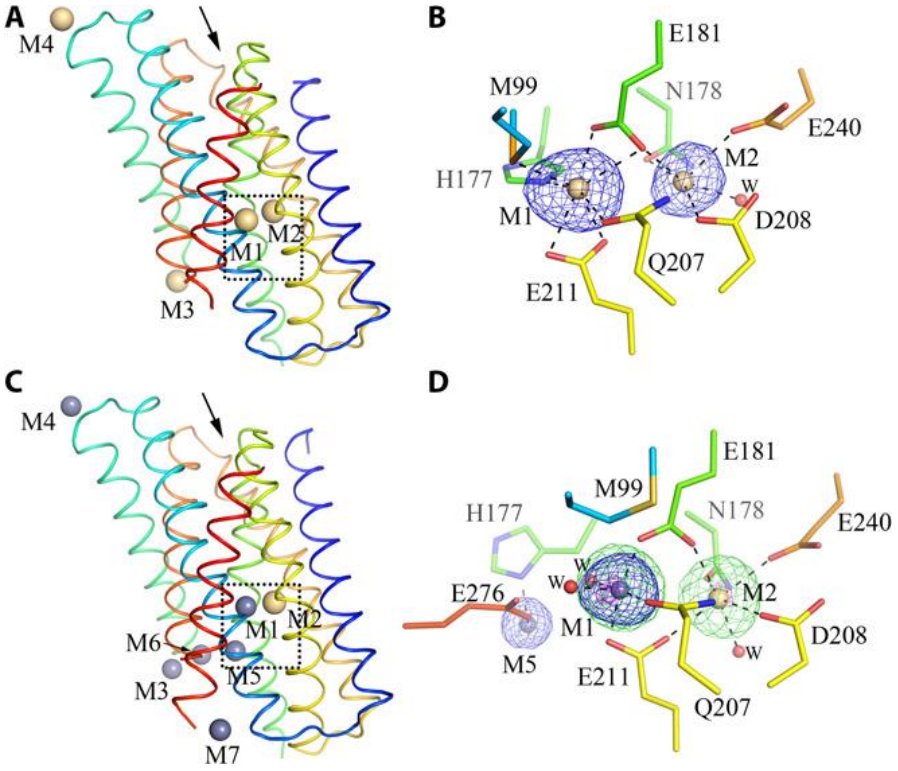

Figure 1-6 - Crystal structure of ZIPB in presence of Cd and Zn. (Adapted from Zhang et al. 2017). A. Crystal structure obtained in presence of Cd. Yellow spheres indicate Cd atoms in binding sites M1 to M4. B. Close up on the coordination of Cd atoms in sites M1 and M2. C. Crystal structure after soaking crystals in ZnCl2. Blue spheres illustrate Zn atoms, yellow indicates Cd. D. Close up on sites M1 and M2 showing the coordination of Zn in M1 and Cd in M2.

The oligomeric status of ZIPs was studied for some members of this family. The conserved proline-alanine-leucine motif was identified in the soluble domains of several members of the LIV-1 subfamily and proved important for dimerization (Zhang, Sui, and Hu 2016; Hu, Wille, and Schmitt-Ulms 2018; Bin, Seo, and Kim 2018). Biochemical data on the human hZIP13 suggested homodimerization in vitro (Bin et al. 2011). Similar results were also reported on the prokaryotic ZIPB, where the purified transporter was detected as two populations corresponding to a monomer and a homodimer (Lin et al.

2010; Zhang et al. 2017). The biological significance of dimerization of this ZIPs remains elusive. Also, whether oligomerization is conserved among subfamilies of ZIPs other than the LIV-1 subfamily and is not yet known due to the lack of biochemical information.

1.3.4 Regulation of ZIPs

In order to respond to nutrient demand ZIPs are transcriptionally and post translationally regulated by their metal substrates such as Zn, Fe, and other divalent metals. The nature of the transcription factors involved in such response varies according to the organism and metal considered. In the case of hZIP4, zinc finger transcription factor Krüppel-like factor 4 (KLF4) was pointed as responsible for its transcript accumulation during Zn deficiency (Liuzzi et al. 2009). Both, the high and low affinity Zn uptake transporter genes Zrt1 and Zrt2 from *Saccharomyces cerevisiae* are induced by direct binding of the zinc-responsive transcriptional activator (Zap1), also a zinc finger transcription factor, to zinc-responsive elements located within their promoters (Zhao et al. 1998). Plant ZIP transcriptional regulation depends vastly on the basic-region leucine zipper (bZIP), responsible for Zn dependent regulation of zinc ZIP transporters, and the bHLH family of transcription factors involved in regulation of Fe transporting ZIPs, such as IRT1 (see section 1.4.4.1) (Assunção et al. 2013; Gao et al. 2019).

At the protein level, eukaryotes use endocytosis to regulate the abundance and localization of ZIP metal transporters. ZIP transporters have been widely characterized to form part of this regulation strategy. In humans for example, hZIP4 is endocytosed during Zn replete conditions. hZIP4 is then recycled to the membrane surface, as long as the Zn concentration is maintained to a minimum micromolar level (Andrews 2008; Kim et al. 2004; Mao et al. 2007; Weaver et al. 2007). On the other hand, Zn excess targets endocytosed hZIP4 directly to degradation. Interestingly, this response is highly conserved in eukaryotes. The yeast ZRT1 transporter undergoes a similar regulation that involves endocytosis and degradation dependent on Zn availability (Gitan et al. 1998; Gitan and Eide 2000; Gitan et al. 2003). Also, the recently described post-translational regulation of Arabidopsis IRT1 follows the same path (Dubeaux et al. 2018), which is described in section 1.4.4.2.

Endocytosis of ZIPs is promoted by ubiquitination. This was first reported for the yeast ZRT1 zinc transporter, and later in mammalian and plant ZIPs (Gitan and Eide 2000; Barberon et al. 2011). Despite the variable nature of the large second intracellular loop of ZIPs, K residues on it are responsible for carrying such modifications. It is worth noticing that metal binding histidine rich motifs are present in this loop as well. The molecular mechanisms integrating metal binding and ubiquitination remain poorly understood. Recent work on the hZIP4, found an LQL motif positioned between the histidine-rich motif and the K residues receiving ubiquitination. This LQL motif, essential for endocytosis, was proposed to change its conformation from a non-functional form in Zn depleted conditions, into a recognizable form that would be detected by the endocytic machinery under normal Zn condition (Zhang et al. 2020). Due to the intrinsic variability of the histidine-rich loop, it is hard to determine whether such a mechanism is true for other ZIPs. The detailed mechanisms of metal binding by IRT1 and coupling with ubiquitination and endocytosis will be described hereafter.

1.3.5 ZIPs in *Arabidopsis thaliana*

In *Arabidopsis thaliana* 15 members of the ZIP family have been identified in the genome. Substrate specificity was studied for several members of this family through yeast complementation assays. As detailed in Table 1, it was shown that ZIP1, ZIP2, ZIP3, ZIP4, ZIP7, ZIP10, ZIP11, ZIP12, IRT1, IRT2 and IRT3 complement the yeast Δ*zrt1*Δ*zrt2* mutant defective for Zn transport; ZIP1, ZIP2, ZIP5, ZIP6, ZIP7, ZIP9 and IRT1 rescue the Δ*smf1* Mn deficient yeast phenotype and IRT1, IRT2, IRT3 and ZIP7 confer Fe transport to *Δfet3Δfet4* yeast mutants (Milner et al. 2013; Lin et al. 2009; Grotz et al. 1998; Vert, Briat, and Curie 2001; Korshunova et al. 1999).

Considering the broad spectrum for transported metals, the actual biological function of ZIPs is therefore dictated by the nature of metals regulating their expression. Among ZIPs, 13 are thought to be involved in the Zn uptake and homeostasis machinery (ZIP1-12 and IRT3), whereas the remaining two are mostly related to Fe transport (IRT1 and IRT2). *ZIP1-12* and *IRT3* are indeed all transcriptionally responsive to Zn deficiency, except for *ZIP6* and *ZIP11* (Grotz et al. 1998; Milner et al. 2013; Assunção, Schat, and Aarts 2010; Jain et al. 2013; Lin et al. 2009). *IRT1* and *IRT2* transcription, on the other hand, responds to Fe limitation suggesting that their biological function is to transport Fe (Vert, Briat, and Curie 2001; Vert et al. 2002) . Their relative expression was also assessed, demonstrating that *ZIP1*, *ZIP2*, *ZIP3*, *ZIP5*, and *ZIP6* are expressed predominantly in roots; *ZIP7* and, to a lesser extent, *ZIP11*, are expressed mostly in shoots, and *ZIP9*, *ZIP10*, and *ZIP12* present a similar expression pattern in root and shoot (Milner et al. 2013). Also, it's been pointed that *ZIP8* may actually be a pseudogene because of its inability for being isolated as predicted in the TAIR database, for being the only ZIP that does not complement yeast mutants in metal uptake and for its poor evidence of expression (Milner et al. 2013). *IRT1*, *IRT2* and *IRT3* are mostly expressed in roots, and the corresponding IRT1 and IRT3 proteins found at the plasma membrane and IRT2 in vesicular compartments as seen by confocal microscopy of GFP fusions in transfected Arabidopsis protoplasts (Vert, Briat, and Curie 2001; Vert et al. 2009; 2002; Lin et al. 2009).

Further characterization was achieved for certain members of this family, with IRT1 being the most studied one (see section 1.4). ZIP1 protein was found at the tonoplast of cells from the root stele and in the shoot, mobilizing Zn from the vacuole, whereas ZIP2 is located at the plasma membrane of root stele cells, loading Zn in the xylem parenchyma (Milner et al. 2013). ZIP4 is expected to mediate Zn transport in chloroplast, given that it possess a potential chloroplast targeting sequence (Grotz et al. 1998). Considering the expression profile and subcellular localization of IRT3, it has been proposed to function as a Zn and low-affinity Fe primary uptake transporter (Lin et al. 2009). Interestingly, IRT3 is phylogenetically closer to ZIP4 than to the other IRTs (Grotz et al. 1998).

Table 1 Yeast mutants complemented by different Arabidopsis thaliana ZIPs. Yeast mutants Δzrt1Δzrt2 are deficient for Zn uptake, Δsmf1 are deficient for Mn uptake and Δfet3Δfet4 are impaired in Fe uptake.

	Yeast mutants complemented
ZIP1	*Δzrt1Δzrt2* *Δsmf1*
ZIP2	*Δzrt1Δzrt2* *Δsmf1*
ZIP3	*Δzrt1Δzrt2*
ZIP4	*Δzrt1Δzrt2*
ZIP5	*Δsmf1*
ZIP6	*Δsmf1*
ZIP7	*Δzrt1Δzrt2* *Δsmf1* *Δfet3Δfet4*
ZIP9	*Δsmf1*
ZIP10	*Δzrt1Δzrt2*
ZIP11	*Δzrt1Δzrt2*
ZIP12	*Δzrt1Δzrt2*
IRT1	*Δzrt1Δzrt2* *Δsmf1* *Δfet3Δfet4*
IRT2	*Δzrt1Δzrt2* *Δfet3Δfet4*
IRT3	*Δzrt1Δzrt2* *Δfet3Δfet4*

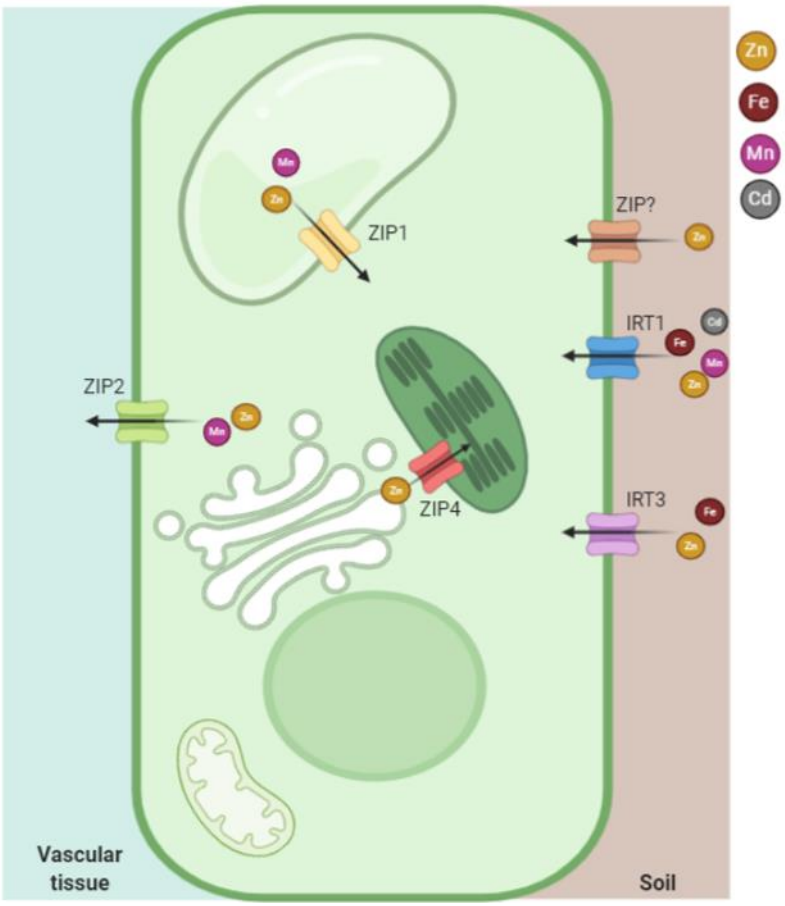

Figure 1-7 ZIP transporters in Arabidopsis thaliana. The current model of Arabidopsis ZIPs locates IRT1 at the plasma membrane, where it constitutes the main entry point of Fe to the cell from the soil. Other metals, such as Zn, Mn and the toxic metal Cd are also internalized by IRT1. IRT3 is also expressed at the plasma membrane and expected to translocate primarily Zn, but also Fe. ZIP1 is located at the vacuole and is expected to mediate transport of Zn and Mn into the cytoplasm. On the other hand, ZIP2 expressed in the stele, is implicated on xylem loading of Zn and Mn. ZIP4 is predicted to mediate Zn transport to chloroplasts. To this day, no specific member of the ZIP family was experimentally proven to be involved in primary uptake of Zn from the rhizosphere, although many members of the family are suspected to take action in such process. Created with BioRender.com

1.4 IRT1: a key protein in metal nutrition

1.4.1 Identification of IRT1

Over the past decades, Fe nutrition in plants has been a widely investigated topic slowly shifting from physiological to molecular studies in the past 25 years. *Arabidopsis thaliana*, being the model dicotyledonous plant of choice, was the first organism in which Fe transporters from the ZIP family were identified. IRT1 was cloned by functional complementation of a yeast a *Saccharomyces cerevisiae* mutant strain deleted for the main low and high affinity genes involved in Fe acquisition (Eide et al. 1996). Such strain consequently fails to grow on iron poor media. Through transformation of *fet3fet4* with an *Arabidopsis thaliana* cDNA library, several clones corresponding to a gene named Iron Regulated Transporter 1 (IRT1) were isolated (Eide et al. 1996). Following studies found similar proteins in a diversity of organisms, such as the Zrt transporter in yeast (Zhao and Eide 1996a). This led to the classification of this proteins into the family described above: Zrt/Irt like Proteins (ZIP) (Guerinot 2000; Grotz et al. 1998).

IRT1 mRNA were early shown to accumulate specifically in roots of iron-deficient Arabidopsis plants suggesting a role in iron absorption from the soil (Eide et al., 1996). Further work indeed demonstrated that IRT1 is the main Fe transporter responsible for iron uptake in Arabidopsis. Knock-out mutations of this gene leads to chlorosis and severe impediments in plant growth, both clear signs of drastic Fe deficiency (Vert et al. 2002; Henriques et al. 2002; Varotto et al. 2002). This effect can only be reverted by the addition of abnormally high amounts of Fe during watering. The use of the GUS reporter allowed the visualization of IRT1 promoter activity in root epidermal cells and confirmed its strong transcriptional regulation by low Fe. Furthermore, an IRT1-GFP fusion protein was found at the plasma membrane when transiently expressed in protoplasts (Vert et al. 2002). Altogether, these evidence support a role for IRT1 as the main Fe transporter involved in direct uptake from the soil.

1.4.2 Substrate specificity of IRT1

As already discussed in sections above, IRT1 was found responsible for internalization of divalent metals other than Fe. Metal transport competition studies coupled to complementation of yeast mutants affected in various metal transporter indeed revealed the ability of IRT1 to transport several metals including Fe, Mn, Zn, Co and Cd (Eide et al. 1996; Korshunova et al. 1999; Vert et al. 2002). Through characterization of Fe^{2+} uptake in the *fet3fet4* yeast mutant an apparent Km of 6 ± 1 μM was measured. Inhibition assays on this mutant revealed that Co, Mn, and Zn inhibited Fe uptake when supplied at 100-fold excess, suggesting a greater affinity for Fe but still potential transport of other metals (Eide et al. 1996). Further investigations, demonstrated that IRT1 is able to complement the yeast *smf1* mutant deficient for Mn uptake. Kinetic assays showed an apparent Km of 9 ± 1 μM, suggesting that Mn is transported in a similar concentration dependent manner as Fe (Korshunova et al. 1999). Additionally, IRT1 complementation was tested in *ctr1* and *zrt1zrt2* mutants defective in Cu and Zn transport, respectively. Cupper deficient strain *ctr1* was unable to grow when overexpressing IRT1, unlike the

zrt1zrt2 mutant that was correctly complemented. The reported apparent Km for Zn transport was of 2.8 ± 0.6 μM (Korshunova et al. 1999). Moreover, the fact that only Fe limitation induces *IRT1* expression, together with the observation that only Fe can complement the chlorosis of *irt1* mutant (Vert et al. 2002) indicated that Fe is the primary substrate of IRT1. From then on, its other substrates were considered as secondary metal substrates being specifically transported by IRT1 (Korshunova et al. 1999; Vert et al. 2002).

Site directed mutagenesis of conserved residues predicted to be involved in metal binding, together with a yeast based uptake essay, showed the importance of certain residues in the specificity of IRT1 for different substrates (Rogers, Eide, and Guerinot 2000). Mutation of Glutamic acid 103 (D103) located at the extracellular loop between TM2 and TM3 to alanine (A) eliminates Zn transport. Fe, Mn and Cd transport however remains unaffected by such mutation. Another mutation in an extracellular loop, on aspartic acid 100 (E100), only eliminated Fe and Mn transport, suggesting that Fe and Mn uptake are mechanistically related. Interestingly, a double mutant, carrying both D103 and E100 substitutions to A, presented Zn transport and was more sensitive to Cd than the independent mutants. This extracellular loop was proposed to be the responsible one for recruiting metal ions before transport. Structural evidence on the Bordetella ZIPB revealed that Cd^{2+} and Zn^{2+} ions were able to bind on this region, contributing further to this hypothesis (Zhang et al. 2017). Another D mutation, this time at the end of TM3 exposed to the cytosol, D136A eliminated Mn and Fe like the D103A mutation, and also to a certain extent Cd uptake. A serine (S) residue located midway through the membranous fraction in TM4 eliminates all transport functions, suggesting that it is of high importance for transport of all the substrates. Additionally, mutations on highly conserved histidine (H) and E residues H96, H197 and H224 together with E228 were detrimental for all transport activity. This showed that IRT1 selectivity can be engineered to transport specific substrate. However, to this date, mechanistic information about the transport of each individual substrate is missing.

1.4.3 Topological aspects of IRT1

The structural and topological aspects regarding IRT1 are still elusive. *Eide et al. 1996* reported on the predicted topology of IRT1 as being composed of eight transmembrane spans (TM), with both N and C termini on the extracellular space. It was noticed later on, that the version of IRT1 used in this study lacked nine amino acids at the N-terminus, which are predicted as part of a signal peptide (Barberon et al. 2011; Zhang et al. 2014). Although significant experimental evidence of a functional signal peptide is still missing, tandem mass spectrometry performed on microsomes isolated from Fe-deficient roots revealed the presence of N-terminal peptides corresponding to IRT1 pointing to the lack of processing for such signal peptide (G. Vert, personal communications). This observation changes the topology model creating a 9th TM, unless the signal peptide is cleaved, and so the N-terminus would be found on the cytosolic compartment whereas the C-terminus on the extracellular side. The plant MxIRT1, discussed in sections above, is the only member of the ZIPs so far to have been experimentally determined to have a signal peptide. The lack of this portion prevents the correct localization of the

protein. Mature MxIRT1 was demonstrated to still have the signal peptide attached (Zhang et al. 2014). Whether this is true for *Arabidopsis thaliana* IRT1 is yet to be determined.

1.4.4 Regulation of *IRT1*

Since the metal concentration range at which plants can properly grow and develop is very limited, a tight regulation of the uptake machineries is crucial to provide enough metals for metabolism and cell structures while preventing deleterious metal overload. Regulation of metal transporters levels in different compartments or tissues together with the expression of intracellular storage/detoxification molecules and proteins are the mechanisms that plants have to tame this effect. For the purpose of this thesis, only the regulation of the Arabidopsis Fe uptake machinery will be discussed in detail in following sections.

1.4.4.1 Transcriptional regulation of *IRT1* expression

Nutrient transport regulation is crucial for finding the right balance between availability and cell requirements without surpassing nutrient toxicity thresholds. To maintain metal homeostasis despite varying concentration of available metals, IRT1 is regulated at different levels. The first point of regulation happens at the transcriptional level of the *IRT1* gene, which is induced by Fe deficiency (Eide et al. 1996; Vert et al. 2002). Several basic Helix-Loop-Helix (bHLH) transcription factors were found responsible for the upregulation of IRT1. Of these, Fer-like Iron Deficiency Induced Transcription Factor 1 (FIT) was pointed as the central actor on the Fe deficiency response, provided that *fit* mutants are chlorotic and die as seedlings in Fe deficiency conditions (Colangelo and Guerinot 2004). FIT function requires heterodimerization with other transcription factors from the Ib subgroup of bHLHs, such as bHLH38, bHLH39, bHLH100, and bHLH101. The formation of heterodimers allows FIT to bind to the *IRT1* promoter as well as to other Fe dependent promoters (Colangelo and Guerinot 2004; Yuan et al. 2008; Sivitz et al. 2012; Selote et al. 2015; Zhang et al. 2015; Li et al. 2016; Liang et al. 2017). Mutants overexpressing *FIT* together with *bHLH38* and *bHLH39* turn IRT1 expression into constitutive expression, whereas single overexpression mutations of one of these genes maintains the responsiveness to Fe deficiency (Yuan et al. 2008). To this date, 448 genes have been shown to be regulated by FIT (Mai, Pateyron, and Bauer 2016). In the same manner, *FIT* expression also responds to Fe starvation, although only mildly, and just like IRT1, it is expressed in the outer cell layer of the root (Jakoby et al. 2004; H. Y. Wang et al. 2007).

Upstream from FIT and Ib bHLH transcription factors, positive regulators from the IVc subgroup of bHLHs (bHLH34, bHLH104, bHLH105 and bHLH115) and the IVb member bHLH121 also named UPSTREAM REGULATOR OF IRT1 (URI) act in response to low iron (Zhang et al. 2015; Li et al. 2016; Liang et al. 2017; Kim et al. 2019; Tissot et al. 2019; Gao et al. 2020). A phosphorylated pool of URI protein accumulates at the root periphery during Fe deficiency conditions. Phosphorylated URI heterodimerizes with subgroup IVc bHLH transcription factors that in turn promote binding of the heterodimers to the promoters of subgroup Ib bHLHs (the aforementioned *bHLH38, bHLH39,*

bHLH100, and *bHLH101*) and of *POPEYE* (*PYE*), *BRUTUS* (*BTS*), and *BRUTUS LIKE 1* (*BTSL1*), besides binding and inducing other Fe-deficiency responsive promoters (Kim et al. 2019; Gao et al. 2020). In accordance with its function, an *uri* mutant lacks the Fe-deficiency response, is highly chlorotic and seedling-lethal in soil, but its phenotype is reversed by supplementation with Fe. Unlike the Ib bHLH transcription factors which enhance the expression of Fe responsive genes like *FIT*, PYE negatively regulates genes involved in Fe mobilization independently from *FIT* (Colangelo and Guerinot 2004; Jakoby et al. 2004; Yuan et al. 2008; Long et al. 2010). The *pye-1* mutant presents strong leaf chlorosis and impaired growth. Also, the FRO3 reductase and the NAS4 nicotianamine synthase are more upregulated in said mutant than in the wild-type in Fe deficiency conditions, indicating the negative regulatory effect of PYE. Additionally, the E3 ubiquitin ligases BTS and BTSL1, are also negative regulators of the Fe deficiency response. They do so by intervening in the proteasome mediated degradation of URI in Fe sufficiency in the case of BTS, and in the destabilization of the FIT protein by BTSL1 together with BTSL2 in a similar manner to URI-BTS (Kim et al. 2019; Rodríguez-Celma et al. 2019). Notably, BTS has been demonstrated to present several types of metal binding domains and to directly bind Fe as well as Zn, possibly through its hemerythrin domain, and therefore inducing its ligase activity (Kobayashi et al. 2013; Selote et al. 2015). Both the *bts* mutant and the *btsls* double mutant fail to down-regulate the Fe deficiency responsive genes, are more tolerant to Fe deficiency but also more prone to accumulate toxic levels of Fe in roots and leaves under Fe sufficiency compared with wild- type plants (Selote et al. 2015; Kim et al. 2019; Rodríguez-Celma et al. 2019). Opposed to the destabilization by BTSL1, FIT activity is positively regulated by phosphorylation by the Fe-deficiency-induced CALCINEURIN B-LIKE- INTERACTING PROTEIN KINASE-11 (CIPK11) (Gratz et al. 2019).

The regulation of the *IRT1* transporter gene expression by Fe limitation integrates both external soil availability signals and the shoot metal content, as shown by split root experiments together with time course expression pattern assessment (Vert, Briat, and Curie 2003). While the Fe deficiency signaling cascade presented above certainly drives *IRT1* expression locally in root epidermis, the nature of long-distance signals and how both are integrated is still unknown.

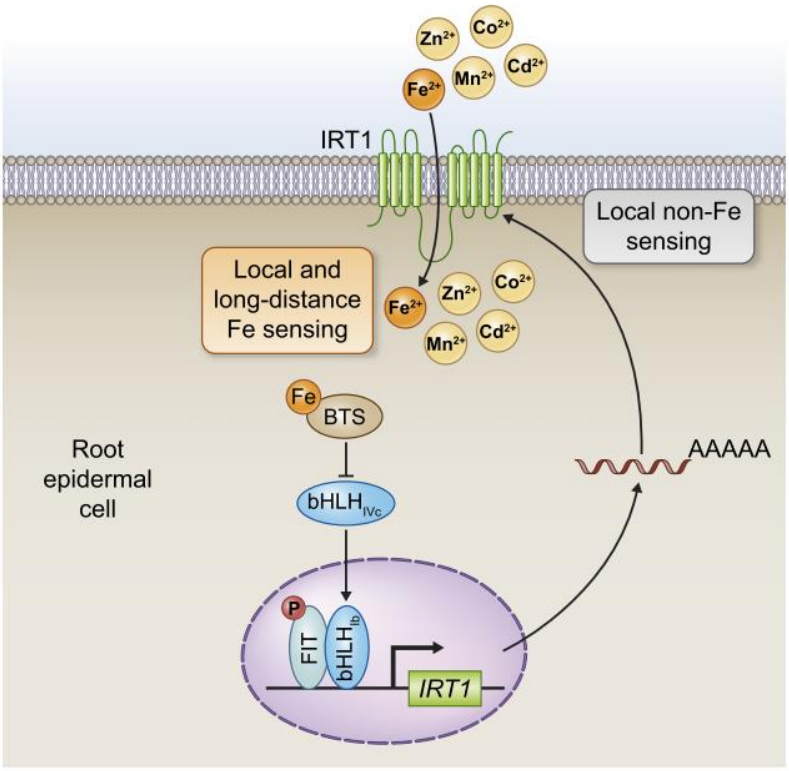

Figure 1-8 - Metal sensing and signaling in the root epidermis. (Adapted from Cointry and Vert, 2019). When plants are in demand for Fe, the IRT1 gene is transcriptionally upregulated in the root epidermis in response to local and long-distance signals underlying Fe availability and the shoot Fe status, respectively. How these signals are integrated is currently unknown. Downstream of BRUTUS (BTS) are found group IVc bHLH transcription factors (bHLH34, 105, 105, 115) that are positive regulators of Fe - deficiency responses. bHLHIVc bind to the promoters of bHLHIb (bHLH38, 39, 100, 101) transcription factors to activate their transcription in Fe-starved plants. bHLHIb heterodimerize with the FIT bHLH transcription factor and bind to IRT1 promoter, therefore driving IRT1 gene expression in Fe -deficient conditions. FIT activity is positively regulated by CALCINEURIN B-LIKE- INTERACTING PROTEIN KINASE-11 (CIPK11)-dependent phosphorylation, represented by a phosphate group attached to FIT. Non- iron metals (Zn, Mn, Co) transported by IRT1 due to their similarity with Fe, are directly sensed by IRT1 in root epidermal cells through a stretch of histidine residues in a cytosolic loop to negatively regulate IRT1.

1.4.4.2 Regulation of IRT1: The regulatory loop as a target for post-translational modifications

In addition to the transcriptional regulation by low Fe, IRT1 protein levels are also regulated for protection in stress conditions. Similar to some ZIPs from other organisms, IRT1 was suspected of being regulated by post-transcriptional modifications. Notably, the mutation of two K residues in the large cytosolic loop in a comparable manner to what has been shown to the yeast Zrt1 zinc transporter, increases IRT1 protein levels. It was therefore suggested that IRT1 undergoes ubiquitin-mediated degradation although no evidence of degradation and ubiquitination was provided.

Previous work from our lab clarified this point and shed light on the complex regulation of IRT1 protein ubiquitination and degradation by non-Fe metal substrates. As already mentioned in sections above, the second intracellular loop of IRT1, located between TM4 and TM5 (that is, if we consider the putative signal peptide to be TM1), presents interesting features. Lysine (K) residues K154 and K179 on this loop are subject to events of ubiquitination. Plants carrying a mutant version of IRT1 in both these

K residues are highly sensitive to Fe. Immunolocalization of the WT and mutant protein together with immunoblotting analyzes revealed that monoubiquitination labeling of this K residues of the loop triggers endocytosis of IRT1 from the PM into early endosomes (EE), and thus the K mutant version of IRT1, incapable of being ubiquitinated, is retained at the PM contributing to toxicity (Barberon et al. 2011). The pool of IRT1 at the EE can be either recycled back into the PM or further modified and targeted to degradation in response to varied external metal availability, as shown by confocal microscopy localization studies using an IRT1 fusion protein to the YFP derivate fluorescent protein mCitrine. The fluorescent mCitrine protein was located after residue 42 of IRT1, between TM1 and TM2, and renders a functional protein that is able to complement the *irt1-1* knock out line (Dubeaux et al. 2018). IRT1 targeting for degradation is driven by the extension of the monoubiquitin labels into larger K63-linked ubiquitin chains, which consist of ubiquitin moieties sequentially bound to the K63 residue of the previous Ubiquitin molecule. This was revealed by immunoblotting of immunopurified IRT1 with Apu3 antibodies, raised to specifically detect K63 linked ubiquitin (Newton et al. 2008; Dubeaux et al. 2018). This type of polyubiquitination was only detected after exposing the plants to an excess of the secondary substrates and it was then proven to target IRT1 to the vacuole for degradation, as seen by confocal microscopy after growing plants in the dark and thus avoiding lytic vacuole activity. The E3 RING ubiquitin ligase Irt1 Degradation Factor 1 (IDF1) was identified as the E3 ligase responsible for the extension of the chains (Shin et al. 2013; Dubeaux et al. 2018). A specific E2 conjugating enzyme involved in IRT1 tagging has not yet been established. The E2 UB-CONJUGATING ENZYMES-35/36 (UBC35/36), responsible for most of the K63 polyUb chain formation in Arabidopsis (Li and Schmidt 2010; Romero-Barrios et al. 2020), is however suspected to take action in this process.

Oftentimes, phosphorylation is needed in advanced to ubiquitination. That is so that the E3 ligases can dock into its substrate better. This is the case for IRT1. Prior to ubiquitination, the action of the CIPK23 kinase is needed. Residues in the proximity of the K residues mentioned above are subject to this kinase, although they have not been identified until this date. Interestingly, action of CIPK23 on IRT1 requires direct non-iron metal binding on a particular PHGHGHGHGP motif in this loop. It is speculated that binding of metals might stimulate structuration on this large loop that allows CIPK23 to act on it. Another hypothesis is that the metals act as the binding mediator between this two proteins.

Addition of K63 polyUbiquitin chains onto IRT1 facilitates the recognition by the Endosomal Sorting Complex Required for Transport (ESCRT) which prompts mobilization of the protein into the vacuole (Dubeaux & Vert, 2017). An ESCRT-associated factor called FAB1, YOTB, VAC1, EEA1-1 (FYVE1) has been shown to interact with both IRT1 and Ubiquitin to elicit proper intracellular sorting of endocytosed IRT1 (Barberon et al. 2014; Gao et al. 2014). The recycling of IRT1 back into the plasma

membrane, is controlled by Sorting Nexin-1 (SNX1), also an endosomal located protein (Ivanov et al. 2014).

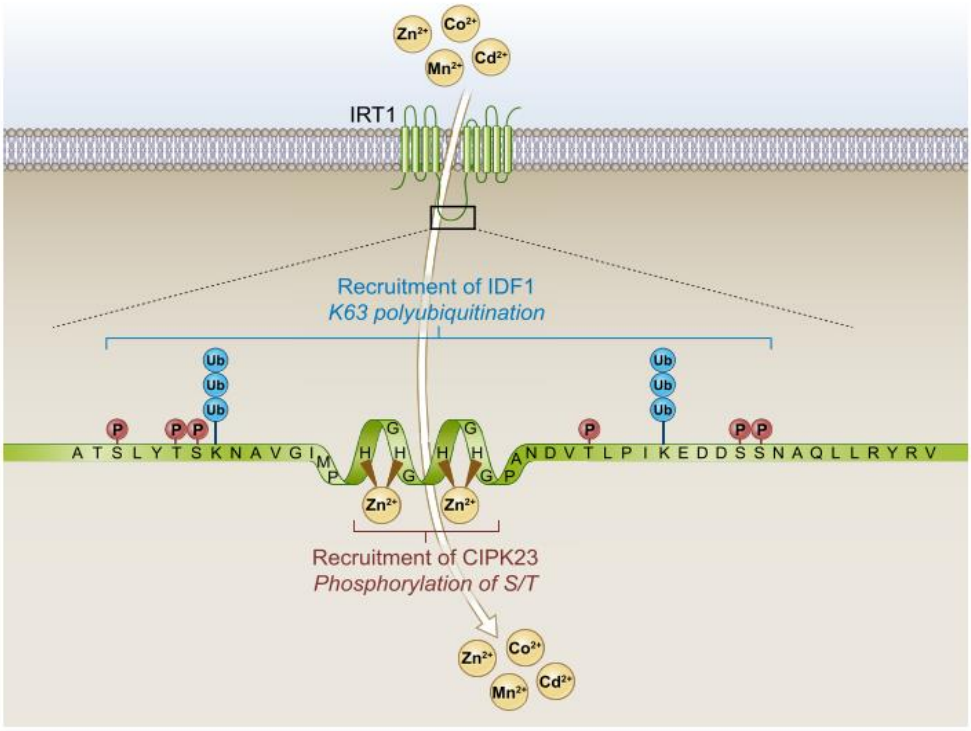

Figure 1-9 - Molecular basis of IRON-REGULATED TRANSPORTER-1 (IRT1) transceptor function. (Adapted from Cointry and Vert, 2019). When plants express high levels of IRT1 in a soil that contains non-iron metals, the flux of the latter is directly sensed by a histidine-rich stretch in IRT1 sitting in an unstructured cytosolic loop at the exit of IRT1 permeation domain. Metal-bound IRT1 recruits the CIPK23 kinase, which in turn phosphorylates serine and threonine residues in the vicinity of the histidine-rich motif. Phosphorylated IRT1 has the ability to interact with the E3 ubiquitin ligase IRONDEFICIENCY FACTOR-1 (IDF1) to promote lysine (K)-63 polyubiquitin-mediated endocytosis and degradation of IRT1.

2 Context and objectives

Deep understanding of biological systems requires multidisciplinarity. Comprehension of the bases of iron uptake by plants is no exception. It is critical to decipher the mechanistic intricacies through which transporters achieve their functions. Research on a wealth of metal transporters reviewed in the previous sections demonstrate the importance of structural and biochemical information in this matter. Despite the fairly known physiological and regulatory mechanisms of IRT1, this protein, as the whole ZIP family of transporters, suffers a tremendous gap in such research. Furthermore, there are great incongruences in the literature regarding the transport mechanisms of ZIPs. It is for that reason that the objectives of this thesis were to navigate these topics. Furthermore, in recent years our lab sat ground in the world of post-translational regulation of membrane transporters by describing the mechanisms of regulation of IRT1 involving phosphorylation by the CIPK23 kinase and subsequent K63 polyubiquitination by the IDF1 E3 ligase. However the molecular basis of the interaction of the regulatory loop of IRT1 with metals and the interacting proteins CIPK23 and IDF1 remain elusive. Therefore, during my thesis I aimed to: a) Develop biochemical tools necessary for the exploration of mechanistic and structural characterization of IRT1 and b) study the molecular basis of the metal-binding event that triggers the regulatory cascade of IRT1.

Our interest in developing biochemical tools for the characterization of IRT1 led us to setting a collaboration with the laboratory of Guillaume Lenoir at the I2BC institute at CEA Saclay. Also, with the aim of achieving the 3D structure of IRT1 we set a collaboration with the laboratory of Hugues Nury and Eva Pebay-Peyroula at IBS, Grenoble. Finally, for studying the structural properties of the IRT1 loop involved in post-translational regulation of the protein by NMR we collaborated with Nelly Morellet at ICSN, Gif sur Yvette, which lead to the preparation of a paper manuscript of which I am first author and will be presented in the second part of the result section. This manuscript will be submitted for publication when ongoing experiments are finished.

3 Results

3.1 Development of tools for the biochemical and structural characterization of IRT1

3.1.1 Expression, solubilization and purification of IRT1

3.1.1.1 Design of functional fusion proteins

Previous work in the team using expression of IRT1 with various affinity tags in Escherichia coli revealed that IRT1 could not be easily purified from bacteria (Licence Pro report of Victor Folcher, supervised by Julie Neveu). Besides, no information about the functionality of IRT1 fusions could be obtained, questioning the relevance of such expression system to express and purify IRT1. I therefore turned to yeast as an expression system to evaluate its suitability to purify significant amounts of functional IRT1 fusions for its biochemical characterization. In collaboration with the team of Guillaume Lenoir at I2BC Paris-Saclay, I designed, cloned and screened for a functional IRT1 fusion protein with an affinity tag in yeast. Our aim was to find a fusion protein that is not only functional for metal transport, but that also has significant expression and that is able to be solubilized by a mild detergent to preserve its functionality and structural properties. To achieve our goals, I used two different tags, the mCitrine fluorescent tag and the Biotin Acceptor Domain (BAD), fused at different position in the IRT1 WT protein (Figure 3-1). Also, we included a Tobacco Etch Virus (TEV) protease cleavage site between IRT1 and the BAD tag for further processing. Taking into account that a fusion IRT1mCitrine protein, where the fluorescent mCitrine tag is located on the first extracellular loop, is able to complement irt1-1 knockout mutant plants and fet3fet4 yeast mutants (Dubeaux et al. 2018), we decided to maintain the tag on this position. We also speculated that the presence of mCitrine may help

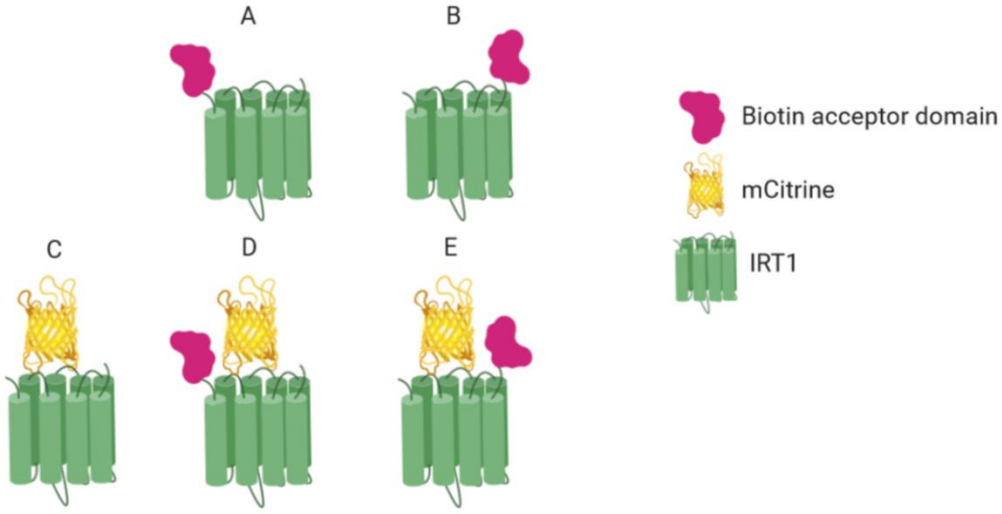

Figure 3-1 Design of protein fusions for purification. Different combinations of the IRT1 protein, the mCitrine fluorescent tag and the biotin acceptor domain tag were cloned into pYEDP60 expression vector in different arrangements. A) Bad-IRT1 B) IRT1-Bad C) IRT1mCitrine D) Bad-IRT1mCitrine E) IRT1mCitrine-Bad.

solubilize the otherwise rather hydrophobic IRT1 protein. The designed fusions were cloned in the PYEDP60 expression vector under control of a galactose inducible promoter and tested for functionality by expression in the W303.1B Δpep4 yeast strain that has been previously used for membrane protein production and purification (Azouaoui et al. 2016). Such strain is deleted for the major vacuolar protease, Proteinase A, which enhances heterologous protein production by preventing degradation of overexpressed proteins.

To assess the functionality of IRT1 fusions, we took advantage of the ability of IRT1 to transport the highly toxic cadmium ions. This was previously shown to yield reduced growth of wild-type yeast strains (Rogers, Eide, and Guerinot 2000; Vert, Briat, and Curie 2001). The W303.1B Δpep4 yeast strain was therefore transformed with the vectors carrying the corresponding IRT1 fusions (*Figure 3-1*). The expression of IRT1 fusions was induced with galactose, and yeast growth assayed by drop test on media containing different concentrations of $CdCl_2$. Yeast carrying the empty vector and the untagged IRT1 protein were used as negative and positive controls, respectively. Such experiment demonstrated that two of the four fusions tested were functional for Cd transport, as visualized by the lack of growth on 5μM $CdCl_2$-containing plates (*Figure 3-2*). Tagging with Bad tag at the N-terminus of IRT1 rendered the proteins non-functional, whereas tagging at the C-terminus maintained transport abilities regardless of the presence of mCitrine. Interestingly, mCitrine enhanced the sensitivity of the yeast to $CdCl_2$, potentially due to a difference of protein levels. It would be interesting to confirm this by performing a western blot using anti-IRT1 antibodies and quantitative RT-PCR to evaluate the influence of mCitrine on IRT1 stability.

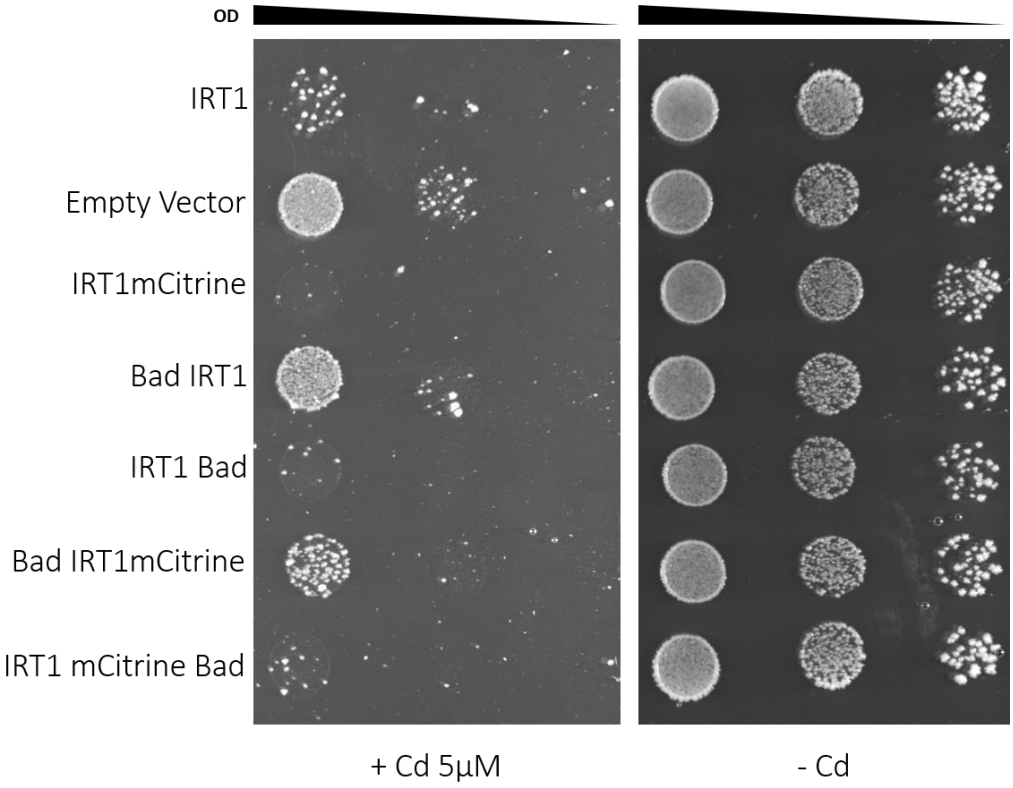

Figure 3-2 Functionality of IRT1 fusions expressed in yeast. W303.1B Δpep4 yeast were transformed with PYEDP60 vectors carrying IRT1 fusion proteins under the control of a galactose inducible promoter. Empty vector transformed yeast were used as negative control and yeast expressing untagged IRT1 as positive control. Yeast were grown in minimal selective media and spotted on plates containing various concentrations of CdCl2. Growth was monitored after 4 days at 28°C.

3.1.1.2 Expression test and solubilization optimization

After having determined what fusions are functional, we next sought to analyze the expression levels of the corresponding fusions expressed in yeast liquid cultures. Overnight yeast cultures in selective media carrying vectors to express the two C-terminal tagged fusions as well as the IRT1mCitrine protein were inoculated and further grown in rich media for 36 hours. Galactose in powder was added to a final concentration of 2 % for induction during 13 hours until cells were harvested and processed for fractionation. We analyzed two different membranous fractions obtained by differential ultracentrifugation, as previously done for other membrane proteins (Azouaoui et al. 2016). Heavy membranes, here called "P2", in reference to being the second pellet obtained after a series of centrifugations, are recovered at 20 000 g and correspond to bigger portions of fractionated membranes. On the other hand, light membranes, from now called "P3", are recovered after a step of ultracentrifugation at 100 000 g. Analyses of the two different membranous fractions demonstrated that all three fusions were recovered in both fractions in comparable amounts (*Figure 3-3*A). Also, the two

proteins containing the mCitrine fluorescent tag were expressed in higher amounts compared to the IRT1Bad fusion.

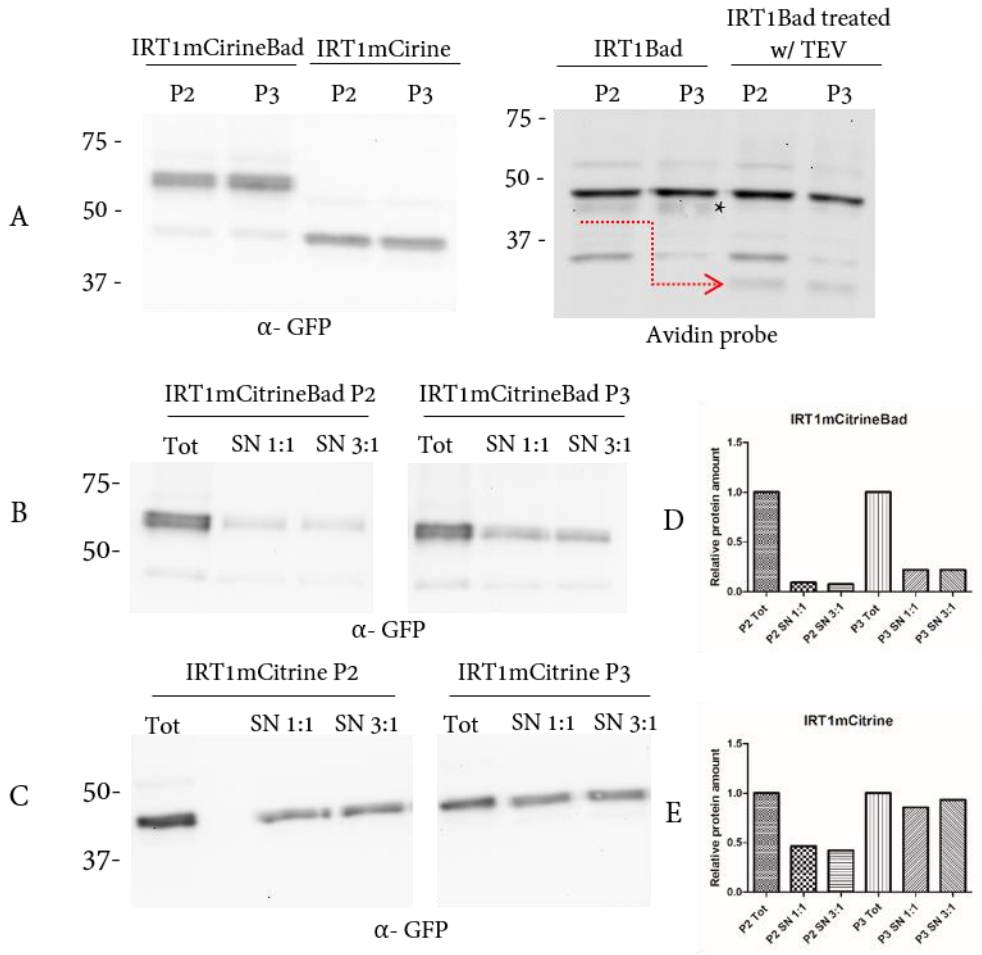

Figure 3-3 Expression and solubilization of IRT1 fusion proteins expressed in yeast. After protein expression, cells were subjected to membrane fractionation followed by sequential steps of centrifugation. We obtained two types of membranes, P2 (heavy membranes) and P3 (light membranes). A) Protein expression in P2 and P3 membranes was analyzed by immunoblotting. Fusions containing the mCitrine fluorescent tag were probed with an anti-GFP antibody, whereas IRT1Bad was probed with an avidin probe. To determine which band corresponds to IRT1Bad, given that the avidin probe recognizes endogenously biotinylated proteins, we treated the samples with the TEV protease, shown by the red arrow. The asterisk indicates the band corresponding to IRT1Bad. B) and C) Solubilization of IRT1mCitrineBad and IRT1mCitrine was carried from P2 and P3 membrane fractions diluted to 2 mg/ml. Detergent was added to final 2 mg/ml (1:1) and 6 mg/ml (3:1) concentrations and solubilization proceeded for 1 hour. Samples were subjected to ultracentrifugation at 100 000 g for 1 hour. Tot refers to the crude extract before centrifugation and 1µg of the "tot" fractions was loaded in each case. SN refers to supernatant after ultracentrifugation and 2µg of these samples were loaded on SDS-PAGE gels. D) and E) Solubilized proteins were quantified relative to the total fractions.

I then focused on the solubilization of the mCitrine-containing fusion proteins by the gentle non-ionic detergent n-dodecyl-β-D-maltopyranoside (DDM) at two detergent: protein ratios (1:1 and 3:1), since it is an appropriate detergent to purify properly folded IRT1 protein compared to harsher detergents. Also, experimental procedures in our laboratory demonstrated the ability of DDM to solubilize IRT1 protein from plant tissues (Dubeaux et al. 2018; Martín-Barranco et al. 2020). This demonstrated that proteins from P3 membranous fractions were better solubilized compared to IRT1mCitrine and IRT1mCitrineBad recovered from P2 type membranes. For the IRT1mCitrine

fusion, the 3:1 detergent to protein ratio solubilized about 75% of the P3 sample, comparable to the 1:1 ratio, where we measured 70% solubilization (*Figure 3-3* E). In the case of IRT1mCitrineBad we estimated a solubilization of ~25% in both conditions for P3 membranes (*Figure 3-3* D).

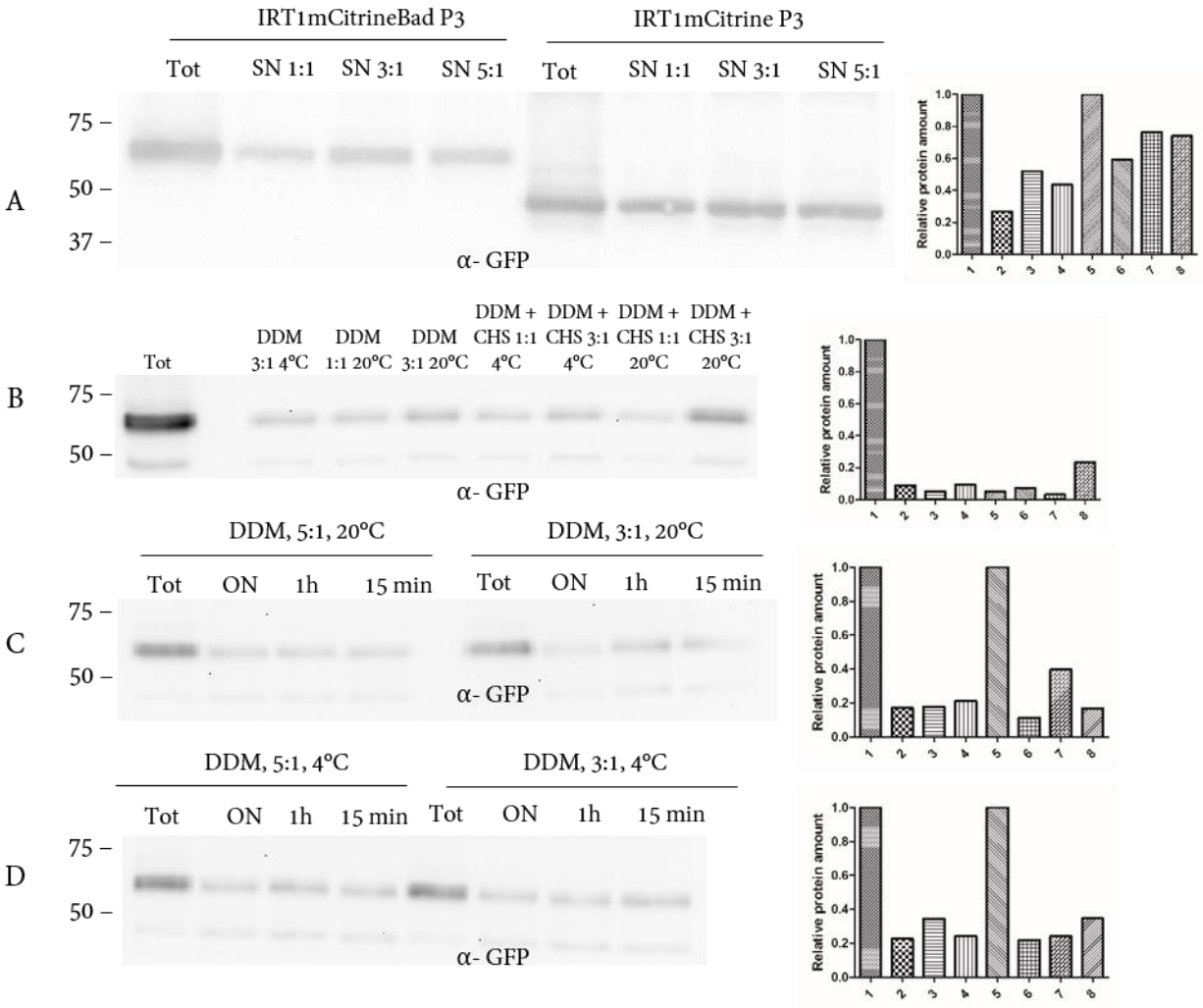

Figure 3-4 Optimization of solubilization. A) Solubilization of IRT1mCitrineBad and IRT1mCitrine was carried from P3 membrane fractions solubilized to 2 mg/ml. Detergent was added to final 2 mg/ml (1:1), 6 mg/ml (3:1) and 10 mg/ml (5:1) concentrations and solubilization proceeded for 1 hour. Samples were subjected to ultracentrifugation at 100 000 g for 1 hour. Tot refers to the crude extract before centrifugation and 2µg of the "tot" fractions was loaded in each case. SN refers to supernatant after ultracentrifugation and 2 µg of these samples were loaded on SDS-PAGE gels. B) Solubilization of IRT1mCitrine Bad from P3 membranes proceeded as in A at the temperatures indicated above each lane. Also, CHS was added to certain samples. C) and D) Solubilization proceeded as in A at different time points indicated above each lane, at 20°C and 4°C respectively. The bar graphs correspond to quantifications normalized to the total fractions.

Further solubilization optimization, where we elevated the detergent:protein ratio (*Figure 3-4* A), did not show any significant increase in the yield of solubilization. Similarly, increase of temperature and addition of CHS, a derivative of cholesterol widely used in protein stabilization (Thompson et al. 2011; Kotov et al. 2019), had little effect on the solubilization of IRT1mCitrineBad. Overall, we observed yields of no more than 25% (*Figure 3-4* B). Likewise, when solubilization was carried out for different time, no significant difference was observed (*Figure 3-4* C and D).

I then tested the solubilization using other harsher detergents than DDM. These were n-Octyl-β-D-Glucopyranoside (OG), 3-cholamidopropyl dimethylammonio 1-propanesulfonate (CHAPS) and Fos-Choline-16 (FC16) (*Figure 3-5*). Solubilization was carried from P3 membranes at 3:1 detergent: protein ratio as previously assayed, and in parallel to DDM to determine whether they presented stronger solubilization yields. We observed that FC16 elicited the highest solubilization yield followed by DDM. OG, CHAPS and a CHAPS+DDM mix, elicit negligible solubilization yields on IRT1mCitrineBad and IRT1mCitrine samples.

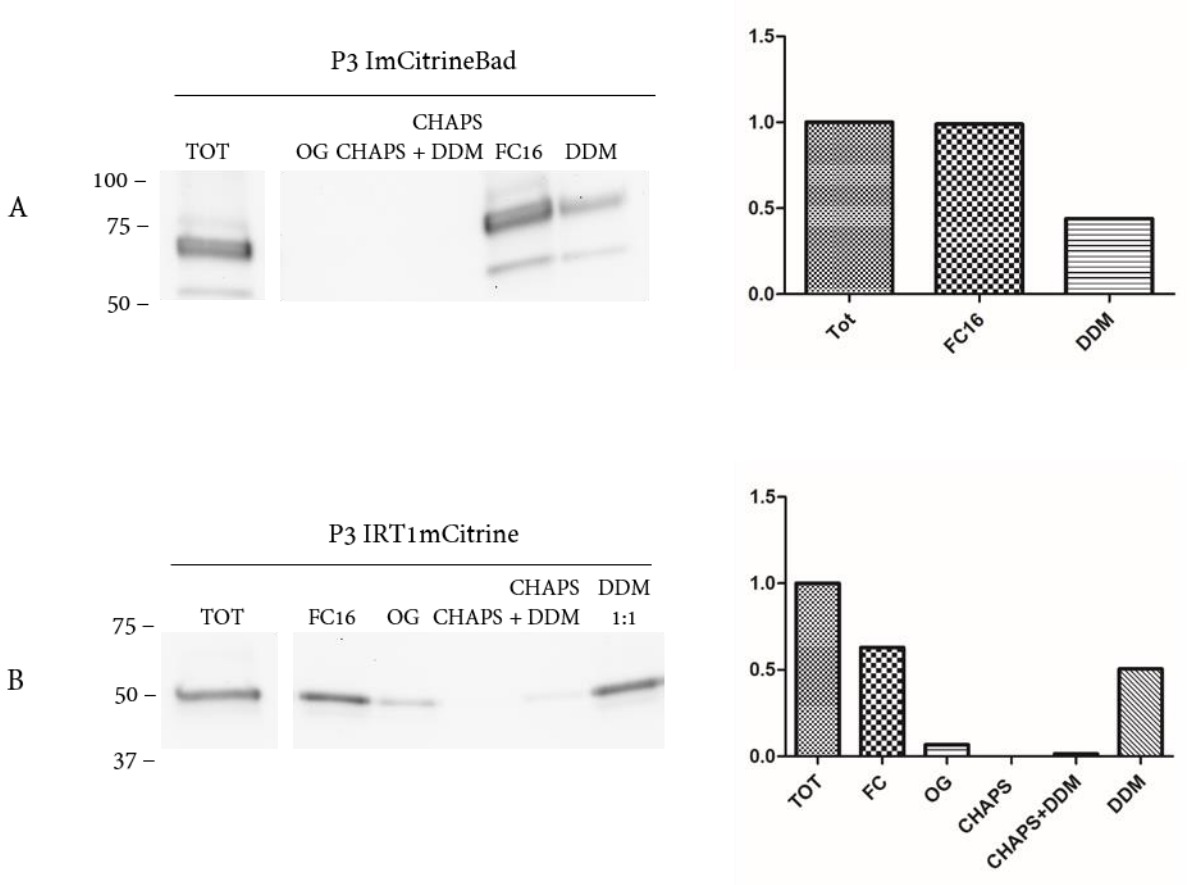

Figure 3-5 Optimization of solubilization in different detergents. A) and B) Solubilization of IRT1mCitrineBad and IRT1mCitrine was carried from P3 membrane fractions solubilized to 2 mg/ml. Detergents were added to final 6 mg/ml (3:1) concentrations and solubilization proceeded for 1 hour at 4°C. Samples were subjected to ultracentrifugation at 100 000 g for 1 hour. Tot refers to the crude extract before centrifugation and 1µg of the "tot" fractions was loaded in each case. SN refers to supernatant after ultracentrifugation and 2µg of these samples were loaded on SDS-PAGE gels. C) and D) Solubilized proteins were quantified relative to the total fractions.

Altogether, solubilization yields for the IRT1mCitrineBad construct were highly variable. FC16 yielded solubilization rates close to 100% whereas DDM yields were 35% in average. Because at this stage we do not count with an assays to determine protein activity in solution, we decided to continue working with both detergents. Whereas DDM tends to keep protein folding intact, this is sometimes not the case for the harsher detergent FC16. On the other hand, solubilization yields of the IRT1mCitrine fusion protein in DDM was consistently about 75%. The addition of CHS had no impact on protein recovery for any of the constructs. Although some of the tested conditions seemed to cause minor effects on the solubilization, these were among the variability present throughout different experiments. For

this reason, we decided to continue our experiments using the solubilization parameters that were the most reproducible and that were optimal for protein stability for IRT1mCitrine and IRT1mCitrineBad (Table 2).

Table 2 Solubilization parameters.

Fusion protein	Membrane type	Detergent	Detergent:protein ratio	Temperature	Time	Solubilization yield
IRT1mCitrine	P3	DDM+CHS	3:1	4°	1h	~75%
IRT1mCitrineBad	P3	DDM+CHS	3:1	4°	1h	~35%
IRT1mCitrineBad	P3	FC16	3:1	4°	1h	~100%

3.1.1.3 Purification strategies

Given the expression and solubilization results, we decided to pursue purification strategies specific for each of the constructs. Because the IRT1mCitrine fusion has no other tag than the mCitrine, we designed a purification strategy based on GFP binding proteins called αReps (Chevrel et al. 2015), that would allow for efficient and affordable purification compared to commercially available GFP traps. On the other hand, the biotin acceptor domain in the IRT1mCitrineBad construct is biotinylated in the yeast, which facilitates capture by the strong avidin-biotin interaction (Jidenko et al. 2006).

3.1.1.3.1 Affinity chromatography on streptavidin sepharose resin

We based the design of our purification strategy on the protocol established for the rabbit sarcoplasmic reticulum Ca^{2+}-ATPase and the yeast lipid flippase P4-ATPase Drs2p (Jidenko et al. 2006; Azouaoui et al. 2016), since established by our collaborators. This strategy consists in incubating the solubilized protein sample containing the BAD domain, which is in vivo biotinylated in the yeast host, with a streptavidin sepharose resin. The strong and highly specific interaction between biotin and streptavidin allows the recovery of a high purity protein sample. The trapped protein is then removed by protease activity by the TEV protease on its specific cleavage site between C-terminal end of IRT1 and the BAD Domain (*Figure 3-6*).

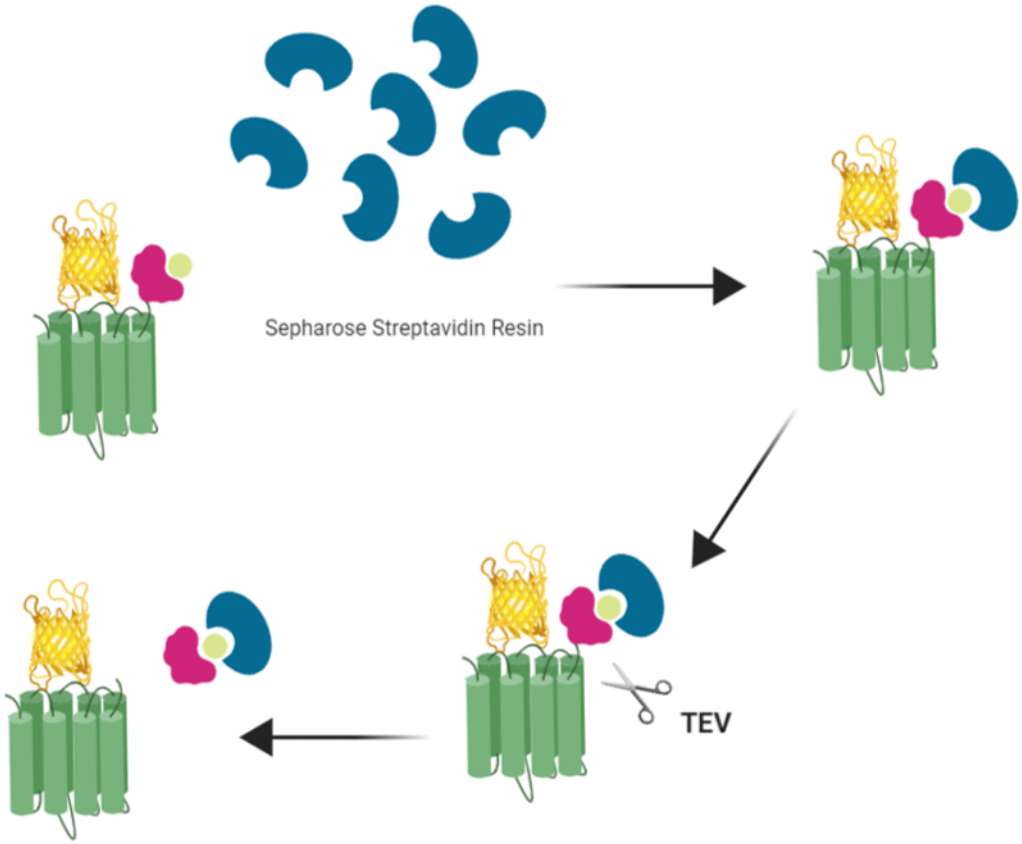

Figure 3-6 Purification on sepharose streptavidin resin. Solubilized IRT1mCitrineBad is incubated with the sepharose streptavidin resin. Unbound proteins are washed away with buffer. The trapped protein is then cleaved by the TEV protease on the TEV protease cleavage site located between IRT1 and the Bad tag.

Because solubilization was more efficient on FC16 and because DDM does not impact on protein folding, we decided to compare purification strategies in both detergents. The different steps of the purification were analyzed by SDS-PAGE followed by Coomasie blue staining or western blot (*Figure 3-7*). As seen in the eluate fraction, IRT1mCitrine is detected at ~50 kDa and its main contaminant is the TEV protease, seen at ~28 kDa in both detergent conditions (*Figure 3-7* A). Comparing the flowthrough (FT) signals to the crude extract (SN), we can observe that most of the protein is lost at the binding step since the intensities of both bands are the same (*Figure 3-7* B). This was observed for purifications in both detergents. We were, however, able to recover IRT1mCitrine in two sequential elution steps (E1 and E2). Interestingly, we observed a shift in the migration of IRT1mCitrine when the sample is treated at 95°C compared to the regular 30°C treatment ($E1_{95°C}$). This may be caused by misfolding of the protein changing the Stokes radius and hence affecting the migration in polyacrylamide gels. To determine whether a fraction of the protein remains bound to the resin even after treatment with the TEV, the resin samples needs to be treated at 95°C in order to detach the captured protein.

We decided to estimate protein concentrations by immunoblotting, based on a calibration curve of purified recombinant mCitrine. We loaded 50 ng, 100 ng, 200 ng and 400 ng of pure mCitrine that we previously purified on SDS-PAGE for immunoblotting. We loaded also 2.5 and 5 µl of a 1/10 dilution

of the original eluate fractions of IRT1mCitrine for protein estimation. By linear regression, we obtained a curve that allowed us to determine the concentration of the eluted protein at approximately 0.2 mg/ml for purifications in DDM+CHS and FC16. This means that the total yield of purification of approximately 0,2 mg IRT1mCitrine/L of culture.

The use of FC16 did not increase the final yield of purification, despite its clear positive effect on solubilization. We reasoned then, to continue our work by using the strategy based on solubilization with DDM+CHS in order to optimize protein stability.

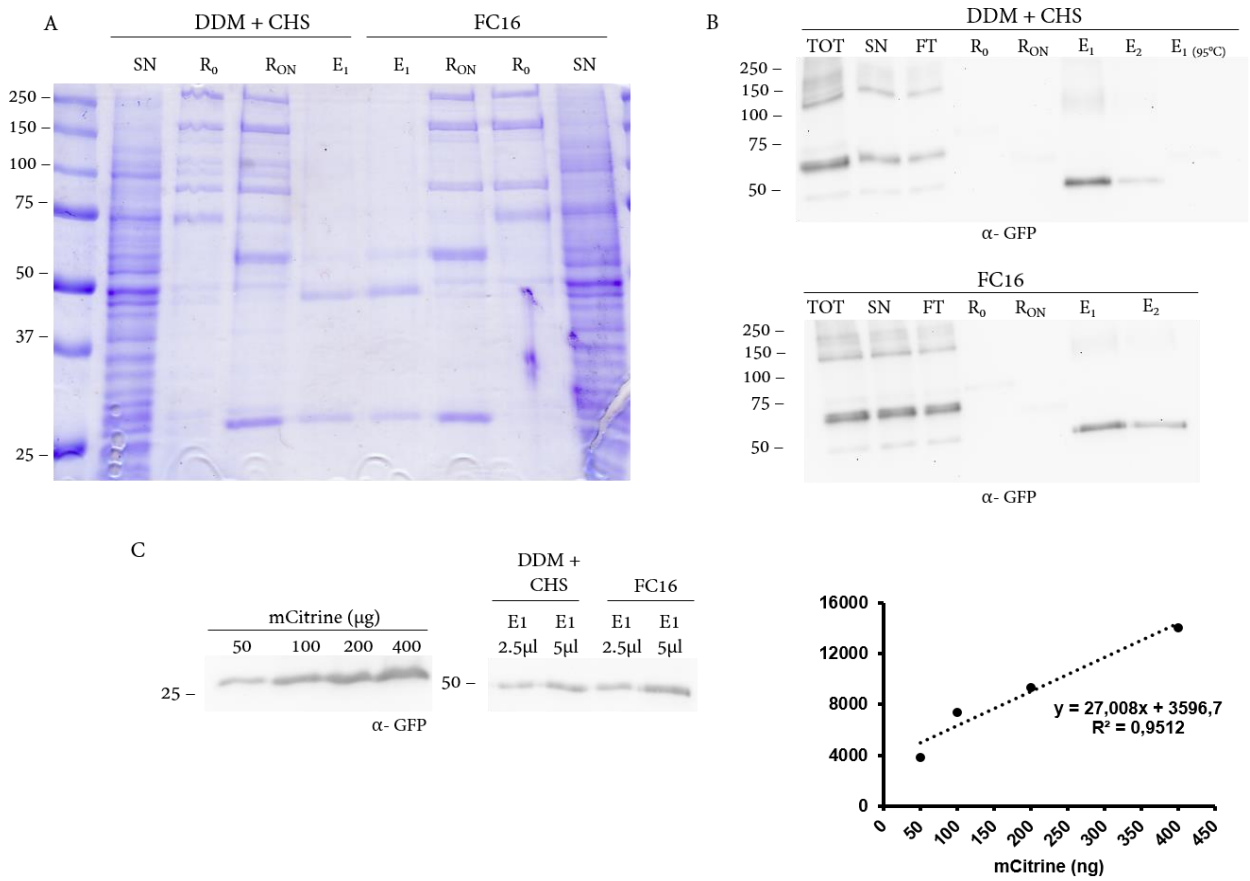

Figure 3-7 Purification on sepharose streptavidin resin. P3 membranes were diluted to 2mg/ml (TOT) and subjected to solubilization with DDM+CHS or FC16 at a final 6mg/ml concentration. The samples were centrifuged at 100 000g and the supernatants (SN) were recovered. Then the SN were incubated with the resin for 2 hours (R_0). The resin was decanted by low speed centrifugation and unbound proteins (FT) were removed. The resin was then washed and finally treated with TEV protease overnight (R_{ON}) for the elution of the bound IRT1mCitrine (E1). E1 was recovered by again decanting the resin at low speed centrifugation. A second elution (E2) was carried by addition of buffer without additional TEV. The protein migration shifts when the sample is treated at 95°C ($E1_{95°C}$). A) Coomasie blue analyses of purification samples in DDM+CHS and FC16. B) Immunodetection of purification samples with GFP antibodies. C) Quantification of purified IRT1mCitrine was based on immunodetection by GFP antibodies. Here, 2.5µl and 5µl of a 1/10 dilution of the pure IRT1mCitrine samples were loaded on SDS-PAGE and immunoblotted together with a mCitrine calibration curve.

As mentioned above, although a portion of the protein is recovered in the elution, the majority is lost in the flow through fraction. In an attempt to increase binding yield, we tried increasing the biotinylation level of the BAD affinity tag. I therefore used a commercial biotinylation kit (Avidity,

BirA500) to incubate P3 membranes and solubilized fractions from P3 membranes with the biotin ligase BirA in a biotin-containing buffer. Reactions were performed at 30°, as recommended by the supplier, and at 4°C in order to maintain conditions optimal for the stability of IRT1mCitrineBad. Immunoblots with an avidin probe capable of binding to biotin, showed that biotinylation was effective in P3 membranes and solubilized fractions, at both 4° and 30° (*Figure 3-8* A-C). The final total amount of protein recovered was however inferior to the initial fraction due to the precipitation of IRT1mCitrineBad (*Figure 3-8* D). This was likely due to the lack of glycerol used in the reaction buffer. Since glycerol is reported to heavily impact on the activity of the BirA biotin ligase according to the manufacturer (Avidity), it was removed from our assay but that clearly impacted on IRT1mCitrine stability.

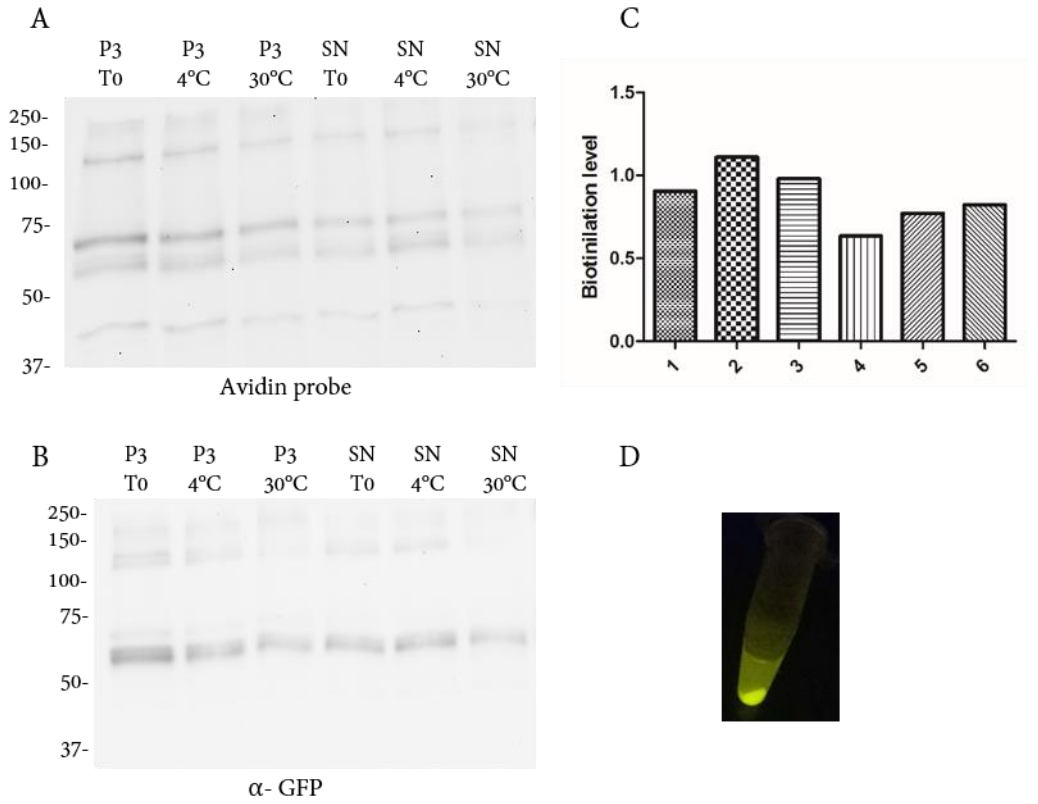

Figure 3-8 Biotinylation of IRT1mCitrineBad. A) A commercial biotinylation kit was used on P3 membrane samples and solubilized P3 membranes at 2 mg/ml following manufacturer recommendations. Recombinant biotin ligase BirA was added to the samples in a biotin-containing buffer. The reaction was carried for 1 hour at 4°C or 30°C degrees. Samples were then immunoblotted with an avidin probe revealing biotinylation levels. B) Same samples as in A, probed with GFP antibodies for normalization of the signals. C) Normalized biotinylation levels. D) The biotinylation reaction was carried in buffer lacking glycerol as recommended by the manufacturer, which prompted to the precipitation of the IRT1mCitrineBad. Here, SN treated at 4°C as an example.

3.1.1.3.2 Alternative purification strategy: αReps

Because the IRT1mCitrine construct was solubilized more than twice as much compared to the IRT1mCitrineBad, we decided to design a purification strategy based on mCitrine trapping by a GFP binding protein, named bGFPd. This artificial binding proteins (αReps) are derived from a natural family of α-helical repeat proteins and were isolated from a library constructed for creating binders with a randomized interaction surface. αReps bind GFP with nanomolar dissociation constants (Chevrel et al. 2015).

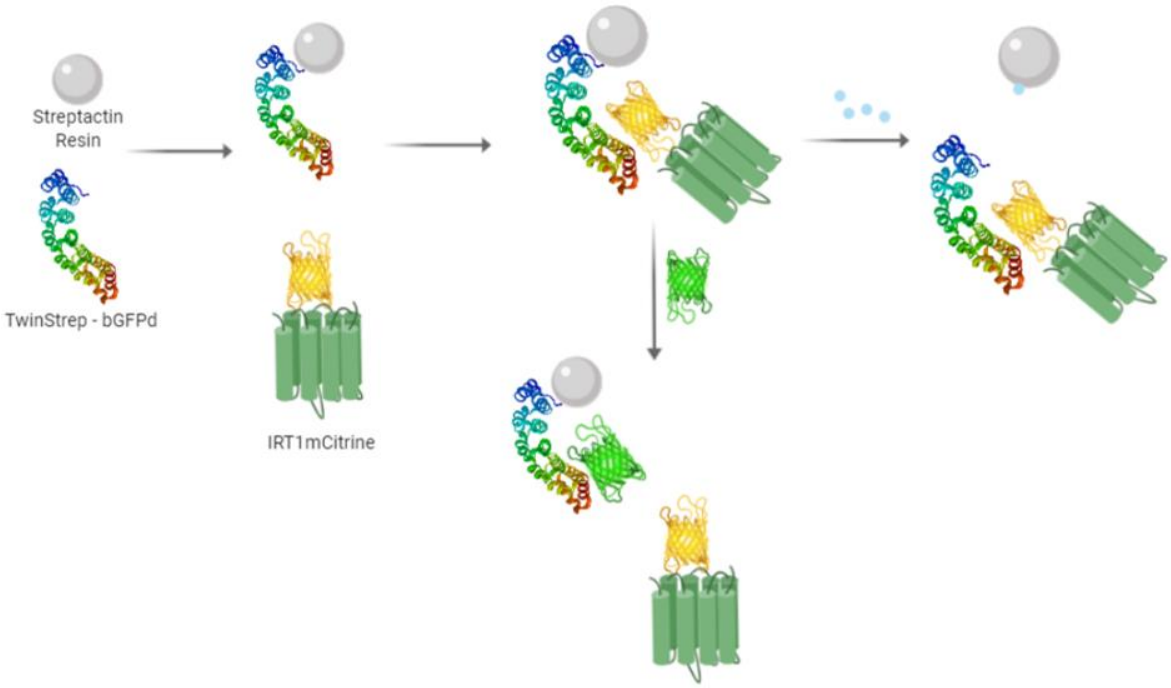

Figure 3-9 Purification strategy using GFP binders. Twinstrep tagged GFP binder "bGFPd" is produced and purified in vitro. The pure protein is then incubated with the streptactin resin. The bound bGFPd-resin complex is then incubated with the solubilized IRT1mCitrineBad protein overnight. Contaminant proteins are washed away before eluting with pure GFP or biotin (blue spheres).

Pure twinstrep-tagged bGFPd was coupled to a streptactin resin and the resulting resin was then incubated with IRT1mCitrine. To disrupt the mCitrine-binder interaction we considered two options, a competition by high amounts of GFP or a biotin elution, which elutes the Twinstrep-bGFPd+IRT1mCitrine complex (*Figure 3-9*). Both approaches presented limitations. First, when recombinant GFP was added as a competitor to IRT1mCitrine, no IRT1mCitrine was detected in the eluate (*Figure 3-10* B). We reasoned the interaction between mCitrine and bGFPd is as strong as the GFP-bGFPd interaction and thus cannot be out competed by GFP. Consequently, the high amount of GFP remaining from the elution step constituted the major component of this sample. Second, the elution with biotin positively resulted in the elution of IRT1mCitrine (*Figure 3-10* C). However, the eluted fraction obtained by used of biotin was significantly less pure than the sample obtained by the streptavidin sepharose resin method (*Figure 3-10* C). Moreover, a comparison of the solubilized fraction

to the unbound material presented a low binding rate (*Figure 3-10* A), similar to the SSR method. For these reasons, we decided to pursue our experiments by using the SSR purification method.

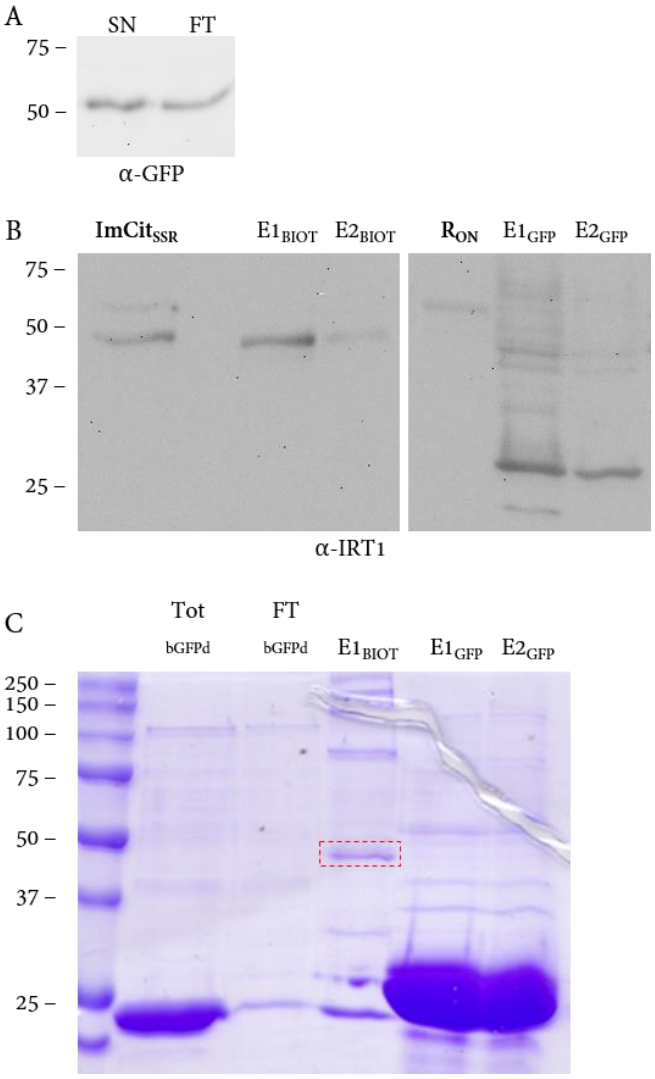

Figure 3-10 Purification in bGFPd. P3 membranes were diluted to 2 mg/ml and subjected to solubilization with DDM+CHS at a final 6 mg/ml concentration. The sample was centrifuged at 100 000 g and the supernatant (SN) was recovered. Then the SN was incubated with the Streptactin Sepharose Resin (previously incubated with bGFPd binders) (R_0) for 2 hours. The resin was decanted by low speed centrifugation and unbound protein (FT) was removed. The resin was then washed and finally treated with biotin or GFP for the elution of the bound IRT1mCitrine ($E1_{BIOT}$ and $E1_{GFP}$ respectively). Second elutions ($E2_{BIOT}$) was carried by a second addition of buffer containing biotin. $E2_{GFP}$ was carried by addition of buffer without additional GFP. Tot bGFPd is the bGFPd sample prior to incubation with Streptactin resin and FT bGFPd is the unbound bGFPd to the streptactin resin.
A) Binding efficiency of IRT1mCitrine from P3 solubilized membrane to the twinstrep-bGFPd bound to Streptactin resin. B) Immunoblotting of elution samples with IRT1 antibody. C) Coomasie blue analyses of elution fractions.

3.1.2 Proteoliposome reconstitution of IRT1

In order to gain insight into the functionality of IRT1 and to characterize its transport mechanism, we decided to reconstitute the purified IRT1mCitrine from the SSR method into liposomes. We based our approach in an existing protocol designed for an amino acid transporter from *Plasmodium falciparum* of similar topological characteristics of IRT1 (full transmembrane transporter of 30 kDa).

Briefly, we started with solubilized lipids in chloroform. A mixture of DOPC and POPE were used in this case. After mixing and drying the mix into a lipidic film in a round bottom flask, it was then resuspended in Mops-Tris buffer. Once the lipidic film was resuspended, we followed a round of sonication and extrusion through a 200 nm followed by a 100 nm filter to homogenize the size of our liposomes. Destabilization of the liposomes was achieved by addition of DDM. This was followed by addition of the pure IRT1mCitrine protein. Removal of destabilizing detergent was carried by Bio-Rad bio beads, made of a polymer that traps detergent molecules (See section 4.7 for detailed explanation).

To determine whether our protein was properly incorporated into the liposomes, we used a sucrose gradient separation by centrifugation strategy. Because empty liposomes are lighter than protein-containing ones, they are found at lower concentrations of sucrose than proteoliposomes when centrifuged in a gradient. The non-reconstituted protein often precipitates in such conditions and is found at the bottom of the tube (*Figure 3-11* A). Parallel to the reconstituted fraction, we ran liposomes that were treated with detergent and bio beads, but instead of the pure protein buffer was added in the place. These samples were loaded on a sucrose gradient. Immunoblot analyzes of top, middle and bottom fractions from the gradient demonstrated the presence of IRT1 in the liposomes (*Figure 3-11* B). We determined approximately 15% of the total protein was recovered reconstituted in the proteoliposomes. Addition of triton is known to disrupt the lipidic particles, and should expose the mCitrine epitope located in the interior of the lipidic layer, allowing the determination of IRT1mCitrine orientation. With this approach, I determined roughly that most of IRT1 was reconstituted in the "mCitrine out" orientation, mCitrine being inserted in the extracellular face of IRT1 protein. Further replicates are needed to improve and confirm such observations. Exposing the samples to an UV lamp also evidenced the presence of IRT1mCitrine in the liposomal fraction obtained at ~10% sucrose (*Figure 3-11* D). Now that the liposome reconstitution of IRT1mCitrine appears feasible, the next step will be to set up transport assays. Incorporation of a metal-sensitive fluorescent probe undergoing metal-dependent quenching appears as the most appropriate strategy to investigate metal transport by IRT1. The fluorophore of choice must be sensitive to metals transported by IRT1 and show spectral properties not interfering with the fluorescence of mCitrine present in IRT1. Calcein deep red (Cayman), a membrane-impermeant fluorescent dye, is an adequate fluorophore for such applications. It is a deep red-emitting version of the green Calcein fluorophore, which is vastly used in metal transport assays (Manatschal et al. 2019; Kato et al. 2019; Billesbølle et al. 2020). It has excitation and emission maxima of 648 and 658 nm respectively, far from the 516 and 529 nm excitation and emission peaks of mCitrine.

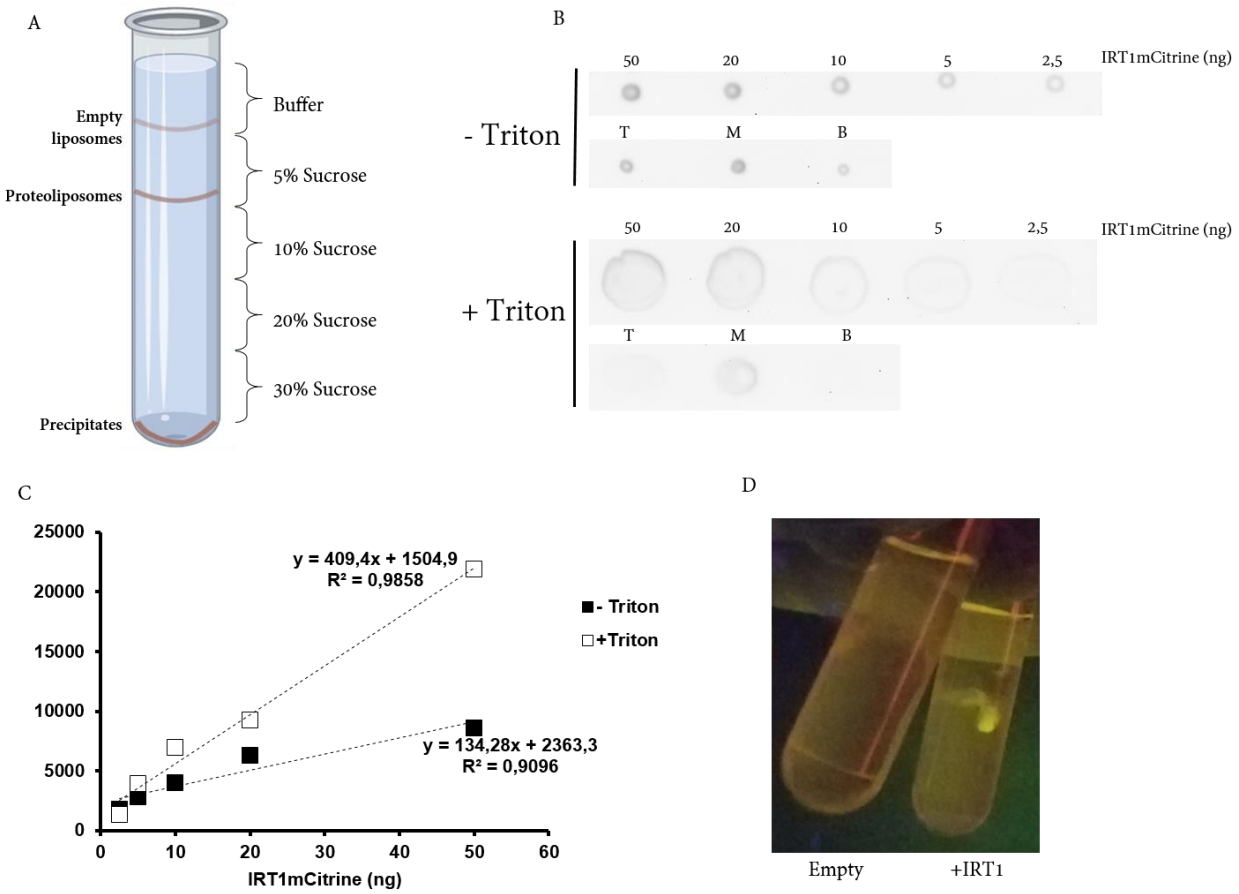

Figure 3-11 Proteoliposome reconstitution. A) Proteoliposomes separate from protein precipitates and empty liposomes during ultracentrifugation in sucrose gradients. B) Detergent destabilized liposomes were reconstituted by addition of pure IRT1mCitrine and resealed by removal of detergent by addition of Biobeads. Reconstituted liposomes were subjected to centrifugation in a sucrose gradient and top (T), middle (M) and bottom (B) fractions were withdrawn for dotblot and immunoblotted with a GFP antibody. The samples were treated with triton for disruption of the lipidic film. Pure protein was used for calibration curves. C) Calibration curve by linear regression of pure protein from the dot blot for determination of the total protein recovery. D) Exposure of gradient separated liposomes without added protein and with addition of IRT1mCitrine.

3.1.3 Biochemical characterization of the full-length IRT1 transporter

3.1.3.1 Structural characterization of IRT1: Cryo electron microscopy

The pure protein sample obtained by the SSR procedure described above was run through size exclusion chromatography (SEC) for further purification of the sample (*Figure 3-12*). Because the elution profile of pure IRT1mCitrine (described in detail in the next section) usually shows two main peaks at 10.5 and 12 ml, we were surprised to find that at higher protein concentrations this behaviour appear to be changed. We expected the intensification of the 10.5 ml peak in such conditions, due to

favoring oligomers at higher concentrations, but we observed a shift of the signal to even larger retention volumes. Deconvolution of overlapping chromatographic peaks showed that indeed, the peak at 10.5 ml increased with respect to the one at 12 ml (*Figure 3-13*). Also, we observe an additional peak at 9 ml that possibly belongs to aggregates, and a shift of the usual 12 ml peak to higher retention volumes, here 13 ml.

Eluted fractions (11-19) (*Figure 3-12*) from FSEC were pulled together. This sample was included in a CryoEM grid for electron microscopy analyses by our collaborators (*Figure 3-14* A).

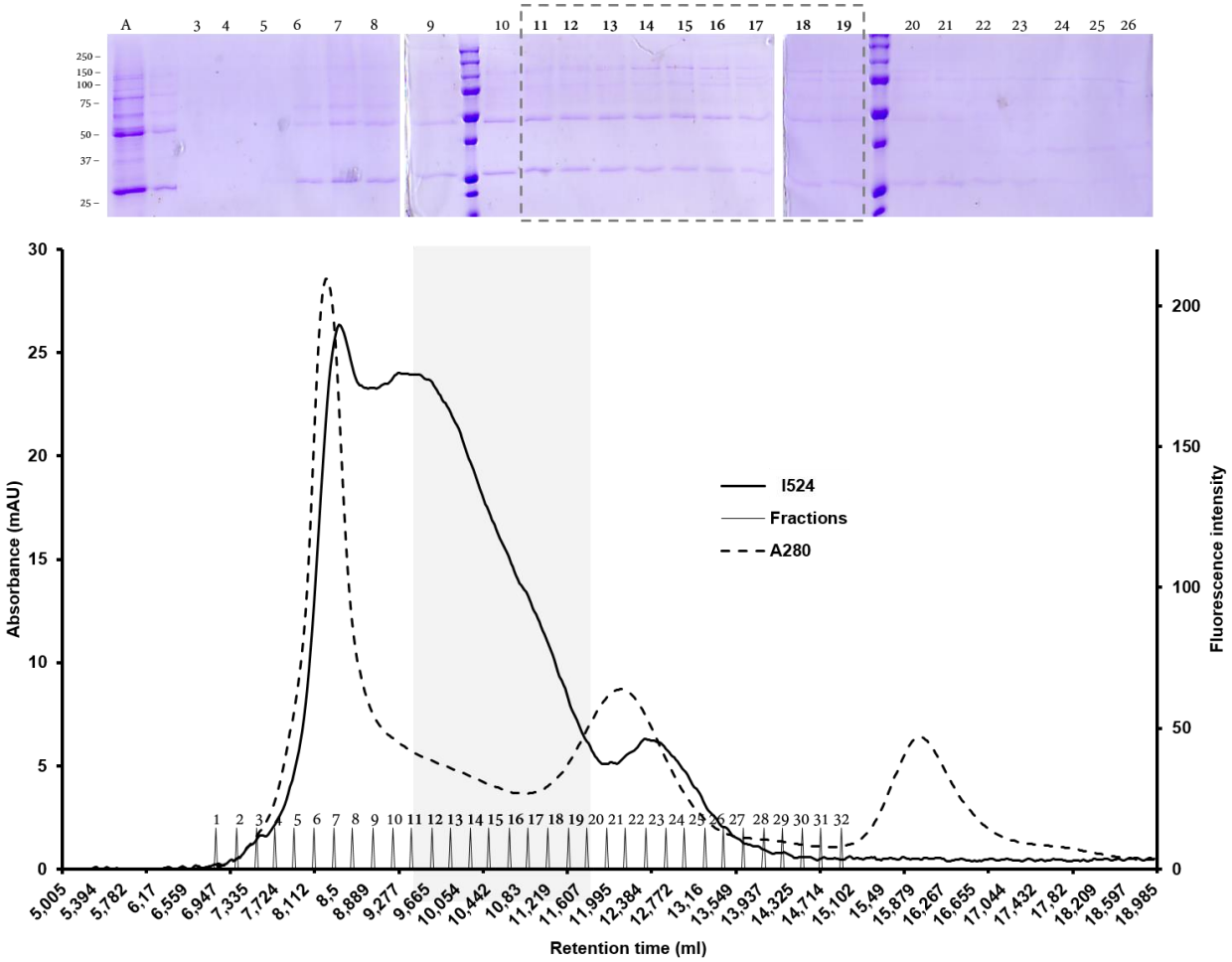

Figure 3-12 Size exclusion chromatography of IRT1mCitrine. The protein was run on a Superdex 200 increase column and monitored by absorbance at 280 nm and fluorescence emitted at 514 nm. Fractions were collected and analyzed on SDS-PAGE followed by coomasie blue staining (3-26). Fractions 11-19 were pooled together and concentrated for further processing. Lane A correspond to the concentrated sample prior to SEC.

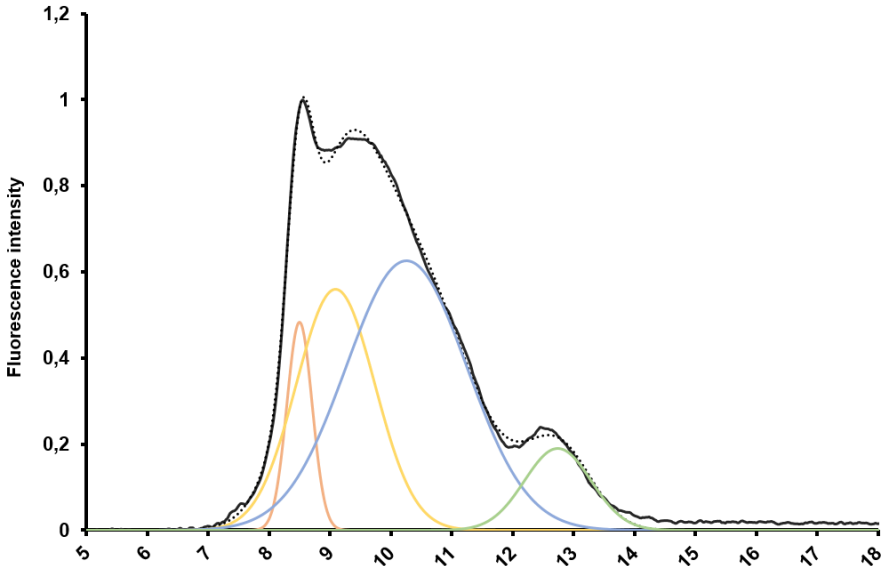

Figure 3-13 Deconvolution of chromatogram from concentrated pure IRT1mCitrine. The chromatogram of the concentrated pure protein was approximated to a sum of Gaussian distributions. Dotted line corresponds to the fitting, full line to the experimental data. Void volume is represented in red. An "aggregate" peak at 9ml in yellow, the favored 10.5ml peak in blue and the 12 ml peak in green (shifted to 13 ml here).

Analyzes of the grid showed a homogenous sample with an elliptic shape and a size of 6x12 nm. A small data collection of 110 micrographs was acquired, with approximately 300 particles per micrograph, this is a total of 33000 particles, and classified in two dimensions. About 16000 particles were selected for 3D modelling (*Figure 3-14* B). Particles chosen from micrographs represented several orientations. The sample size was however not enough to observe all possible orientations, and "top views" were missing. Despite this limitation, 3D reconstitutions showed vague elliptic blobs. In the future we hope to scale up our purification strategy in order to produce a sample large enough for CryoEM.

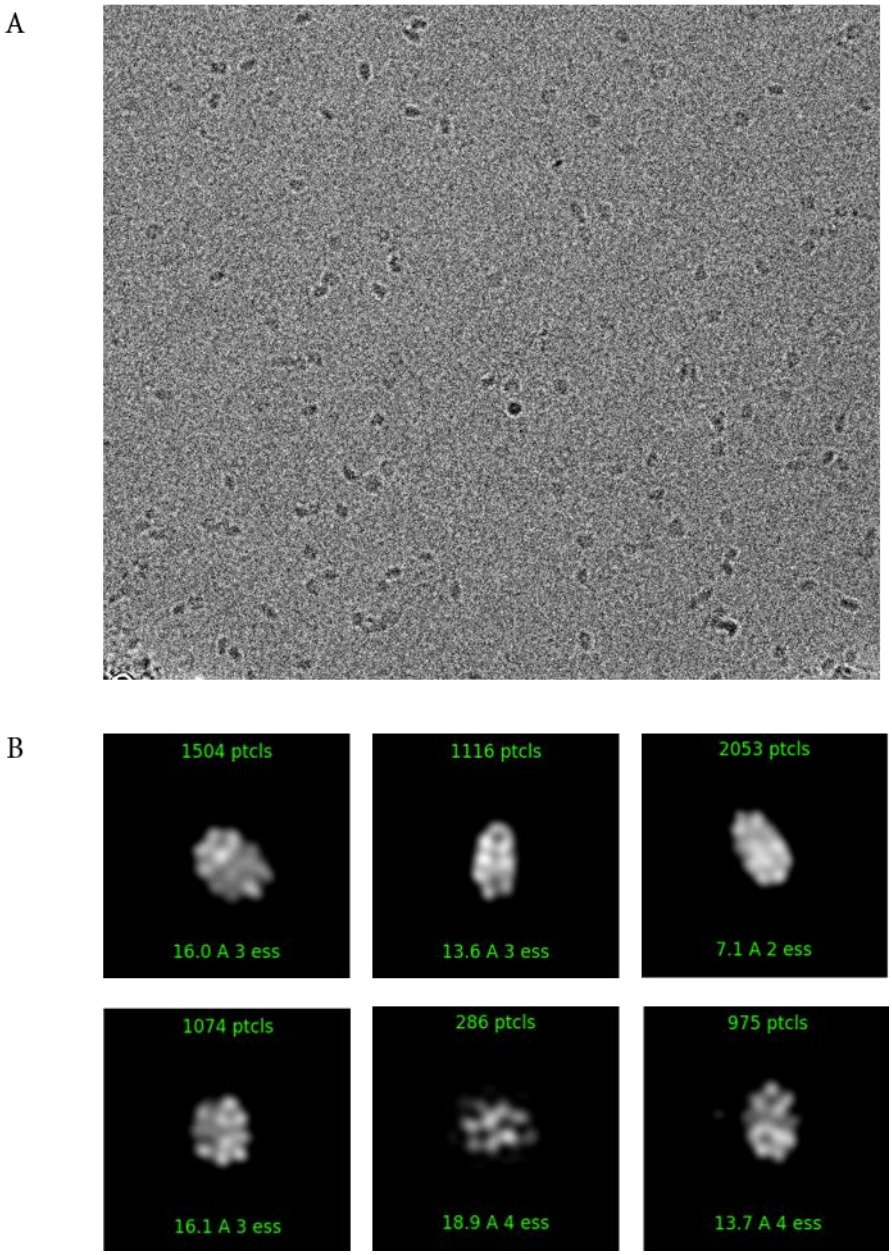

Figure 3-14 CryoEM preliminary results. A) Representative micrograph of IRT1mCitrine. B) Representative 2D class averages of IRT1mCitrine particle images.

3.1.3.2 Oligomeric status of IRT1

The characterization of several ZIP proteins demonstrated their ability to form oligomers (Lin et al. 2010; Zhang, Sui, and Hu 2016; Zhang et al. 2017; Hu, Wille, and Schmitt-Ulms 2018; Bin, Seo, and Kim 2018). We therefore wondered if IRT1 also has the ability to form multimers and pursued different techniques for the determination of its oligomeric status in vitro and in vivo.

Fluorescence coupled size exclusion chromatography (F-SEC) of the purified IRT1mCitrine sample presented an elution profile with three peaks. A first peak at about 7 ml corresponding to the void volume, and two more peaks at about 10.5 and 12 ml as previously mentioned (*Figure 3-15* A). A

calibration curve demonstrated that the peaks at 10.5 and 12 ml correspond to particles of an apparent molecular weight of 208 kDa and 140.6 kDa respectively (*Figure 3-15* B and C). The peak corresponding to the smaller molecule is of higher intensity than the other. Such behavior of pure proteins in size exclusion chromatography is often due to oligomerization. Considering the theoretical molecular weight calculated with the ExPASy ProtParam Tool, IRT1mCitrine has a weight of 64.6 kDa. The peak at 140.6 kDa is very close to the 136.6 kDa calculated for a monomer of IRT1mCitrine with a DDM micelle (72 kDa according to the supplier). The larger 208 kDa molecule corresponds with the estimated molecular weight of a dimer of IRT1mCitrine plus a DDM micelle which is 201.2 kDa. This elution profile was observed consistently between purification replicates when no more than 500 µg of protein were run on a 25 ml F-SEC column, however the intensities of each peak varied while the "monomer" peak remained the majoritarian in most cases. At higher protein quantities the elution profile appears shifted to higher molecular weights (*Figure 3-12*). Interestingly, when we monitored the absorbance at 280 nm, only the void volume was detected together with a peak at about 13 ml corresponding to DDM mixed micelles. We reasoned that no IRT1mCitrine is detected by absorbance at 280 nm due to the protein being highly diluted in the SEC column, in addition to its poor aromatic residue content. Data collected from FSEC allowed us to calculate hydrodynamic radius values for both species, which were 4.2 and 5.3 nm (*Figure 3-15* D). To verify that the behavior of IRT1mCitrine in FSEC was not an artefact from the purification, we decided to analyze P3 solubilized membranes prior to purification. In this sample, IRT1mCitrineBad is found in a complex environment containing diverse proteins and lipids. The elution profile of the solubilized membranes showed a similar shape to that of the pure protein, indicating that oligomerization of IRT1mCitrine is independent of the purification procedure (*Figure 3-15* E). Here, the monomer peak was also more intense than that of the putative dimer. A slight shift towards higher retention volumes was observed for the P3 solubilized membranes in comparison to the pure protein. This is in accordance with the additional 10 kDa resulting from the uncleaved Bad tag. A shoulder at about 9.5 ml is seen for the chromatogram of the pure protein, but it is absence in the one of the P3 solubilized membranes. This possibly corresponds to aggregates as seen above, and matches the result from the deconvolution of the chromatogram from highly concentrated protein (*Figure 3-13*).

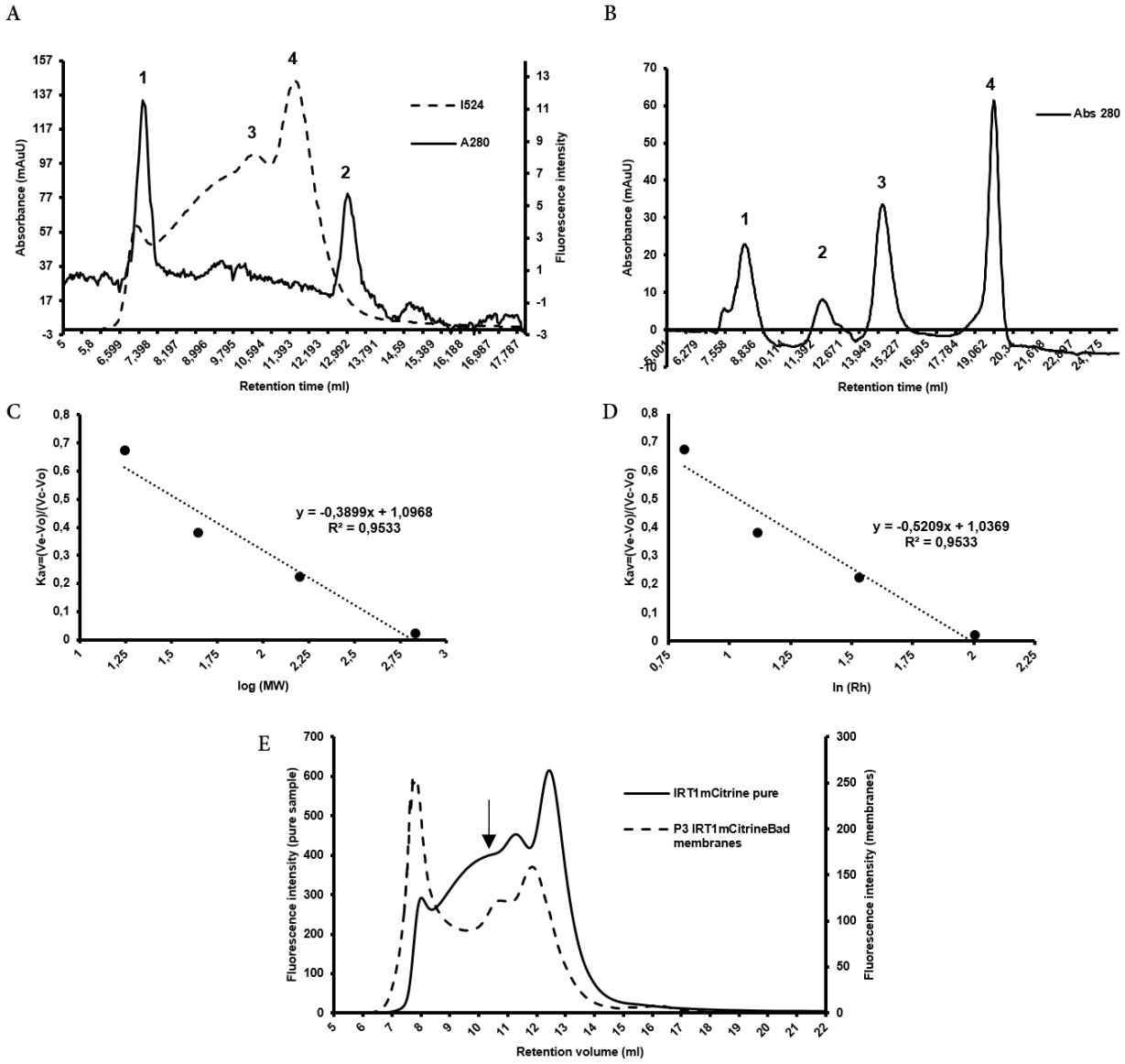

Figure 3-15 Size exclusion chromatography of pure IRT1mCitrine and P3 IRT1mCitrineBad membranes. A) Elution profile of IRT1mCitrine. The peaks correspond to 1) Void volume 2) Detergent mixed micelles 3) Oligomer 4) Monomer. B) Elution profile of proteins used for calibration: 1) thyroglobulin, 2) γ-globulin, 3) ovalbumin and 4) myoglobin. C) and D) Calibration curves plotted using the gel-phase distribution coefficient (Kav) versus logarithm of the molecular weight (Log(MW)) and hydrodynamic radius (Ln(Rh))respectively. Kav= (Ve-Vo)/(Vc-Vo), where Ve= elution volume, Vo= column void volume. E) Superimposed elution profiles of pure IRT1mCitrine and P3 membranes solubilized in DDM+CHS. The shift of P3 membranes towards smaller retention volumes is due to the presence of the Bad tag (10 kDa) fused to IRT1mCitrine. The arrow shows the shoulder corresponding to aggregates in purified IRT1mCitrine samples.

To further evaluate the possible oligomerization of IRT1 in vitro, we took advantage of analytical ultracentrifugation experiments which combine ultracentrifugation with optical monitoring systems (AUC). Here, we took advantage if the mCitrine fusion to monitor sedimentation from fluorescence signals. To this purpose, purified IRT1mCitrine proteins were sent to the Plateforme Biophysique AUC-PAOL in Grenoble for AUC analyses by Christine Ebel. Conflicting evidence was however obtained. When protein samples at 3, 1 and 0.3 µM are run on AUC, it was observed that 97 ± 2% of the total signal is found in a massif of peaks at sedimentation coefficients between 0.2 and 8 S. The mean of this

signals was found at 2.69 ± 0.1 S with the maximum at 1.61 ± 0.09 S. The two hydrodynamic radius (R_H) values determined from SEC data, 4.2 nm and 5.3 nm, were used here. Considering the R_H value of 4.2 nm, the main peak would correspond to a 121 kDa particle with 0.8 g of DDM bound per gram of protein, with a globular shape as determined by the SEDFIT v 16.1c software. If we consider the R_H to be 5.3 nm, then the 1.61 S peak corresponds to a 162 kDa molecule with 1.5 g/g detergent per protein, with an elongated shape corresponding to a monomer. Also, this parameters are fitting to the size of a dimer with no bound DDM, which is highly unlikely given the highly hydrophobic nature of IRT1 and the detergent content in the buffer. An additional sedimentation experiment at 0.03 µM presented a shift of the massif of peaks towards lower molecular weights, with a mean value of 1.69 S and the maximum at 1.16 S plus a shoulder at 1.94 S, suggesting the dissociation of a complex. This is however unlikely due to the evidence at higher concentrations for a monomer. As for FSEC, we decided to include P3 solubilized membranes. Again, four concentrations were analyzed: 1, 0.33 and 0.1µM. Similarly, we observed a massif of peaks between 0.2 and 8 S, for 96 ± 4% of the total signal. The mean and maximum s-values decreased when the concentration decreased. These are summarized in Table 3. This behaviour suggests the dissociation of larger species. The maximum at 0.1 µM was matching the values obtained for the pure sample. Also, in the sample at 0.01 µM, the distribution of peaks is shifted to lower values, with the maximum s-value at 1S, similar to the one obtained for the pure IRT1mCitrine at 0.03 µM.

Table 3 Sedimentation coefficients of IRT1mCitrine pure and in P3 solubilized membranes.

Sample	Concentration (µM)	Mean s-value	Max s-value
Pure IRT1mCitrine	3	2. 69 S	1.61 S
	1	2. 69 S	1.61 S
	0.3	2. 69 S	1.61 S
	0.03	1.69 S	1.16 S
Solubilized P3 membranes	1	2.7 S	1.87 S
	0.33	2.42 S	1.66 S
	0.1	2.33 S	1.61S
	0.01	1.11 S	1 S

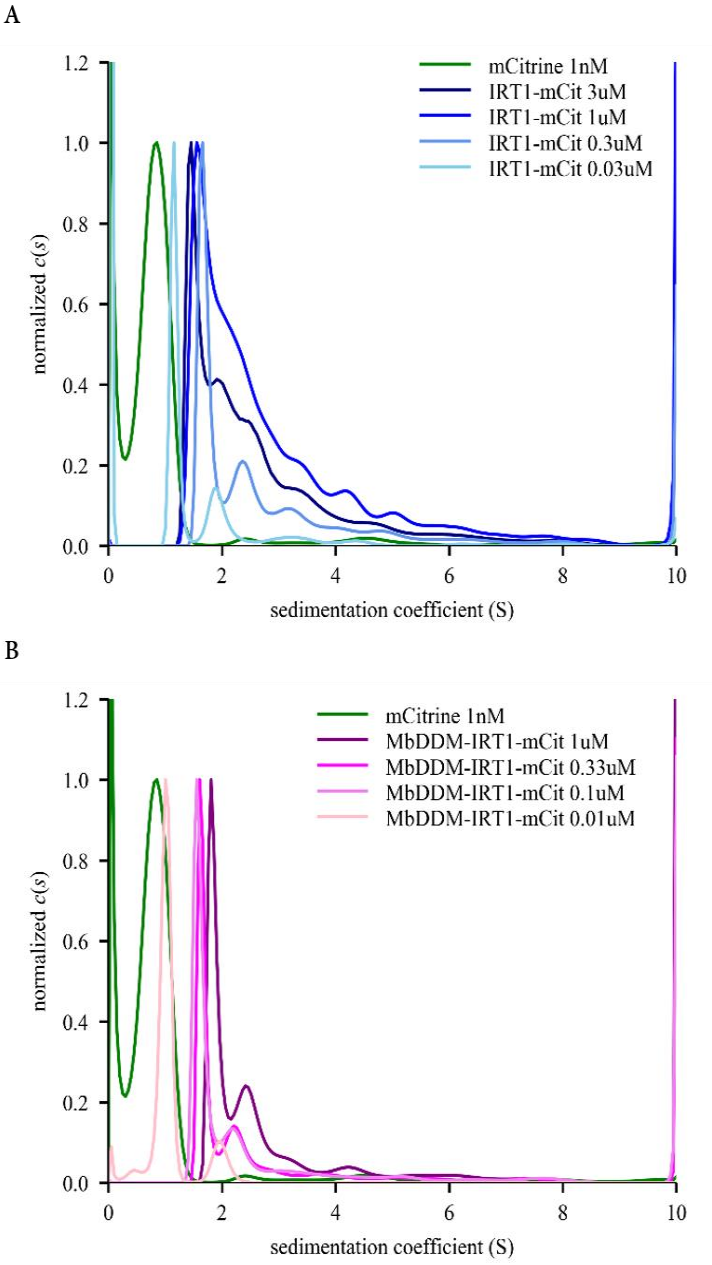

Figure 3-16 Sedimentation profile of pure IRT1mCitrine. Fluorescence signals were recorded for four dilutions of A) the IRT1mCitrine protein (IRT1-mCit) and B) solubilized P3 IRT1mCitrine membranes in DDM+CHS (MbDDM-IRT1-mCit). Pure mCitrine was run as a control.

To examine the oligomeric state of IRT1 and evaluate if IRT1 functions as a monomer or oligomer, we decided to implement in vivo protein-protein interaction experiments. We first use bimolecular fluorescence complementation (BiFC) in *Nicotiana benthamiana* leaves that allows to detect protein-protein interaction in vivo and visualize the site of interaction in the cell by confocal microscopy. BiFC is based on the reconstitution of a fluorescent protein from two separate N- and C- terminal domains fused to proteins of interest when they are in close proximity. Here, we used a system based on the N-terminal ($mCit^{Nter}$) and the C-terminal domains ($mCit^{Cter}$) of mCitrine, equivalent to what has been

originally described for GFP (Kerppola 2008). Transient expression of IRT1-mCit^{Nter} and IRT1-mCit^{Cter} under control of the CaMV35S constitutive promoter in tobacco leaves yielded a fluorescent signal outlining the edges of the cell and likely corresponding to the plasma membrane (*Figure 3-17*A). This suggests that a positive interaction between differently tagged IRT1 occurs in vivo at the cell surface, but this will have to be confirmed by co-expressing a known plasma membrane marker fused to CFP for example. To validate the BiFC results, we used the Arabidopsis plasma membrane-localized receptor-kinase BRI1, which is not supposed to interact with IRT1, as a first negative control. As expected, no BiFC signal could be observed using BRI1mCit^{Cter} and the IRT1mCit^{Nter}. However, the use of BRI1 is not adequate since BRI1 is tagged on its C-terminus oriented towards the cytosol while IRT1 is tagged at the C-terminal side predicted to be facing the extracellular space. If the predicted topology of IRT1 is correct, no BiFC interaction can occur between BRI1 and IRT1, making of BRI1 an irrelevant control. The use of a plasma membrane protein tagged on its extracellular face with mCit^{Cter} would serve a better control and will have to be generated in the future. Regardless, the fact that the functionality of C-terminally tagged IRT1 cannot be checked in the BiFC system, and that these fusions are overexpressed in leaves where IRT1 is not expressed point to the need of other approaches to study the in vivo oligomerization of IRT1.

We therefore carried out co-immunoprecipitation (Co-IP) of tagged versions of IRT1 stably expressed in Arabidopsis plants. First, I used the previously characterized 35S::IRT1-mCitrine line in the WT background where endogenous *IRT1* is also expressed (Dubeaux et al., 2018). Co-IP was performed on roots of iron-deficient plants to induce endogenous *IRT1* expression. Root samples were ground and protein solubilized before ultracentrifugation at 100 000 g for removal of insoluble material. Solubilized proteins from 35S::IRT1-mCitrine or WT counterpart were then subjected to immunoprecipitation with GFP-agarose magnetic beads (Chromotek), which also recognize mCitrine. The presence of endogenous IRT1 was detected using anti-IRT1 antibodies. IRT1-mCitrine was efficiently IPed from 35S::IRT1-mCitrine-expressing plants, although the corresponding protein was not observed in the input fraction due to low expression level. Regardless, endogenous IRT1 protein was detected after IRT1-mCitrine IP (*Figure 3-17* B). Endogenous IRT1 was however not seen after IP in WT plants, suggesting that IRT1 is able to interact with itself in vivo. To further validate this observation, I used a double transgenic line expressing the functional IRT1-mCitrine fusion under the control of *IRT1* promoter in the *irt1-1* mutant background (Dubeaux et al. 2018) and transformed with IRT1-mScarlet also driven by *IRT1* promoter. Co-IP was performed on roots of iron-deficient plants to induce *IRT1-mCitrine and IRT1-mScarlet* expression. I used *irt1-1*/IRT1::IRT1-mCitrine plants as negative control. IRT1-mCitrine was IPed from both control and the double transgenic lines, but IRT1-mScarlet could only be detected in the double transgenic line (*Figure 3-17* C), confirming the ability of IRT1 to oligomerize. Considering that IRT1 has been already observed in discrete foci at the plasma membrane, it is likely to be present in membrane microdomains. However, I think the results from co-IP experiments are in favor of IRT1 oligomerization since the ultracentrifugation step should prevent detection of the different forms of IRT1 present in the same unsolubilized microdomains.

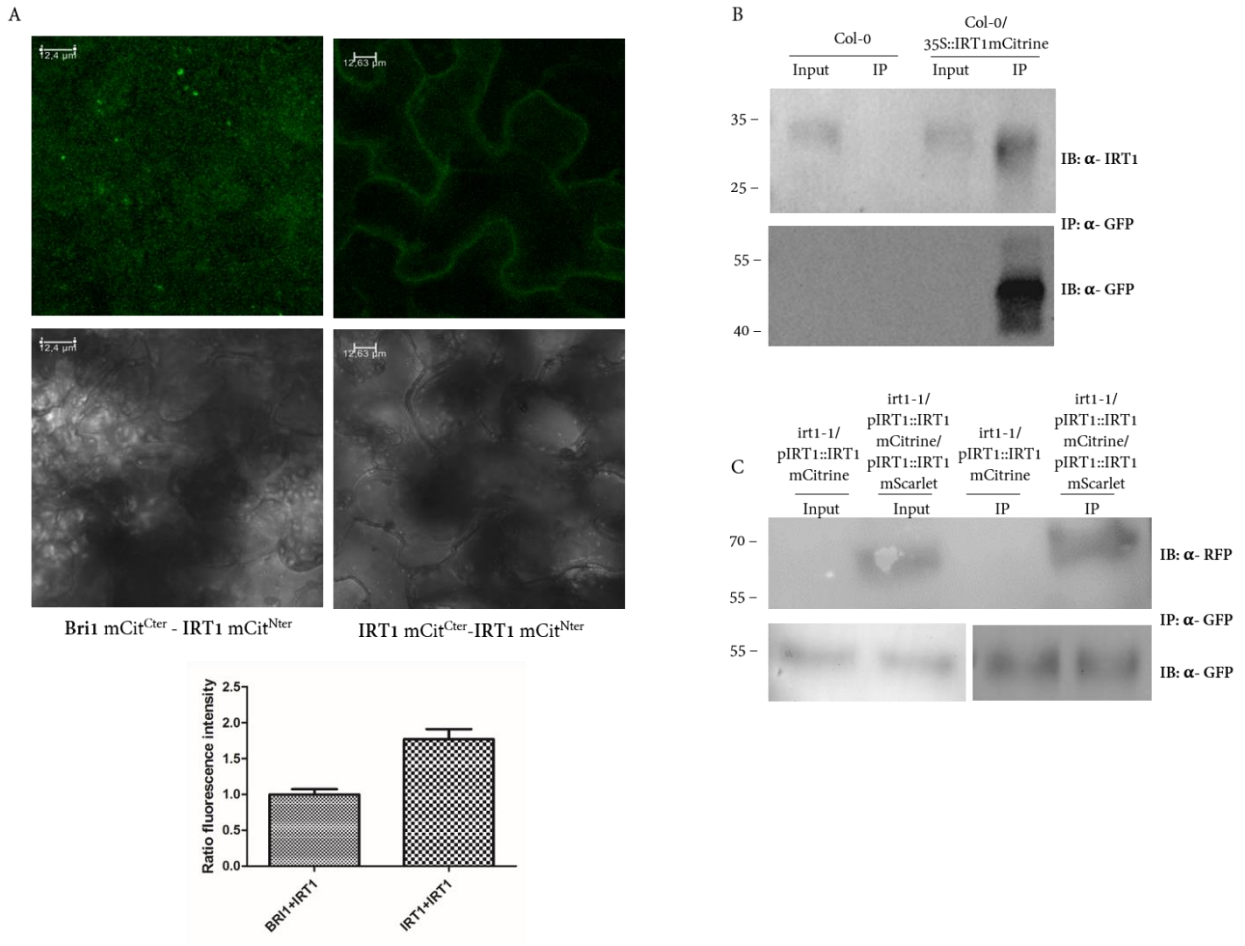

Figure 3-17 In planta oligomerization of IRT1. A) BiFC of IRT1+BRI1 and IRT1+IRT1. Quantification from two independent biological replicates with at least 5 technical replicates each, normalized to negative control. B) Co-immunoprecipitations of endogenous IRT1 and constitutively expressed IRT1mCitrine. 1) Roots of Col-0 WT plants. 2) Roots of Col-0/35S::IRT1mCitrine. C) Co-immunoprecipitations of IRT1mCitrine and IRT1mScarlet. 1) Roots of irt1-1/pIRT1::IRT1mCitrine plants. 2) Roots of irt1-1/pIRT1::IRT1mCitrine/pIRT1::IRT1mScarlet plants.

3.2 Metal-binding properties of the disordered loop from the Arabidopsis metal transceptor IRT1

Virginia Cointry[1], Nelly Morellet[2], Julie Neveu[1] and Grégory Vert[1, 3].

[1] Plant Science Research Laboratory (LRSV), UMR5546 CNRS/Université Toulouse 3, 24 chemin de Borde Rouge, 31320 Auzeville-Tolosane, France.

[2] Institut de Chimie des Substances Naturelles (ICSN), CNRS UPR 2301, Université Paris-Saclay, 91198 Gif sur Yvette cedex, France.

[3] Electronic address: Gregory.Vert@lrsv.ups-tlse.fr

3.2.1 Abstract

The Arabidopsis IRT1 transporter is a plasma membrane protein from plant root epidermal cells that constitutes the principal soil Fe uptake pathway. Besides Fe, IRT1 transports other non-Fe divalent metals such as Zn, Mn, Co and Cd. We previously reported that the second intracellular loop between transmembrane domains TM4 and TM5 is involved in the post-translational regulation of IRT1 by its non-iron metal substrates. Upon excess of these metals, IRT1 undergoes phosphorylation by the CIPK23 kinase, creating a docking site for the IDF1 E3 ubiquitin ligase that subsequently K63 polyubiquitinates IRT1. This triggers the vacuolar targeting and degradation of IRT1 to limit the overaccumulation of highly reactive non-iron metals. Interestingly, this metal-dependent downregulation of IRT1 requires the presence of four histidine (H) residues in the second intracellular loop. Initial biochemical characterization revealed that non-Fe metals bind to said H residues, allowing IRT1 to sense non-Fe metal levels thus acting as a transceptor controlling its own degradation. Here, we better characterize the metal binding properties and structure of this loop to shed light on the molecular basis of IRT1 response to non-iron metal excess. We demonstrate using microscale thermophoresis that the intracellular loop of IRT1 binds Zn in the micromolar range and Cd in the millimolar range through the four H residues, while binding affinities for Co and Mn could not be measured. Using circular dichroisms (CD) and NMR spectroscopy, we first uncovered that the IRT1 loop is unstructured in the absence and presence of metals. We confirmed by NMR the ability of H residues to coordinate metals, possibly with the help of aspartic acid (D) residue 173. Biochemical and genetic characterization however failed to confirm the role of D173 in metal binding by IRT1. Altogether, our data provides further evidence of how the second intracellular loop of IRT1 senses high cytosolic divalent metal concentrations and regulates the plasma membrane levels of IRT1.

3.2.2 Introduction

The first-row transition metal iron is the most abundant and used metal in cells (Waldron et al. 2009). Iron is widely used as a cofactor, participating in oxidation-reduction reactions. In plants, iron

is of great importance due to its involvement in respiration chains, chlorophyll synthesis and photosynthesis (Briat et al. 1995). In nature, iron is often unavailable to organisms because it is found as insoluble ferric compounds. Lack of this metal impacts deeply on plant growth and leads to chlorosis (Briat et al. 1995). On the other hand, an excess of iron is detrimental to cells due to its redox properties and participation in the Fenton reaction that leads to reactive oxygen species formation (Gratão et al. 2005). For these reasons, living organisms including plants need to tightly control metal uptake.

Dicotyledonous plants, such as *Arabidopsis thaliana*, developed acquisition mechanisms based on the solubilization and reduction of the soil ferric iron (Fe^{3+}) insoluble oxides into ferrous iron (Fe^{2+}). This is mediated by the AHA2 proton pump, involved in soil acidification together with the FRO2 ferric chelate reductase, which reduces Fe^{3+} to Fe^{2+} (Robinson et al. 1999; Connolly et al. 2003; Wu et al. 2005; Santi and Schmidt 2009). In Arabidopsis, the main transporter involved in the uptake of ferrous iron is the Iron Regulated Transporter 1 (IRT1) (Vert et al. 2002), one of the founding members of the family of ZIP transporters, widely distributed across all kingdoms of life (Guerinot 2000). The Arabidopsis IRT1 has a broad substrate range as it was shown to transport other essential divalent heavy-metals than ferrous iron, such as zinc, cobalt and manganese (Eide et al. 1996; Korshunova et al. 1999; Rogers, Eide, and Guerinot 2000; Vert, Briat, and Curie 2001; Vert et al. 2002; Barberon et al. 2011). The *irt1-1* knockout mutant plants are highly chlorotic and show growth impairment, a phenotype that can be reversed by the addition of high amounts of iron in watering solutions (Vert et al. 2002). IRT1 localizes to the plasma membrane and is strongly expressed in iron-deficient root epidermal cells (Vert et al. 2002; Barberon et al. 2011). This clearly points to the major role of IRT1 in soil iron acquisition. The chlorosis of *irt1* mutants is however not complemented by the other divalent metal substrates of IRT1, indicating that these constitute secondary substrates aspecifically transported by IRT1.

In recent years, the molecular mechanisms of the regulation of *IRT1* expression by its metal substrates was uncovered. Transcriptional regulation of *IRT1* involves a cascade of bHLHs transcription factors, where the major iron response regulator FIT heterodimerizes with other Ib bHLH transcription factors, and binds to the *IRT1* promoter upon iron deficiency (Colangelo and Guerinot 2004; Yuan et al. 2008; Sivitz et al. 2012; Selote et al. 2015; Zhang et al. 2015; Li et al. 2016; Liang et al. 2017). More recently, a post-translational regulation of *IRT1* by its non-iron metal substrates Zn, Mn and Co has been reported. Non-iron metal availability indeed regulates the subcellular localization of IRT1. In the absence of non-iron metals, IRT1 sits at the cell surface to take up low available iron. Increasing non-iron metals levels leads to partial IRT1 internalization in early endosomes as a result of its multimonoubiquitination on lysine residues K154 and K179 by a yet to be characterized E3 ubiquitin ligase (Barberon et al. 2011). Higher non-iron metal levels trigger IRT1 phosphorylation by the CIPK23 kinase and the recruitment of the E3 ubiquitin ligase IDF1 (Dubeaux et al. 2018). IDF1 elongates monoubiquitin moieties into K63 polyUbiquitin chains, thus leading to IRT1 targeting to the vacuole for degradation. Fe availability has however no influence on IRT1 protein localization (Barberon et al. 2011; Dubeaux et al. 2018).

The cytosolic loop of IRT1 located between transmembrane domains 4 and 5 has been shown to bind metals in vitro (Dubeaux et al. 2018). A remarkable characteristic of IRT1 and related transporters is the presence of a PHGHGHGHGP motif at the center of such loop. Inductively coupled plasma mass spectrometry (ICP-MS) confirmed the ability of these H residues to bind Zn and Mn in vitro (Dubeaux et al. 2018). Such repetition of H has also been shown to be required for the non-iron metal dependent endocytosis of IRT1 as an $IRT1_{4HA}$ mutant version fails to be degraded upon metal excess (Dubeaux et al. 2018). Metal binding to H residues was shown to drive the recruitment of CIPK23 and IRT1 endocytosis (Dubeaux et al. 2018).

To obtain mechanistic insight into how IRT1 binds and senses non-iron metals and how does that mediate the recruitment of CIPK23, we biochemically characterized the metal binding and structure of IRT1 intracellular loop. We provide further evidence that this loop binds Zn and Cd in vitro using the four H residues while affinities towards Mn and Co were not possible to measure. Furthermore, we provide evidence that the loop of IRT1 is a disordered domain, both in absence and presence of metals with the presence of a rigid turn involving an AVGI motif. We also characterized the possible contribution of residue D173 to metal coordination. Overall, our work provides additional biochemical and structural insight into the ZIP family of metal transporters.

3.2.3 Results

3.2.3.1 The regulatory loop of IRT1 is disordered

To have a first glance at the structural characteristics of the IRT1 loop, we decided to perform far-UV circular dichroism (CD) on a chemically synthesized peptide corresponding to the intracellular loop located between TM4 and TM5 of IRT1. The ^{143}DSMATSLYTSKNAVGIMPHGHGHGHGPANDVTLPIKEDDSSN^{186} peptide sequence encompasses all important residues required for phosphorylation, ubiquitination and contains the four H residues that have been previously associated to metal binding and sensing (Dubeaux et al. 2018). Typical tridimensional structures as beta sheet and alfa helixes give positive ellipticity signals at around 190 and 200 nm respectively, and negative signals at 210-220 nm. Here, spectra recorded from 190 to 240 nm in pH 6.7 at room temperature showed a spectrum typical of a peptide in a random coil conformation, with a single negative peak at 198 nm (*Figure 3-18*A).

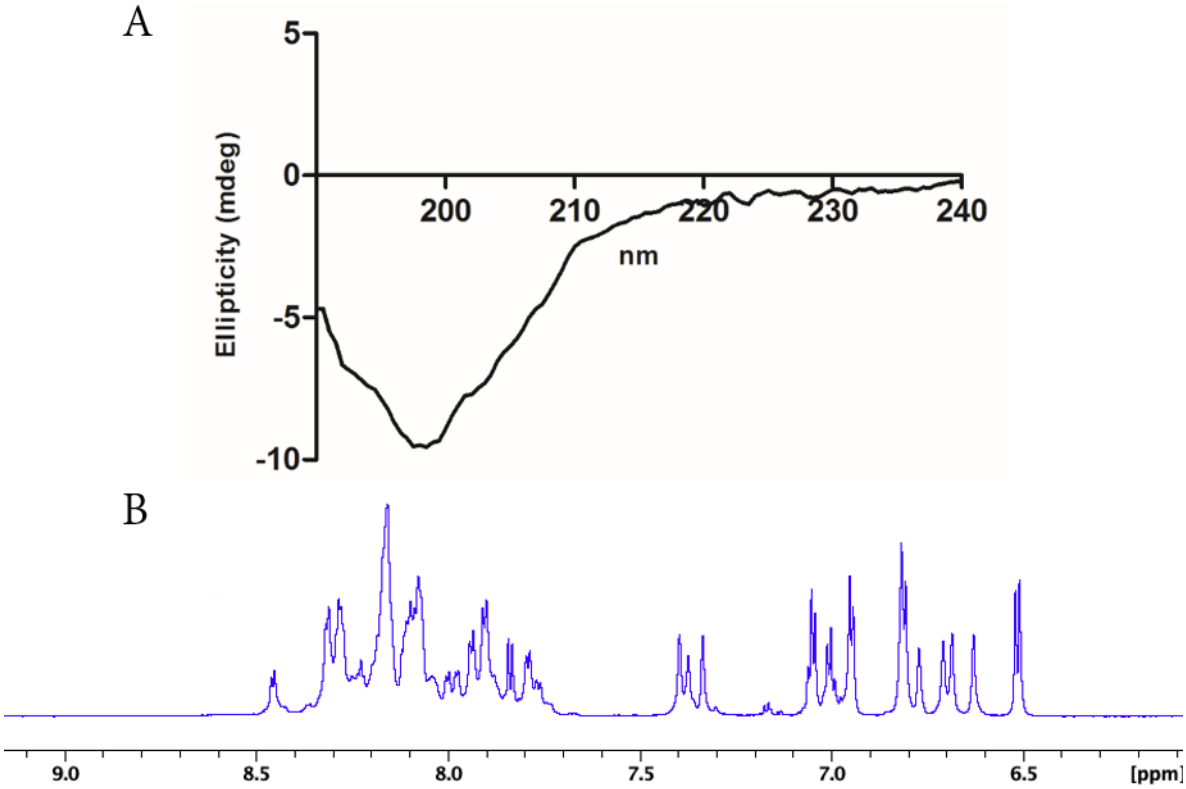

Figure 3-18 IRT1loopWT is a disordered peptide A) Far-UV circular dichroism spectra of the IRT1loop at 25µM in 10mM Tris pH 7 from 190 to 240 nm. Corrections of the final peptide concentrations were done with each addition of Zn. B) 1D ^{1}H spectra of the IRT1 loop peptide recorded at pH 6.7, 5°C, on a 800 MHz spectrometer. Only the amide and the aromatic proton are shown.

To obtain deeper insight into the structure of the IRT1 loop, we turned to NMR spectroscopy, which allow us to obtain atomic resolution data unlike CD. One dimension (1D) ^{1}H NMR spectra were recorded at pH 6.7 in the absence of metals. In accordance with the CD data obtained, 1D ^{1}H NMR spectra were poorly dispersed, a characteristic of peptides in random coil conformations (*Figure 3-18* B). Furthermore, two dimension (2D) H^{1}-H^{1} NOESY spectra of the IRT1 loop, showed that despite our previous observations of the peptide adopting a rather unstructured conformation, medium-range NOEs observed here, indicate the presence of a turn involving the ^{155}AVGI^{160} hydrophobic residues (α156/HN159, α157/HN159) (*Figure 3-19* A). Also, we observed that the cross peak intensities of the histidine-rich domain of the IRT1 loop decreased relative to the other signals of the peptide, resulting probably from chemical exchange (*Figure 3-19* B).

Despite the lack of clear secondary structure, we generated structures using the NOE-derived distance restraints with the program CYANA. As expected, except for the ^{155}AVGI^{160} turn (*Figure 3-19* C), no secondary structure was observed.

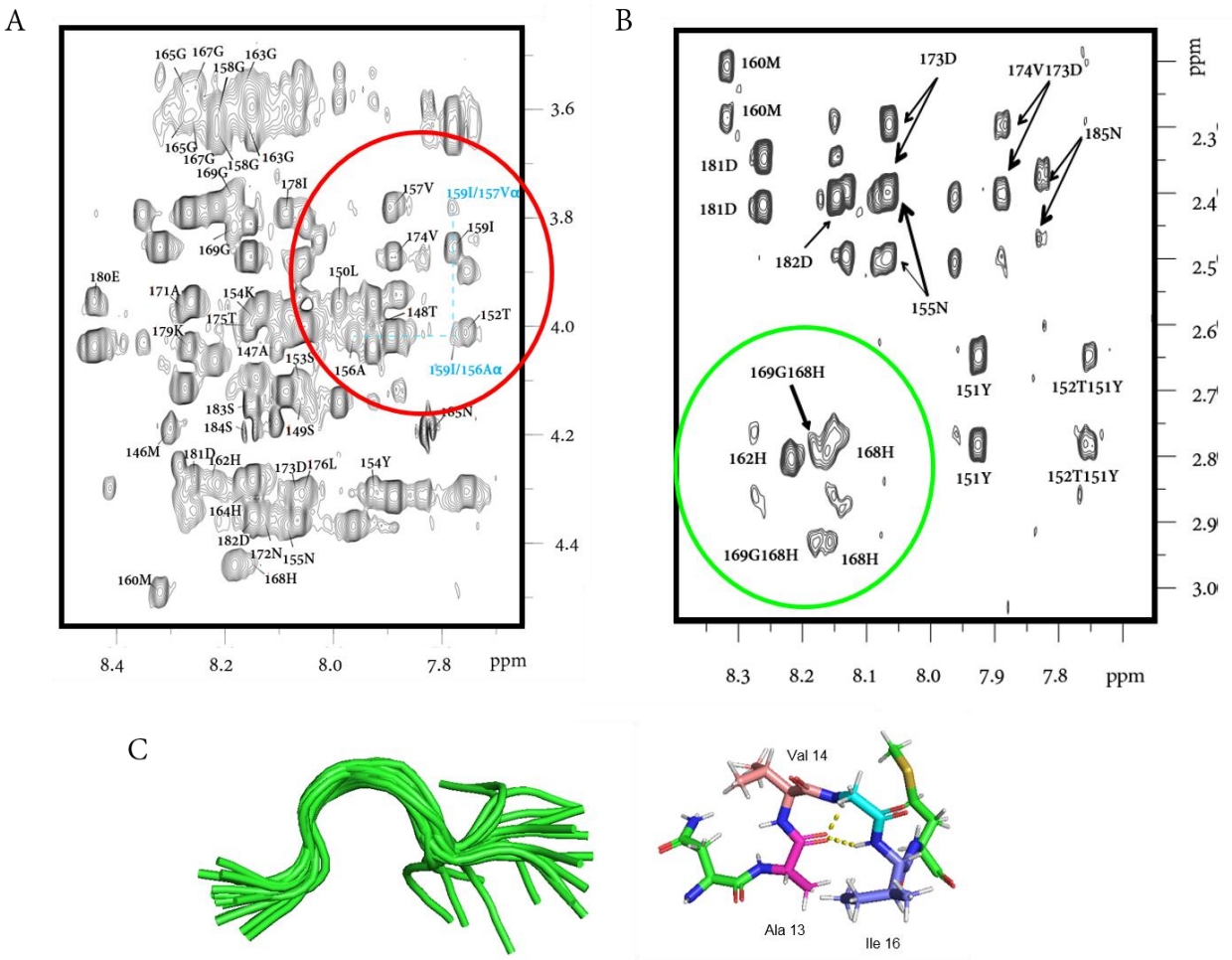

Figure 3-19 Residues AVGI make a turn in the loop of IRT1. A) Select region of the NOESY spectra recorded on 500 µM of IRT1 loop at pH 6.7, 5°C, 150mM NaCl at 800MHz. The labels in black indicate the HN(i),Hα(i) correlations, and in blue those corresponding to the HN(i),Hα(i-2) and HN(i),Hα(i-3) of Ile159, the latter indicated in the red circle B) Selected regions of the NOESY spectra recorded on the wild-type IRT1 loop peptide. The green circle indicates histidine resonances. The spectra was recorded from 500 µM of the peptides in buffer at pH 6.7 and 150mM NaCl, at 5°C on an 800 MHz spectrometer. C) Superimposition of the structures of the IRT1 loop calculated by the program CYANA (green). The turn involving the three hydrophobic residues: Ala13, Val14 and Ile16 in licorice representation.

We observed that the histidine-rich domain can exist as loops or more extended conformations with several possible orientations of the histidine residues relative to each other (*Figure 3-19* C and *Figure 3-20*). Moreover, in several structures, D173 is located at the proximity of the histidines (*Figure 3-20*). Interestingly, the C-terminal end of the loop appears to be more mobile than the N-terminus. This might, however, not be of biological relevance, given that the loop is constrained by its adjacent transmembrane domains.

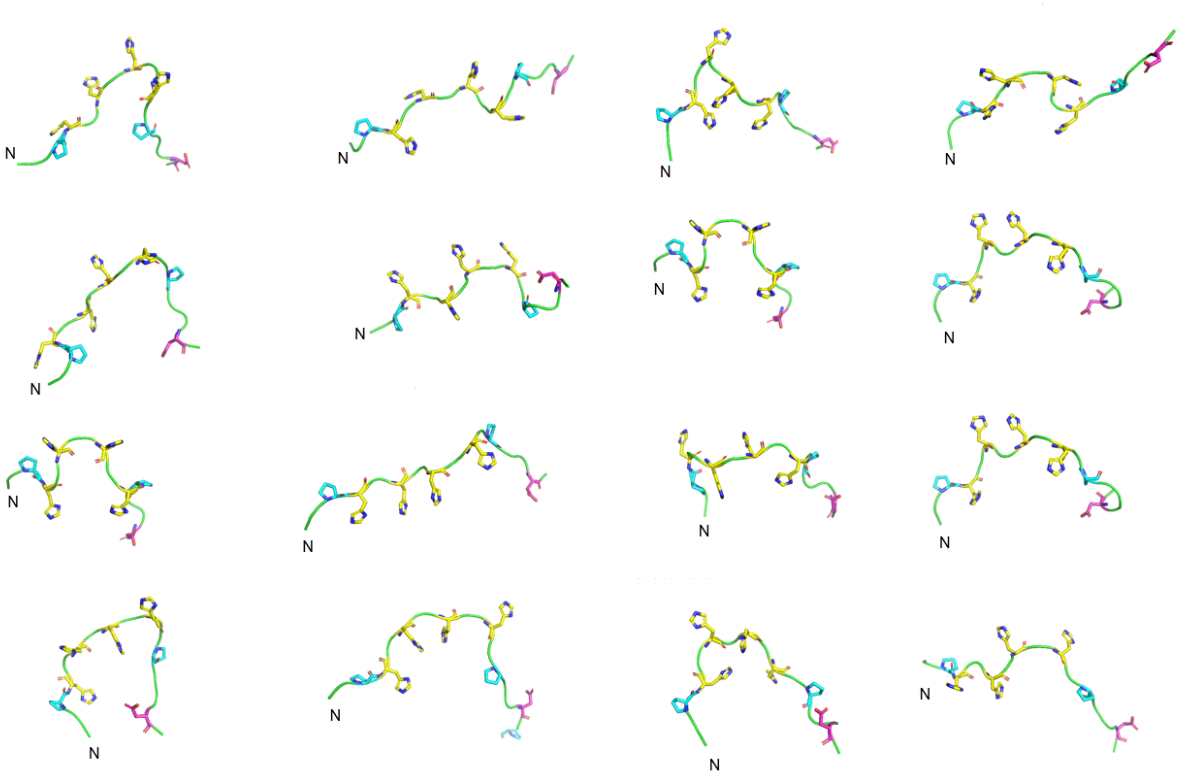

Figure 3-20 Structures of the histidine-rich domain showing the many possible orientations of the histidine residues relative to each other. Histidines are represented in yellow, prolines in blue and aspartic acid 30 in pink.

3.2.3.2 Impact of metal binding on the structure of IRT1 loop

In order to determine whether the structural properties of the loop were impacted by interaction with the secondary metal substrates of IRT1, we performed a titration by sequential equimolar additions of Zn^{2+} on the peptide followed by recording of CD spectra (*Figure 3-21* A). With each addition of Zn^{2+}, the final concentration of the peptide was corrected to avoid dilution effects. We observed a saturable increase in ellipticity with each addition of the substrate but the overall shape of the spectra remained the same. In particular, no evidence of typical structures such as alfa-helixes or beta sheets appeared. Overall, binding of Zn^{2+} did not seem to impact on the secondary structure of the IRT1 loop as visualized by CD. Similarly, 1D H^1 NMR spectra in presence of Zn^{2+} showed a similar dispersion of the signals to the spectra recorded in absence of the metal, again suggesting that even in presence of Zn^{2+}, the peptide remains disordered (*Figure 3-21* B).

To obtain a deeper understanding of the molecular interaction of the IRT1 loop with its substrates, H^1-H^1 NOESY spectra of the IRT1 peptide were recorded at pH 6.7 in the absence of metal substrates and in the presence of 2 equimolar Zn^{2+}. Superimposition of these spectra indicated that the histidine-

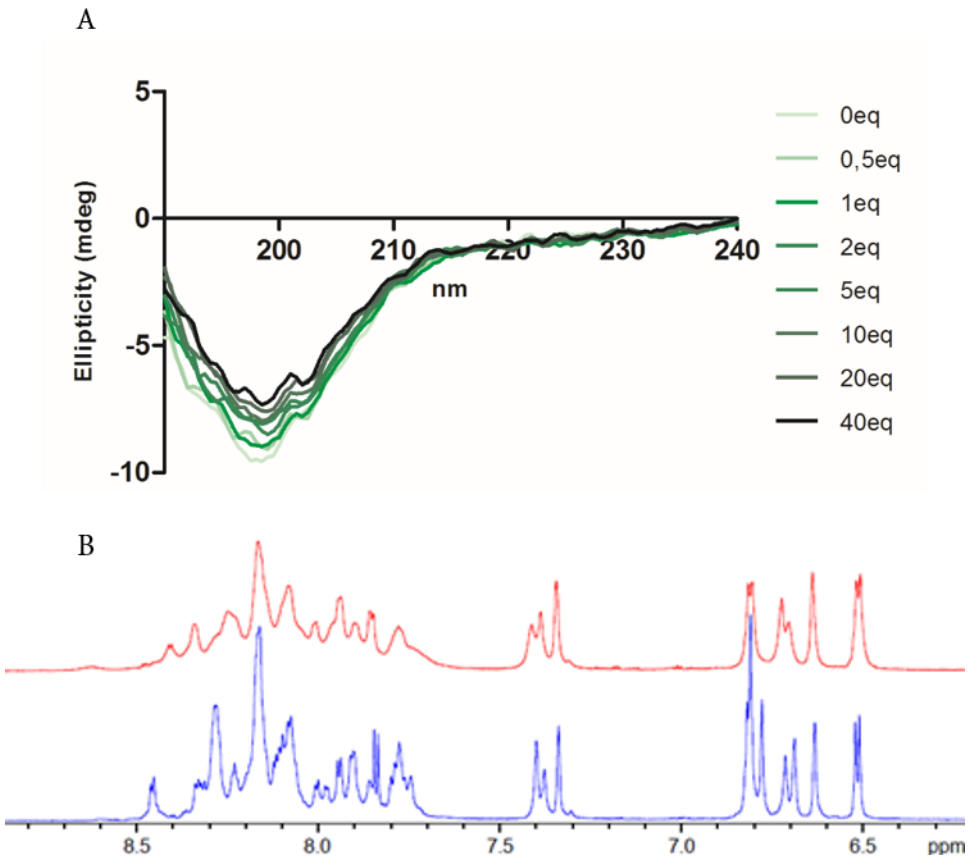

Figure 3-21 IRT1loopWT is a disordered peptide in presence and absence of Zn. A) Far-UV circular dichroism spectra of the IRT1loop from 190 to 240 nm. Additions of 0 to 40 equivalents of Zn were added to a 25µM solution of the peptide in 10mM Tris pH 7. Corrections of the final peptide concentrations were done with each addition of Zn. B) 1D ^{1}H spectra of the IRT1 loop peptide recorded in absence (blue) and presence (red) of Zn at pH 6.7, 5°C, on a 800 MHz spectrometer. Only the amide and the aromatic proton are shown.

rich fragment of the IRT1 loop is implicated in binding of Zn^{2+}, since all the proton resonances of this motif (162H, 164H, 166H and 168H) disappeared upon addition of Zn^{2+} (*Figure 3-22* A). Further analyzes of our data indicated that signals corresponding to an aspartic acid residue (D173) located to the right of the histidine stretch behaved in a similar manner to the histidines (*Figure 3-22* A), disappearing after addition of Zn^{2+}, suggesting a possible implication in metal coordination.

To better characterize the role of individual histidine residues and the mentioned aspartic acid (D173) present in the wild type loop, we decided to also record H^{1}-H^{1} NOESY spectra of different mutants. We designed three mutants on the PHGHGHGHGP motif where histidines were replaced with phenylalanine, threonine or asparagine, in order to remove the charges on this sites and maintain the structure of the residue; and a mutant where aspartic acid 173 was replaced by asparagine, as illustrated in *Figure 3-22*. We observed that in presence of Zn^{2+}, the line width for all the peptides increased drastically (*Figure 3-22* A, B, C, E) except for the mutant peptide with four mutated histidines (*Figure 3-22* D). Broadening of the signals indicate that the metal-bound loop undergoes dynamic interchange among different metal-bound states. Interestingly, the mutants with only the two first or two last histidines of the stretch mutated to uncharged residues, are still able to complex Zn^{2+}. Conversely, when

the four histidines are mutated, the peptide no longer has the ability to complex Zn^{2+}. These results suggest that either the histidines constitute a single binding site where at least two histidines are required for metal binding or that there are two binding sites formed by residues 162H/164H and 166H/168H respectively. The latter is rather improbable given that complexing of Zn^{2+} normally requires four amino acid ligands (Laitaoja, Valjakka, and Jänis 2013). Furthermore, when replacing the aspartic acid in position 173 with the uncharged amino acid asparagine, the signal no longer responded to addition of Zn^{2+} (*Figure 3-22* E), suggesting that aspartic acid 173 is indeed involved in metal binding.

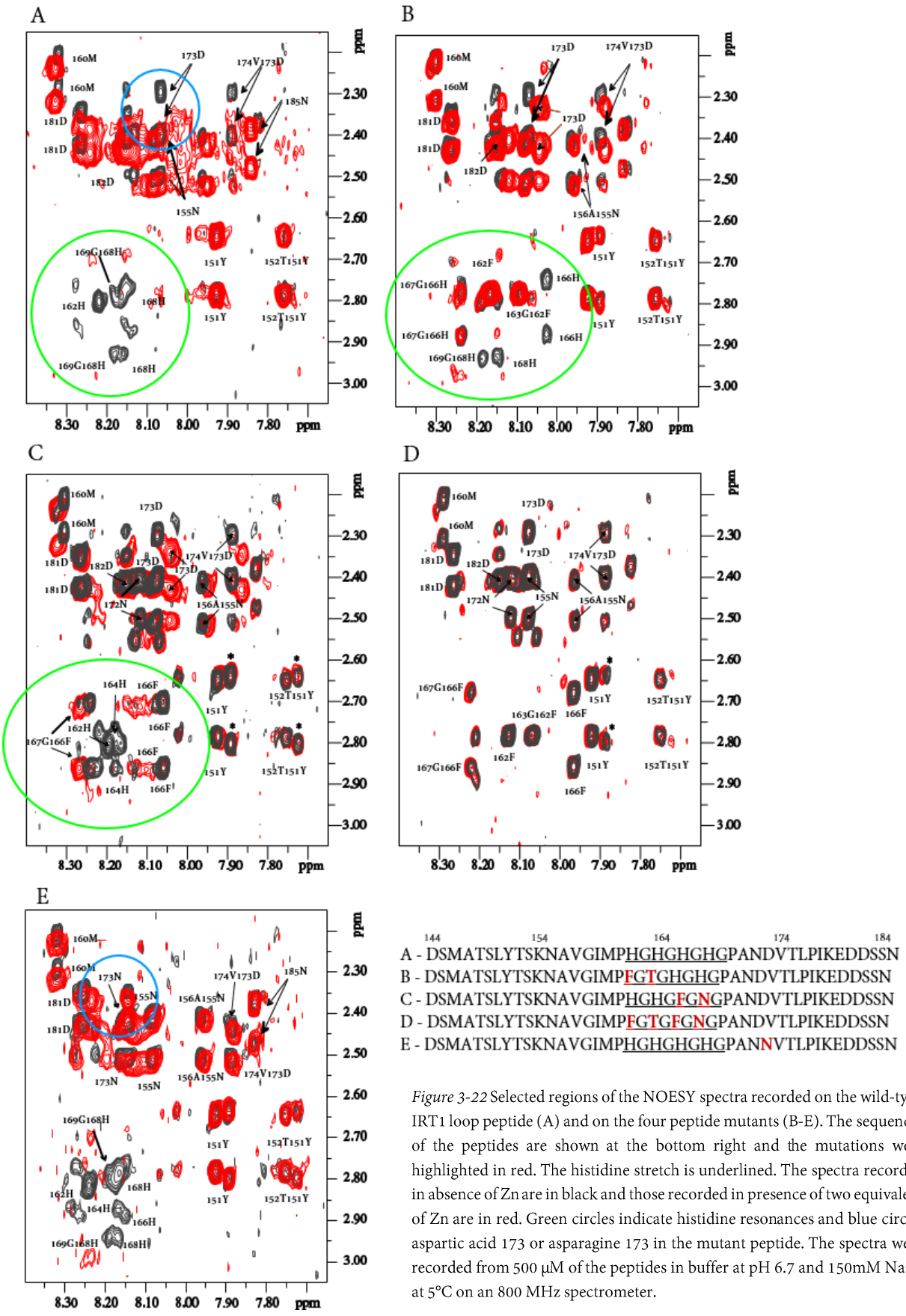

Figure 3-22 Selected regions of the NOESY spectra recorded on the wild-type IRT1 loop peptide (A) and on the four peptide mutants (B-E). The sequences of the peptides are shown at the bottom right and the mutations were highlighted in red. The histidine stretch is underlined. The spectra recorded in absence of Zn are in black and those recorded in presence of two equivalent of Zn are in red. Green circles indicate histidine resonances and blue circles aspartic acid 173 or asparagine 173 in the mutant peptide. The spectra were recorded from 500 µM of the peptides in buffer at pH 6.7 and 150mM NaCl, at 5°C on an 800 MHz spectrometer.

Finally, we analyzed the chemical shift variations in the absence and in the presence of 2 equimolar Zn^{2+} of each residue. Here, we found that the residues located to the left of the histidine-rich fragment are very little affected by Zn^{2+} binding, whereas those located on the right undergo significant chemical shift variations (*Figure 3-23* A). The same behaviour is observed for the peptides with mutations on two histidines and for the aspartic acid mutant (*Figure 3-23* B, D, E), although less intense than for the wild-type peptide. As expected, the peptide with the four histidines mutated presented no chemical shift variation (*Figure 3-23* C). These results are in line with the structural models calculated with the software CYANA, where residues to the right of the histidines are more mobile that the rest of the loop in solution. Whether this property is present in the full length protein remains unanswered.

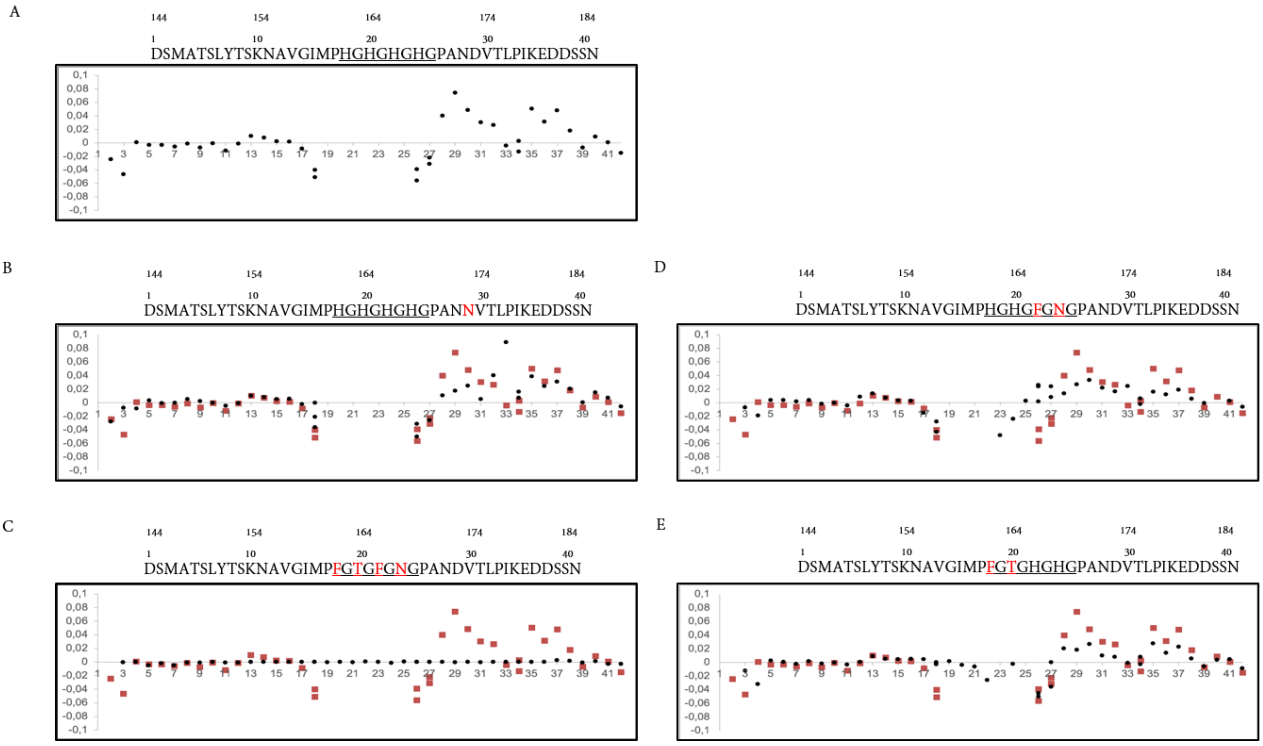

Figure 3-23 Chemical shift variations in presence and absence of two molar equivalent of Zn of WT and mutants. Sequences of the peptides are indicated on the top of each graph. A) Chemical shift variation of the WT, B) to E) Superimposition of chemical shift variations of mutant (black) and WT (red) peptides.

3.2.3.3 Metal binding affinities of IRT1 variable loop

To quantify the binding affinity of metals transported and sensed by IRT1, a binding curve for Zn^{2+} was first obtained by plotting changes in ellipticity at 198 nm from CD experiments against the concentration of ligand (*Figure 3-24* A), as done before for other proteins (Hussain and Siligardi 2016). The measured values were fitted to a one-site binding model with GraphPad Prism. A value of Kd of 15.91 ± 7.3 µM was obtained in this way. However, this value may be statistically irrelevant since only one data set was recorded in CD at that stage.

In order to precisely quantify the interaction between the IRT1 loop and non-iron metals, and further confirm observations from CD experiments and from ICP-MS previously reported (Dubeaux et

al. 2018), we performed microscale thermophoresis (MST) experiments using the technology from Nanotemper. Here, fluorescently labelled molecules are subjected to increased concentrations of a ligand, and their thermophoresis properties are measured while a temperature gradient is applied over time. Recombinant fusion proteins harboring an MBP affinity tag at the N-terminus of the loop of IRT1 (MBP-IRT1loop) and a mutant version of this protein carrying substitutions of the four central histidine residues to alanine (MBP-IRT1loop4HA) were overexpressed in *Escherichia coli*. The proteins were purified by affinity to an amylose resin, washed with an EDTA-containing buffer in order to remove putative bound metals, and eluted in HEPES 10mM pH 7, NaCl 150mM buffer that is compatible with MST assays. The MBP-IRT1loop fusions were fluorescently labelled with an NH2 binding probe in the MBP domain, in order to avoid interference of the probe with the metal ligand. We first used Zn as substrate, as it was shown to bind to IRT1 peptide and its excess drives IRT1 endocytosis. As suggested by Nanotemper, a constant concentration of the peptide was titrated with a one in half serial dilution of the ligand, $ZnCl_2$ in this case, and thermophoresis was measured. The binding affinity of the MBP-IRT1loop protein was determined at 15 ± 5.8 μM when fitted to the Kd model (*Figure 3-24* B), assuming a 1:1 stoichiometry of reaction. Data was obtained from three independent protein labelling reactions with at least two technical replicates each time. The value obtained here was almost identical to that obtained from the CD data. Binding tests performed with mutant peptide for the four H residues (MBP-IRT1loop4HA) indicated no binding. Despite this, mutant data points were recorded and revealed that they did not fit to a binding curve, demonstrating that the histidines in this stretch are absolutely essential for metal binding (*Figure 3-24*).

Furthermore, we decided to test binding of the non-iron metals Co, Mn and Cd, previously reported to being transported by IRT1 (Eide et al. 1996; Korshunova et al. 1999; Rogers, Eide, and Guerinot 2000; Vert, Briat, and Curie 2001; Vert et al. 2002; Barberon et al. 2011) (*Figure 3-25*). Binding of such metals to the PHGHGHGHP motif had already been previously assessed by isothermal titration calorimetry (ITC) (Grossoehme et al. 2006). Our MST approach however failed to measure binding affinities of the IRT1 loop to Co and Mn consistently, since data points obtained for both metals failed to fit to a binding

A

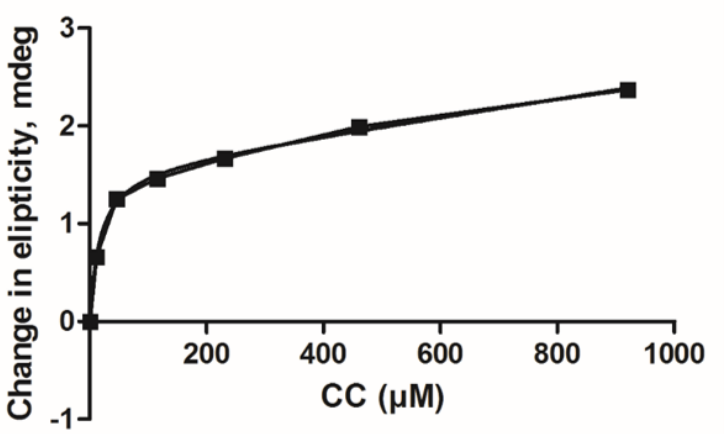

Target Name	Ligand Name	Kd	Kd Confidence	Std. Error	R^2
• IRT1loopWT	ZnCl2	15.91 µM	7,305 µM	2,25	0,9987

B

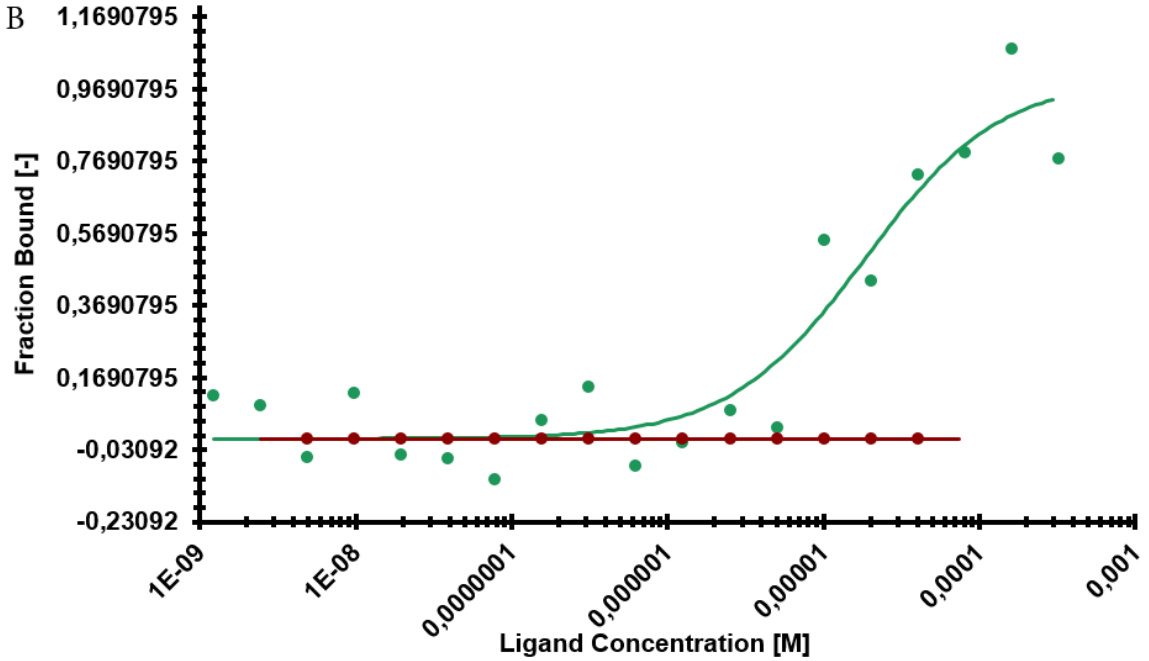

Target Name	Ligand Name	Kd	Kd Confidence	Std. Error of Regression	Signal to noise ratio
• IRT1loopWT	ZnCl2	15 µM	5,85 µM	0,41	9,05

Figure 3-24 Binding affinity of IRT1 for Zn. A) Change in ellipticity from CD data. Titration on 20µM IRT1 synthetic peptide in Tris pH 7 at 25°C. Data was fitted to a one site binding model with Graphpad prism. Calculated parameter of the fit are shown at the bottom of the graph. B) Microscale thermophoresis of IRT1loopWT (green) and IRT1loop4HA (red). Dots represent the average dose response of biological duplicates with technical duplicates each.

model. However, measures for Cd did fit to a Kd model, with a 1:1 stoichiometry, as previously done for Zn. The Kd for Cd was determined at 4.44 ± 1.47 mM. These results are in accordance with affinities measured by ITC, where it was determined that the histidine stretch of IRT1 was able to bind several metals with relative stabilities in accordance to the Irving-Williams series (Grossoehme et al. 2006). Furthermore, the MBP-IRT1loop4HA mutant peptide failed in binding Cd, indicating that the observed binding is indeed related to the histidine stretch (data not shown).

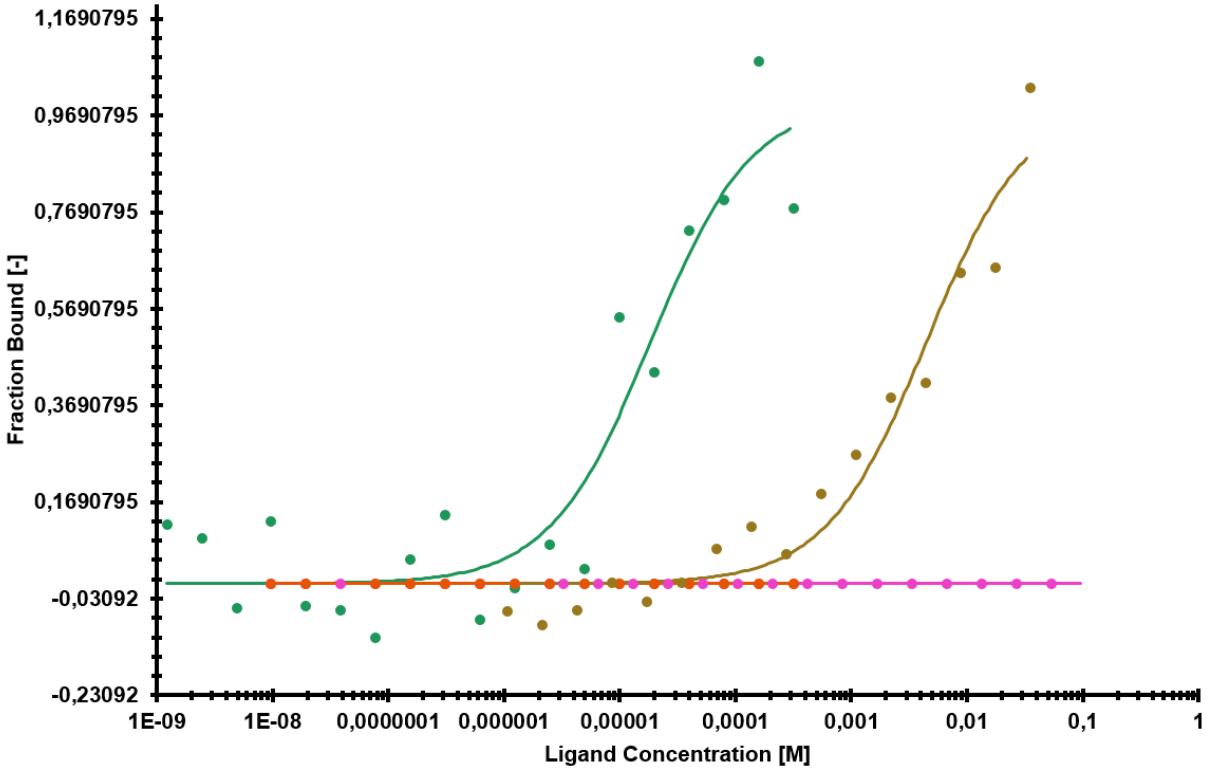

Target Name	Ligand Name	Kd	Kd Confidence	Std. Error of Regression	Signal to noise ratio
IRT1loopWT	ZnCl2	15 µM	5,85 µM	0,41	9,05
IRT1loopWT	CdCl2	4,44 mM	1,47 mM	1,24	13,17

Figure 3-25 Binding affinity of IRT1 for different non-iron metals determined by Microscale thermophoresis. The affinity of the IRT1loopWT for Zn (green), Cd (brown), Mn (pink) and Co (orange) was measured and fitted to a Kd model. Dots represent the average dose response of biological replicates with technical duplicates each.

3.2.3.4 Analysis of the role of aspartic acid 173

Having established the affinity of the loop for the substrate metals of IRT1, we decided to investigate whether residue D173 contributes to metal coordination and to responses to metal excess. In particular, because of the potential implication of aspartic acid 173 (D173) in metal binding revealed by NMR, and the particular position it is predicted to adopt with respect to the histidine stretch, we wondered the importance of this amino acid in the context of the full-length protein in planta. To analyze this, we took advantage of the previously reported fluorescently tagged version of IRT1, here called

IRT1mCitrine, which has been demonstrated to complement the *irt1-1* knockout Arabidopsis plants and a yeast mutant defective in high and low-affinity iron uptake, Δ*fet3*Δ*fet4*. A point mutation was therefore introduced in the loop of IRT1 to replace aspartic acid 173 with asparagine. This mutant protein, called $IRT1_{D173N}$, was expressed in the *irt1-1* Arabidopsis knockout line under control of the endogenous pIRT1 promoter (pIRT1::$IRT1_{D173N}$mCitrine). The obtained homozygous plants showed a chlorotic and growth impaired phenotype similar to *irt1* mutants, as seen by the measured chlorophyll content and root length (*Figure 3-26*). RNA and protein levels were assessed in order to determine whether the lack of complementation came from compromised *IRT1* expression. For Arabidopsis lines, here called 6.4 and 13.8, both RNA and $IRT1_{D173N}$mCitrine protein levels were comparable to the previously reported IRT1mCitrine complemented line (*Figure 3-27*). The chlorotic phenotype of $IRT1_{D173N}$mCitrine-expressing plants could be reversed by addition of Fe excess to the watering solution (data not shown). All these observations were signs of a lack of complementation by the mutant protein, although being expressed to wild-type levels.

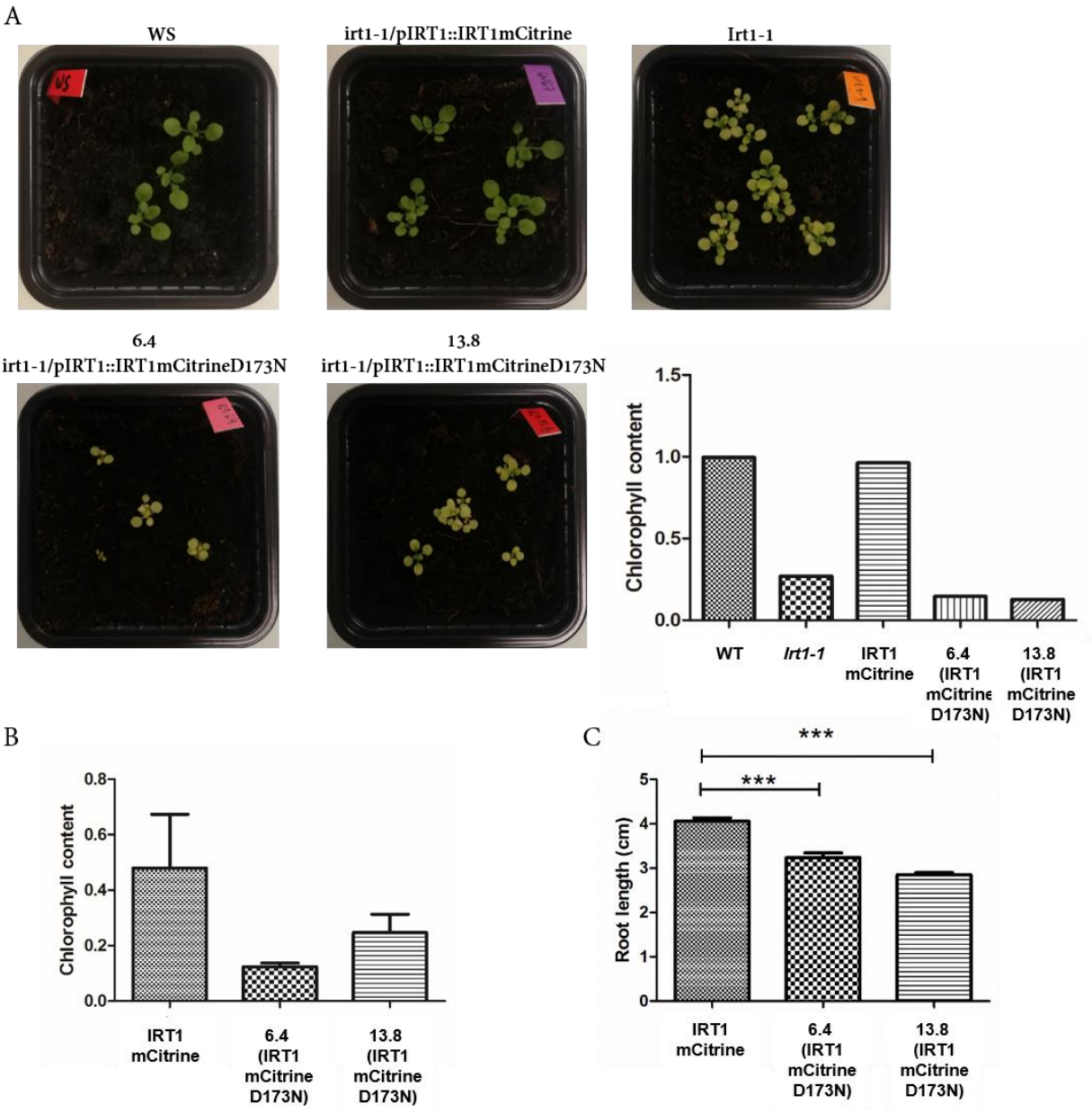

Figure 3-26 IRT1mCitrineD173N is unable to complement the *irt1-1* Arabidopsis knockout line. Mutant plants were transformed by floral dipping and selected by screening according to antibiotic resistance. A) Homozygous plants were grown in soil in parallel to wild type plants (WS), a complemented line expressing IRT1mCitrine and the *irt1-1* mutant. Chlorophyll content was measured from soil grown plants. B) Chlorophyll content was measured from aerial tissue recovered from plants grown for 12 days in square plates on MS/2 media lacking iron. Statistical analyses was done from biological duplicates with n=2. C) Root length was measured from scanned plates grown for 12 days in square plates on MS/2 media lacking iron. Statistical analyses was done from biological duplicates with n=30.

To decipher if the lack of complementation arose from improper subcellular localization of $IRT1_{D173N}$, confocal imaging of 15-day old plant roots vertically grown in square plates in iron-deficient media was carried out. These experiments revealed that the localization of the $IRT1_{D173N}$ protein was different from wild-type IRT1. $IRT1_{D173N}$ indeed localized to intracellular structures resembling the endoplasmic reticulum (ER) while wild-type IRT1 was observed at the plasma membrane and endosomes as previously reported (Barberon et al., 2011 ; Dubeaux et al., 2018) (*Figure 3-28*). Co-

localization with an appropriate ER marker will have to be performed to corroborate this observation. We, therefore, reasoned that lack of complementation was due to the mislocalization of the $IRT1_{D173N}$ protein.

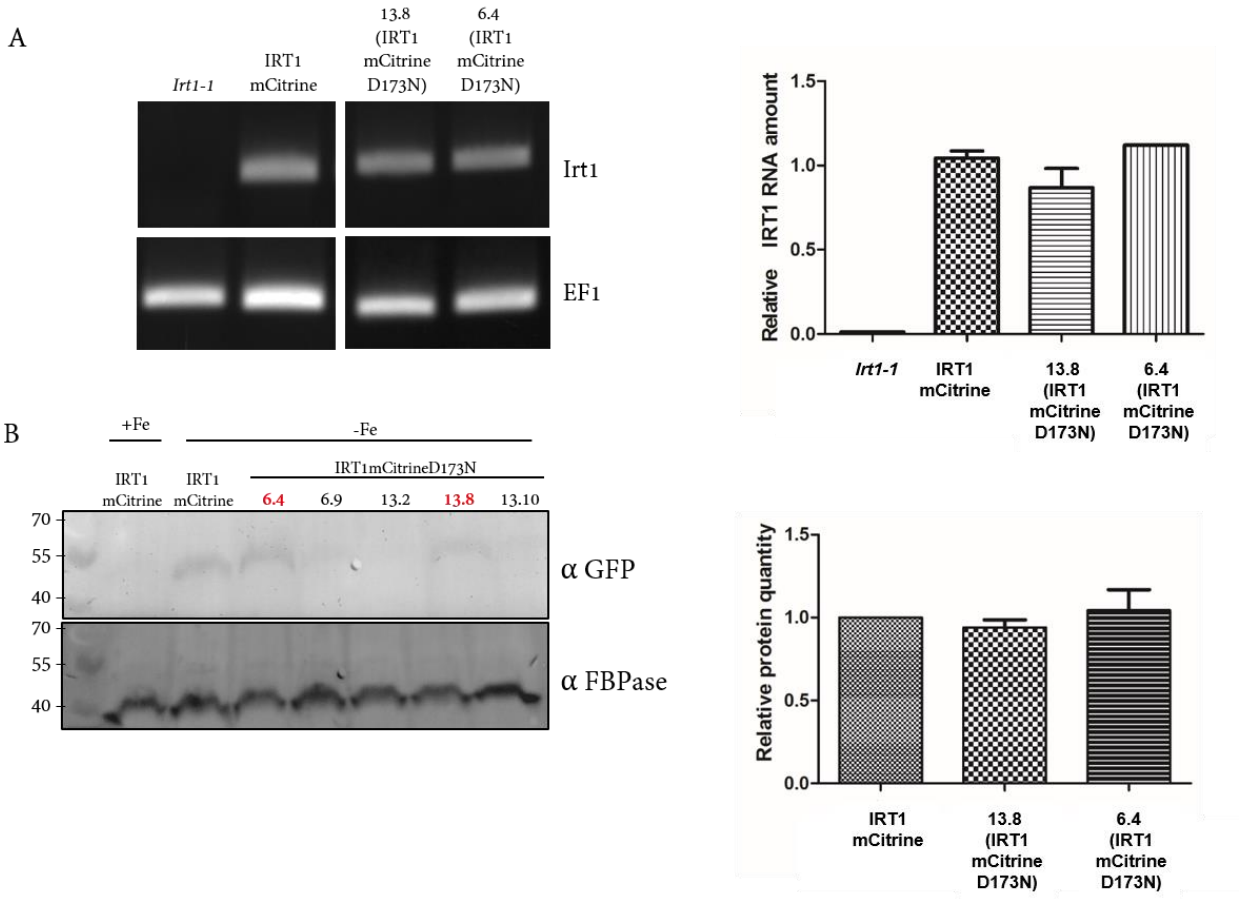

Figure 3-27 IRT1mCitrineD173N is expressed to similar levels of the complemented line. A) RNA was extracted from roots of 12 day old plants grown in MS/2 media vertically grown in square plates. RT-PCR was performed on these samples to amplify sequences on the irt1 and elongation factor 1 (EF1) as a housekeeping control. Quantifications were done relative to the housekeeping gene. Error bars represent duplicates. For line 6.4 a single value was measured. B) Total protein was extracted from roots of plants vertically grown for 12 days in MS/2 media. Total protein samples were run on SDS-PAGE and immunoblotted n PVDF membranes with GFP antibodies recognizing mCitrine and anti-FBPase antibody recognizing the constitutively expressed FBPase as a control. Quantifications were done relative to the IRT1mCitrine complemented line.

To further determine whether the D173N mutation renders the protein functional or not, we expressed the $IRT1_{D173N}$ mutant protein under control of a constitutive promoter in the yeast *Δfet3Δfet4* mutant, deleted for the high and low iron affinity uptake mechanisms. Yeast cells transformed with the empty vector as a negative control, the wild type IRT1 as positive control and the $IRT1_{D173N}$ mutant, were grown for 3 days in selective media containing 0, 25 or 50 μM Fe-EDTA to prove protein functionality (*Figure 3-29*). Yeast expressing the $IRT1_{D173N}$ protein grew to the same extent as yeast carrying the wild type IRT1 protein in low iron media, meaning that $IRT1_{D173N}$ is actually functional for metal transport. We speculated that this discrepancy between the observed complementation of yeast but not of plants could be due to the fact that the $IRT1_{D173N}$ expression in yeast was carried under a

constitutive promoter, and that the overexpressed protein escapes the ER quality control to localize to the plasma membrane and mediate metal transport.

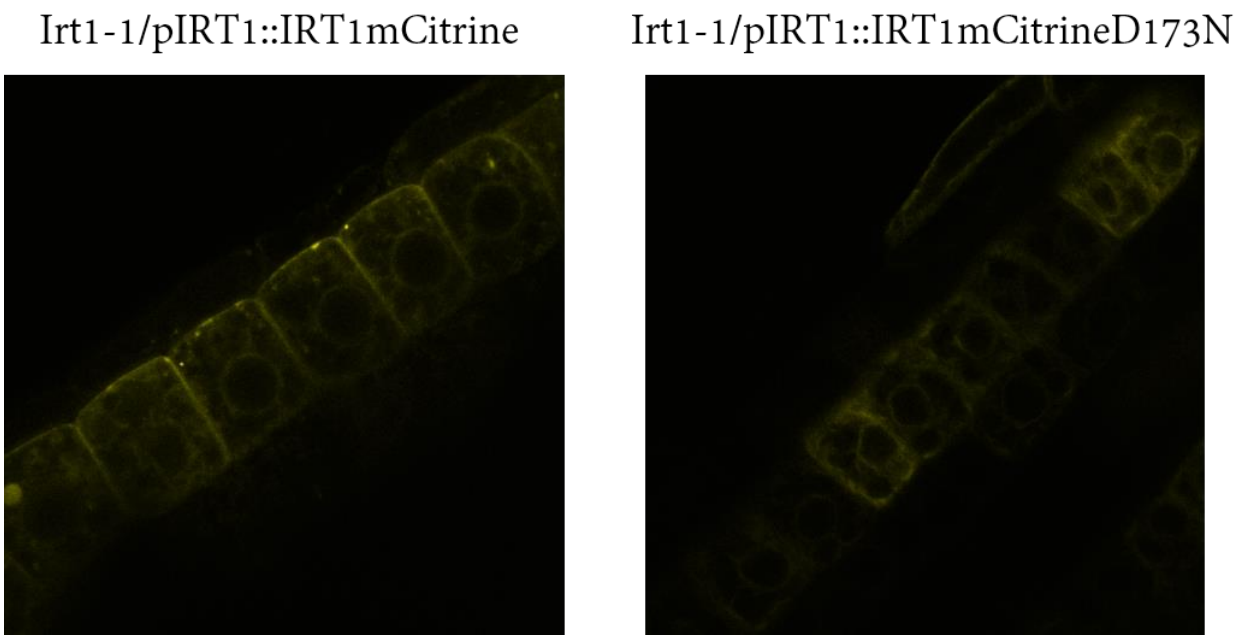

Figure 3-28 Confocal imaging of roots of 15 day old plants vertically grown in MS/2 in absence of iron showing the subcellular localization of the fluorescently tagged proteins.

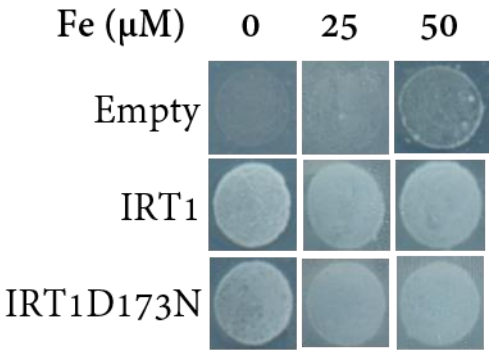

Figure 3-29 Complementation of the *Δfet3Δfet4* yeast strain deficient in iron uptake, by the IRT1 wild type and the IRT1D173N proteins. Yeast transformed with the empty vector were plated as a negative control. Three independent colonies of each were plated in this conditions. The figure shows representative colonies.

To inquire about the role of the D173 residue, we finally generated and purified a recombinant protein fusion of the loop with aspartic acid 173 replaced by asparagine, with the same methodology described above for the wild type and histidine mutant loops. As done previously for the wild type and four histidine mutant peptides, the MBP-IRT1$_{D173N}$ mutant loop fusion was labelled with a fluorescent probe on the NH2 end, and subjected to microscale thermophoresis. The IRT1loop wild type peptide was used as a control. Binding curves for Zn^{2+} were determined in the same concentration range as the previous experiments and fitted to the Kd model, considering a stoichiometry of 1:1. Superimposition

of the binding curves obtained for the mutant and the wild type peptides as a function of the ligand-bound fraction demonstrate they behave in the same manner (*Figure 3-30*). The Kd value determined for the IRT1loop$_{D173N}$ was 21 µM ± 6.29 µM, which considering the error of the measure is not significantly different to that of the wild type peptide although being reproducibly lower.

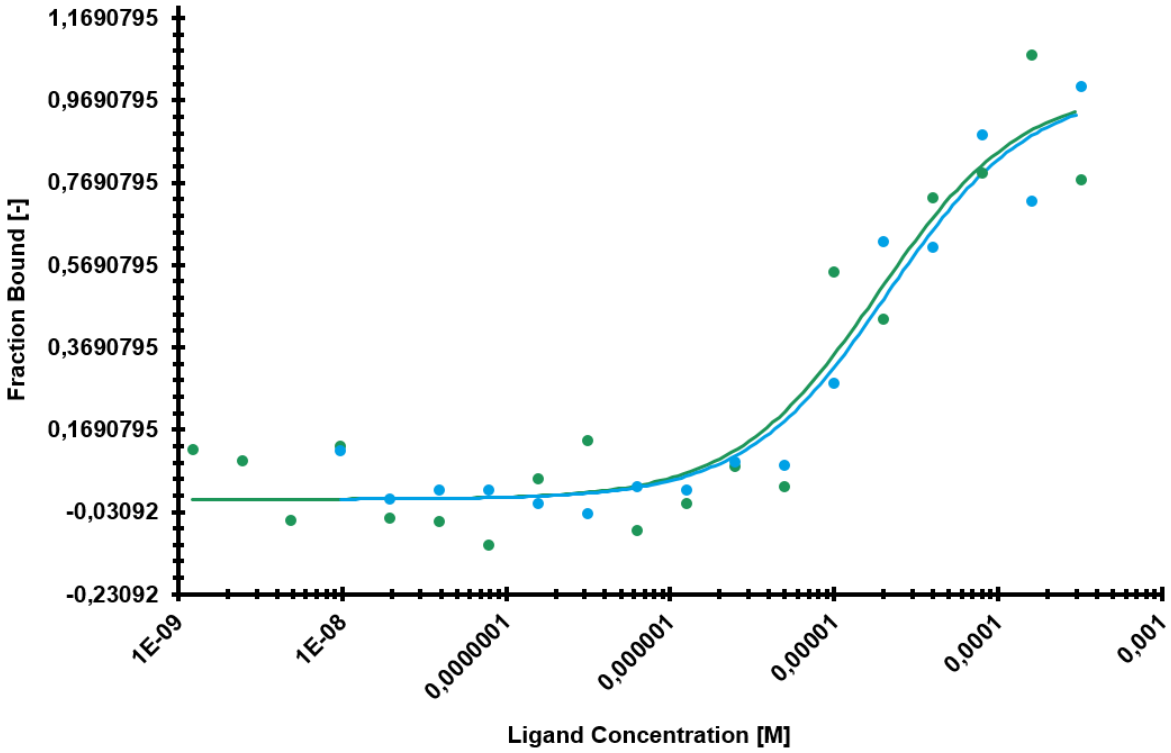

Target Name	Ligand Name	Kd	Kd Confidence	Std. Error of Regression	Signal to noise ratio
• IRT1loopWT	ZnCl2	15 µM	5,85 µM	0,41	9,05
• IRT1loopD173N	ZnCl2	21 µM	6,29 µM	0,97	12,77

Figure 3-30 Microscale Thermophoresis of IRT1loopWT (green) and IRT1loopD173N (blue). Dots represent the average dose response of biological duplicates with technical duplicates each.

3.2.4 Discussion

To cope with the changing nutrient availability and nutrient demand, plants developed strategies that allow them to control the surface expression of nutrient transporters. This is the case for the Arabidopsis IRT1 iron transporter that is controlled by various metal substrates at different levels, i.e transcription is regulated by low Fe and post-translation by Zn, Mn and Co. The post-translational regulation of IRT1 at the plasma membrane consists in phosphorylation by the CIPK23 kinase followed by K63 polyubiquitin labelling by the IDF1 E3 ligase on the large intracellular loop, upon direct binding of non-iron metals on a histidine-stretch located in this portion of the protein.

Here we show that the regulatory loop of IRT1 is a disordered peptide which can adopt various conformations. This characteristic appears to be conserved among ZIPs, such as is the case of the human

ZIP4 zinc transporter (Bafaro et al. 2015; 2019). This is however not reserved to ZIP transporters only. Other families of transporters, like the Arabidopsis MTP1 vacuolar zinc transporter, also possess disordered intracellular loops with metal binding motifs (Tanaka et al. 2013). Previously, it has been proposed that metal binding on the histidines of the IRT1 loop might trigger structuration (Cointry and Vert 2019), which would consequently trigger protein-protein interactions with regulator proteins. We demonstrate here that even in the presence of Zn^{2+}, the IRT1 loop remains unstructured, suggesting that the molecular mechanism intervening in the recruitment of downstream factors such as CIPK23 are unrelated to structural changes. However, because the histidines resonances disappear upon addition of Zn^{2+}, we are not able to determine whether this particular stretch adopts a particular conformation in such conditions. Moreover, we observed that despite adopting random coil conformations, a motif formed by AVGI residues forms a turn. We hypothesize that a turn of these characteristics, in the portion of the protein less influenced by metal binding, might have a role in exposing the histidine stretch located to its right. This is also supported by the presence of two proline residues flanking the metal binding site. Disruption of this AVGI turn or of the two prolines by point mutations would allow us to better understand the role of such a structure in an otherwise mainly disordered peptide.

The importance of the histidines stretch of the IRT1 loop in its post-translational regulation has been previously established by direct mutagenesis and homologous expression in Arabidopsis. Confocal microscopy demonstrated that plants harboring a protein mutated for the four histidines fail to show IRT1 phosphorylation and degradation upon non-iron metal excess (Dubeaux et al. 2018). We show here further evidence of the histidine stretch being of absolute importance for Zn^{2+} coordination. Both NMR and MST experiments demonstrated intense perturbations upon mutation of all four histidines, completely abolishing metal binding. Also, we inquired in the effect of double mutants of proximal histidines in Zn binding. We observed that two histidines are still able to coordinate metals. This behaviour may be due to all four histidines, and putatively aspartic acid 173, forming a single binding site in which Zn^{2+} can still be coordinated by the remaining residues when two of these are mutated. Such mutant, with only two histidines mutated might bind Zn^{2+} with lower affinity than the wild type, although this hypothesis is yet to be tested. Another possibility is the formation of two distinct metal-binding sites formed by H162/H164 and H166/H168 respectively, however, this is rather improbable given that binding of Zn^{2+} usually requires at least four coordinating amino acids (Laitaoja, Valjakka, and Jänis 2013). Furthermore, previous isothermal calorimetry experiments on a synthetic peptide mimicking only the PHGHGHGHGP stretch of the IRT1 loop demonstrated a stoichiometry of 1:1 for metal binding (Grossoehme et al. 2006). Interestingly, the intracellular loop of the human ZIP4 was shown by atomic absorption spectroscopy together with site-directed mutagenesis to possess two binding sites. It is worth noting that the loop of the human ZIP4 contains six histidine residues plus a cysteine, forming two binding sites with a yet unknown bridging amino acid, in accordance with stable Zn^{2+} coordination by four ligands. In the case of the IRT1loop, evidence suggests that a single binding site is present in this position formed by the four histidines and possibly aspartic acid 173, however, additional unidentified binding residues might be involved.

We report here the binding affinity of the IRT1 loop to Zn^{2+} at 15 ± 5.85 µM as measured by MST. This result was further supported by determination of the Kd from CD experiments which gave a value of 15.91 ± 7.3 µM. This is close to the 25 µM Kd obtained for the binding affinity of the intracellular loop of the MTP1 vacuolar Zn transporter determined by isothermal titration calorimetry (Tanaka et al. 2013). Micromolar intracellular concentrations of free Zn^{2+} are far from the experimentally determined nanomolar concentrations in plants grown in excess conditions (Lanquar et al. 2014). However, the determined affinity in vitro may not resemble the real Kd in vivo since interactions of the loop with the lipidic membrane and the hydrophobic domains of IRT1 are not taken into account in these assays. Nonetheless, we shall not discard that micromolar concentrations of metals might occur in specific regions of the cell such as in the proximal region of the membrane, upon translocation of metals into the cytosol. Development of ratiometric zinc sensors would allow us to study the concentration and distribution of Zn inside plant cells and would help us look for possible microenvironment close to the plasma membrane where higher concentrations of Zn would be found. Interestingly, measures of the kinetic parameters of Zn transport by IRT1 from yeast based assays determined that the apparent Km value in this condition was of 2.8 ± 0.6 µM (Korshunova et al. 1999), further supporting that IRT1 works at micromolar concentration ranges.

We were also able to determine a millimolar Kd value of 4.44 ± 1.47 mM for Cd. This is in accordance with the ability of the histidine stretch of IRT1 to bind metals with a relative stability consistent with the Irving-Williams series as stablished by Grossoehme et al. 2006, where affinity towards Cd was lower than for Zn but higher than for Mn and Co. Consistently, for the latter two, we failed to measure a binding affinity by MST. This is possibly explained by the concentrations used in this assay that never reached higher than millimolar concentrations. To date Cd has been reported to be transported by IRT1 (Vert et al. 2002), however, whether it takes a part in the post-translational regulation remains elusive. Unpublished observation done by Julien Spielmann in our team indicate that growing plants in absence of Fe, Zn, Co and Mn, but with 50 µM Cd, induces internalization of IRT1 into endosomes, suggesting a possible implication in the regulation of IRT1. Such condition is however mildly toxic to plants. Furthermore, it was observed that subjecting the plants to a two-fold concentration, 100 µM Cd, is detrimental and plants die within 24 hours. Taking this into account, our determined millimolar affinity constant would then be biologically irrelevant. On the other hand, post-translational regulation of IRT1 by Cd may involve a different mechanism than regulation by the other non-iron metals. A different domain of the protein than the second intracellular loop may be involved in such regulation, where binding sites may have a higher affinity for Cd. This hypothesis could be tested by analyzing whether the $IRT1_{4HA}$mCitrine mutant responds to Cd in the same manner as the wild-type protein.

Our MST experimental approach allows us to determine the impact of specific mutation on the binding affinity of the IRT1 loop. We found that a single mutation on aspartic acid 173 does not impact much on the binding affinity of the loop for Zn^{2+}. Despite not showing significant binding affinity differences to the wild type, we cannot discard the hypothesis of aspartic acid 173 contributing to the

metal coordination in the loop. In this mutant, Zn^{2+} binding might be stabilized by the remaining histidine stretch. A similar behaviour has been observed when single point mutations were introduced in the equivalent loop of the human ZIP4 and did not impact on the overall determined Kd, except for three particular residues (Bafaro et al. 2015). Interestingly, the single mutation on aspartic acid 173 to asparagine had a great impact on proper protein localization in planta. This effect could be due to misfolding of the protein and ER retention due to the ER quality control machinery. We were surprised by this behaviour since single and multiple mutants on this region of IRT1 have been previously shown to properly localize to the plasma membrane and complement the *irt1-1* knockout line (Barberon et al. 2011; Dubeaux et al. 2018). We speculate that aspartic acid 173 may play an important role in trafficking of IRT1, by being part or in proximity of an ER exit signal. We found no conserved ER exit signals in this region of the protein, however we may not discard that unknown exit signal motifs implicated in this pathway may be present. Interestingly, residue 173 is adjacent to a V residue and in close proximity to an L, both hydrophobic residues that are often involved in signaling proteins out of the ER (Mancias and Goldberg 2005). Surprisingly, overexpression of $IRT1_{D173N}$ in yeast complemented the iron-deficient phenotype of the yeast host. We believe that overexpression of the mutant protein in yeast may help by-pass protein quality controls in the ER, whereas low expression in plants might not be sufficient to generate the same response. Regardless, this proves that $IRT1_{D173N}$ is functional for metal transport, although retained at the ER when expressed in plants. Whether mutation of aspartic acid 173 to asparagine impacts on the post-translational regulation of IRT1 remains to be determined, however the protein needs to be targeted to the plasma membrane. An approach to do so, would be to generate Arabidopsis plants expressing $IRT1_{D173N}$mCitrine in an ER quality control mutant background. In the past, approaches of this nature allowed to target the usually ER-retained BRI1-5 brassinolide receptor kinase to the plasma membrane (Hong et al. 2008). With these approaches, BRI1-5 localized at the plasma membrane complemented the dwarf phenotype generated by the *bri1-5* knockout mutation. A similar approach would allow us to direct $IRT1_{D173N}$mCitrine to the plasma membrane and finally determine whether it complements the *irt1-1* mutant background and to assess if it elicits a non-iron metal excess endocytosis response.

3.2.5 Materials and methods

3.2.5.1 Circular dichroism

Circular dichroism (CD) spectra were recorded on a Jasco J-815 spectropolarimeter equipped with a temperature controller operating at room temperature. CD spectra ranging from 190 to 240 nm were recorded in a 1-mm path length cuvette. Sample concentrations were at 25 µM, in 10mM Tris, pH 7.0, and the data presented are an average of 3 scans.

3.2.5.2 Sample preparation and NMR experiments

The peptide IRT1loop WT and the four peptide mutants were first dissolved at pH 3.5 at a final concentration around 500 µM in the presence of 150 mM NaCl. The pH was then adjusted to 6.7. In a

second time two equivalents of $ZnCl_2$ with respect to the peptide concentrations were added and the pH was again adjusted to 6.7. Two-dimensional phase-sensitive 1H Clean-TOCSY (Griesinger et al. 1988) with 60 ms spin lock, and NOESY experiments (Kumar, Ernst, and Wüthrich 1980) with 200 ms mixing time were recorded at 5 and 20°C on an AVANCE Bruker 800.13 MHz spectrometer, with a spectral width of 8013 Hz, without sample spinning, with 2k real points in t2 and 512 t1-increments. Pulsed-field gradient-based WATERGATE was used for water suppression (Piotto, Saudek, and Sklenář 1992). The data were processed using TopSpin 3.6 software (Bruker). π/3 and π/6 phase-shifted sine bell window function were applied prior to Fourier transformation in both dimensions (t1 and t2).

3.2.5.3 NMR structure of IRT1loopWT

Interproton distance restraints were derived from the two-dimensional ^1H NOESY (with a 200 ms mixing time and at 5°C) using CcpNmr 2.4 (Vranken et al. 2005) and used to generate IRT1 loop structures with the program CYANA version 3.98.5 (Güntert, Mumenthaler, and Wüthrich 1997). We used the standard CYANA protocol of seven iterative cycles of NOE assignment and structure calculation, followed by a final structure calculation. In each cycle, the structure calculation started from 200 randomized conformers, and the standard CYANA simulated annealing schedule was used with 10,000 torsion angle dynamics steps per conformer. Graphic representations were prepared with PyMOL (Schrodinger n.d.).

3.2.5.4 Cloning expression and purification of proteins for Microscale thermophoresis

IRT1loop and IRT1loop4HA from pDNR221 vectors already available in our laboratory were cloned in the pMal vector, containing an MBP tag on the N-terminal from the MCS. The IRT1loopD173N was introduced on the pMal-IRT1loop vector by the SPRINP method as described in Edelheit, Hanukoglu, and Hanukoglu 2009. Vectors were transformed into BL21 DE3 E. coli. In general, 1 L of LB supplemented with glucose at 0.2% final concentration and ampicillin was inoculated with 10 ml of an overnight high density culture of cells containing the fusion plasmids pMal containing IRT1loopWT, IRT1loop4HA or IRT1loopD173N. Cultures were grown at 37°C. When OD600 reached 0.5, expression was induces by addition of IPTG to a final concentration of 0.3 mM. Cell cultures were incubated at 20°C overnight. Pellets were recovered by centrifugation at 10000g for 40 minutes at 4°C, then suspended in HEPES 10mM pH 7, NaCl 150mM in 30ml/L culture. Suspended cells were stored until further processing at -80°C.

Affinity purification of the MBP-IRT1loop variants was performed in batch. Frozen cell suspensions were thawed. Lysozyme was added for cell wall disruption and then the suspensions were sonicated with 8 pulses of 45 seconds while kept in ice. Clarification of the lysate was performed at 20000g for 30 minutes. The supernatant (crude extract) was recovered and stored in ice. Separately, 500 µl amylose resin (NEB) was washed according to providers specifications. Washed amylose resin was incubated into the crude extract in rotation at 4°C for 1h30. The resin was then pelleted at 500 g, and flow through

was discarded. 2 washing steps were performed with HEPES 10mM pH 7, NaCl 150mM, 1mM EDTA followed by a two more washes in the same buffer without EDTA. Three consecutive elutions were carried with HEPES 10mM pH 7, NaCl 150mM, Maltose 10mM.

3.2.5.5 Microscale thermophoresis

Binding experiments were performed by microscale thermophoresis with a Monolith NT.115 (NanoTemper Technologies, Munich, Germany). MBP-IRT1loop variants were labelled with the Monolith NT™ Protein Labeling Kit RED according to the instructions provided by the manufacturer, using a 1:3 protein:dye molar ratio. For Zn binding experiments, the labelled protein (20 nM) was incubated with a range of titrant concentrations made by serial dilutions (1:1), in 50 mM Tris buffer pH 7.4, 10 mM $MgCl_2$, 150 mM NaCl, 0.05% Tween 20, in PCR tubes, at room temperature for 10 min. Premium treated capillaries (NanoTemper Technologies) were loaded and the measurements were performed at 25°C, 40% LED power and 40% microscale thermophoresis power, 20 s laser-on time, 1 s laser-off time. All the experiments were repeated at least twice with two independent protein labelling reactions. Binding data were analyzed using MO.AFFINITY ANALYSIS software (NanoTemper Technologies).

3.2.5.6 Constructions and generation of Arabidopsis IRT1mCitrineD173N transgenic lines

To assay the effect of the IRT1D173N point mutation, the SPRINP (single-primer reactions in parallel) method was performed as described in Edelheit, Hanukoglu, and Hanukoglu 2009 in a pDNR221 containing the IRT1mCitrine sequence. Final destination vectors for expression in plants were obtained by multisite Gateway® recombination using the entry vector described above, an entry vector containing the IRT1 promoter sequence and the pGBKT7 GW (gentamycin resistance in plants) destination plasmid. After verification by sequencing, the final constructions were introduced in *Agrobacterium tumefaciens* strain AGL0. *Arabidopsis thaliana* was then transformed following the floral dip protocol described in Clough and Bent 1998.

3.2.5.7 Plant material and growth conditions

Arabidopsis thaliana wild type plants (WS), the previously described irt1-1/pIRT1::IRT1-mCitrine (Dubeaux et al. 2018), and the transgenic lines irt1-1/IRT1::IRT1D173N-mCitrine generated in this study were vertically grown in sterile conditions at 21°C with 16 h light/8 h dark cycles, using half-strength Murashige and Skoog (MS/2) medium (Murashige and Skoog 1962). MS/2 contained 1% sucrose, 1% agar and physiological concentrations (25µM) of non-Fe IRT1 metal substrates (Zn, Mn, Co). Plants were grown in absence of iron to induce the iron-deficiency response (-Fe +Metals).

For microscopy analysis, transgenic lines expressing IRT1mCitrineD173N under the control of IRT1 promoter, were first grown 15 days on a -Fe +Metals medium to ensure protein expression.

For phenotypic analysis, plants were grown during 12 days in absence of iron with physiological concentrations of non-iron metals. The resulting material was used to perform immunoblots on root protein extracts, RNA extractions from roots and measurement of chlorophyll content in leaves.

For IRT1mCitrineD173N functionality test, irt1-1/IRT1::IRT1-mCitrineD173N transgenic lines, irt1-1/IRT1::IRT1-mCitrine mutant, irt1-1 and WS plants were grown during 12 days in absence of iron (no addition to MS media) with physiological concentrations (25 µM) of non-iron metals.

For plant cultures in soil, plants were grown at 21°C under long day conditions.

3.2.5.8 Extraction of root total proteins and immunoblots

Total proteins were extracted from around 100 mg of roots grinded in liquid nitrogen and directly resuspended in 2X SDS sample buffer (300 µl of buffer per 100 mg of tissue). Samples were heated at 65°C during 10 min, centrifuged 10 min at 20 000 g and finally supernatants were collected and directly used for SDS-PAGE. Immunoblot analysis were performed as previously described (Barberon et al. 2011). Immunodetection of mCitrine fusion proteins was performed using an anti-GFP antibody conjugated to horseradish peroxidase (HRP) (Miltenyi Biotec 130-091-833, 1/5,000). Loading controls were obtained by using rabbit anti-FBPase (1/5,000, Agrisera). The anti-rabbit IgG (Bio-Rad 170-6515) secondary antibody coupled to HRP and diluted 1/20,000 were used for the loading control. Detection of HRP chemiluminescence was performed using SuperSignal West Dura Extended Duration Substrate (Thermo Scientific) in a Chemidoc Touch Imaging system (Bio-Rad).

3.2.5.9 RNA extractions and RT-PCR

RNA extractions were performed using the Nucleospin RNA extraction kit (Macherey-Nagel) as indicated by the manufacturer. DNA was removed from all RNA samples using rDNase treatment. RNA integrity was then verified by agarose gel electrophoresis. Reverse transcription was performed on 0.25 µg of total RNA with M-MLV Reverse Transcriptase (Promega) and oligo(dT)$_{15}$ according to specifications of the manufacturer.

The resulting cDNA was used for RT-PCR. The amplification program was as following: one cycle of pre-incubation at 95°C for 300 sec, followed by 40 cycles of amplification including 3 steps (95°C 30 sec, 63°C 30 sec, 72°C 30 sec). EDF1α gene was used as reference gene to normalize the results.

3.2.5.10 Root length analyses

Primary root length was measured from plants that grew vertically *in vitro* (see the section Plant material and growth conditions). The plates were scanned, and root lengths were measured from pictures using Fiji image software (http://fiji.sc/).

3.2.5.11 Chlorophyll content

In order to determine the chlorophyll content, 30-100mg of leaves were weighted and placed in a 1.5ml Eppendorf tube. 1ml of 96% Ethanol (VWR) was added. The samples were incubated 48h at RT

covered in aluminum foil and placed in a rotation wheel. After this incubation, the solution was diluted in 96% ethanol (VWR). This dilution (between 3 and 10 times) varies according to the concentration of chlorophyll (determined visually according to the color). This was done so that the absorbance at 649nm and 665nm does not exceed 0.6. The chlorophyll content of each sample was determined using the equation below (Wintermans and De Mots 1965):

Chl_{tot} = (6.1 x (A665) + 20.4 x (A649)) x dilution / fresh weight

3.2.5.12 Yeast complementation assay

Iron uptake assays were performed using the pDR195 vector harboring the constitutive expression of IRT1 (already available in our laboratory), IRT1D173N (point mutation generated by SPRINP, single-primer reactions in parallel, method as described in Edelheit, Hanukoglu, and Hanukoglu 2009 in the pDR195-IRT1 vector) or empty vector in *Δfet3Δfet4* Saccharomyces cerevisiae. FeCl3 was used for a final iron concentration of 25 μM.

4 Materials and methods

4.1 Cloning, expression and membrane fractionation of heterologous proteins for purification from yeast

The IRT1 and IRT1mCitrine were amplified from pDNR221 entry vectors available in our laboratory and the biotin acceptor domain was amplified from a yeast expression vector kindly provided by the laboratory of Dr. Guillaume Lenoir. Restriction sites were introduced during the PCR amplification for restriction digestion cloning on the final PYEDP60 expression vector.

The vector was transformed in the W303.B Δpep4 strain and grown in SD-agar media for 3 days. Colonies were picked and inoculated into 5 ml of warm SD medium supplemented with 2 % dextrose and -Ura aminoacid dropout mix just before inoculation (pre-culture PC1) and incubated for 24 hours at 28 °C. Next, 1 ml of PC1 was inoculated into 50 ml of pre-warmed SD medium supplemented with dextrose 2% and dropout mix (PC2). After 24 hours, 8 fernbach flasks containing 500 ml YPGE2X medium (2% yeast extract, 2% bactopeptone, 1 % dextrose and 2.7 % ethanol) each, were inoculated with PC2 so that OD_{600} is about 0.5, and the culture was incubated at 28 °C and 130 rpm for 36 hours. For induction, the cultures were transferred into a water/ice bath for 10 min to allow cooling. Expression was then induced by addition of 2 % galactose directly into the Fernbach flasks, before being incubated at 18 °C and 130 rpm for 13 hours. Finally, a second induction was performed by adding 2 % (w/v) galactose and incubation at 18°C was continued for 5 more hours.

Posterior steps for yeast harvesting and subsequent membrane fractionation were carried out at 4°C. To begin, cultures were poured into 1 liter polycarbonate bottles and centrifuged at 4000 g for 9 min (4000 rpm in a Beckman JLA8.1000 rotor), at 4°C. Supernatants were discarded and cold sterile water was then used to resuspend pellets (250 mL for 0.5 L culture). After resuspension, yeasts were centrifuged at 4000 g for 10 min at 4°C (~ 4600 rpm in a Beckman JLA 10.500 rotor). The mass of pellets (w_p) was weighed at this step (usually w_p ~ 65 g) and then resuspended with a volume equivalent to 2 w_p of TEKS buffer (50 mM Tris-HCl pH 7,5, 1 mM EDTA, 0,1 M KCl, 0,6 M Sorbitol) and incubated for about 15 min at 4°C. Cells resuspended in TEKS were centrifuged under the same low-speed conditions as above (4,000 g, 9 min, and 4°C, in tabletop Eppendorf 5430 centrifuge). Supernatants were discarded and the pellets stored at -80°C after freezing in bags or falcon tubes in liquid N_2 until further processing.

For membrane fractionation, pellets were thawed and then resuspended in 1 volume of TES buffer (50 mM Tris-HCl pH 7.5, 1 mM EDTA, and 0.6 M sorbitol) in an agate pot. Then, 2 tablets of PIC were added, as well as PMSF to a final concentration of 1mM. A volume equal to 1.5 volume of the resuspension volume of 0.5 mm glass beads were added. Yeast cells were then broken with a Pulverisette 6 planetary mill (Fritsch), by shaking them with the beads for 3 min at 450 rpm first, followed by a 30 sec pause and additional shaking for 3 min at 450 rpm in the reverse direction. The broken cells were recovered by pipetting and beads were rinsed with a volume equivalent to 1.5 w_p of TES buffer. The suspension was first centrifuged at low speed (1000 g) for 20 min at 4 °C, to give pellet

P1 and supernatant S1. S1 was then centrifuged at 20 000g for 20 min at 4 °C, to give pellet P2 and supernatant S2. P2 were resuspended in the remaining buffer and stored at -80°C after flash freezing in liquid N_2. Lastly, S2 was centrifuged at 100 000 g for 1 h at 10 °C, to give pellet P3 and supernatant S3. The P3 membrane fraction was finally resuspended in a volume equivalent to 0.2 w_p, with HS buffer (20 mM Hepes-Tris pH 7.4, 0.3 M sucrose, 0.1 mM $CaCl_2$). P3 membrane fractions are frozen in liquid N_2 and stored at -80 °C.

4.2 Protein assay

The protein content of P2 and P3 membrane fractions was measured using the 'BCA' method. The assay mixture consists in 10 µl of a diluted sample (diluted 10 times), 2 % SDS (w/v), in a total volume of 25 µl (adjusted with MilliQ water). For the standard curve, 0 to 80 µg of BSA (0-8 µl from a 10 mg/mL stock solution from New England Biolabs) was mixed with 2 % SDS (w/v) and 10 µl of a either TES or HS buffer, and again adjusted with water to 25 µl. 200 µl of a 50:1 (v:v) BCA:Cu^{2+} mix (BCA = Bicinchoninic acid stock solution, #B9643 Sigma Aldrich which contains 0.95 % sodium carbonate, 2 % sodium bicarbonate, 1 % bicinchoninic acid sodium salt and 0.16 % sodium tartrate in 0.1 M sodium hydroxide (Smith *et al* Anal Biochem (1985))), 3,2 mM $CuSO_4$ (from a 4 % (w/v), *i.e.* 160 mM, stock solution) was added into every tube and incubated for at least 30 minutes at 37 °C. 100 or 200 µl aliquots were placed in a 96 well plate. Absorbance at 562 nm was measured on an Epoch microplate spectrophotometer (Biotek).

4.3 Solubilization assays

P2 or P3 membranes were diluted to a final total protein concentration of 2 mg/ml in SSR buffer supplemented with 1 mM PMSF and an EDTA-free 1x antiproteases cocktail (MOPS-Tris 50mM pH 7, KCl 100mM, MgCl2 5mM and Glycerol 20% w/v) independently of the solubilization volume, which was of 200 µl for solubilization optimization trials, and of 60 ml for purification purposes. Detergents (stock 200 mg/ml in Tris-Cl 200 mM pH 8) or DDM+CHS mixture (stock 100 mg/ml DDM, 20 mg/ml CHS in Tris-Cl 200 mM pH8) were added to a final concentration of 2 mg/ml, 6 mg/ml or 10 mg/ml depending on the detergent: protein ratio assayed, 1:1, 3:1 or 5:1 respectively. Mix was done in a rotation wheel in centrifuge tubes for 15 minutes, 1 hour or overnight. The samples were then centrifuged at 100 000 g for 1 hour at 4°C. Supernatants were recovered for WB analyze or purification.

4.4 Purification on Streptavidin Sepharose resin (SSR)

For 60 mL of solubilized membranes at 2 mg/mL we used 1 ml of Streptavidin Sepharose Resin. For equilibration, the resin was first centrifuged for 3 minutes at 500 g (SW4400 rotor in a Allegra X30 Beckman centrifuge) to remove ethanol, then resuspended in 3 volumes of SSR buffer containing 0,5 mg/ml DDM, washed for 5 minutes, before centrifugation for 3 minutes at 500 g again and supernatant withdrawal. This washing step was repeated two times. The pre-equilibrated resin was mixed with the supernatant and incubated in rotation for 2 hours at 4°C to allow binding. The tubes were then

centrifuged at 500 g (SW4400 rotor in an Allegra X30 Beckman centrifuge,) for 3 min, and followed by removal of the flow-through (FT). Unbound material was removed by 4 consecutive washing steps consisting of adding 3 volumes of SSR supplemented with detergent, incubating in rotation for 10 minutes and removal by centrifugation at 500 g for 2 minutes.

IRT1mCitrine was released from the resin by overnight TEV cleavage of the Bad tag. Per 60 ml of initial solubilized material, 250 µg of TEV were added and incubated on rotation overnight in the cold room, typically 250 µl of a 1 mg/ml stock solution, together with one volume resin (1ml) of SSR+DDM buffer. At the end of the overnight incubation, one additional volume of SSR+DDM buffer was added to the resuspended and overnight-treated resin, and incubated on the wheel for 5 more minutes at 4 °C. Next, the resin was sedimented by centrifugation and the supernatant, *i.e.* the first "eluted" fraction, was collected (E1). The resin was again resuspended with 2 volumes of SSR+DDM buffer, left on the wheel for 5 min, and centrifuged for recovery of a second "eluted" fraction (E2). Elution samples were flash frozen in N2 and stored at -80°C.

4.5 Purification of bGFPd, GFP and mCitrine

For expression and purification of soluble proteins, GFP, mCitrine and bGFPd, BL21 (DE3) cells were transformed with pET-15b-mCitrine-Hisx6 vector cloned by restriction in our lab, pTTQ18-GFP-Hisx10 or pQE80L-bGFPd-TwinStrep kindly gifted by Dr. Jose Luis Vazquez-Ibar and Dr. Philippe Minard respectively. Cells were grown at 37°C in LB containing the appropriate antibiotic to an OD_{600} of 0.6. Protein expressions were induced by addition of 0.5 mM IPTG and incubated overnight at 37°C for GFP and bGFPd and at 20°C for mCitrine. Cells were harvested by centrifugation and resuspended in corresponding lysis buffers, then frozen in liquid N2 until further processing. Thawed cells were sonicated and purification proceeded as described here:

- ✓ For purification of GFP through a 1ml HisTrap FF column previously washed and equilibrated in lysis buffer (20 mM Tris, pH 7.5, 200 mM NaCl) with 5 mM Imidazole, sample was loaded with a syringe and the appropriate adapter. Then, washed by sequential steps of 20 ml of lysis buffer 5 mM Imidazole, followed by 20 ml lysis buffer with 20 mM Imidazole. Next, by 20 ml lysis buffer with 30 mM Imidazole. GFP was eluted with 5 ml lysis Buffer containing 150 mM Imidazole (E1) and 5 mL lysis Buffer with 300 mM Imidazole (E2).
- ✓ For purification of mCitrine through a HisTrap FF Crude column containing 5 mL of Ni-NTA resin connected to an AKTA purifier system, equilibrated with 5 column volumes (CV) of buffer A (Tris-Cl 50 mM pH7.5, NaCl 300 mM, glycerol 10% (v/v) and 25 mM Imidazole), followed by 5 CV of buffer B (Tris-Cl 50 mM pH7.5, NaCl 300 mM, glycerol 10% (v/v) and 500 mM Imidazole) and finally with 10 more CV of buffer A at flow 5 mL/min. Sample was then loaded on the column at 2 mL/min from a superloop. Next, 25 CV of buffer A were applied at 2 mL/min (until reaching A280nm~0). Fractions of 10 mL were collected. For the elution fractions of 5 mL were collected by applying a gradient from 5 to 100% of buffer B in 20 CV.

- ✓ For bGFPdTwinstrep, the StrepTactin Superflow High capacity resin was washed and equilibrated by pelleting at low velocity at 4°C (1000g). The resin was equilibrated with 3 ml of W buffer (30ml of Tris 20mM, NaCl 200mM pH 7.5 and PIC) for 5 min in a rotation wheel twice. The equilibrated resin was added on the cell lysate and placed in the rotation wheel at 4°C for 1 hour. The flowthrough was then removed, and the unbound protein washed out by addition of 3 ml W buffer and centrifugation. Elution was achieved by 3 sequential additions of 1 ml of Buffer E (100 mM Tris/HCl pH 8.0, 150 mM NaCl, 1 mM EDTA, 2.5 mM desthiobiotin) obtaining 3 eluate fractions (E1, E2 and E3).

Protein concentrations were determined by spectroscopic properties (A514, A280), with extinction coefficients obtained from ProtParam Expasy of each particular protein on a nanodrop.

4.6 Purification of IRT1 with bGFPd

The bGFPd used in this assay has a twin strep tag that allows binding to a StrepTactin Superflow High capacity resin. The StrepTactin Superflow High capacity resin was first washed and equilibrated by three consecutive additions of SSR buffer (MOPS-Tris 50mM pH 7, KCl 100mM, MgCl2 5mM and Glycerol 20% w/v) containing DDM+CHS 0.5 mg/ml ($SSR_{DDM+CHS}$) (DDM+CHS stock solution is 100 mg/ml DDM with 20 mg/ml CHS). Next, 15.2 nmol of bGFPd were diluted in 1 ml of $SSR_{DDM+CHS}$. The resin was then resuspended with the bGFPd dilution and incubated in a cold room for 2 hours. 3 washing steps followed for removal of unbound bGFPd with $SSR_{DDM+CHS}$. Next, 2.5 ml of solubilized P3 IRT1mCitrine at 5 mg/ml in 15 mg/ml DDM+CHS in SSR supplemented with PIC and PMSF (see section 2.3 for solubilization details) were incubated with the bGFPd bound resin during an overnight incubation at 4°C. Washing of the resin was carried 3 times with $SSR_{DDM+CHS}$. Elutions were carried by addition of 100 µl of GFP at 8 mg/ml (296 µM) 29.6 nmol in this case, supplemented with DDM+CHS to 0.5 mg/ml, and incubated ON. After incubation, the mix was centrifuged and the supernatant recovered (E1). A second elution consisted in addition of 100 µl of buffer, incubated for 10 minutes in the rotation wheel and centrifuged for recovery of the supernatant as E2. Another elution strategy was the addition of 100µl of BXT buffer containing biotin in a similar manner to the previously described GFP elution.

4.7 Proteoliposome reconstitution

In a round bottom flask 160 µl of DOPC in chloroform at 100 mg/ml and 8 µl POPE in chloroform at 100mg/ml with 6 mg cholesterol (added in powder) were mixed. The flask was placed in the rotavap to dry with vacuum in rotation for 20 minutes. The flask was then incubated in a vacuum bell overnight. The resulting lipidic film was resuspended with 2 ml of buffer Mops-Tris 50mM pH 7, KCl 100mM by vigorous pipetting. The flask was placed at 37°C for 20 min for better resuspension. The solubilized lipids were sonicated for 5 minutes at 37°C. After sonication, the liposomes were extruded with a hand extruder, first through a membrane of 0.2 µm, then through a 0.1 µm one. Rsat (saturation

concentration) and Rsol (solubilization concentration) were determined by diluting the liposomes to 7.5 ml with buffer and destabilizing 100µl of this dilution with 0-9 µg of DDM at 25°C while shaking for 3 hours. In this work reconstitution was carried at Rsat.

For reconstitution 3ml of the liposome preparation were destabilized with 60 µl of DDM at 10 mg/ml and incubated in a rotating wheel for 3 hours. 500 µl of IRT1mCit, corresponding to approximately 100 µg was added to the destabilized liposomes and incubated in a rotation wheel at room temperature for 1h. 20x mass detergent of bio-beads (BioRad) were added (6 mg x20 = 120 mg) and incubation proceeded for 1h in rotation. Additional 40x mass (240 mg) of biobeads were added and kept at room temp. The last addition of bio beads was of 40x (240 mg) in a new tube and kept overnight in the cold in rotation.

For determining the reconstitution rate, half of the volume of liposomes were placed in an ultracentrifuge tube and centrifuged at 200 000g for 1h at 4°C for concentration. The pelleted liposomes were resuspended in 300 µl of buffer for running in a sucrose gradient. The sucrose gradient was set up by sequential additions of 560 µl of a 30%, 20%, 10% and 5% sucrose solution in 10mM HEPES/NaOH pH 7.4, 100mM NaCl and 10% DDM. This was followed by a final layer of buffer lacking sucrose. The 30% sucrose solution was prepared by a 1:1 mixture of a 60% sucrose solution and the liposome preparation. Gradient tubes were then loaded into a rotor and centrifuged at 100 000 g, for 1 hour, at 4°C with acceleration and deceleration set at 9. To determine the presence of protein in the gradient, 3 fractions (bottom, middle and top) were withdrawn for a dot blot. Also, the liposomes were checked for fluorescence.

For a dotblot followed by immunoblotting a standard curve was prepared by mixing 10 µl of pure IRT1mCitrine protein with 70 µl of 10 mM HEPES/NaOH pH 7.4, 100 mM NaCl and 10% DDM buffer. Dilutions were made (1/2, 1/5, 1/10, 1/20, 1/40). Next 4 µl of each dilution was deposited in a PVDF membrane previously incubated in methanol and washed in transfer buffer. 4µl of each fraction (top, middle and bottom) from the gradient were also loaded. The same was repeated in presence of Triton. For this, 8µl of each of the above mentioned fractions were mixed with 1µl of Triton 10%. Again 4µl of each sample was deposited in the membrane. Immunoblotting was followed as per usual, by blocking in a 5% milk solution, followed by incubation with an HRP coupled anti-GFP antibody, three washing steps of TBS-T buffer and then revealed by addition of BioRad chemiluminescent peroxidase substrate. Quantification of the blots was done by Quantity One software.

4.8 CryoEM sample preparation and image recording

3.5 µl of IRT1mCitrine sample were deposited on a glow-discharged (25 mA, 50 s) Quantifoil copper-rhodium R 1.2/1.3 grid, blotted at 8°C for 10 s at force 0 using a Mark IV Vitrobot and plunge-frozen in liquid ethane.

Test datasets were recorded on a Glacios electron microscope at the IBS. Movies (40 frames) were acquired with SerialEM on a Gatan K2 Summit camera. Raw movies were aligned and summed with MotionCor2, within Relion. CTF estimation for non dose-weighted sums was calculated using GCTF. Particles were picked with Cryolo. All subsequent steps were carried out in Cryosparc.

4.9 Size exclusion chromatography

IRT1mCitrine an P3 solubilized membranes, SEC was run on a Superdex 200 Increase 10/300 column on an ÄKTA purifier system at 4 °C in SSR without glycerol and 0.03 mg ml^{-1} DDM. For preparative purposes, the peak fractions were pooled and concentrated using a centrifugal concentrator with a cut-off of 50 kDa, and stored at −80 °C for later use.

4.10 Analytical ultracentrifugation

All experiments were conducted at 4°C. Sedimentation velocity (SV) experiments were performed on a Beckman Coulter XL-I analytical ultracentrifuge with a rotor Anti-50 at a speed of 42,000 rpm. We used Al-Epon double sector 1.2 cm optical path centerpieces equipped with sapphire windows filled with, 150 µl, 45 µl or 4.5 µl of sample plus 300 µl, 405 µl and 445.5 µl of buffer respectively. The buffer used was MOPS-Tris 50 mM pH7.0, 100 mM KCl, 20% Glycerol, supplemented with 0.5 mg/ml or 6 mg/ml DDM for concentrated and diluted samples respectively). Sedimentation profiles were acquired overnight using fluorescence at 527 nm. SV Analysis Analyses were typically made considering a total of 16 h sedimentation. The programs used for data analysis, SEDFIT, v 16.1c and Gussi 1.4.2 (freely available at http:// www.analyticalultracentrifugation.com) are described in detail on the web site. *s20w*, for protein-detergent complex, was calculated using a mean vbar value, corresponding to 1g/g of bound detergent.

4.11 Cadmium and iron transport tests in yeast

Cadmium uptake assays were performed in the expression strain *Saccharomyces cerevisiae* W303.b Δpep4. Vectors pYEDP60 harboring the expression of the different fusion proteins were transformed by the lithium acetate method. Transformed yeast were grown in SGF-Ura media, complemented with galactose to induce the expression of the mentioned proteins and 50µM CdCl2. Growth control was grown in SGF-Ura with galactose in absence of CdCl2.

4.12 Plant material and growth conditions

Arabidopsis thaliana wild type plants (Col-0), the previously described irt1-1/pIRT1::IRT1-mCitrine and Col0/35S::IRT1-mCitrine lines (Dubeaux et al. 2018) and the irt1-1/pIRT1::IRT1-mCitrine/IRT1::IRT1-mScarlet previously generated in our laboratory were vertically grown in sterile conditions at 21°C with 16 h light/8 h dark cycles, using half-strength Murashige and Skoog (MS/2) medium (Murashige and Skoog 1962). MS/2 contained 1% sucrose, 1% agar and physiological concentrations (25µM) of non-Fe IRT1 metal substrates (Zn, Mn, Co). Depending on the experiment,

plants were grown in absence of iron to induce the iron-deficiency response and in presence of physiological concentrations of IRT1 secondary substrates Zn, Mn and Co (-Fe +Metals).

For immunoprecipitation, irt1-1/IRT1::IRT1-mCitrine, irt1-1/ IRT1::IRT1-mCitrine/IRT1::IRT1-mScarlet, Col0/35S::IRT1-mCitrine transgenic lines and Col-0 wild-type plants, used as a negative control, were initially grown during 8 days on MS/2 medium containing 50 µM Fe-EDTA, then transferred during 4 days onto a -Fe +Metals medium to induce IRT1-mCitrine and IRT1-mScarlet expression.

4.13 Immunopurifications

Immunopurification (IP) were performed on approximatively 500 mg of *Arabidopsis* roots, mostly as previously described (Dubeaux et al. 2018). Briefly, for co-IP analysis between IRT1mCitrine and endogenous IRT1, as well as for coIP analysis between IRT1mCitrine and IRT1mScarlet, roots grinded in liquid nitrogen were resuspended in IRT1 solubilization buffer (50 mM Tris-HCl pH 7.4, 150 mM NaCl, 5 mM EDTA, 1% n-Dodecyl β-D-maltoside (DDM) and plant specific protease inhibitors (Sigma-Aldrich)), using 300 µl of buffer per 100 mg of tissue. After two successive centrifugations at 3 800 g for 10 min at 4 °C, the resulting supernatants were collected and solubilization of membrane proteins was continued for 1h 30 min at 4 °C on a rotating wheel. Samples were then centrifuged at 100 000 g for 1 h at 4 °C to remove unsolubilized material and supernatants containing solubilized proteins were recovered for IPs. mCitrine fusion proteins were immunopurified using GFP-Trap®_MA magnetic beads (Chromotek), following the instructions of the manufacturers. Before elution, extensive washes were performed with IRT1 solubilization buffer.

4.14 Extraction of root total proteins and immunoblots

Total proteins were extracted from around 100 mg of roots grinded in liquid nitrogen and directly resuspended in 2X SDS sample buffer (300 µl of buffer per 100 mg of tissue). Samples were heated at 65°C during 10 min, centrifuged 10 min at 20 000 g and finally supernatants were collected and directly used for SDS-PAGE. Immunoblot analysis were performed as previously described (Barberon et al. 2011). Immunodetection of mCitrine fusion proteins was performed using an anti-GFP antibody conjugated to horseradish peroxidase (HRP) (Miltenyi Biotec 130-091-833, 1/5,000). mScarlet fusion proteins were monitored with a mouse anti-RFP antibody (Chromotek, 1/5,000). Immunodetection of endogenous IRT1 protein was performed using an affinity-purified antipeptide IRT1 antibody diluted 1/3,000 (Séguéla et al. 2008). Depending on the primary antibody, the anti-rabbit IgG (Bio-Rad 170-6515) or the anti-mouse IgG (Bio-Rad 172-1011) secondary antibodies both coupled to HRP and diluted 1/20,000 were used. Detection of HRP chemiluminescence was performed using SuperSignal West Dura Extended Duration Substrate (Thermo Scientific) in a Chemidoc Touch Imaging system (Bio-Rad).

4.15 Confocal microscopy

For BiFC constructs, both halves of mCitrine (N-terminal: 1-154 and C-terminal: 155-238) were amplified by PCR, then cloned into the p2rp3 vector by BP reaction. Infiltrated tobacco leaves with the corresponding vectors were pierced to obtain leaf discs. They were mounted in water viewed on a Leica TCS SP8 confocal laser scanning microscope (www.leica-microsystems.com/home/). Excitation of mCitrine used the 514 nm laser line. Laser intensity and detection settings were kept constant when required. Before imaging, care was taken to always be below saturation levels.

5 Discussion and perspectives

Organisms require Fe and other divalent metals to accomplish basic life functions. The ZIP family of transporters is a major family of proteins involved in the primary uptake as well as in the distribution of divalent metals, mainly Fe and Zn, but also Mn and Co, across all kingdoms of life. The Arabidopsis IRT1 protein, the founding member of the ZIP family, has been vastly characterized since its discovery and still serves as a model for the ZIP transporters. Because metal nutrition needs to be tightly regulated in order to prevent malnutrition or toxicity, research has recently been focused on the mechanisms regulating ZIPs in animals and plants. Particularly, in our laboratory, the post-translational regulation of IRT1 has been widely investigated, turning IRT1 into a model protein for the understanding of the endocytic machinery in Arabidopsis. However, a major gap still exists when it comes to the metal transport mechanism itself, the structural and topological characteristics of the protein and the basic molecular mechanisms driving the regulation of IRT1 protein. For these reasons, my PhD work has focused in narrowing these gaps by implementing for the first time technical approaches needed for structural and mechanistic characterization of the IRT1 protein. Such approaches allowed us to gather some structural and biophysical information on IRT1, which complements what has been recently reported for the human ZIP4 zinc transporter or for the distantly related bacterial ZIP transporter from *Bordetella bronchiseptica*.

5.1 Development of technical approaches for the study of the IRT1 transporter

To date, from a total of more than 170,000 tridimensional structures of proteins reported in the literature, only 1,209 of those correspond to single membrane proteins (https://blanco.biomol.uci.edu/mpstruc). This gap is partly due to the challenges presented by the purification of membrane proteins. Their hydrophobic nature makes them prone to aggregation in vitro. Usage of detergents can solve this problem, however, addition of surfactants often negatively affects the functioning and folding of proteins. Thorough optimization is therefore required in the design of these strategies. During my PhD work, I established a detailed protocol for the production and purification of a functional fluorescently-tagged version of IRT1 expressed in yeast. This protocol consists in the expression of the IRT1 protein in the heterologous yeast host W303.B Δpep4 in rich media at high OD, followed by differential fractionation of membranes and purification through the high affinity and specific interaction between a biotin acceptor domain (BAD) affinity tag and avidin. Yields of purification for our IRT1mCitrine fusion were around 0.2 mg/L culture. The yield of binding of the affinity tag to the avidin resin was however low and hampered our ability to improve recovery. Attempts to further biotinylate the affinity BAD tag failed to increase further the binding yield. This may be due to a saturation of the epitopes of the avidin resin in the volume of sample we worked. Adjusting the crude extract:resin ratio may help us optimize the parameters in order to achieve a

purification strategy in which solubilized IRT1mCitrine is not lost during the resin-binding step. Such strategy would allow us to increase the overall yield of purification per liter of culture. In the eventuality where we find an optimal crude extract:resin ratio, we may also assay the purification with protein solubilized by FC16. The significantly higher solubilization yield of this detergent may indeed increase even more the yield of purification but we would still face a problem of determining whether the structure and function of IRT1 in this condition are affected. Furthermore, we believe changing the type of affinity tag and resin may not be of help at that stage given that the avidin-biotin affinity is one of the higher affinities described, which allows us to obtain a fairly pure sample in only one step of purification. It is worth noting that purification yields in the range of 1-10 mg/L culture are considered "high" for membrane proteins (Mohanty and Wiener 2004; Su et al. 2013; Feroz et al. 2018). We believe that with the strategies mentioned above, our purification system may be optimized to achieve yields close to this range. Nonetheless, a similar strategy to the one described in my PhD work has been used for the purification of the rabbit sarco/endoplasmic reticulum Ca^{2+}-ATPase with a yield of 0.3 mg/L culture, which finally lead to the successful crystallization of this protein (Jidenko et al. 2005; 2006).

We were able to establish a protocol for the characterization of the transport parameters of IRT1 by integrating our pure IRT1-mCitrine protein into proteoliposomes. Analyzes by immunoblotting of proteoliposomal fractions treated with triton, allowed us to estimate the orientation of the incorporated protein. Preliminary results suggested that the "mCitrine out" orientation is the favored one, given that the amount of protein quantified in samples with and without triton is similar. In the case the protein would adopt both orientations equally, we would expect to observe twice as much signal in the triton-treated sample, because of the disruption of the lipidic film exposing the internal mCitrine protein. Further reconstitution assays will allow us to determine if these observations are reproducible. Furthermore, we may adopt an additional strategy for determining the orientation of our protein, such as protease accessibility to cleave the mCitrine, followed by ultracentrifugation and immunoblotting of the supernatant to detect the mCitrine protein. In the future we hope to use IRT1mCitrine reconstituted proteoliposome to investigate the transport mechanism of IRT1. We favor the use of a fluorescent probe that can be incorporated in liposomes during preparation and that is quenched by divalent metals in the interior of the liposomes, if the orientation of the IRT1mCitrine protein is indeed "mCitrine out". This orientation of IRT1 will allow us to search for the optimal kinetic assay conditions by easily exchanging the extra liposomal buffer, given that the transport would be carried from the extra liposomal space to the interior. Considering that mCitrine is present in our system, a fluorophore such as Calcein deep red needs to be used as a reporter in the interior of the liposomes. The excitation and emission spectra of Calcein deep red does not overlap with that of mCitrine, given that it has excitation and emission peaks at 648 and 658 nm respectively, while mCitrine excitation and emission peaks are at 516 and 529 nm. Alternatively, we may turn to the use of radioisotopes, but such experiments would need to be performed in an institute where Fe, Zn, Mn, Co and Cd isotopes can be used.

Because there is conflicting evidence regarding the mechanism of transport of ZIPs, we need to design experiments that allow us to screen varied transport conditions. Given that HCO^- has been

proposed as a co-transported molecule by other ZIPs such as the mouse ZIP8 and ZIP14 (Liu et al. 2008; Girijashanker et al. 2008), we believe it is needed to investigate its effect on metal transport by IRT1 by adding it in the extra liposomal buffer. Furthermore, varied pH conditions between intra- and extraliposomal solutions might result in efficient transport. A problem to be faced in such an approach might be the instability of Fe^{2+} in solution. Addition of a reducing agent such as ascorbate to testing buffers has been previously used as a solution to this problem in yeast based uptake assays (D. R. Dix et al. 1994; Eide et al. 1996). Also, we propose the study of the transport of the secondary substrates besides the principal substrate Fe^{2+}. Kinetic parameters indicating the affinity to the substrate and the speed of the transport have been previously reported from cell-based assays for the uptake of Fe, Zn and Mn. It was determined that apparent Km and Vmax, for all three substrates were in the low micromolar range when IRT1 was expressed in yeasts (Eide et al. 1996; Korshunova et al. 1999). Knowing the previously measured velocity and affinity parameters will allow us to determine the concentrations in which we should set our experiments. Although the mentioned values obtained in yeast constitute an apparent approximation of the kinetics of transport by IRT1, measures of this kind are usually influenced by other metal transporters present in the cell. Proteoliposomes constitute an adequate environment for the study of transport of substrate across lipidic membranes without the interference of additional proteins. Furthermore, the lipidic composition of the liposomes can be adjusted to match that of the plasma membrane of plant root cells.

The purified protein harbors mCitrine, which we think may be an advantage. First, previous work in our laboratory evidenced that the addition of a fluorescent tag in amino acid position 42, on the first extracellular loop, does not affect IRT1 function in planta (Dubeaux et al. 2018). Second, the presence of mCitrine increased the IRT1 expression and purification from the yeast host. Not only mCitrine likely stabilizes IRT1 protein, but often, the addition of soluble domains to highly hydrophobic proteins increases the overall solubility and stability, such as the case of Maltose Binding Protein (MBP) fusions (Kapust and Waugh 1999). Third, the presence of mCitrine on the protein allowed us to analyze the behaviour of the protein in vitro through fluorescence coupled techniques such as F-SEC and AUC. Finally, the presence of mCitrine may turn out to be a major advantage during structural analyses regarding the molecular weight of the sample. Our purification strategy reported here has proven to generate an IRT1-mCitrine protein sample that was suitable for preliminary CryoEM trials. We hope in the future to enlarge the amount of sample in this assay in order to obtain sufficient data for modelling of the tridimensional structure of IRT1. Besides, the molecular weight of our protein (36.7 kDa for IRT1) would be too small to solve the structure by CryoEM. With the addition of mCitrine (64.6 kDa for the IRT1mCitrine fusion), the purified protein now resides close to the limit of detection for this technique, of about 50 kDa, which constitutes one of the main limitations for deciphering the structure through CryoEM. The fact that IRT1 forms oligomers will also help reach a sufficient molecular weight suitable for structure determination. For the latter, highly concentrated samples should be analyzed, in order to favor the formation of dimer as seen by F-SEC. Besides, a strategy that may be of use to improve structure determination of IRT1mCitrine is the reconstitution in nanodiscs. Nanodiscs are lipidic

bilayer discs surrounded by a protein scaffold that keeps the disc intact and membrane proteins can be inserted in the lipidic bilayer (Denisov and Sligar 2016). This strategy creates larger particles, an advantage for CryoEM approaches, that are stable in solution, and gives the advantage of having proteins in an environment similar to the original. Strategies of this nature have been successfully used for determination of the structures of several transmembrane transporters in recent years (Roh et al. 2018; Reid, Kern, and Brohawn 2020; Arkhipova, Guskov, and Slotboom 2020).

The structure of the only ZIP described until today, the *Bordetella bronchiseptica* ZIP, has been achieved through lipidic cubic phase crystallography (T. Zhang et al. 2017). This approach requires protein amounts at least 10 times larger than CryoEM. In the case of the Bordetella ZIP, such a protein quantity is easier to achieve since prokaryotic expression hosts are characterized for yielding high expression levels. In the case of Arabidopsis IRT1, a eukaryotic heterologous host is more suitable for its expression because it may perform all the post-translational modifications needed for proper folding, but presents often lower expression yields than prokaryotic ones. The yield of purification by the SSR method reported in this thesis remains too low for crystallography applications and further optimization of this method would be required.

5.2 Determination of the oligomeric status of IRT1

As part of the structural characterization of IRT1, we deciphered whether oligomerization, a trait seen before in some ZIPs (Bin et al. 2011; Zhang, Sui, and Hu 2016), especially in the LIV1-subfamily, was also shared by IRT1. Analyses of our pure IRT1mCitrine protein on FSEC allowed us to observe the presence of two different molecular size particles that correlate with the estimated values expected for a monomer and for a dimer with bound detergent. These in vitro experiments demonstrated the predominance of the monomer specie over the putative dimer. We hoped that increasing the concentration of the protein might favor oligomerization, and the dimer peak would be the major form in this condition. Indeed, we found after deconvolution of our chromatogram that increasing the concentration favored the formation of putative dimers. Besides the in vitro analyses, we have observed the oligomeric state of IRT1 *in planta*. By BiFC and co-immunoprecipitation, we were indeed able to determine self-interactions of IRT1. It is important to note that in the case of BiFC i) proper negative controls were missing in order to determine whether the interaction seen was of biological relevance, and that ii) topological issues of IRT1 render this approach poorly conclusive because of the orientation of the tags. We believe that co-immunoprecipitation itself is sufficient to conclude on the ability of IRT1 to oligomerize in vivo. It is worth noticing that the role of the oligomerization of other ZIPs has not been described yet. Analyses of the oligomerization in varied metal conditions would help us understand if the oligomerization plays a part in the regulation of the transporter as a response to metal overload or deficit. Importantly, the interaction of IRT1 with the AHA2 H+-ATPase and the FRO2 reductase has been shown to be disrupted upon metal excess, and triggered by IRT1 phosphorylation by CIPK23 (Martín-Barranco et al. 2020). Whether phosphorylation of IRT1 and the ability to sense metals also controls oligomeric status would also have to be tested by taking advantage of mutant

versions of IRT1 with point mutations affecting both parameters ($IRT1_{S/TxA}$, $IRT1_{S/TxD}$ and $IRT1_{4HA}$). Another possible role for oligomerization could be its direct participation in transport, as it is the case for YiiP transporters that requires dimerization for the formation of a metal translocation pore (Lu and Fu 2007). This hypothesis is however weak, given that the structure of the Bordetella ZIPB demonstrated an intrinsic metal translocation path within the monomeric protein (T. Zhang et al. 2017), and even though sequence alignments demonstrate low identity among ZIPs, the specific residues involved in metal translocation appear to be conserved (Krishna et al. 2020). The function of oligomerization in regulation is very well exemplified by the Arabidopsis NRT1 transporter, where dimerization lowers the affinity of the protein toward the substrate nitrate in comparison to the monomer with a high affinity (Sun et al. 2014). Interestingly, this oligomerization event is inhibited by phosphorylation. A further example of dimerization intervening in nutrient uptake are the AMT ammonium transporters. AMT1 has been demonstrated to participate in homo- and hetero-dimerization. The roles of such behaviour remain elusive, but is has been proposed that the heterodimerization of AMT1.1 with the AMT1.2 paralog, might form a heteromeric protein in which distinct paralogs reconstitute a single functional transporter (Ludewig et al. 2003). Similar implications for the IRT1 transporter need to be studied. This thesis reports on the homodimerization of the transporter. Similar experiments as the ones described here, like immunoprecipitation, can be performed between IRT1 and its close iron transporter homologue, IRT2. Sucrose transporters SUT are a known examples for forming such structures. Three SUT paralogs with different substrate binding affinities, SUT1, SUT2 and SUT4 were found to interact with each other (Reinders et al. 2002). Heterodimeric complexes may present different affinities than homodimers or monomeric species. The proteoliposome reconstitution of IRT1 reported in this thesis presents a unique tool for the study of transport kinetics of IRT1 in varied homooligomeric forms if known (if affected by phosphorylation for example), or for heterodimers. Further research on the events triggering oligomerization is therefore required. A constitutive oligomerized form of IRT1 would greatly enrich our knowledge in this subject. Evidently, resolution of the structure of IRT1 would be highly informative on the mechanisms and interface of oligomerization. Interestingly, in LIV-1 ZIP members, oligomerization occurs through a PAL motif in an ectodomain located in the N-terminal region of the ZIP, which is missing in IRT1 (Zhang et al. 2019; Pocanschi et al. 2013; Bin, Seo, and Kim 2018).

We have obtained contrasting data regarding oligomerization of IRT1 from AUC analyzes. The evidence suggested that at 3, 1 and 0.3 µM, purified IRT1mCitrine is present as a monomer in solution and that a dimer would be possible only if no detergent is bound. The latter is very unlikely given the hydrophobic nature of IRT1 and the detergent concentration in the assay buffer. Surprisingly, the sedimentation profile of a highly diluted IRT1mCitrine sample, at 0.03 µM, pointed to putative dissociation events, which would be impossible if the sample is monomeric at higher concentrations. A similar behaviour was observed for AUC analyzes of solubilized P3 membranes in DDM+CHS, where the mean s-value decreased together with the concentration (1, 0.33 and 0.1µM), suggesting the dissociation of the larger species. Again, at 0.01 µM, the distribution of peaks from solubilized

membranes shifted to lower sedimentation coefficients. Although the overall AUC data suggests that monomeric IRT1 is the predominant form, the sedimentation profiles at low concentrations point to possible minor oligomerization events. F-SEC data has shown that indeed, the monomeric form of IRT1mCitrine was the predominant in those experiments, however a putative dimeric species is present as well. A detailed analyses of IRT1mCitrine in higher resolution AUC chambers or at higher concentration of proteins could help us understand this behaviour.

5.3 Molecular mechanisms driving the post-translational regulation of IRT1

Regulators of IRT1 protein have been described in recent years, such as the IDF1 E3 ligase and the CIPK23 kinase (Shin et al. 2013; Dubeaux et al. 2018). The latter has been established to phosphorylate residues on the second intracellular loop of IRT1 triggering the recruitment of the IDF1 E3 ligase which decorates K residues K154 and K179 present in the same loop with K63 polyubiquitin chains. The tagging of IRT1 with K63 linked Ub triggers its endocytosis and targeting to the vacuole. This process is controlled by the intracellular metal concentration (Dubeaux et al. 2018). When metals other than Fe reach elevated intracellular levels due to high transport activity by IRT1, they bind to the loop of IRT1 which in turn recruits the CIPK23 to this site. In this work, we determined that the binding affinity of one of these non-iron metals, Zn^{2+} is in the micromolar range. Specifically, binding affinity was of 15 μM as determined by two independent techniques, microscale thermophoresis and circular dichroism. Previously, by using fluorescent probes, it was determined that intracellular concentrations of Zn^{2+} in plant roots are in the nanomolar range, specifically, 0.4 nM was determined for plants in normal growth conditions and 2 nM for metal excess conditions (Lanquar et al. 2014). The approach to determine such concentrations gives the mean concentration in the cytoplasm. Concentrations of metals may be transiently higher in specific regions of the cells, for instance in the plasma membrane proximal area upon metal translocation. Therefore, ratiometric fluorescent sensors allowing to determine the spatial distribution of Zn across the cell, and more importantly at the vicinity of the plasma membrane are required. Besides Zn, affinity measures to Cd fell in the millimolar range, although such concentrations of Cd are improbable to accumulate in plants cells because of the toxicity of this metal. As mentioned in section 3.2, preliminary results from other members of our laboratory indicate that Cd may also drive the endocytosis of IRT1 upon excess. We propose that additional binding sites with higher affinities for Cd may therefore be present in other intracellular regions of IRT1 or that Cd sensing is achieved by other sensors in plant cells. Determining whether the histidine mutant $IRT1_{4HA}$ responds in the same manner as the wild-type protein to Cd remains to be determined. Previous research demonstrated that mutation of aspartic acid 144 to alanine, at the interface between TM4 and the second intracellular loop, eliminated transport of Cd in yeast, indicating a putative binding site for Cd involving this aminoacid (Rogers, Eide, and Guerinot 2000). Mutation of this residue and analyzes of its response to Cd may shed light on whether it is involved in regulation by Cd.

Besides Zn, we were not able to measure binding affinities for Co and Mn. It is important to note that the concentrations used in this assay were never higher than 100 millimolar, which may be the reason for this. Microscale thermophoresis experiments at higher concentrations could be initiated with the goal to determine binding affinities for this metals, however the biological relevance of metal binding in such elevated concentrations would be difficult to reconcile with the fact that Mn excess of 500 µM triggers the depletion of IRT1 from the plasma membrane (Dubeaux et al. 2018). Nonetheless, it is important to note that our in vitro assay does not take into account potentially important interactions of the loop with other regions of IRT1 and thus, the parameters described for the loop of IRT1 are apparent.

During this work we provide evidence for the possible involvement of an additional residue in metal binding in the intracellular loop of IRT1. We hypothesize that residue D173 acts together with the histidine stretch in metal coordination as seen by NMR. On the other hand, microscale thermophoresis failed in demonstrating its role in Zn binding. Possibly, in this case, the metal ligand is still able to bind to the remaining histidine residues. In line with this, mutants on two of the four histidines do appear to still complex Zn^{2+}, as seen by NMR. In the future, it would be interesting to determine the binding affinity of double histidine mutants to gather further evidence of the remaining two histidines and aspartic acid residues still being able to complex Zn^{2+}. Moreover, measures of binding affinity on triple mutants of two histidines (162H/164H or 166H/168H) plus D173N may reveal an ability to complex Zn^{2+} with significantly lower affinity if not at all. Experiments of this nature would allow us to better determine if D173 indeed takes part in metal complexing together with the histidine stretch. In addition, we found that mutation of D173 to asparagine had no impact in protein transport function in vivo, as demonstrated by yeast complementation assays. Opposite to this, in plants, the D173N mutation of IRT1 impacted deeply in protein localization. Instead of being delivered to the plasma membrane, IRT1mCitrine$_{D173N}$ was indeed retained at the endoplasmic reticulum (ER). We do not know at that stage if the mutant protein is misfolded although not impacting metal transport per se, or if D173 may be involved or indirectly affect an ER exit signal. In order to study whether D173N impacts in the post-translational regulation of IRT1, we propose to generate plants expressing the mutant IRT1mCitrine$_{D173N}$ in a line with deficient ER quality control. For instance in an Arabidopsis line where the Hsp70 chaperone BiP, involved in binding to hydrophobic exposed regions of misfolded proteins in the ER, is silenced. Such approach has previously been used for targeting the ER-retained allele of the BRI1 receptor kinase, bri1-5, to the plasma membrane where it complemented the mutant phenotype (Hong et al. 2008). BRI1 is a leucine-rich-repeat receptor–like kinase that functions as a cell surface receptor for brassinosteroids, which loss-of function mutations lead to dwarf plants. The bri1-5 allele contains a C69Y mutation at the receptor domain which leads to retention of the protein at the ER, however this mutation does not impair its function, as seen in BiP silenced plants which allow bri1-5 to reach the plasma membrane and reverse the dwarf phenotype. Importantly, we would first need to determine whether the BiP is involved in the retention of IRT1mCitrine$_{D173N}$, by co-immunoprecipitation for instance, with IRT1mCitrine as a control. Another option for an approach of

this kind may be the crossing of our irt1-1/pirt1::IRT1$_{D173N}$mCitrine line with the ER quality control double mutant *hrd1a hrd1b*. This line is defective in two HRD1 ubiquitin ligase homologs, which are involved in tagging misfolded proteins at the ER for degradation. Like the BiP silenced line, usage of the *hrd1a hrd1b* double mutant allowed for the complementation of the *bri1-9* mutant, containing a S662F mutation, by eliminating the ER-associated degradation of this protein (Su et al. 2011). Alternately, we may also analyze whether overexpression of the IRT1mCitrine$_{D173N}$, under the constitutively active 35S promoter of the cauliflower mosaic virus behaves as in yeast, forcing the location of the protein to the plasma membrane.

During this work we also investigated the molecular mechanisms that trigger the recruitment of the CIPK23 kinase upon metal binding. We had hypothesized that metal binding might trigger structuration of the loop (Cointry and Vert 2019). We have now collected structural data of the loop by CD and NMR that indicated that it remains unstructured even when metal is bound. We therefore speculate that a different molecular mechanism may be involved in recruiting the CIPK23. A possibility is that the metals may function as a "glue" between these two proteins. Metal ligands found in protein-protein interfaces are often overlooked. An analyses of oligomeric structures determined that 4-5% of non-redundant oligomeric proteins present biologically relevant first row transition metals at their interface. Moreover, Zn constitutes 40% of the metal ligand involved in those interfaces (Song et al. 2014). Metals in protein-protein interfaces can help stabilize such interaction, but they can also be implicated in transient protein-protein complexes. An example of the latter is the interaction between the lymphocyte-specific protein tyrosine kinase (Lck) to the T cell co-receptors CD4 and CD8, to phosphorylate them. This interaction is triggered by binding of Zn in two cysteine residues of the Lck kinase and two cysteines in the receptors, both located in unstructured tails of these proteins (P. W. Kim et al. 2003). We think a similar mechanisms might occur between CIPK23 and the IRT1loop. Therefore, we now need to determine whether CIPK23 has metal binding properties. I expressed and purified CIPK23 from E. coli and performed preliminary MST experiments. These indicate that indeed, the CIPK23 kinase is able to bind metal ions, although biological replicates are needed for sufficient statistically relevant results (data not shown) and controls are required. One such control may be CIPK9, a close homologue to CIPK23 that does not interact with IRT1, as seen by yeast two hybrid (Dubeaux et al. 2018). Analyses of the readily available 3D structure of CIPK23 together with directed mutagenesis will hopefully allow us to determine metal binding sites and thus, allow us to decipher whether direct metal binding on CIPK23 is equally important as direct metal binding on the IRT1 loop for the interaction of these two. Moreover, deciphering the tridimensional structure of the IRT1loop-CIPK23 complex would shed light in this event. This may however be complex to achieve given the mobile nature of the IRT1loop.

5.4 Perspectives

Achieving the tridimensional structure of IRT1 would make a strong impact in the research on ZIP transporters, and on plant membrane proteins in general. Structures of plant proteins, and especially of

membrane proteins are underrepresented in the literature. Furthermore, knowing the tridimensional structure of IRT1 would open the doors to the possibility of using it as a biotechnological tool. Specific amino acids involved in recruiting metals from the soil, in translocation and in regulatory mechanisms can be identified from the structure. Kinetic measures of IRT1 together with information we may collect from its 3D structure constitute a major starting point in utilizing efficient and specific IRT1 based phytoremediation and/or biofortification strategies. Usage of IRT1 as a biofortification tool has been reported for two different crops of agricultural interest, rice and cassava (Boonyaves et al. 2017; Narayanan et al. 2019). Overexpression of the Arabidopsis IRT1 transporter together with the chelator protein ferritin, for increased metal tolerance, and the Arabidopsis nicotianamine synthase, for elevated metal reduction capacities, in rice plants increased iron content in grain by 3.8 fold compared to the wild type (Boonyaves et al. 2017). Furthermore, for the staple crop cassava the approach used was based in expressing the stabilized mutant version of IRT1, mutated in residues K154 and K179, which prevents the internalization of IRT1 from the plasma membrane upon metal overload by its inability of being ubiquitinated, combined with the expression of the Arabidopsis ferritin 1 (FER1) protein, which creates a tolerance to intracellular metal overload by sequestration (Narayanan et al. 2019). This approach led to plants that were able to take up and storage 7 to 18 more times iron and 3 to 10 more times zinc than the wild type, making it an attractive crop for agricultural purposes with the caveat that other noxious metals such as Cd may also overaccumulate. By gathering biochemical and structural data on IRT1, we may combine the mentioned approaches with modification of specific residues to change the specificity of the whole protein. Direct mutagenesis of conserved, putative metal-binding residues of IRT1 has been previously reported to change the specificity of transport (Rogers, Eide, and Guerinot 2000). In this work, mutants with increased affinity towards iron, manganese and cadmium and towards zinc and cadmium were reported. Furthermore, the lack of specific data on the role of individual residues in metal selectivity at the time of this publication, impeded the specific manipulation of IRT1 for generating a transporter with increased affinity towards only one metal. Particularly, increasing the affinity of IRT1 to Cd is of greater interest in phytoremediation approaches.

From an agronomical point of view, biofortification approaches mentioned above, where the iron accumulation is more than 10 times elevated, may be of concern. High accumulating plants may harm soils by depleting their iron content and causing agricultural erosion. Generating plants with mild accumulation levels of metals, would be a compromise between fortification of the crop and soil conservation. We propose the generation of variants of IRT1 with modified affinity towards the regulating, non-iron metals. For instance, a mutant with lower affinity towards the non-iron metals but that still has a post-translational response, would in theory allow a higher metal accumulation than wild-type plants. The IRT1loop with two histidines mutated reported in this work, would be a candidate for an approach of this type. Moreover, we first need to assess whether impairment of the metal complexing site of the loop of IRT1 by mutating two histidines indeed lowers the binding affinity. Next, we need to generate plants to determine whether the regulation of IRT1 still takes place in these conditions. Likewise, generating IRT1 mutants that are downregulated at lower concentrations of metals than the

wild-type, would be of interest for agricultural applications in heavy-metal contaminated soils that are normally inadequate for food production. By increasing the affinity of IRT1 to the non-iron metals and maintaining its post-translational regulation, we may obtain plants that are resistant to heavy-metal polluted soils. One such mutant may be achieved by addition of metal binding residues in the proximity of the histidine stretch, or by substituting histidine residues with other metal binding residues that may increase the affinity, like cysteines for example (Cao et al. 2017). In either case, specifically modulating the affinity towards metals by modifying the IRT1loop is a promising tool for designing engineered plants adequate to different types of soil.

The structure of IRT1, may in the future be used as a model for other eukaryotic ZIPs, allowing an accurate recognition of specific residues involved in metal uptake, sensing and regulation, based on structural analysis. Furthermore, the expression and purification protocols, plus the proteoliposome reconstitution approach reported in this thesis can be adapted for other eukaryotic ZIPs. Of particular interest would be to develop such approaches for ZIP proteins of medical relevance. The human ZIP4 and ZIP13 are classical examples of ZIPs involved in health issues by their loss of function mutant alleles. The loss of function mutation of the ZIP4 protein is implicated in Acrodermatitis Enterophatica, a genetic disorder in which malfunctioning of the ZIP4 leads to poor dietary Zn uptake (Dufner-Beattie et al. 2003). Similarly, the Ehler-Danlos syndrome is caused by a G64D mutation on the ZIP13 which leads to misfolding of the transporter and its subsequent degradation, and thus a poor Zn distribution in connective tissues (Bin et al. 2014). Development of in vitro techniques that allow the biochemical characterization of these transporters are much needed. Biochemical and structural characterization of these ZIPs may allow the development of specific drugs that block the degradation of these transporters, by preventing their cellular internalization and thus, increasing Zn uptake by being retained at the plasma membrane. An approach of these characteristics was assayed in in vitro cell cultures expressing a mutant ZIP13 carrying the G64D mutation responsible for Ehler-Danlos syndrome, and consisted in pharmacological treatment with Bortezomib, a proteasome inhibitor, which indeed helped restabilizing protein levels and consequently the intracellular Zn concentration (Bin et al. 2014). Furthermore, such therapeutic approach may give rise to a number of side-effects given that this drug inhibits approximately 30% of proteasome-mediated protein degradation, thus affecting normal cell functions (Thibaudeau and Smith 2019). By determining the structure of these transporters, specific drugs with minimal side-effects may be developed.

6 Conclusions

To summarize, the experiments carried out during my thesis allowed us to begin the structural and detailed functional characterization of the main iron transporter of *Arabidopsis thaliana*. In the future, we hope that additional structural and functional information gathered from IRT1 will allow a better understanding of plant metal homeostasis and the manipulation of metal transport/sensitivity at will. Of particular interest are the development of biofortification and phytoremediation strategies and the

development of homologous strategies for the study of other eukaryotic ZIPs including in humans. We demonstrated that the IRT1 transporter, as other ZIPs, forms oligomers. The biological relevance of this particularity needs to be studied in the near future. We speculate that oligomerization may play a role in the regulation of IRT1 transport and metal sensing to fine tune metal homeostasis. During this work we also focused on studying the molecular mechanisms that drive the metal related post-transcriptional mechanisms of IRT1. We established that the mechanisms of recruitment of regulator proteins may not be structuration of the intracellular loop upon metal binding as initially thought. Further research with a focus on the regulator protein CIPK23 needs to take place in order to examine the mechanism of interaction. Finally, we were surprised to identify a putative metal binding residue in the second intracellular loop of IRT1. Until now, it was believed that only the histidine stretch located at the center of the IRT1 loop was implicated in metal binding and regulation. Further data needs to be gathered by in vitro and in vivo approaches in order to determine the specific role of aspartic acid 173.

7 Synthèse en français

Le fer, métal de transition, est un nutriment essentiel pour tous les organismes vivants. Il est impliqué dans de nombreux processus cellulaires car il est principalement utilisé comme cofacteur par une multitude de protéines. Bien qu'il soit l'un des éléments les plus abondants sur terre, le fer est souvent indisponible car il précipite dans le sol, formant des complexes insolubles. Les plantes utilisent une stratégie combinée pour absorber le fer du sol. Dans les cellules épidermiques de la racine, la pompe à protons AHA2 déclenche l'acidification du sol, tandis que la réductase FRO2 réduit les composés ferriques insolubles en ions ferreux solubles. Le fer ferreux est ensuite absorbé par la racine grâce au transporteur de fer IRT1, qui appartient à la famille des transporteurs ZIP, largement répandue. Outre le fer, IRT1 peut également transporter des métaux non ferreux (Zn, Mn, Co et Cd), qui sont également appelés substrats secondaires. Des rapports récents ont démontré qu'IRT1 détecte directement les substrats secondaires par le biais d'un tronçon riche en histidine dans la deuxième boucle intracellulaire (Dubeaux et al., 2018). Dans des conditions d'excès des substrats non ferreux, ces métaux se lient aux résidus histidine. La liaison métallique déclenche le recrutement de la kinase CIPK23, qui phosphoryle certains résidus sur la boucle d'IRT1. La phosphorylation, à son tour, permet le recrutement de la ligase E3 IDF1 qui ubiquitine IRT1 et le cible pour la dégradation par la voie endocytique.

A ce jour, les informations sur les caractéristiques structurelles d'IRT1, ses mécanismes de transport, la base de la sélectivité de transport d'IRT1 et les mécanismes moléculaires conduisant les événements de régulation tels que le recrutement de la kinase CIPK23 font défaut. Ce manque de connaissances existe pour la plupart des membres de la famille ZIP. Ce travail décrit l'initiation d'étapes cruciales pour réaliser la caractérisation biochimique de cette protéine. Ici, nous sommes les premiers à rapporter avoir établi un protocole optimisé pour l'expression hétérologue, la solubilisation et la purification de la protéine IRT1 dans des cellules de levure. De plus, nous avons déterminé une procédure technique pour l'étude du transporteur IRT1 dans des protéoliposomes, ce qui permettra l'étude de son mécanisme de transport dans le futur. Les deux approches techniques rapportées ici posent les jalons pour l'avenir de la caractérisation structurelle et mécanique d'IRT1, et pour les transporteurs ZIP en général. L'échantillon généré par notre protocole a été d'une qualité suffisante pour permettre une caractérisation préliminaire de la structure par microscopie électronique cryogénique avec nos collaborateurs. D'autres collectes de données sont nécessaires pour obtenir une structure à haute résolution d'IRT1. Nous avons également examiné la capacité d'IRT1 à former des dimères à la fois in vivo et in vitro, en soumettant l'échantillon pur à une chromatographie d'exclusion de taille couplée à la fluorescence et à ultracentrifugation analytique, ainsi qu'à des techniques in vivo telles que la co-immunoprécipitation et la complémentation bimoléculaire par fluorescence. La signification biologique de la dimérisation d'IRT1 ainsi que le mécanisme moléculaire déclenchant cet événement restent à déterminer.

De plus, nous avons étudié la nature du mécanisme moléculaire piloté par la liaison métallique sur la boucle d'IRT1. Nous avons déterminé par dichroïsme circulaire et RMN l'absence de structure

tridimensionnelle sur ladite portion de la protéine, même en présence des substrats secondaires qui déclenchent la voie de régulation d'IRT1. Nous fournissons ici des preuves supplémentaires de la liaison métallique sur la boucle d'histidines, ainsi qu'une quantification de cette interaction in vitro. De plus, nous avons déduit le rôle d'un résidu d'acide aspartique, positionné à proximité de l'histidine, qui semble avoir un rôle dans la liaison métallique.

8 Bibliography

Ajeesh Krishna, T. P., T. Maharajan, G. Victor Roch, Savarimuthu Ignacimuthu, and Stanislaus Antony Ceasar. 2020. "Structure, Function, Regulation and Phylogenetic Relationship of ZIP Family Transporters of Plants." *Frontiers in Plant Science* 11 (May): 662. https://doi.org/10.3389/fpls.2020.00662.

Alagarasan, Ganesh, Mahima Dubey, Kumar S. Aswathy, Girish Chandel, Rosalba Giugno, Vincenzo Bonnici, Ganesh Alagarasan alagarasan, et al. 2017. "Genome Wide Identification of Orthologous ZIP Genes Associated with Zinc and Iron Translocation in Setaria Italica." *Frontiers in Plant Science* 8 (May). https://doi.org/10.3389/fpls.2017.00775.

Alloway, Brian J. 2004. *Zinc in Soils and Crop Nutrition*. Brussels: IZA Publications, International Zinc Association, Scientific Research Publishing. www.fertilizer.org.

Alloway, Brian J. 2013. "Heavy Metals and Metalloids as Micronutrients for Plants and Animals BT - Heavy Metals in Soils: Trace Metals and Metalloids in Soils and Their Bioavailability." In , edited by Brian J Alloway, 195–209. Dordrecht: Springer Netherlands. https://doi.org/10.1007/978-94-007-4470-7_7.

Andrews, Glen K. 2008. "Regulation and Function of Zip4, the Acrodermatitis Enteropathica Gene." *Biochemical Society Transactions* 36 (6): 1242–46. https://doi.org/10.1042/BST0361242.

Argüello, José M, Eren Elif, and Manuel González-Guerrero. 2007. "The Structure and Function of Heavy Metal Transport P 1B-ATPases." *Biometals* 20: 233–48. https://doi.org/10.1007/s10534-006-9055-6.

Arkhipova, Valentina, Albert Guskov, and Dirk J. Slotboom. 2020. "Structural Ensemble of a Glutamate Transporter Homologue in Lipid Nanodisc Environment." *Nature Communications* 11 (1): 1–9. https://doi.org/10.1038/s41467-020-14834-8.

Arrivault, Stéphanie, Toralf Senger, and Ute Krämer. 2006. "The Arabidopsis Metal Tolerance Protein AtMTP3 Maintains Metal Homeostasis by Mediating Zn Exclusion from the Shoot under Fe Deficiency and Zn Oversupply" 46 (5): 861–79. https://doi.org/10.1111/j.1365-313X.2006.02746.x.

Askwith, Candice, David Eide, Anthony Van Ho, Philip S. Bernard, Liangtao Li, Sandra Davis-Kaplan, David M. Sipe, and Jerry Kaplan. 1994. "The FET3 Gene of S. Cerevisiae Encodes a Multicopper Oxidase Required for Ferrous Iron Uptake." *Cell* 76 (2): 403–10. https://doi.org/10.1016/0092-8674(94)90346-8.

Assunção, Ana G.L., Daniel P. Persson, Søren Husted, Jan K. Schjørring, Ross D. Alexander, and Mark G.M. Aarts. 2013. "Model of How Plants Sense Zinc Deficiency." *Metallomics*. Metallomics. https://doi.org/10.1039/c3mt00070b.

Assunção, Ana G L, Henk Schat, and Mark G M Aarts. 2010. "Regulation of the Adaptation to Zinc Deficiency in Plants." *Plant Signaling & Behavior* 5 (12): 1553–55. https://doi.org/10.4161/psb.5.12.13469.

Azouaoui, Hassina, Cédric Montigny, Aurore Jacquot, Raphaëlle Barry, Philippe Champeil, Guillaume Lenoir, and Lenoir G. Azouaoui H, Montigny C, Jacquot A, Barry R, Champeil P. 2016. "Coordinated Overexpression in Yeast of a P4-ATPase and Its Associated Cdc50 Subunit: The Case of the Drs2p/Cdc50p Lipid Flippase Complex BT - P-Type ATPases: Methods and Protocols." In , edited by Maike Bublitz, 37–55. New York, NY: Springer New York. https://doi.org/10.1007/978-1-4939-3179-8_6.

Bafaro, Elizabeth M., Sagar Antala, Tuong Vi Nguyen, Stephen P. Dzul, Brian Doyon, Timothy L. Stemmler, and Robert E. Dempski. 2015. "The Large Intracellular Loop of HZIP4 Is an Intrinsically Disordered Zinc Binding Domain." *Metallomics* 7 (9): 1319–30. https://doi.org/10.1039/c5mt00066a.

Bafaro, Elizabeth M., Mark W. Maciejewski, Jeffrey C. Hoch, and Robert E. Dempski. 2019. "Concomitant Disorder and High-affinity Zinc Binding in the Human Zinc- and Iron-regulated Transport Protein 4 Intracellular Loop." *Protein Science* 28 (5): 868–80. https://doi.org/10.1002/pro.3591.

Barberon, Marie, Guillaume Dubeaux, Cornelia Kolb, Erika Isono, Enric Zelazny, and Grégory Vert. 2014. "Polarization of IRON-REGULATED TRANSPORTER 1 (IRT1) to the Plant-Soil Interface Plays Crucial Role in Metal Homeostasis." *Proceedings of the National Academy of Sciences of the United States of America* 111 (22): 8293–98. https://doi.org/10.1073/pnas.1402262111.

Barberon, Marie, Enric Zelazny, Stéphanie Robert, Geneviève Conéjéro, Cathy Curie, Jirí Friml, and Grégory Vert. 2011. "Monoubiquitin-Dependent Endocytosis of the Transporter Controls Iron Uptake in Plants." *Proceedings of the National Academy of Sciences of the United States of America* 108: e450–58. https://doi.org/10.1073/pnas.1100659108/-/DCSupplemental.www.pnas.org/cgi/doi/10.1073/pnas.1100659108.

Benoist, Bruno De, and Erin Mclean. 2008. *Worldwide Prevalence of Anaemia 1993-2005 Who Global Database on Anaemia.*

Billesbølle, Christian B., Caleigh M. Azumaya, Rachael C. Kretsch, Alexander S. Powers, Shane Gonen, Simon Schneider, Tara Arvedson, Ron O. Dror, Yifan Cheng, and Aashish Manglik. 2020. "Structure of Hepcidin-Bound Ferroportin Reveals Iron Homeostatic Mechanisms." *Nature* 586 (7831): 807–11. https://doi.org/10.1038/s41586-020-2668-z.

Bin, Bum-Ho, Juyeon Seo, and Sung Tae Kim. 2018. "Function, Structure, and Transport Aspects of ZIP and ZnT Zinc Transporters in Immune Cells." *Journal of Immunology Research* 2018. https://doi.org/10.1155/2018/9365747.

Bin, Bum-Ho, Shintaro Hojyo, Toshiaki Hosaka, Jinhyuk Bhin, Hiroki Kano, Tomohiro Miyai, Mariko Ikeda, et al. 2014. "Molecular Pathogenesis of Spondylocheirodysplastic Ehlers-Danlos Syndrome Caused by Mutant ZIP13 Proteins." *EMBO Molecular Medicine* 6 (8): 1028–42. https://doi.org/10.15252/emmm.201303809.

Bin, Bum Ho, Toshiyuki Fukada, Toshiaki Hosaka, Satoru Yamasaki, Wakana Ohashi, Shintaro Hojyo, Tomohiro Miyai, Keigo Nishida, Shigeyuki Yokoyama, and Toshio Hirano. 2011. "Biochemical Characterization of Human ZIP13 Protein: A Homo-Dimerized Zinc Transporter Involved in the Spondylocheiro Dysplastic Ehlers-Danlos Syndrome." *Journal of Biological Chemistry* 286 (46): 40255–65. https://doi.org/10.1074/jbc.M111.256784.

Boonyaves, Kulaporn, Ting Ying Wu, Wilhelm Gruissem, and Navreet K. Bhullar. 2017. "Enhanced Grain Iron Levels in Iron-Regulated Metal Transporter, Nicotianamine Synthase, and Ferritin Gene Cassette." *Frontiers in Plant Science* 8 (FEBRUARY). https://doi.org/10.3389/fpls.2017.00130.

Bozzi, Aaron T., Lukas B. Bane, Wilhelm A. Weihofen, Abhishek Singharoy, Eduardo R. Guillen, Hidde L. Ploegh, Klaus Schulten, and Rachelle Gaudet. 2016. "Crystal Structure and Conformational Change Mechanism of a Bacterial Nramp-Family Divalent Metal Transporter." *Structure* 24 (12): 2102–14. https://doi.org/10.1016/j.str.2016.09.017.

Bozzi, Aaron T., Christina M. Zimanyi, John M. Nicoludis, Brandon K. Lee, Casey H. Zhang, and Rachelle Gaudet. 2019. "Structures in Multiple Conformations Reveal Distinct Transition Metal and Proton Pathways in an Nramp Transporter." *ELife* 8 (February). https://doi.org/10.7554/eLife.41124.

Briat, Jean-François, Isabelle Fobis-Loisy, Nicole Grignon, Stéphane Lobréaux, Nadine Pascal, Gil Savino, Séverine Thoiron, Nicolaus Wirén, and Olivier Wuytswinkel. 1995. "Cellular and Molecular Aspects of Iron Metabolism in Plants." *Biology of the Cell* 84 (1–2): 69–81. https://doi.org/10.1016/0248-4900(96)81320-7.

Burleigh, Stephen H., Brian K. Kristensen, and Iben Ellegaard Bechmann. 2003. "A Plasma Membrane Zinc Transporter from Medicago Truncatula Is Up-Regulated in Roots by Zn Fertilization, yet down-Regulated by Arbuscular Mycorrhizal Colonization." *Plant Molecular Biology* 52 (5): 1077–88. https://doi.org/10.1023/A:1025479701246.

Byers, B R, and J E L Arceneaux. 1998. *Iron Transport and Storage in Microorganisms, Plants, and Animals.* Edited by A Sigel and H Sigel. 35th ed. Marcel Dekker, Inc., New York.

Cailliatte, Rémy, Adam Schikora, Jean François Briat, Stéphane Mari, and Catherine Curie. 2010. "High-Affinity Manganese Uptake by the Metal Transporter Nramp1 Is Essential for Arabidopsis Growth in Low Manganese Conditions." *Plant Cell* 22 (3): 904–17. https://doi.org/10.1105/tpc.109.073023.

Cakmak, Smail, Kemal Y. Gülüt, Horst Marschner, and Robin D. Graham. 1994. "Effect of Zinc and Iron Deficiency on Phytosiderophore Release in Wheat Genotypes Differing in Zinc Efficiency." *Journal of Plant Nutrition* 17 (1): 1–17. https://doi.org/10.1080/01904169409364706.

Cao, Xiaoyong, Xiuzhen Hu, Xiaojin Zhang, Sujuan Gao, Changjiang Ding, Yonge Feng, and Weihua Bao. 2017. "Identification of Metal Ion Binding Sites Based on Amino Acid Sequences." *PLoS ONE* 12 (8). https://doi.org/10.1371/journal.pone.0183756.

Cellier, Mathieu, Abdelmajid Belouchi, and Phihppe Gros. 1996. "Resistance to Intracellular Infections: Comparative Genomic Analysis of Nramp."

Charlang, G, B Ng, N H Horowitz, and R M Horowitz. 1981. "Cellular and Extracellular Siderophores of Aspergillus Nidulans and Penicillium Chrysogenum." *Molecular and Cellular Biology* 1 (2): 94–100. https://doi.org/10.1128/mcb.1.2.94.

Chen, Xing Zhen, Ji Bin Peng, Adiel Cohen, Hannah Nelson, Nathan Nelson, and Matthias A. Hediger. 1999. "Yeast SMF1 Mediates H+-Coupled Iron Uptake with Concomitant Uncoupled Cation Currents." *Journal of Biological Chemistry* 274 (49): 35089–94. https://doi.org/10.1074/jbc.274.49.35089.

Cherezov, Vadim, Nicole Höfer, Doletha M.E. Szebenyi, Olga Kolaj, J. Gerard Wall, Richard Gillilan, Vasundara Srinivasan, Christopher P. Jaroniec, and Martin Caffrey. 2008. "Insights into the Mode of Action of a Putative Zinc Transporter CzrB in Thermus Thermophilus." *Structure* 16 (9): 1378–88. https://doi.org/10.1016/j.str.2008.05.014.

Chevrel, Anne, Agathe Urvoas, Ines Li De La Sierra-Gallay, Magali Aumont-Nicaise, Sandrine Moutel, Michel Desmadril, Franck Perez, et al. 2015. "Specific GFP-Binding Artificial Proteins (ARep): A New Tool for in Vitro to Live Cell Applications." *Bioscience Reports* 35 (4): 223. https://doi.org/10.1042/BSR20150080.

Chu, Heng Hsuan, Suzana Car, Amanda L. Socha, Maria N. Hindt, Tracy Punshon, and Mary Lou Guerinot. 2017. "The Arabidopsis MTP8 Transporter Determines the Localization of Manganese and Iron in Seeds." *Scientific Reports* 7 (1). https://doi.org/10.1038/s41598-017-11250-9.

Chu, Heng Hsuan, Jeff Chiecko, Tracy Punshon, Antonio Lanzirotti, Brett Lahner, David E. Salt, and Elsbeth L. Walker. 2010. "Successful Reproduction Requires the Function of Arabidopsis YELLOW STRIPE-LIKE1 and YELLOW STRIPE-LIKE3 Metal-Nicotianamine Transporters in Both Vegetative and Reproductive Structures." *Plant Physiology* 154 (1): 197–210. https://doi.org/10.1104/pp.110.159103.

Clough, Steven J., and Andrew F. Bent. 1998. "Floral Dip: A Simplified Method for Agrobacterium-Mediated Transformation of Arabidopsis Thaliana." *Plant Journal* 16 (6): 735–43. https://doi.org/10.1046/j.1365-313X.1998.00343.x.

Cockrell, Allison, Sean P. McCormick, Michael J. Moore, Mrinmoy Chakrabarti, and Paul A. Lindahl. 2014. "Mössbauer, EPR, and Modeling Study of Iron Trafficking and Regulation in Δccc1 and CCC1-up Saccharomyces Cerevisiae." *Biochemistry* 53 (18): 2926–40. https://doi.org/10.1021/bi500002n.

Cointry, Virginia, and Grégory Vert. 2019. "The Bifunctional Transporter-receptor <scp>IRT</Scp> 1 at the Heart of Metal Sensing and Signalling." *New Phytologist* 223 (3): 1173–78. https://doi.org/10.1111/nph.15826.

Colangelo, Elizabeth P., and Mary Lou Guerinot. 2004. "The Essential Basic Helix-Loop-Helix Protein FIT1 Is Required for the Iron Deficiency Response." *Plant Cell* 16 (12): 3400–3412. https://doi.org/10.1105/tpc.104.024315.

Conklin, D S, J A McMaster, M R Culbertson, and C Kung. 1992. "COT1, a Gene Involved in Cobalt Accumulation in Saccharomyces Cerevisiae." *Molecular and Cellular Biology* 12 (9): 3678–88.

https://doi.org/10.1128/mcb.12.9.3678.

Conklin, Douglas S., Michael R. Culbertson, and Ching Kung. 1994. "Interactions between Gene Products Involved in Divalent Cation Transport in Saccharomyces Cerevisiae." *MGG Molecular & General Genetics* 244 (3): 303–11. https://doi.org/10.1007/BF00285458.

Connolly, Erin L., Nathan H. Campbell, Natasha Grotz, Charis L. Prichard, and Mary Lou Guerinot. 2003. "Overexpression of the FRO2 Ferric Chelate Reductase Confers Tolerance to Growth on Low Iron and Uncovers Posttranscriptional Control." *Plant Physiology* 133 (3): 1102–10. https://doi.org/10.1104/pp.103.025122.

Conte, Sarah, David Stevenson, Ian Furner, and Alan Lloyd. 2009. "Multiple Antibiotic Resistance in Arabidopsis Is Conferred by Mutations in a Chloroplast-Localized Transport Protein." *Plant Physiology* 151 (2): 559–73. https://doi.org/10.1104/pp.109.143487.

Coudray, Nicolas, Salvatore Valvo, Minghui Hu, Ralph Lasala, Changki Kim, Martin Vink, Ming Zhou, et al. 2013. "Inward-Facing Conformation of the Zinc Transporter YiiP Revealed by Cryoelectron Microscopy." *Proceedings of the National Academy of Sciences of the United States of America* 110 (6): 2140–45. https://doi.org/10.1073/pnas.1215455110.

Courville, Pascal, Roman Chaloupka, Frédéric Veyrier, and Mathieu F.M. Cellier. 2004. "Determination of Transmembrane Topology of the Escherichia Coli Natural Resistance-Associated Macrophage Protein (Nramp) Ortholog." *Journal of Biological Chemistry* 279 (5): 3318–26. https://doi.org/10.1074/jbc.M309913200.

Curie, Catherine, Jose M. Alonso, Marie Le Jean, Joseph R. Ecker, Jean-François François Briat, Jose M Alonso †, Marie Le Jean, Joseph R. Ecker, and Jean-François François Briat. 2000. *Involvement of NRAMP1 from Arabidopsis Thaliana in Iron Transport*. Vol. 347. Portland Press Ltd. https://doi.org/10.1042/0264-6021:3470749.

Curie, Catherine, Zivile Panaviene, Clarisse Loulergue, Stephen L Dellaporta, Jean-Francois Briat, and Elsbeth L Walker. 2001. "Maize Yellow Stripe1 Encodes a Membrane Protein Directly Involved in Fe(III) Uptake." *Nature* 409 (6818): 346–49. https://doi.org/10.1038/35053080.

Dancis, A., D. G. Roman, G. J. Anderson, A. G. Hinnebusch, and R. D. Klausner. 1992. "Ferric Reductase of Saccharomyces Cerevisiae: Molecular Characterization, Role in Iron Uptake, and Transcriptional Control by Iron." *Proceedings of the National Academy of Sciences of the United States of America* 89 (9): 3869–73. https://doi.org/10.1073/pnas.89.9.3869.

Delhaize, Emmanuel, Benjamin D. Gruber, Jon K. Pittman, Rosemary G. White, Helen Leung, Yansong Miao, Liwen Jiang, Peter R. Ryan, and Alan E. Richardson. 2007. "A Role for the AtMTP11 Gene of Arabidopsis in Manganese Transport and Tolerance." *Plant Journal* 51 (2): 198–210. https://doi.org/10.1111/j.1365-313X.2007.03138.x.

Demidchik, Vadim, Helen C. Bowen, Frans J.M. Maathuis, Sergey N. Shabala, Mark A. Tester, Philip J. White, and Julia M. Davies. 2002. "Arabidopsis Thaliana Root Non-Selective Cation Channels Mediate Calcium Uptake and Are Involved in Growth." *The Plant Journal* 32 (5): 799–808. https://doi.org/10.1046/j.1365-313X.2002.01467.x.

Denisov, Ilia G., and Stephen G. Sligar. 2016. "Nanodiscs for Structural and Functional Studies of Membrane Proteins." *Nature Structural and Molecular Biology* 23 (6): 481–86. https://doi.org/10.1038/nsmb.3195.

Desbrosses-Fonrouge, Anne Garlonn, Katrin Voigt, Astrid Schröder, Stéphanie Arrivault, Sébastien Thomine, and Ute Krämer. 2005. "Arabidopsis Thaliana MTP1 Is a Zn Transporter in the Vacuolar Membrane Which Mediates Zn Detoxification and Drives Leaf Zn Accumulation." *FEBS Letters* 579 (19): 4165–74. https://doi.org/10.1016/j.febslet.2005.06.046.

Deshpande, Chandrika N., T. Alex Ruwe, Ali Shawki, Vicky Xin, Kyle R. Vieth, Erika V. Valore, Bo Qiao, et al. 2018. "Calcium Is an Essential Cofactor for Metal Efflux by the Ferroportin Transporter Family."

Nature Communications 9 (1). https://doi.org/10.1038/s41467-018-05446-4.

DiDonato, Raymond J., Louis A. Roberts, Tamara Sanderson, Robynn Bosler Eisley, and Elsbeth L. Walker. 2004. "Arabidopsis Yellow Stripe-Like2 (YSL2): A Metal-Regulated Gene Encoding a Plasma Membrane Transporter of Nicotianamine-Metal Complexes." *Plant Journal* 39 (3): 403–14. https://doi.org/10.1111/j.1365-313X.2004.02128.x.

Divol, Fanchon, Daniel Couch, Geneviève Conéjéro, Hannetz Roschzttardtz, Stéphane Mari, and Catherine Curie. 2013. "The Arabidopsis Yellow Stripe Like4 and 6 Transporters Control Iron Release from the Chloroplast." *Plant Cell* 25 (3): 1040–55. https://doi.org/10.1105/tpc.112.107672.

Dix, David, Jamie Bridgham, Margaret Broderius, and David Eide. 1997. "Characterization of the FET4 Protein of Yeast EVIDENCE FOR A DIRECT ROLE IN THE TRANSPORT OF IRON*." http://www-jbc.stanford.edu/jbc/.

Dix, David R, Jamie T. Bridgham, Margaret A. Broderius, Craig A. Byersdorfer, and David J. Eide. 1994. "The FET4 Gene Encodes the Low Affinity Fe(II) Transport Protein of Saccharomyces Cerevisiae." *Journal of Biological Chemistry* 269 (42): 26092–99. https://doi.org/10.1016/S0021-9258(18)47163-3.

Dubeaux, Guillaume, Julie Neveu, Enric Zelazny, and Grégory Vert. 2018. "Metal Sensing by the IRT1 Transporter-Receptor Orchestrates Its Own Degradation and Plant Metal Nutrition." *Molecular Cell* 69 (6): 953-964.e5. https://doi.org/10.1016/j.molcel.2018.02.009.

Dufner-Beattie, Jodi, Fudi Wang, Yien Ming Kuo, Jane Gitschier, David Eide, and Glen K. Andrews. 2003. "The Acrodermatitis Enteropathica Gene ZIP4 Encodes a Tissue-Specific, Zinc-Regulated Zinc Transporter in Mice." *Journal of Biological Chemistry* 278 (35): 33474–81. https://doi.org/10.1074/jbc.M305000200.

Durrett, Timothy P., Walter Gassmann, and Elizabeth E. Rogers. 2007. "The FRD3-Mediated Efflux of Citrate into the Root Vasculature Is Necessary for Efficient Iron Translocation." *Plant Physiology* 144 (1): 197–205. https://doi.org/10.1104/pp.107.097162.

Edelheit, Oded, Aaron Hanukoglu, and Israel Hanukoglu. 2009. "Simple and Efficient Site-Directed Mutagenesis Using Two Single-Primer Reactions in Parallel to Generate Mutants for Protein Structure-Function Studies." *BMC Biotechnology* 9 (1): 61. https://doi.org/10.1186/1472-6750-9-61.

Ehrnstorfer, Ines A., Eric R. Geertsma, Els Pardon, Jan Steyaert, and Raimund Dutzler. 2014. "Crystal Structure of a SLC11 (NRAMP) Transporter Reveals the Basis for Transition-Metal Ion Transport." *Nature Structural and Molecular Biology* 21 (11): 990–96. https://doi.org/10.1038/nsmb.2904.

Ehrnstorfer, Ines A., Cristina Manatschal, Fabian M. Arnold, Juerg Laederach, and Raimund Dutzler. 2017. "Structural and Mechanistic Basis of Proton-Coupled Metal Ion Transport in the SLC11/NRAMP Family." *Nature Communications* 8 (January). https://doi.org/10.1038/ncomms14033.

Eide, D., M. Broderius, J. Fett, and M. L. Guerinot. 1996. "A Novel Iron-Regulated Metal Transporter from Plants Identified by Functional Expression in Yeast." *Proceedings of the National Academy of Sciences* 93 (11): 5624–28. https://doi.org/10.1073/pnas.93.11.5624.

Eroglu, Seckin, Ricardo F.H. Giehl, Bastian Meier, Michiko Takahashi, Yasuko Terada, Konstantin Ignatyev, Elisa Andresen, Hendrik Küpper, Edgar Peiter, and Nicolaus von Wirén. 2017. "Metal Tolerance Protein 8 Mediates Manganese Homeostasis and Iron Reallocation during Seed Development and Germination." *Plant Physiology* 174 (3): 1633–47. https://doi.org/10.1104/pp.16.01646.

Eroglu, Seckin, Bastian Meier, Nicolaus von Wirén, and Edgar Peiter. 2016. "The Vacuolar Manganese Transporter Mtp8 Determines Tolerance to Iron Deficiency-Induced Chlorosis in Arabidopsis." *Plant Physiology* 170 (2): 1030–45. https://doi.org/10.1104/pp.15.01194.

Feroz, Hasin, Hyeyoung Kwon, Jing Peng, Hyeonji Oh, Bryan Ferlez, Carol S. Baker, John H. Golbeck, Guillermo C. Bazan, Andrew L. Zydney, and Manish Kumar. 2018. "Improving Extraction and Post-Purification Concentration of Membrane Proteins." *Analyst* 143 (6): 1378–86. https://doi.org/10.1039/c7an01470h.

Forbes, John R., and Phillippe Gros. 2001. "Divalent-Metal Transport by NRAMP Proteins at the Interface of Host-Pathogen Interactions." *Trends in Microbiology*. Elsevier. https://doi.org/10.1016/S0966-842X(01)02098-4.

Fourcroy, Pierre, Patricia Sisó-Terraza, Damien Sudre, María Savirón, Guilhem Reyt, Frédéric Gaymard, Anunciación Abadía, Javier Abadia, Ana Álvarez-Fernández, and Jean-François François Briat. 2014. "Involvement of the ABCG37 Transporter in Secretion of Scopoletin and Derivatives by Arabidopsis Roots in Response to Iron Deficienc." *New Phytologist* 201 (1): 155–67. https://doi.org/10.1111/nph.12471.

Franz, Marie C., Jonai Pujol-Giménez, Nicolas Montalbetti, Miguel Fernandez-Tenorio, Timothy R. Degrado, Ernst Niggli, Michael F. Romero, and Matthias A. Hediger. 2018. "Reassessment of the Transport Mechanism of the Human Zinc Transporter SLC39A2." *Biochemistry* 57 (26): 3976–86. https://doi.org/10.1021/acs.biochem.8b00511.

Gaither, L. Alex, and David J. Eide. 2000. "Functional Expression of the Human HZIP2 Zinc Transporter." *Journal of Biological Chemistry* 275 (8): 5560–64. https://doi.org/10.1074/jbc.275.8.5560.

———. 2001. "Eukaryotic Zinc Transporters and Their Regulation." *BioMetals* 14 (3–4): 251–70. https://doi.org/10.1023/A:1012988914300.

Ganasen, Menega, Hiromi Togashi, Hanae Takeda, Honami Asakura, Takehiko Tosha, Keitaro Yamashita, Kunio Hirata, et al. 2018. "Structural Basis for Promotion of Duodenal Iron Absorption by Enteric Ferric Reductase with Ascorbate." *Communications Biology* 1 (1). https://doi.org/10.1038/s42003-018-0121-8.

Gao, Caiji, Ming Luo, Qiong Zhao, Renzhi Yang, Yong Cui, Yonglun Zeng, Jun Xia, and Liwen Jiang. 2014. "A Unique Plant ESCRT Component, FREE1, Regulates Multivesicular Body Protein Sorting and Plant Growth." *Current Biology* 24 (21): 2556–63. https://doi.org/10.1016/j.cub.2014.09.014.

Gao, Fei, Kevin Robe, Mathilde Bettembourg, Nathalia Navarro, Valérie Rofidal, Véronique Santoni, Frédéric Gaymard, et al. 2020. "The Transcription Factor BHLH121 Interacts with BHLH105 (ILR3) and Its Closest Homologs to Regulate Iron Homeostasis in Arabidopsis." *Plant Cell* 32 (2): 508–24. https://doi.org/10.1105/tpc.19.00541.

Gao, Fei, Kevin Robe, Frederic Gaymard, Esther Izquierdo, and Christian Dubos. 2019. "The Transcriptional Control of Iron Homeostasis in Plants: A Tale of BHLH Transcription Factors?" *Frontiers in Plant Science* 10 (January): 6. https://doi.org/10.3389/fpls.2019.00006.

Gao, Huiling, Wenxiang Xie, Changhong Yang, Jingyi Xu, Jingjun Li, Hua Wang, Xi Chen, and Chao-Feng Feng Huang. 2018. "NRAMP2, a Trans-Golgi Network-Localized Manganese Transporter, Is Required for Arabidopsis Root Growth under Manganese Deficiency." *New Phytologist* 217 (1): 179–93. https://doi.org/10.1111/nph.14783.

Garrick, Michael D. 2011. "Human Iron Transporters." *Genes and Nutrition*. BioMed Central. https://doi.org/10.1007/s12263-010-0184-8.

Georgatsou, E, and D Alexandraki. 1994. "Two Distinctly Regulated Genes Are Required for Ferric Reduction, the First Step of Iron Uptake in Saccharomyces Cerevisiae." *Molecular and Cellular Biology* 14 (5): 3065–73. https://doi.org/10.1128/mcb.14.5.3065.

Girijashanker, Kuppuswami, Lei He, Manoocher Soleimani, Jodie M Reed, Hong Li, Zhiwei Liu, Bin Wang, Timothy P Dalton, Daniel W Nebert, and Mol Pharmacol Author. 2008. "Slc39a14 Gene Encodes ZIP14, A Metal/Bicarbonate Symporter: Similarities to the ZIP8 Transporter Author Manuscript." *Mol Pharmacol* 73 (5): 1413–23. https://doi.org/10.1124/mol.107.043588.

Gitan, Raad S., and David J. Eide. 2000. "Zinc-Regulated Ubiquitin Conjugation Signals Endocytosis of the Yeast ZRT1 Zinc Transporter." *Biochem. J.* Vol. 346. Portland Press Ltd. https://doi.org/10.1042/bj3460329.

Gitan, Raad S, Huan Luo, Jacquelyn Rodgers, Margaret Broderius, and David Eide. 1998. "Zinc-Induced

Inactivation of the Yeast ZRT1 Zinc Transporter Occurs through Endocytosis and Vacuolar Degradation*." http://www.jbc.org/.

Gitan, Raad, Monir Shababi, Michelle Kramer, and eide. 2003. "A Cytosolic Domain of the Yeast Zrt1 Zinc Transporter Is Required for Its Post-Translational Inactivation in Response to Zinc and Cadmium." *Article in Journal of Biological Chemistry* 278 (41): 39558–64. https://doi.org/10.1074/jbc.M302760200.

Gollhofer, Julia, Roman Timofeev, Ping Lan, Wolfgang Schmidt, and Thomas J. Buckhout. 2014. "Vacuolar-Iron-Transporter1-Like Proteins Mediate Iron Homeostasis in Arabidopsis." Edited by Stephan Neil Witt. *PLoS ONE* 9 (10): e110468. https://doi.org/10.1371/journal.pone.0110468.

Gourdon, Pontus, Xiang Yu Liu, Tina Skjorringe, J. Preben Morth, Lisbeth Birk Møller, Bjorn Panyella Pedersen, and Poul Nissen. 2011. "Crystal Structure of a Copper-Transporting PIB-Type ATPase." *Nature* 475 (7354): 59–65. https://doi.org/10.1038/nature10191.

Grass, Gregor, Markus Otto, Beate Fricke, Christopher J. Haney, Christopher Rensing, Dietrich H. Nies, and Doreen Munkelt. 2005. "FieF (YiiP) from Escherichia Coli Mediates Decreased Cellular Accumulation of Iron and Relieves Iron Stress." *Archives of Microbiology* 183 (1): 9–18. https://doi.org/10.1007/s00203-004-0739-4.

Gratão, Priscila L., Andrea Polle, Peter J. Lea, and Ricardo A. Azevedo. 2005. "Making the Life of Heavy Metal-Stressed Plants a Little Easier." *Functional Plant Biology*. CSIRO PUBLISHING. https://doi.org/10.1071/FP05016.

Gratz, Regina, Prabha Manishankar, Rumen Ivanov, Philipp Köster, Inga Mohr, Ksenia Trofimov, Leonie Steinhorst, et al. 2019. "CIPK11-Dependent Phosphorylation Modulates FIT Activity to Promote Arabidopsis Iron Acquisition in Response to Calcium Signaling." *Developmental Cell* 48 (5): 726-740.e10. https://doi.org/10.1016/j.devcel.2019.01.006.

Gries, Dirk, Sylke Brunn, David E. Crowley, and David R. Parker. 1995. "Phytosiderophore Release in Relation to Micronutrient Metal Deficiencies in Barley." *Plant and Soil* 172 (2): 299–308. https://doi.org/10.1007/BF00011332.

Griesinger, C., G. Otting, K. Wüthrich, and R. R. Ernst. 1988. "Clean Tocsy for 1H Spin System Identification in Macromolecules." *Journal of the American Chemical Society* 110 (23): 7870–72. https://doi.org/10.1021/ja00231a044.

Grossoehme, Nicholas E., Shreeram Akilesh, Mary Lou Guerinot, and Dean E. Wilcox. 2006. "Metal-Binding Thermodynamics of the Histidine-Rich Sequence from the Metal-Transport Protein IRT1 of Arabidopsis Thaliana." *Inorganic Chemistry* 45 (21): 8500–8508. https://doi.org/10.1021/ic0606431.

Grotz, Natasha, Tama Fox, Erin Connolly, Walter Park, Mary Lou Guerinot, and David Eide. 1998. "Identification of a Family of Zinc Transporter Genes from Arabidopsis That Respond to Zinc Deficiency." *Proceedings of the National Academy of Sciences of the United States of America* 95 (12): 7220–24. https://doi.org/10.1073/pnas.95.12.7220.

Guerinot, Mary Lou. 2000. "The ZIP Family of Metal Transporters." *Biochimica et Biophysica Acta - Biomembranes* 1465 (1–2): 190–98. https://doi.org/10.1016/S0005-2736(00)00138-3.

Guffanti, Arthur A., Yi Wei, Sacha V. Rood, and Terry A. Krulwich. 2002. "An Antiport Mechanism for a Member of the Cation Diffusion Facilitator Family: Divalent Cations Efflux in Exchange for K+ and H+." *Molecular Microbiology* 45 (1): 145–53. https://doi.org/10.1046/j.1365-2958.2002.02998.x.

Gulec, Sukru, Gregory J. Anderson, and James F. Collins. 2014. "Mechanistic and Regulatory Aspects of Intestinal Iron Absorption." *American Journal of Physiology - Gastrointestinal and Liver Physiology*. American Physiological Society. https://doi.org/10.1152/ajpgi.00348.2013.

Gunshin, Hiromi, Bryan Mackenzie, Urs V. Berger, Yoshimi Gunshin, Michael F. Romero, Walter F. Boron, Stephan Nussberger, John L. Gollan, and Matthiaa A. Hediger. 1997. "Cloning and Characterization of a Mammalian Proton-Coupled Metal-Ion Transporter." *Nature* 388 (6641): 482–88.

https://doi.org/10.1038/41343.

Güntert, P., C. Mumenthaler, and K. Wüthrich. 1997. "Torsion Angle Dynamics for NMR Structure Calculation with the New Program DYANA." *Journal of Molecular Biology* 273 (1): 283–98. https://doi.org/10.1006/jmbi.1997.1284.

Guthrie, Gregory J., Tolunay B. Aydemir, Catalina Troche, Alyssa B. Martin, Shou Mei Chang, and Robert J. Cousins. 2015. "Influence of ZIP14 (Slc39A14) on Intestinal Zinc Processing and Barrier Function." *American Journal of Physiology - Gastrointestinal and Liver Physiology* 308 (3): G171–78. https://doi.org/10.1152/ajpgi.00021.2014.

Haydon, Michael J., and Christopher S. Cobbett. 2007. "Transporters of Ligands for Essential Metal Ions in Plants: Research Review." *New Phytologist*. John Wiley & Sons, Ltd. https://doi.org/10.1111/j.1469-8137.2007.02051.x.

He, Lei, Kuppuswami Girijashanker, Timothy P. Dalton, Jodie Reed, Hong Li, Manoocher Soleimani, and Daniel W. Nebert. 2006. "ZIP8, Member of the Solute-Carrier-39 (SLC39) Metal-Transporter Family: Characterization of Transporter Properties." *Molecular Pharmacology* 70 (1): 171–80. https://doi.org/10.1124/mol.106.024521.

Henriques, Rossana, Markus Klein, Enrico Martinoia, Urs Feller, Jeff Schell, Maria S Pais, and Csaba Koncz. 2002. "Knock-out of Arabidopsis Metal Transporter Gene IRT1 Results in Iron Deficiency Accompanied by Cell Differentiation Defects." *Plant Molecular Biology* 50: 587–97.

Heymann, Petra, Joachim F. Ernst, and Günther Winkelmann. 2000. "A Gene of the Major Facilitator Superfamily Encodes a Transporter for Enterobactin (Enb1p) in Saccharomyces Cerevisiae." *BioMetals* 13 (1): 65–72. https://doi.org/10.1023/A:1009250017785.

Hoch, Eitan, Wei Lin, Jin Chai, Michal Hershfinkel, Dax Fu, and Israel Sekler. 2012. "Histidine Pairing at the Metal Transport Site of Mammalian ZnT Transporters Controls Zn2+ over Cd2+ Selectivity." *Proceedings of the National Academy of Sciences of the United States of America* 109 (19): 7202–7. https://doi.org/10.1073/pnas.1200362109.

Hong, Zhi, Hua Jin, Tzvi Tzfira, and Jianming Li. 2008. "Multiple Mechanism-Mediated Retention of a Defective Brassinosteroid Receptor in the Endoplasmic Reticulum of Arabidopsis." *Plant Cell* 20 (12): 3418–29. https://doi.org/10.1105/tpc.108.061879.

Hu, Jian, Holger Wille, and Gerold Schmitt-Ulms. 2018. "The Evolutionary UnZIPping of a Dimerization Motif—a Comparison of ZIP and PrP Architectures." *Pathogens* 7 (1). https://doi.org/10.3390/pathogens7010004.

Huang, Sheng, Akimasa Sasaki, Naoki Yamaji, Haruka Okada, Namiki Mitani-Ueno, and Jian Feng Ma. 2020. "The ZIP Transporter Family Member OsZIP9 Contributes to Root Zinc Uptake in Rice under Zinc-Limited Conditions." *Plant Physiology* 183 (3): 1224–34. https://doi.org/10.1104/pp.20.00125.

Hussain, Dawar, Michael J. Haydon, Yuwen Wang, Edwin Wong, Sarah M. Sherson, Jeff Young, James Camakaris, Jeffrey F. Harper, and Christopher S. Cobbett. 2004. "P-Type ATPase Heavy Metal Transporters with Roles in Essential Zinc Homeostasis in Arabidopsis." *Plant Cell* 16 (5): 1327–39. https://doi.org/10.1105/tpc.020487.

Hussain, Rohanah, and Giuliano Siligardi. 2016. "Characterisation of Conformational and Ligand Binding Properties of Membrane Proteins Using Synchrotron Radiation Circular Dichroism (SRCD)." In *Advances in Experimental Medicine and Biology*, 922:43–59. Springer New York LLC. https://doi.org/10.1007/978-3-319-35072-1_4.

Ishimaru, Yasuhiro, Motofumi Suzuki, Takashi Tsukamoto, Kazumasa Suzuki, Mikio Nakazono, Takanori Kobayashi, Yasuaki Wada, et al. 2006. "Rice Plants Take up Iron as an Fe3+-Phytosiderophore and as Fe2+." *Plant Journal* 45 (3): 335–46. https://doi.org/10.1111/j.1365-313X.2005.02624.x.

Ivanov, Rumen, Tzvetina Brumbarova, Ailisa Blum, Anna Maria Jantke, Claudia Fink-Straube, and Petra Bauer. 2014. "SORTING NEXIN1 Is Required for Modulating the Trafficking and Stability of the

Arabidopsis IRON-REGULATED TRANSPORTER1." *Plant Cell* 26 (3): 1294–1307. https://doi.org/10.1105/tpc.113.116244.

Jain, Ajay, Bhaskaran Sinilal, Gurusamy Dhandapani, Richard B. Meagher, and Shivendra V. Sahi. 2013. "Effects of Deficiency and Excess of Zinc on Morphophysiological Traits and Spatiotemporal Regulation of Zinc-Responsive Genes Reveal Incidence of Cross Talk between Micro- and Macronutrients." *Environmental Science and Technology* 47 (10): 5327–35. https://doi.org/10.1021/es400113y.

Jakoby, Marc, Hong Yu Wang, Wim Reidt, Bernd Weisshaar, and Petra Bauer. 2004. "FRU (BHLH029) Is Required for Induction of Iron Mobilization Genes in Arabidopsis Thaliana." *FEBS Letters* 577 (3): 528–34. https://doi.org/10.1016/j.febslet.2004.10.062.

Jáuregui-Lobera, Ignacio. 2014. "Iron Deficiency and Cognitive Functions." *Neuropsychiatric Disease and Treatment*. Dove Medical Press Ltd. https://doi.org/10.2147/NDT.S72491.

Jensen, Laran T, Mispa Ajua-Alemanji, and Valeria Cizewski Culotta. 2003. "The Saccharomyces Cerevisiae High Affinity Phosphate Transporter Encoded by PHO84 Also Functions in Manganese Homeostasis*." https://doi.org/10.1074/jbc.M307413200.

Jidenko, Marie, Guillaume Lenoir, José M. Fuentes, Marc le Maire, and Christine Jaxel. 2006. "Expression in Yeast and Purification of a Membrane Protein, SERCA1a, Using a Biotinylated Acceptor Domain." *Protein Expression and Purification* 48 (1): 32–42. https://doi.org/10.1016/j.pep.2006.03.001.

Jidenko, Marie, Rikke C. Nielsen, Thomas Lykke Møller Sørensen, Jesper V. Møller, Marc Le Maire, Poul Nissen, and Christine Jaxel. 2005. "Crystallization of a Mammalian Membrane Protein Overexpressed in Saccharomyces Cerevisiae." *Proceedings of the National Academy of Sciences of the United States of America* 102 (33): 11687–91. https://doi.org/10.1073/pnas.0503986102.

Kai, Kosuke, Masaharu Mizutani, Naohiro Kawamura, Ryotaro Yamamoto, Michiko Tamai, Hikaru Yamaguchi, Kanzo Sakata, and Bun Ichi Shimizu. 2008. "Scopoletin Is Biosynthesized via Ortho-Hydroxylation of Feruloyl CoA by a 2-Oxoglutarate-Dependent Dioxygenase in Arabidopsis Thaliana." *Plant Journal* 55 (6): 989–99. https://doi.org/10.1111/j.1365-313X.2008.03568.x.

Kambe, Taiho, Jim Geiser, Brett Lahner, David E. Salt, and Glen K. Andrews. 2008. "Slc39a1 to 3 (Subfamily II) Zip Genes in Mice Have Unique Cell-Specific Functions during Adaptation to Zinc Deficiency." *American Journal of Physiology - Regulatory Integrative and Comparative Physiology* 294 (5): R1474. https://doi.org/10.1152/ajpregu.00130.2008.

Kambe, Taiho, Tomoyuki Suzuki, Masaya Nagao, and Yuko Yamaguchi-Iwai. 2006. *Sequence Similarity and Functional Relationship among Eukaryotic ZIP and CDF Transporters. Genomics, Proteomics and Bioinformatics*. Vol. 4. Beijing Genomics Institute. https://doi.org/10.1016/S1672-0229(06)60010-7.

Kamizono, Akihito, Masafumi Nishizawa, Yutaka Teranishi, Kousaku Murata, and Akira Kimura. 1989. "Identification of a Gene Conferring Resistance to Zinc and Cadmium Ions in the Yeast Saccharomyces Cerevisiae." *MGG Molecular & General Genetics* 219 (1–2): 161–67. https://doi.org/10.1007/BF00261172.

Kapust, Rachel B., and David S. Waugh. 1999. " Escherichia Coli Maltose-Binding Protein Is Uncommonly Effective at Promoting the Solubility of Polypeptides to Which It Is Fused ." *Protein Science* 8 (8): 1668–74. https://doi.org/10.1110/ps.8.8.1668.

Kato, Takafumi, Kaoru Kumazaki, Miki Wada, Reiya Taniguchi, Takanori Nakane, Keitaro Yamashita, Kunio Hirata, et al. 2019. "Crystal Structure of Plant Vacuolar Iron Transporter VIT1." *Nature Plants* 5 (3): 308–15. https://doi.org/10.1038/s41477-019-0367-2.

Kawachi, Miki, Yoshihiro Kobae, Tetsuro Mimura, and Masayoshi Maeshima. 2008. "Deletion of a Histidine-Rich Loop of AtMTP1, a Vacuolar Zn 2+/H+ Antiporter of Arabidopsis Thaliana, Stimulates the Transport Activity." *Journal of Biological Chemistry* 283 (13): 8374–83. https://doi.org/10.1074/jbc.M707646200.

Kerkeb, Loubna, Indrani Mukherjee, Iera Chatterjee, Brett Lahner, David E Salt, and Erin L Connolly. 2008. "Iron-Induced Turnover of the Arabidopsis IRON-REGULATED TRANSPORTER1 Metal Transporter Requires Lysine Residues 1[W][OA]." *Plant Physiology* 146: 1964–73. https://doi.org/10.1104/pp.107.113282.

Kerppola, R. E., and G. F.L. Ames. 1992. "Topology of the Hydrophobic Membrane-Bound Components of the Histidine Periplasmic Permease. Comparison with Other Members of the Family." *Journal of Biological Chemistry* 267 (4): 2329–36. https://europepmc.org/article/MED/1733937.

Kerppola, Tom K. 2008. "Bimolecular Fluorescence Complementation (BiFC) Analysis as a Probe of Protein Interactions in Living Cells." *Annual Review of Biophysics*. https://doi.org/10.1146/annurev.biophys.37.032807.125842.

Kim, Byung Eun, Fudi Wang, Jodi Dufner-Beattie, Glen K. Andrews, David J. Eide, and Michael J. Petris. 2004. "Zn2+-Stimulated Endocytosis of the MZIP4 Zinc Transporter Regulates Its Location at the Plasma Membrane." *Journal of Biological Chemistry* 279 (6): 4523–30. https://doi.org/10.1074/jbc.M310799200.

Kim, Leah, Kaitlyn Tsuyuki, Fengling Hu, Emily Park, Jingwen Zhang, Jennifer Gallegos Iraheta, Ju-Chen Chia, et al. 2020. "Ferroportin 3 Is a Dual-Targeted Mitochondrial/Chloroplast Iron Exporter Necessary for Iron Homeostasis in Arabidopsis." *BioRxiv*, July, 2020.07.15.203646. https://doi.org/10.1101/2020.07.15.203646.

Kim, Peter W., Zhen Yu J. Sun, Stephen C. Blacklow, Gerhard Wagner, and Michael J. Eck. 2003. "A Zinc Clasp Structure Tethers Lck to T Cell Coreceptors CD4 and CD8." *Science* 301 (5640): 1725–28. https://doi.org/10.1126/science.1085643.

Kim, Sun A., Tracy Punshon, Antonio Lanzirotti, Angtao Li, José M. Alonso, Joseph R. Ecker, Jerry Kaplan, and Mary Lou Guerinot. 2006. "Localization of Iron in Arabidopsis Seed Requires the Vacuolar Membrane Transporter VIT1." *Science* 314 (5803): 1295–98. https://doi.org/10.1126/science.1132563.

Kim, Sun A, Ian S Lacroix, Scott A Gerber, and Mary Lou. 2019. "The Iron Deficiency Response in Arabidopsis Thaliana Requires the Phosphorylated Transcription Factor URI." https://doi.org/10.1073/pnas.1916892116.

Kim, Yu Young, Hyunju Choi, Shoji Segami, Hyung Taeg Cho, Enrico Martinoia, Masayoshi Maeshima, and Youngsook Lee. 2009. "AtHMA1 Contributes to the Detoxification of Excess Zn(II) in Arabidopsis." *Plant Journal* 58 (5): 737–53. https://doi.org/10.1111/j.1365-313X.2009.03818.x.

Kobayashi, Takanori, Seiji Nagasaka, Takeshi Senoura, Reiko Nakanishi Itai, Hiromi Nakanishi, and Naoko K. Nishizawa. 2013. "Iron-Binding Haemerythrin RING Ubiquitin Ligases Regulate Plant Iron Responses and Accumulation." *Nature Communications* 4 (1): 1–12. https://doi.org/10.1038/ncomms3792.

Korshunova, YuliaO. O., David Eide, W Gregg Clark, Mary Lou Guerinot, HimadriB. B. Pakrasi, W. Gregg Clark, Mary Lou Guerinot, and HimadriB. B. Pakrasi. 1999. "The IRT1 Protein from *Arabidopsis Thaliana* Is a Metal Transporter with a Broad Substrate Range." *Plant Molecular Biology* 40 (1): 37–44. https://doi.org/10.1023/A:1026438615520.

Kotov, Vadim, Kim Bartels, Katharina Veith, Inokentijs Josts, Udaya K.Tiruttani Subhramanyam, Christian Günther, Jörg Labahn, et al. 2019. "High-Throughput Stability Screening for Detergent-Solubilized Membrane Proteins." *Scientific Reports* 9 (1): 1–19. https://doi.org/10.1038/s41598-019-46686-8.

Kroh, Gretchen E, and Marinus Pilon. 2020. "Regulation of Iron Homeostasis and Use in Chloroplasts."

Kumar, Anil, R. R. Ernst, and K. Wüthrich. 1980. "A Two-Dimensional Nuclear Overhauser Enhancement (2D NOE) Experiment for the Elucidation of Complete Proton-Proton Cross-Relaxation Networks in Biological Macromolecules." *Topics in Catalysis* 95 (1): 1–6. https://doi.org/10.1016/0006-291X(80)90695-6.

Küry, Sébastien, Brigitte Dréno, Stéphane Bézieau, Stéphanie Giraudet, Monia Kharfi, Ridha Kamoun, and Jean Paul Moisan. 2002. "Identification of SLC39A4, a Gene Involved in Acrodermatitis Enteropathica." *Nature Genetics* 31 (3): 239–40. https://doi.org/10.1038/ng913.

Kwok, Ernest Y., Scott Severance, and Daniel J. Kosman. 2006. "Evidence for Iron Channeling in the Fet3p-Ftr1p High-Affinity Iron Uptake Complex in the Yeast Plasma Membrane." *Biochemistry* 45 (20): 6317–27. https://doi.org/10.1021/bi052173c.

Laitaoja, Mikko, Jarkko Valjakka, and Janne Jänis. 2013. "Zinc Coordination Spheres in Protein Structures." *Inorganic Chemistry* 52 (19): 10983–91. https://doi.org/10.1021/ic401072d.

Lan, Ping, Wenfeng Li, Tuan Nan Wen, Jeng Yuan Shiau, Yu Ching Wu, Wendar Lin, and Wolfgang Schmidt. 2011. "ITRAQ Protein Profile Analysis of Arabidopsis Roots Reveals New Aspects Critical for Iron Homeostasis." *Plant Physiology* 155 (2): 821–34. https://doi.org/10.1104/pp.110.169508.

Lanquar, Viviane, Guido Grossmann, Jan L. Vinkenborg, Maarten Merkx, Sébastien Thomine, and Wolf B. Frommer. 2014. "Dynamic Imaging of Cytosolic Zinc in Arabidopsis Roots Combining FRET Sensors and RootChip Technology." *New Phytologist* 202 (1): 198–208. https://doi.org/10.1111/nph.12652.

Lanquar, Viviane, Françoise Lelièvre, Susanne Bolte, Cécile Hamès, Carine Alcon, Dieter Neumann, Gérard Vansuyt, et al. 2005. "Mobilization of Vacuolar Iron by AtNRAMP3 and AtNRAMP4 Is Essential for Seed Germination on Low Iron." *EMBO Journal* 24 (23): 4041–51. https://doi.org/10.1038/sj.emboj.7600864.

Lasswell, Jamie, Luise E Rogg, David C Nelson, Catherine Rongey, and Bonnie Bartel. 2000. "Cloning and Characterization of IAR1 , a Gene Required for Auxin Conjugate Sensitivity in Arabidopsis." *The Plant Cell.* Vol. 12. www.plantcell.org.

Lee, Sichul, and Gynheung An. 2009. "Over-Expression of OsIRT1 Leads to Increased Iron and Zinc Accumulations in Rice." *Plant, Cell and Environment* 32 (4): 408–16. https://doi.org/10.1111/j.1365-3040.2009.01935.x.

Li, Liangtao, Opal S. Chen, Diane Mc Vey Ward, and Jerry Kaplan. 2001. "CCC1 Is a Transporter That Mediates Vacuolar Iron Storage in Yeast." *Journal of Biological Chemistry* 276 (31): 29515–19. https://doi.org/10.1074/jbc.M103944200.

Li, Suzhen, Xiaojin Zhou, Yaqun Huang, Liying Zhu, Shaojun Zhang, Yongfeng Zhao, Jinjie Guo, Jingtang Chen, and Rumei Chen. 2013. "Identification and Characterization of the Zinc-Regulated Transporters, Iron-Regulated Transporter-like Protein (ZIP) Gene Family in Maize." *BMC Plant Biology* 13 (1). https://doi.org/10.1186/1471-2229-13-114.

Li, Wenfeng, and Wolfgang Schmidt. 2010. "A Lysine-63-Linked Ubiquitin Chain-Forming Conjugase, UBC13, Promotes the Developmental Responses to Iron Deficiency in Arabidopsis Roots." *Plant Journal* 62 (2): 330–43. https://doi.org/10.1111/j.1365-313X.2010.04150.x.

Li, Xiaoli, Huimin Zhang, Qin Ai, Gang Liang, and Diqiu Yu. 2016. "Two BHLH Transcription Factors, BHLH34 and BHLH104, Regulate Iron Homeostasis in Arabidopsis Thaliana." *Plant Physiology* 170 (4): 2478–93. https://doi.org/10.1104/pp.15.01827.

Liang, Gang, Huimin Zhang, Xiaoli Li, Qin Ai, and Diqiu Yu. 2017. "BHLH Transcription Factor BHLH115 Regulates Iron Homeostasis in Arabidopsis Thaliana." *Journal of Experimental Botany* 68 (7): 1743–55. https://doi.org/10.1093/jxb/erx043.

Lin, Wei, Jin Chai, James Love, and Dax Fu. 2010. "Selective Electrodiffusion of Zinc Ions in a Zrt-, Irt-like Protein, ZIPB." *Journal of Biological Chemistry* 285 (50): 39013–20. https://doi.org/10.1074/jbc.M110.180620.

Lin, Ya-Fen Fen, Hong-Ming Ming Liang, Shu-Yi Yi Yang, Annegret Boch, Stephan Clemens, Chyi-Chuann Chuann Chen, Jing-Fen Fen Wu, Jing-Ling Ling Huang, and Kuo-Chen Chen Yeh. 2009. "Arabidopsis IRT3 Is a Zinc-Regulated and Plasma Membrane Localized Zinc/Iron Transporter." *New Phytologist* 182 (2): 392–404. https://doi.org/10.1111/j.1469-8137.2009.02766.x.

Liu, Zhiwei, Hong Li, Manoocher Soleimani, Kuppuswami Girijashanker, Jodie M. Reed, Lei He, Timothy P. Dalton, and Daniel W. Nebert. 2008. "Cd 2+ versus Zn 2+ Uptake by the ZIP8 HCO 3 −-Dependent Symporter: Kinetics, Electrogenicity and Trafficking." *Biochemical and Biophysical Research Communications* 365 (4): 814–20. https://doi.org/10.1016/j.bbrc.2007.11.067.

Liuzzi, Juan P., Liang Guo, Shou-Mei Chang, and Robert J. Cousins. 2009. "Krüppel-like Factor 4 Regulates Adaptive Expression of the Zinc Transporter *Zip4* in Mouse Small Intestine." *American Journal of Physiology-Gastrointestinal and Liver Physiology* 296 (3): G517–23. https://doi.org/10.1152/ajpgi.90568.2008.

Long, Terri A., Hironaka Tsukagoshi, Wolfgang Busch, Brett Lahner, David E. Salt, and Philip N. Benfey. 2010. "The BHLH Transcription Factor POPEYE Regulates Response to Iron Deficiency in Arabidopsis Roots." *Plant Cell* 22 (7): 2219–36. https://doi.org/10.1105/tpc.110.074096.

López-Millán, Ana Flor, Danielle R. Ellis, and Michael A. Grusak. 2004. "Identification and Characterization of Several New Members of the ZIP Family of Metal Ion Transporters in Medicago Truncatula." *Plant Molecular Biology* 54 (4): 583–96. https://doi.org/10.1023/B:PLAN.0000038271.96019.aa.

Lu, Min, and Dax Fu. 2007. "Structure of the Zinc Transporter YiiP." *Science* 317 (5845): 1746–48. https://doi.org/10.1126/science.1143748.

Ludewig, Uwe, Stephanie Wilken, Binghua Wu, Wolfgang Jost, Petr Obrdlik, Mohamed El Bakkoury, Anne Marie Marini, et al. 2003. "Homo- and Hetero-Oligomerization of Ammonium Transporter-1 NH +4 Uniporters." *Journal of Biological Chemistry* 278 (46): 45603–10. https://doi.org/10.1074/jbc.M307424200.

MacDiarmid, Colin W., L. Alex Gaither, and David Eide. 2000. "Zinc Transporters That Regulate Vacuolar Zinc Storage in Saccharomyces Cerevisiae." *EMBO Journal* 19 (12): 2845–55. https://doi.org/10.1093/emboj/19.12.2845.

Macgregor, Margaret W. 1963. "Maternal Anaemia as a Factor in Prematurity and Perinatal Mortality." *Scottish Medical Journal* 8 (4): 134–40. https://doi.org/10.1177/003693306300800402.

Mai, Hans Jörg, Stéphanie Pateyron, and Petra Bauer. 2016. "Iron Homeostasis in Arabidopsis Thaliana: Transcriptomic Analyses Reveal Novel FIT-Regulated Genes, Iron Deficiency Marker Genes and Functional Gene Networks." *BMC Plant Biology* 16 (1). https://doi.org/10.1186/s12870-016-0899-9.

Manatschal, Cristina, Jonai Pujol-Gimé Nez, Marion Poirier, Jean-Louis Reymond, Matthias A Hediger, and Raimund Dutzler. 2019. "Mechanistic Basis of the Inhibition of SLC11/NRAMP-Mediated Metal Ion Transport by Bis-Isothiourea Substituted Compounds." https://doi.org/10.7554/eLife.51913.

Mancias, Joseph D., and Jonathan Goldberg. 2005. "Exiting the Endoplasmic Reticulum." *Traffic*. John Wiley & Sons, Ltd. https://doi.org/10.1111/j.1600-0854.2005.00279.x.

Mao, Xiaoqing, Byung Eun Kim, Fudi Wang, David J. Eide, and Michael J. Petris. 2007. "A Histidine-Rich Cluster Mediates the Ubiquitination and Degradation of the Human Zinc Transporter, HZIP4, and Protects against Zinc Cytotoxicity." *Journal of Biological Chemistry* 282 (10): 6992–7000. https://doi.org/10.1074/jbc.M610552200.

Marschner, H. 1995. *Mineral Nutrition of Higher Plants*. 2nd ed. London: Academic press. https://doi.org/10.1006/anbo.1996.0155.

Marsh, H. V., H. J. Evans, and G. Matrone. 1963. "Investigations of the Role of Iron in Chlorophyll Metabolism. II. Effect of Iron Deficiency on Chlorophyll Synthesis." *Plant Physiology* 38 (6): 638–42. https://doi.org/10.1104/pp.38.6.638.

Martín-Barranco, Amanda, Julien Spielmann, Guillaume Dubeaux, Grégory Vert, and Enric Zelazny. 2020. "Dynamic Control of the High-Affinity Iron Uptake Complex in Root Epidermal Cells." *Plant Physiology* 184 (3): 1236–50. https://doi.org/10.1104/pp.20.00234.

Mathews, Wendy R., Fudi Wang, David J. Eide, and Mark Van Doren. 2005. "Drosophila Fear of Intimacy Encodes a Zrt/IRT-like Protein (ZIP) Family Zinc Transporter Functionally Related to Mammalian

ZIP Proteins." *Journal of Biological Chemistry* 280 (1): 787–95. https://doi.org/10.1074/jbc.M411308200.

McKie, A. T., D. Barrow, G. O. Latunde-Dada, A. Rolfs, G. Sager, E. Mudaly, M. Mudaly, et al. 2001. "An Iron-Regulated Ferric Reductase Associated with the Absorption of Dietary Iron." *Science* 291 (5509): 1755–59. https://doi.org/10.1126/science.1057206.

McKie, Andrew, Paola Marciani, Andreas Rolfs, Karen Brennan, Kristina Wehr, Dalna Barrow, Silvia Miret, et al. 2000. "A Novel Duodenal Iron-Regulated Transporter, IREG1, Implicated in the Basolateral Transfer of Iron to the Circulation." *Molecular Cell* 5 (2): 299–309. https://doi.org/10.1016/S1097-2765(00)80425-6.

Mcmahon, Robert J., and Robert J. Cousins. 1998. "Regulation of the Zinc Transporter ZnT-1 by Dietary Zinc." *Proceedings of the National Academy of Sciences of the United States of America* 95 (9): 4841–46. https://doi.org/10.1073/pnas.95.9.4841.

Merchant, Sabeeha S. 2010. "Future Perspectives in Plant Biology The Elements of Plant Micronutrients 1." *Plant Physiology Ò* 154: 512–15. https://doi.org/10.1104/pp.110.161810.

Milner, Matthew J., Jesse Seamon, Eric Craft, and Leon V. Kochian. 2013. "Transport Properties of Members of the ZIP Family in Plants and Their Role in Zn and Mn Homeostasis." *Journal of Experimental Botany* 64 (1): 369–81. https://doi.org/10.1093/jxb/ers315.

Mino, Yoshiki, Toshimasa Ishida, Nagayo Ota, Masatoshi Inoue, Kyosuke Nomoto, Tsunematsu Takemoto, Hisashi Tanaka, and Yukio Sugiura. 1983. "Mugineic Acid-Iron(III) Complex and Its Structurally Analogous Coball(III) Complex: Characterization and Implication for Absorption and Transport of Iron in Gramineous Plants." *Journal of the American Chemical Society* 105 (14): 4671–76. https://doi.org/10.1021/ja00352a024.

Mohanty, Arun K., and Michael C. Wiener. 2004. "Membrane Protein Expression and Production: Effects of Polyhistidine Tag Length and Position." *Protein Expression and Purification* 33 (2): 311–25. https://doi.org/10.1016/j.pep.2003.10.010.

Montanini, Barbara, Damien Blaudez, Sylvain Jeandroz, Dale Sanders, and Michel Chalot. 2007. "Phylogenetic and Functional Analysis of the Cation Diffusion Facilitator (CDF) Family: Improved Signature and Prediction of Substrate Specificity." *BMC Genomics* 8 (1): 107. https://doi.org/10.1186/1471-2164-8-107.

Moreau, Sophie, Rowena M. Thomson, Brent N. Kaiser, Ben Trevaskis, Mary Lou Guerinot, Michael K. Udvardi, Alain Puppo, and David A. Day. 2002. "GmZIP1 Encodes a Symbiosis-Specific Zinc Transporter in Soybean." *Journal of Biological Chemistry* 277 (7): 4738–46. https://doi.org/10.1074/jbc.M106754200.

Mori, Satoshi, and Naoko Nishizawa. 1987. "Methionine as a Dominant Precursor of Phytosiderophores in Graminaceae Plants." *Plant and Cell Physiology* 28 (6): 1081–92. https://doi.org/10.1093/oxfordjournals.pcp.a077388.

Morrissey, Joe, Ivan R. Baxter, Joohyun Lee, Liangtao Li, Brett Lahner, Natasha Grotz, Jerry Kaplan, David E. Salt, and Mary Lou Guerinot. 2009. "The Ferroportin Metal Efflux Proteins Function in Iron and Cobalt Homeostasis in Arabidopsis." *Plant Cell* 21 (10): 3326–38. https://doi.org/10.1105/tpc.109.069401.

Murashige, Toshio, and Folke Skoog. 1962. "A Revised Medium for Rapid Growth and Bio Assays with Tobacco Tissue Cultures." *Physiologia Plantarum* 15 (3): 473–97. https://doi.org/10.1111/j.1399-3054.1962.tb08052.x.

Narayanan, Narayanan, Getu Beyene, Raj Deepika Chauhan, Eliana Gaitán-Solís, Jackson Gehan, Paula Butts, Dimuth Siritunga, et al. 2019. "Biofortification of Field-Grown Cassava by Engineering Expression of an Iron Transporter and Ferritin." *Nature Biotechnology* 37 (2): 144–51. https://doi.org/10.1038/s41587-018-0002-1.

Newton, Kim, Marissa L. Matsumoto, Ingrid E. Wertz, Donald S. Kirkpatrick, Jennie R. Lill, Jenille Tan, Debra Dugger, et al. 2008. "Ubiquitin Chain Editing Revealed by Polyubiquitin Linkage-Specific Antibodies." *Cell* 134 (4): 668–78. https://doi.org/10.1016/j.cell.2008.07.039.

Nozoye, Tomoko, Hiromi Nakanishi, and Naoko K. Nishizawa. 2013. "Characterizing the Crucial Components of Iron Homeostasis in the Maize Mutants Ys1 and Ys3." *PLoS ONE* 8 (5). https://doi.org/10.1371/journal.pone.0062567.

Philpott, Caroline C. 2006. "Iron Uptake in Fungi: A System for Every Source." *Biochimica et Biophysica Acta - Molecular Cell Research*. Elsevier. https://doi.org/10.1016/j.bbamcr.2006.05.008.

Piotto, Martial, Vladimir Saudek, and Vladimir Sklenář. 1992. "Gradient-Tailored Excitation for Single-Quantum NMR Spectroscopy of Aqueous Solutions." *Journal of Biomolecular NMR* 2 (6): 661–65. https://doi.org/10.1007/BF02192855.

Pocanschi, Cosmin L., Sepehr Ehsani, Mohadeseh Mehrabian, Holger Wille, William Reginold, William S. Trimble, Hansen Wang, et al. 2013. "The ZIP5 Ectodomain Co-Localizes with PrP and May Acquire a PrP-Like Fold That Assembles into a Dimer." Edited by Ilia V. Baskakov. *PLoS ONE* 8 (9): e72446. https://doi.org/10.1371/journal.pone.0072446.

Prasad, A S. 1991. "Discovery of Human Zinc Deficiency and Studies in an Experimental Human Model." *The American Journal of Clinical Nutrition* 53 (2): 403–12. https://doi.org/10.1093/ajcn/53.2.403.

Przybyszewska, Justyna, and Ewa Zekanowska. 2014. "The Role of Hepcidin, Ferroportin, HCP1, and DMT1 Protein in Iron Absorption in the Human Digestive Tract." *Przeglad Gastroenterologiczny*. Termedia Publishing House Ltd. https://doi.org/10.5114/pg.2014.45102.

Purohit, Rahul, Matthew O. Ross, Sharon Batelu, April Kusowski, Timothy L. Stemmler, Brian M. Hoffman, and Amy C. Rosenzweig. 2018. "Cu+-Specific CopB Transporter: Revising P1B-Type ATPase Classification." *Proceedings of the National Academy of Sciences of the United States of America* 115 (9): 2108–13. https://doi.org/10.1073/pnas.1721783115.

Reid, Michelle S., David M. Kern, and Stephen Graf Brohawn. 2020. "Cryo-EM Structure of the Potassium-Chloride Cotransporter KCC4 in Lipid Nanodiscs." *ELife* 9 (April). https://doi.org/10.7554/eLife.52505.

Reinders, Anke, Waltraud Schulze, Christina Kühn, Laurence Barker, Alexander Schulz, John M. Ward, and Wolf B. Frommer. 2002. "Protein-Protein Interactions between Sucrose Transporters of Different Affinities Colocalized in the Same Enucleate Sieve Element." *Plant Cell* 14 (7): 1567–77. https://doi.org/10.1105/tpc.002428.

Roberts, Louis A., Abbey J. Pierson, Zivile Panaviene, and Elsbeth L. Walker. 2004. "Yellow Stripe1. Expanded Roles for the Maize Iron-Phytosiderophore Transporter." *Plant Physiology* 135 (1): 112–20. https://doi.org/10.1104/pp.103.037572.

Robinson, Nigel J., Catherine M. Procter, Erin L. Connolly, and Mary Lou Guerinot. 1999. "A Ferric-Chelate Reductase for Iron Uptake from Soils." *Nature* 397 (6721): 694–97. https://doi.org/10.1038/17800.

Rodríguez-Celma, Jorge, James M. Connorton, Inga Kruse, Robert T. Green, Marina Franceschetti, Yi Tze Chen, Yan Cui, Hong Qing Ling, Kuo Chen Yeh, and Janneke Balk. 2019. "Arabidopsis BRUTUS-LIKE E3 Ligases Negatively Regulate Iron Uptake by Targeting Transcription Factor FIT for Recycling." *Proceedings of the National Academy of Sciences of the United States of America* 116 (35): 17584–91. https://doi.org/10.1073/pnas.1907971116.

Rogers, E. E., D. J. Eide, and M. L. Guerinot. 2000. "Altered Selectivity in an Arabidopsis Metal Transporter." *Proceedings of the National Academy of Sciences* 97 (22): 12356–60. https://doi.org/10.1073/pnas.210214197.

Roh, Soung Hun, Nicholas J. Stam, Corey F. Hryc, Sergio Couoh-Cardel, Grigore Pintilie, Wah Chiu, and Stephan Wilkens. 2018. "The 3.5-Å CryoEM Structure of Nanodisc-Reconstituted Yeast Vacuolar ATPase Vo Proton Channel." *Molecular Cell* 69 (6): 993-1004.e3.

https://doi.org/10.1016/j.molcel.2018.02.006.

Romero-Barrios, Natali, Dario Monachello, Ulla Dolde, Aloysius Wong, Helene San Clemente, Anne Cayrel, Alexander Johnson, et al. 2020. "Advanced Cataloging of Lysine-63 Polyubiquitin Networks by Genomic, Interactome, and Sensor-Based Proteomic Analyses." *The Plant Cell* 32 (1): 123–38. https://doi.org/10.1105/tpc.19.00568.

Santi, Simonetta, and Wolfgang Schmidt. 2009. "Dissecting Iron Deficiency-Induced Proton Extrusion in Arabidopsis Roots." *New Phytologist* 183 (4): 1072–84. https://doi.org/10.1111/j.1469-8137.2009.02908.x.

Schaaf, Gabriel, Annegret Honsbein, Anderson R. Meda, Silvia Kirchner, Daniel Wipf, and Nicolaus Von Wirén. 2006. "AtIREG2 Encodes a Tonoplast Transport Protein Involved in Iron-Dependent Nickel Detoxification in Arabidopsis Thaliana Roots." *Journal of Biological Chemistry* 281 (35): 25532–40. https://doi.org/10.1074/jbc.M601062200.

Schaaf, Gabriel, Uwe Ludewig, Bülent E. Erenoglu, Satoshi Mori, Takeshi Kitahara, and Nicolaus Von Wirén. 2004. "ZmYS1 Functions as a Proton-Coupled Symporter for Phytosiderophore- and Nicotianamine-Chelated Metals." *Journal of Biological Chemistry* 279 (10): 9091–96. https://doi.org/10.1074/jbc.M311799200.

Schmidt, Holger, Carmen Günther, Michael Weber, Cornelia Spörlein, Sebastian Loscher, Christoph Böttcher, Rainer Schobert, and Stephan Clemens. 2014. "Metabolome Analysis of Arabidopsis Thaliana Roots Identifies a Key Metabolic Pathway for Iron Acquisition." *PLoS ONE* 9 (7). https://doi.org/10.1371/journal.pone.0102444.

Scholl, Theresa O., and Mary L. Hediger. 1994. "Anemia and Iron-Deficiency Anemia: Compilation of Data on Pregnancy Outcome." In *American Journal of Clinical Nutrition*. Vol. 59. American Society for Nutrition. https://doi.org/10.1093/ajcn/59.2.492S.

Schrodinger, L. n.d. "Schrodinger, L. (2010) The PyMOL Molecular Graphics System, Version 1.3r1. - References - Scientific Research Publishing." Accessed November 8, 2020. https://www.scirp.org/(S(vtj3fa45qm1ean45vvffcz55))/reference/ReferencesPapers.aspx?ReferenceID=1571978.

Séguéla, Mathilde, Jean François Briat, Grégory Vert, and Catherine Curie. 2008. "Cytokinins Negatively Regulate the Root Iron Uptake Machinery in Arabidopsis through a Growth-Dependent Pathway." *Plant Journal* 55 (2): 289–300. https://doi.org/10.1111/j.1365-313X.2008.03502.x.

Selote, Devarshi, Rozalynne Samira, Anna Matthiadis, Jeffrey W. Gillikin, and Terri A. Long. 2015. "Iron-Binding E3 Ligase Mediates Iron Response in Plants by Targeting Basic Helix-Loop-Helix Transcription Factors1[Open]." *Plant Physiology* 167 (1): 273–86. https://doi.org/10.1104/pp.114.250837.

Shayeghi, Majid, Gladys O. Latunde-Dada, Jonathan S. Oakhill, Abas H. Laftah, Ken Takeuchi, Neil Halliday, Yasmin Khan, et al. 2005. "Identification of an Intestinal Heme Transporter." *Cell* 122 (5): 789–801. https://doi.org/10.1016/j.cell.2005.06.025.

Shin, Lung-Jiun, Jing-Chi Lo, Guan-Hong Chen, Judy Callis, Hongyong Fu, and Kuo-Chen Yeh. 2013. "IRT1 DEGRADATION FACTOR1, a RING E3 Ubiquitin Ligase, Regulates the Degradation of IRON-REGULATED TRANSPORTER1 in Arabidopsis C W OPEN." *The Plant Cell* 25: 3039–51. https://doi.org/10.1105/tpc.113.115212.

Shojima, Shinsuke, Naoko Kishi Nishizawa, Shinji Fushiya, Shigeo Nozoe, Tomohiro Irifune, and Satoshi Mori. 1990. "Biosynthesis of Phytosiderophores: In Vitro Biosynthesis of 2′-Deoxymugineic Acid from L-Methionine and Nicotianamine." *Plant Physiology* 93 (4): 1497–1503. https://doi.org/10.1104/pp.93.4.1497.

Silva, Deepika De, Sandra Davis-Kaplan, Jennifer Fergestad, and Jerry Kaplan. 1997. "Purification and Characterization of Fet3 Protein, a Yeast Homologue of Ceruloplasmin." *Journal of Biological*

Chemistry 272 (22): 14208–13. https://doi.org/10.1074/jbc.272.22.14208.

Sivitz, Alicia B., Victor Hermand, Catherine Curie, and Grégory Vert. 2012. "Arabidopsis BHLH100 and BHLH101 Control Iron Homeostasis via a FIT-Independent Pathway." *PLoS ONE* 7 (9). https://doi.org/10.1371/journal.pone.0044843.

Smith, Aaron T, Kyle P Smith, and Amy C Rosenzweig. 2014. "Diversity of the Metal-Transporting P 1B-Type ATPases." https://doi.org/10.1007/s00775-014-1129-2.

Song, Woon Ju, Pamela A. Sontz, Xavier I. Ambroggio, and F. Akif Tezcan. 2014. "Metals in Protein–Protein Interfaces." *Annual Review of Biophysics* 43 (1): 409–31. https://doi.org/10.1146/annurev-biophys-051013-023038.

Stearman, Robert, Daniel S. Yuan, Yuko Yamaguchi-Iwai, Richard D. Klausner, and Andrew Dancis. 1996. "A Permease-Oxidase Complex Involved in High-Affinity Iron Uptake in Yeast." *Science* 271 (5255): 1552–57. https://doi.org/10.1126/science.271.5255.1552.

Su, Pin Chuan, William Si, Deidre L. Baker, and Bryan W. Berger. 2013. "High-Yield Membrane Protein Expression from E. Coli Using an Engineered Outer Membrane Protein F Fusion." *Protein Science* 22 (4): 434–43. https://doi.org/10.1002/pro.2224.

Su, Wei, Yidan Liu, Yang Xia, Zhi Hong, and Jianming Li. 2011. "Conserved Endoplasmic Reticulum-Associated Degradation System to Eliminate Mutated Receptor-like Kinases in Arabidopsis." *Proceedings of the National Academy of Sciences of the United States of America* 108 (2): 870–75. https://doi.org/10.1073/pnas.1013251108.

Sun, Ji, John R. Bankston, Jian Payandeh, Thomas R. Hinds, William N. Zagotta, and Ning Zheng. 2014. "Crystal Structure of the Plant Dual-Affinity Nitrate Transporter NRT1.1." *Nature* 507 (7490): 73–77. https://doi.org/10.1038/nature13074.

Suzuki, Motofumi, Michiko Takahashi, Takashi Tsukamoto, Satoshi Watanabe, Shinpei Matsuhashi, Junshi Yazaki, Naoki Kishimoto, et al. 2006. "Biosynthesis and Secretion of Mugineic Acid Family Phytosiderophores in Zinc-Deficient Barley." *Plant Journal* 48 (1): 85–97. https://doi.org/10.1111/j.1365-313X.2006.02853.x.

Suzuki, Motofumi, Takashi Tsukamoto, Haruhiko Inoue, Satoshi Watanabe, Shinpei Matsuhashi, Michiko Takahashi, Hiromi Nakanishi, Satoshi Mori, and Naoko K. Nishizawa. 2008. "Deoxymugineic Acid Increases Zn Translocation in Zn-Deficient Rice Plants." *Plant Molecular Biology* 66 (6): 609–17. https://doi.org/10.1007/s11103-008-9292-x.

Takahashi, Ryuichi, Khurram Bashir, Yasuhiro Ishimaru, Naoko K. Nishizawa, and Hiromi Nakanishi. 2012. "The Role of Heavy-Metal ATPases, HMAs, in Zinc and Cadmium Transport in Rice." *Plant Signaling and Behavior* 7 (12): 1605. https://doi.org/10.4161/psb.22454.

Tanaka, Natsuki, Miki Kawachi, Takashi Fujiwara, and Maeshima Masayoshi. 2013. "Zinc-Binding and Structural Properties of the Histidine-Rich Loop of Arabidopsis Thaliana Vacuolar Membrane Zinc Transporter MTP1." *FEBS Open Bio* 3: 218–24. https://doi.org/10.1016/j.fob.2013.04.004.

Tandy, Sarah, Mark Williams, Aime Leggett, Marta Lopez-Jimenez, Markos Dedes, Bala Ramesh, Surjit Kaila Srai, and Paul Sharp. 2000. "Nramp2 Expression Is Associated with PH-Dependent Iron Uptake across the Apical Membrane of Human Intestinal Caco-2 Cells." *Journal of Biological Chemistry* 275 (2): 1023–29. https://doi.org/10.1074/jbc.275.2.1023.

Taniguchi, Reiya, Hideaki E. Kato, Josep Font, Chandrika N. Deshpande, Miki Wada, Koichi Ito, Ryuichiro Ishitani, Mika Jormakka, and Osamu Nureki. 2015. "Outward-and Inward-Facing Structures of a Putative Bacterial Transition-Metal Transporter with Homology to Ferroportin." *Nature Communications* 6 (October). https://doi.org/10.1038/ncomms9545.

Taylor, Kathryn M., and Robert I. Nicholson. 2003. "The LZT Proteins; The LIV-1 Subfamily of Zinc Transporters." *Biochimica et Biophysica Acta - Biomembranes*. Elsevier. https://doi.org/10.1016/S0005-2736(03)00048-8.

Thibaudeau, Tiffany A., and David M. Smith. 2019. "A Practical Review of Proteasome Pharmacology." *Pharmacological Reviews* 71 (2): 170–97. https://doi.org/10.1124/pr.117.015370.

Thomine, Sébastien, Françoise Lelièvre, Elise Debarbieux, Julian I. Schroeder, and Hélène Barbier-Brygoo. 2003. "AtNRAMP3, a Multispecific Vacuolar Metal Transporter Involved in Plant Responses to Iron Deficiency." *Plant Journal* 34 (5): 685–95. https://doi.org/10.1046/j.1365-313X.2003.01760.x.

Thomine, Sébastien, Rongchen Wang, John M. Ward, Nigel M. Crawford, and Julian I. Schroeder. 2000. "Cadmium and Iron Transport by Members of a Plant Metal Transporter Family in Arabidopsis with Homology to Nramp Genes." *Proceedings of the National Academy of Sciences of the United States of America* 97 (9): 4991–96. https://doi.org/10.1073/pnas.97.9.4991.

Thompson, Aaron A., Jeffrey J. Liu, Eugene Chun, Daniel Wacker, Huixian Wu, Vadim Cherezov, and Raymond C. Stevens. 2011. "GPCR Stabilization Using the Bicelle-like Architecture of Mixed Sterol-Detergent Micelles." *Methods* 55 (4): 310–17. https://doi.org/10.1016/j.ymeth.2011.10.011.

Tissot, Nicolas, Kevin Robe, Fei Gao, Susana Grant-Grant, Jossia Boucherez, Fanny Bellegarde, Amel Maghiaoui, et al. 2019. "Transcriptional Integration of the Responses to Iron Availability in Arabidopsis by the BHLH Factor ILR3." *New Phytologist* 223 (3): 1433–46. https://doi.org/10.1111/nph.15753.

Varotto, Claudio, Daniela Maiwald, Paolo Pesaresi, Peter Jahns, Francesco Salamini, and Dario Leister. 2002. "The Metal Ion Transporter IRT1 Is Necessary for Iron Homeostasis and Efficient Photosynthesis in Arabidopsis Thaliana." *The Plant Journal* 31 (5): 589–99. https://doi.org/10.1046/j.1365-313X.2002.01381.x.

Verret, Frédéric, Antoine Gravot, Pascaline Auroy, Nathalie Leonhardt, Pascale David, Laurent Nussaume, Alain Vavasseur, and Pierre Richaud. 2004. "Overexpression of AtHMA4 Enhances Root-to-Shoot Translocation of Zinc and Cadmium and Plant Metal Tolerance." *FEBS Letters* 576 (3): 306–12. https://doi.org/10.1016/j.febslet.2004.09.023.

Vert, Grégory A, Jean-François Briat, and Catherine Curie. 2003. "Dual Regulation of the Arabidopsis High-Affinity Root Iron Uptake System by Local and Long-Distance Signals 1." https://doi.org/10.1104/pp.102.016089.

Vert, Grégory, Marie Barberon, Enric Zelazny, Mathilde Séguéla, Jean François Briat, and Catherine Curie. 2009. "Arabidopsis IRT2 Cooperates with the High-Affinity Iron Uptake System to Maintain Iron Homeostasis in Root Epidermal Cells." *Planta* 229 (6): 1171–79. https://doi.org/10.1007/s00425-009-0904-8.

Vert, Grégory, Jean François Briat, and Catherine Curie. 2001. "Arabidopsis IRT2 Gene Encodes a Root-Periphery Iron Transporter." *Plant Journal* 26 (2): 181–89. https://doi.org/10.1046/j.1365-313X.2001.01018.x.

Vert, Grégory, Natasha Grotz, Fabienne Dédaldéchamp, Frédéric Gaymard, Mary Lou Guerinot, Jean François Briat, and Catherine Curie. 2002. "IRT1, an Arabidopsis Transporter Essential for Iron Uptake from the Soil and for Plant Growth." *Plant Cell* 14 (6): 1223–33. https://doi.org/10.1105/tpc.001388.

Vidal, Silvia M., Danielle Malo, Kyle Vogan, Emil Skamene, and Philippe Gros. 1993. "Natural Resistance to Infection with Intracellular Parasites: Isolation of a Candidate for Bcg." *Cell* 73 (3): 469–85. https://doi.org/10.1016/0092-8674(93)90135-D.

Vranken, Wim F., Wayne Boucher, Tim J. Stevens, Rasmus H. Fogh, Anne Pajon, Miguel Llinas, Eldon L. Ulrich, John L. Markley, John Ionides, and Ernest D. Laue. 2005. "The CCPN Data Model for NMR Spectroscopy: Development of a Software Pipeline." *Proteins: Structure, Function and Genetics* 59 (4): 687–96. https://doi.org/10.1002/prot.20449.

Waldron, Kevin J, Julian C Rutherford, Dianne Ford, and Nigel J Robinson. 2009. "Metalloproteins and Metal Sensing" 460 (August). https://doi.org/10.1038/nature08300.

Wallner, Anja, Michael Blatzer, Markus Schrettl, Bettina Sarg, Herbert Lindner, and Hubertus Haas. 2009. "Ferricrocin, a Siderophore Involved in Intra- and Transcellular Iron Distribution in Aspergillus Fumigatus." *Applied and Environmental Microbiology* 75 (12): 4194–96. https://doi.org/10.1128/AEM.00479-09.

Wang, Fudi, Byung Eun Kim, Michael J. Petris, and David J. Eide. 2004. "The Mammalian Zip5 Protein Is a Zinc Transporter That Localizes to the Basolateral Surface of Polarized Cells." *Journal of Biological Chemistry* 279 (49): 51433–41. https://doi.org/10.1074/jbc.M408361200.

Wang, Hong Yu, Marco Klatte, Marc Jakoby, Helmut Bäumlein, Bernd Weisshaar, and Petra Bauer. 2007. "Iron Deficiency-Mediated Stress Regulation of Four Subgroup Ib BHLH Genes in Arabidopsis Thaliana." *Planta* 226 (4): 897–908. https://doi.org/10.1007/s00425-007-0535-x.

Wang, Kaituo, Oleg Sitsel, Gabriele Meloni, Henriette Elisabeth Autzen, Magnus Andersson, Tetyana Klymchuk, Anna Marie Nielsen, Douglas C Rees, Poul Nissen, and Pontus Gourdon. 2014. "Structure and Mechanism of Zn2+-Transporting P-Type ATPases." *Nature* 514 (7253): 518–22. https://doi.org/10.1038/nature13618.

Wang, Kun, Bing Zhou, Yien Ming Kuo, Jason Zemansky, and Jane Gitschier. 2002. "A Novel Member of a Zinc Transporter Family Is Defective in Acrodermatitis Enteropathica." *American Journal of Human Genetics* 71 (1): 66–73. https://doi.org/10.1086/341125.

Waters, Brian M., Heng Hsuan Chu, Raymond J. DiDonato, Louis A. Roberts, Robynn B. Eisley, Brett Lahner, David E. Salt, and Elsbeth L. Walker. 2006. "Mutations in Arabidopsis Yellow Stripe-Like1 and Yellow Stripe-Like3 Reveal Their Roles in Metal Ion Homeostasis and Loading of Metal Ions in Seeds." *Plant Physiology* 141 (4): 1446–58. https://doi.org/10.1104/pp.106.082586.

Waters, Brian M., and David J. Eide. 2002. "Combinatorial Control of Yeast FET4 Gene Expression by Iron, Zinc, and Oxygen." *Journal of Biological Chemistry* 277 (37): 33749–57. https://doi.org/10.1074/jbc.M206214200.

Weaver, Benjamin P., Jodi Dufner-Beattie, Taiho Kambe, and Glen K. Andrews. 2007. "Novel Zinc-Responsive Post-Transcriptional Mechanisms Reciprocally Regulate Expression of the Mouse Slc39a4 and Slc39a5 Zinc Transporters (Zip4 and Zip5)." *Biological Chemistry* 388 (12): 1301–12. https://doi.org/10.1515/BC.2007.149.

Welch, Ross M., and Robin D. Graham. 2004. "Breeding for Micronutrients in Staple Food Crops from a Human Nutrition Perspective." In *Journal of Experimental Botany*, 55:353–64. J Exp Bot. https://doi.org/10.1093/jxb/erh064.

White, Christopher, and Geoffrey M. Gadd. 1987. "The Uptake and Cellular Distribution of Zinc in Saccharomyces Cerevisiae." *Journal of General Microbiology* 133 (3): 727–37. https://doi.org/10.1099/00221287-133-3-727.

Wiles, Amy M., Fred Naider, and Jeffrey M. Becker. 2006. "Transmembrane Domain Prediction and Consensus Sequence Identification of the Oligopeptide Transport Family." *Research in Microbiology* 157 (4): 395–406. https://doi.org/10.1016/j.resmic.2005.10.004.

Williams, Lorraine E., Jon K. Pittman, and J. L. Hall. 2000. "Emerging Mechanisms for Heavy Metal Transport in Plants." *Biochimica et Biophysica Acta - Biomembranes*. Vol. 1465. Elsevier. https://doi.org/10.1016/S0005-2736(00)00133-4.

Wintermans, J. F.G.M., and A. De Mots. 1965. "Spectrophotometric Characteristics of Chlorophylls a and b and Their Phenophytins in Ethanol." *BBA - Biophysics Including Photosynthesis* 109 (2): 448–53. https://doi.org/10.1016/0926-6585(65)90170-6.

Wirén, Nicolaus Von, Horst Marschner, and Volker Romheld. 1996. "Roots of Iron-Efficient Maize Also Absorb Phytosiderophore-Chelated Zinc." *Plant Physiol.* Vol. 11.

Wu, Huilan, Lihua Li, Juan Du, Youxi Yuan, Xudong Cheng, and Hong Qing Ling. 2005. "Molecular and Biochemical Characterization of the Fe(III) Chelate Reductase Gene Family in Arabidopsis Thaliana."

Plant and Cell Physiology 46 (9): 1505–14. https://doi.org/10.1093/pcp/pci163.

Wu, Jian, Fang Jie Zhao, Artak Ghandilyan, Barbara Logoteta, Myriam Olortegui Guzman, Henk Schat, Xiaowu Wang, and Mark G.M. Aarts. 2009. "Identification and Functional Analysis of Two ZIP Metal Transporters of the Hyperaccumulator Thlaspi Caerulescens." *Plant and Soil* 325 (1): 79–95. https://doi.org/10.1007/s11104-009-0151-6.

Yamaguchi, Masayoshi. 1998. "Role of Zinc in Bone Formation and Bone Resorption." *The Journal of Trace Elements in Experimental Medicine* 11 (2-3): 119–35. https://doi.org/10.1002/(SICI)1520-670X(1998)11:2/3<119::AID-JTRA5>3.0.CO;2-3.

Yip, Ray, and Usha Ramakrishnan. 2002. "Experiences and Challenges in Developing Countries." In *Journal of Nutrition*, 132:827S-830S. American Institute of Nutrition. https://doi.org/10.1093/jn/132.4.827s.

Yu, Yu, Aimin Wu, Zhuzhen Zhang, Guang Yan, Fan Zhang, Lihong Zhang, Xiaoyun Shen, et al. 2013. "ScienceDirect Characterization of the GufA Subfamily Member SLC39A11 / Zip11 as a Zinc Transporter" 24: 1697–1708. https://doi.org/10.1016/j.jnutbio.2013.02.010.

Yuan, Youxi, Huilan Wu, Ning Wang, Jie Li, Weina Zhao, Juan Du, Daowen Wang, and Hong Qing Ling. 2008. "FIT Interacts with AtbHLH38 and AtbHLH39 in Regulating Iron Uptake Gene Expression for Iron Homeostasis in Arabidopsis." *Cell Research* 18 (3): 385–97. https://doi.org/10.1038/cr.2008.26.

Yun, Cheol Won, Tracy Ferea, Jared Rashford, Orly Ardon, Patrick O. Brown, David Botstein, Jerry Kaplan, and Caroline C. Philpott. 2000. "Desferrioxamine-Mediated Iron Uptake in Saccharomyces Cerevisiae. Evidence for Two Pathways of Iron Uptake." *Journal of Biological Chemistry* 275 (14): 10709–15. https://doi.org/10.1074/jbc.275.14.10709.

Yun, Cheol Won, John S. Tiedeman, Robert E. Moore, and Caroline C. Philpott. 2000. "Siderophore-Iron Uptake in Saccharomyces Cerevisiae: Identification of Ferrichrome and Fusarinine Transporters." *Journal of Biological Chemistry* 275 (21): 16354–59. https://doi.org/10.1074/jbc.M001456200.

Zhang, Chi, Dexin Sui, Tuo Zhang, and Jian Hu. 2020. "Molecular Basis of Zinc-Dependent Endocytosis of Human ZIP4 Transceptor." *Cell Reports* 31 (4): 107582. https://doi.org/10.1016/j.celrep.2020.107582.

Zhang, Fusuo, Volker Römheld, and Horst Marschner. 1989. "Effect of Zinc Deficiency in Wheat on the Release of Zinc and Iron Mobilizing Root Exudates." *Zeitschrift Für Pflanzenernährung Und Bodenkunde* 152 (2): 205–10. https://doi.org/10.1002/jpln.19891520211.

Zhang, Jie, Bing Liu, Mengshu Li, Dongru Feng, Honglei Jin, Peng Wang, Jun Liu, Feng Xiong, Jinfa Wang, and Hong Bin Wang. 2015. "The BHLH Transcription Factor BHLH104 Interacts with IAA-LEUCINE RESISTANT3 and Modulates Iron Homeostasis in Arabidopsis." *Plant Cell* 27 (3): 787–805. https://doi.org/10.1105/tpc.114.132704.

Zhang, Peng, Song Tan, James O Berry, Peng Li, Na Ren, Shuang Li, Guang Yang, Wei-Bing Wang, Xiao-Ting Qi, and Li-Ping Yin. 2014. "An Uncleaved Signal Peptide Directs the Malus Xiaojinensis Iron Transporter Protein Mx IRT1 into the ER for the PM Secretory Pathway." *Int. J. Mol. Sci* 15: 20413–33. https://doi.org/10.3390/ijms151120413.

Zhang, Tuo, Eziz Kuliyev, Dexin Sui, and Jian Hu. 2019. "The Histidine-Rich Loop in the Extracellular Domain of ZIP4 Binds Zinc and Plays a Role in Zinc Transport." *Biochemical Journal* 476 (12): 1791–1803. https://doi.org/10.1042/BCJ20190108.

Zhang, Tuo, Jian Liu, Matthias Fellner, Chi Zhang, Dexin Sui, and Jian Hu. 2017. "Crystal Structures of a ZIP Zinc Transporter Reveal a Binuclear Metal Center in the Transport Pathway."

Zhang, Tuo, Dexin Sui, and Jian Hu. 2016. "Structural Insights of ZIP4 Extracellular Domain Critical for Optimal Zinc Transport." https://doi.org/10.1038/ncomms11979.

Zhang, Yu, Yong Han Xu, Hong Yin Yi, and Ji Ming Gong. 2012. "Vacuolar Membrane Transporters OsVIT1 and OsVIT2 Modulate Iron Translocation between Flag Leaves and Seeds in Rice." *Plant Journal* 72 (3): 400–410. https://doi.org/10.1111/j.1365-313X.2012.05088.x.

Zhao, Hui, Edward Butler, Jacquelyn Rodgers, Thomas Spizzo, Sara Duesterhoeft, and David Eide. 1998.

"Regulation of Zinc Homeostasis in Yeast by Binding of the ZAP1 Transcriptional Activator to Zinc-Responsive Promoter Elements." *Journal of Biological Chemistry* 273 (44): 28713–20. https://doi.org/10.1074/jbc.273.44.28713.

Zhao, Hui, and David Eide. 1996a. "The Yeast ZRT1 Gene Encodes the Zinc Transporter Protein of a High-Affinity Uptake System Induced by Zinc Limitation." *Proceedings of the National Academy of Sciences of the United States of America* 93 (6): 2454–58. https://doi.org/10.1073/pnas.93.6.2454.

———. 1996b. "The ZRT2 Gene Encodes the Low Affinity Zinc Transporter in Saccharomyces Cerevisiae." *Journal of Biological Chemistry* 271 (38): 23203–10. https://doi.org/10.1074/jbc.271.38.23203.

Ziegler, Jörg, Stephan Schmidt, Nadine Strehmel, Dierk Scheel, and Steffen Abel. 2017. "Arabidopsis Transporter ABCG37/PDR9 Contributes Primarily Highly Oxygenated Coumarins to Root Exudation." *Scientific Reports* 7 (1): 1–11. https://doi.org/10.1038/s41598-017-03250-6.

Zohn, Irene E., Ivana De Domenico, Andrew Pollock, Diane Mc Vey Ward, Jessica F. Goodman, Xiayun Liang, Amaru J. Sanchez, Lee Niswander, and Jerry Kaplan. 2007. "The Flatiron Mutation in Mouse Ferroportin Acts as a Dominant Negative to Cause Ferroportin Disease." *Blood* 109 (10): 4174–80. https://doi.org/10.1182/blood-2007-01-066068.

ÉCOLE DOCTORALE
Sciences du végétal : du gène à l'écosystème (SEVE)

Titre : Caractérisation biochimique du transporteur IRT1 et de son mécanisme de régulation

Mots clés : IRT1, transport de métaux, acquisition du fer, protéines membranaires

Résumé : Le fer est un nutriment clé pour tous les organismes vivants et il est impliqué dans de nombreux processus cellulaires. Bien qu'il soit l'un des éléments les plus abondants sur terre, le fer est souvent indisponible car il précipite dans le sol, formant des complexes insolubles. Les plantes absorbent le fer du sol à travers les cellules épidermiques de la racine en utilisant le transporteur de fer IRT1 qui appartient à la famille de transporteurs ZIP largement répandue. Outre le fer, l'IRT1 peut également transporter des métaux non ferreux (Zn, Mn, Co et Cd), que nous appelons également les substrats secondaires. Notre équipe a récemment montré que l'IRT1 agit comme un transcepteur, détectant directement les métaux non ferreux à l'aide d'un motif riche en histidine dans une boucle intracellulaire non structurée (Dubeaux et al. 2018). Brièvement, sous un excès de métal non ferreux, les métaux se lient aux histidines recrutant la kinase CIPK23. La phosphorylation, à son tour, permet le recrutement de la ligase IDF1 E3 qui ubiquitine IRT1 et la cible pour la dégradation par la voie endocytique.
À ce jour, nous en savons encore très peu sur les caractéristiques structurelles de l'IRT1, ses mécanismes de transport, la base de la sélectivité de transport de l'IRT1 et les mécanismes moléculaires à l'origine des événements de régulation tels que le recrutement de la kinase CIPK23. Un tel écart existe pour toutes les ZIP eucaryotes. Au cours de ce travail, nous avons initié des étapes cruciales pour réaliser la caractérisation biochimique de cette protéine. Ici, nous sommes les premiers à rapporter avoir établi un protocole optimisé pour l'expression hétérologue, la solubilisation et la purification d'une protéine variante IRT1 dans les cellules de levure.
En outre, nous avons déterminé une procédure technique pour l'étude du transporteur IRT1 dans les protéoliposomes.
Les deux approches techniques rapportées ici ont jeté les bases de l'avenir de la caractérisation structurelle et mécanique de l'IRT1 et des ZIP eucaryotes en général. L'échantillon généré par notre protocole a abouti à une qualité suffisante pour la caractérisation préliminaire de la structure par microscopie électronique cryogénique en collaboration avec nos collaborateurs. De plus, nous avons pu étudier les propriétés oligomères de l'IRT1 in vitro, en soumettant l'échantillon pur à une chromatographie d'exclusion de taille couplée par fluorescence et à une ultracentrifugation analytique, et par des techniques in vivo telles que la co-immunoprécipitation et la complémentation de fluorescence bimoléculaire.
En outre, nous avons étudié la nature du mécanisme moléculaire induit par la liaison du métal sur la boucle de l'IRT1. Nous avons déterminé par dichroïsme circulaire et RMN l'absence de structure tridimensionnelle sur ladite partie de la protéine, même en présence des substrats secondaires qui déclenchent la voie régulatrice de l'IRT1. Nous fournissons ici, des preuves supplémentaires de la liaison des métaux sur la boucle de l'histidine, ainsi qu'une quantification de cette interaction in vitro. De plus, nous avons déduit le rôle d'un résidu d'acide aspartique, également présent dans la boucle de régulation, qui semble avoir un rôle dans la liaison directe des métaux.

Université Paris-Saclay
Espace Technologique / Immeuble Discovery
Route de l'Orme aux Merisiers RD 128 / 91190 Saint-Aubin, France

ÉCOLE DOCTORALE
Sciences du végétal : du gène à l'écosystème (SEVE)

Title: Biochemical characterization of the IRT1 transporter and of its regulatory mechanism

Keywords : IRT1, metal transport, iron acquisition, membrane proteins

Abstract: Iron is a key nutrient for all living organisms and it is involved in many cellular processes. Despite being one of the most abundant elements on earth, iron often is unavailable because it precipitates in soil, forming insoluble complexes. Plants take up iron from the soil through the epidermic cells of the root using the IRT1 iron transporter that belongs to the widely distributed ZIP family of transporters. Aside from iron, IRT1 can also transport non-iron metals (Zn, Mn, Co and Cd), which we also refer to as the secondary substrates. It was recently shown by our team that IRT1 acts as a transceptor, directly sensing non-iron metals using a histidine-rich stretch in an unstructured intracellular loop (Dubeaux et al., 2018). Shortly, under non-iron metal excess, metals bind to the histidines recruiting the CIPK23 kinase. Phosphorylation, in turn, allows the recruitment of the IDF1 E3 ligase that ubiquitinates IRT1 and targets it for degradation through the endocytic pathway.
To date, we still know very little about the structural characteristics of IRT1, its transport mechanisms, the basis of IRT1 transport selectivity and the molecular mechanisms driving regulation events such as the recruitment of the CIPK23 kinase. Such a gap exist for all the eukaryotic ZIPs. During the course of this work, we initiated crucial steps for achieving the biochemical characterization of this protein. Here, we are the first to report having established an optimized protocol for the heterologous expression, solubilization and purification of an IRT1 variant protein in yeast cells. Also, we determined a technical procedure for the study of the IRT1 transporter in proteoliposomes. Both technical approaches reported here set ground in the future of the structural and mechanical characterization of IRT1, and eukaryotic ZIPs in general. The sample generated by our protocol resulted in a quality enough for preliminary characterization of the structure by cryogenic electron microscopy together with our collaborators. Additionally, we were able to investigate the oligomeric properties of IRT1 in vitro, by subjecting the pure sample to fluorescent coupled size exclusion chromatography and analytical ultracentrifugation, and by in vivo techniques such as co-immunoprecipitation and bimolecular fluorescence complementation.
Furthermore, we investigated the nature of the molecular mechanism driven by metal binding on the loop of IRT1. We determined by circular dichroism and NMR the absence of tridimensional structure on said portion of the protein, even in presence of the secondary substrates that trigger the regulatory path of IRT1. We provide here, further evidence of metal binding on the histidine loop, as well as a quantification of this interaction in vitro. Additionally, we inferred on the role of an aspartic acid residue, present in the regulatory loop as well, which appears to have a role in metal binding.

Université Paris-Saclay
Espace Technologique / Immeuble Discovery
Route de l'Orme aux Merisiers RD 128 / 91190 Saint-Aubin, France